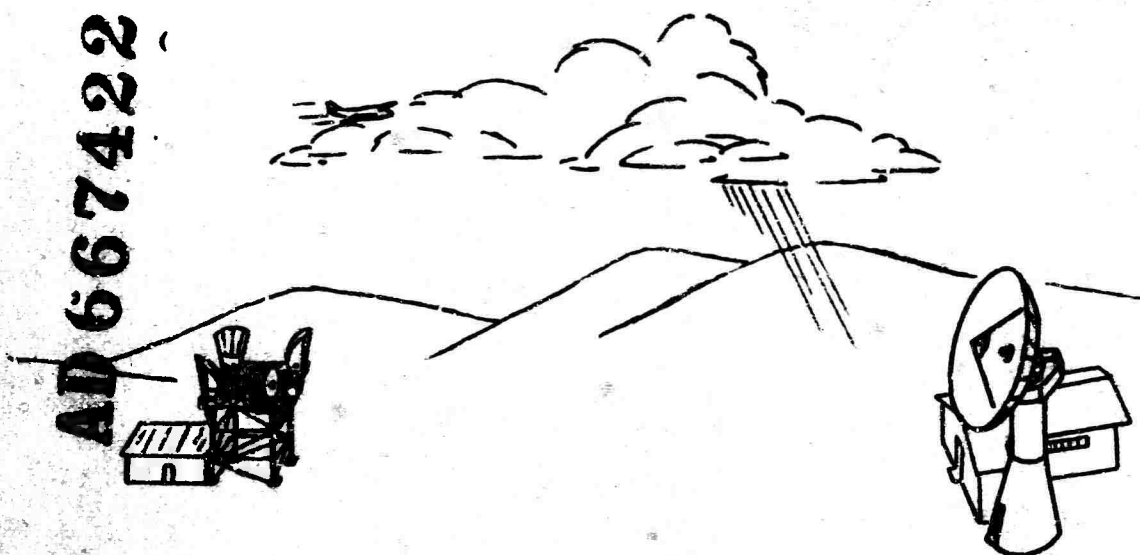


Know Library
FEDERAL COMMUNICATIONS COMMISSION...U.S. AIR FORCE

POPSI PROJECT

AD 667422



REPORT NO. R-6801

By
Roger B. Corey
Daniel B. Hutton
Gary S. Kelagian

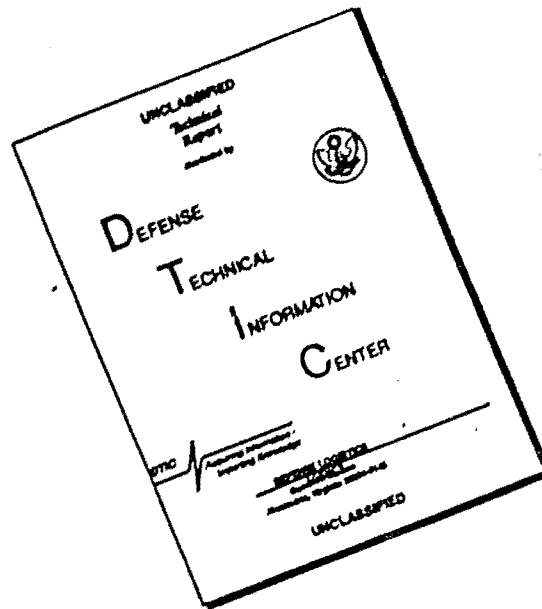


AD 667422
RECEIVED
APR 15 1968

RESEARCH DIVISION
OFFICE OF THE CHIEF ENGINEER
FEDERAL COMMUNICATIONS COMMISSION
WASHINGTON, D.C. 20554
March 15, 1968

This document has been approved
for public release and sale; its
distribution is unlimited

DISCLAIMER NOTICE



THIS DOCUMENT IS BEST QUALITY AVAILABLE. THE COPY FURNISHED TO DTIC CONTAINED A SIGNIFICANT NUMBER OF PAGES WHICH DO NOT REPRODUCE LEGIBLY.

FEDERAL COMMUNICATIONS COMMISSION
OFFICE OF CHIEF ENGINEER
RESEARCH DIVISION

REPORT NO. R-6801

March 15, 1968

FCC/USAF POPSI PROJECT

By
Roger B. Carey
Daniel B. Hutton
Gary S. Kalagian

Washington, D. C.

CONTENTS

	Page No.
1.0 Summary	1
2.0 Introduction	2
2.1 Past Research	
2.2 POPSI, A Cooperative Project	
3.0 Transmitting Site and Equipment	2
3.1 Location	
3.2 Transmitter and Transmitting Antenna Control	
4.0 Receiving Sites and Equipment	3
4.1 Antennas	
4.2 Receivers and Recorders	
5.0 Path Configurations and Sampling Technique	4
5.1 Antenna Alignment	
5.2 Sample Intervals	
6.0 Main Beam Common Volumes	5
6.1 On-Path Common Volumes	
6.2 Off-Path Common Volumes	
7.0 Basic Propagation Equation	6
7.1 Interference Criteria	7
8.0 Probability Distribution Curves	8
8.1 Transmitting Antenna On-Path	
8.2 Transmitting Antenna Off-Path	
9.0 Separation and Identification of Propagation Modes	9
9.1 Mode Separation Technique	10
10.0 Meteorological Data	12
10.1 Weather Radar	
10.2 RAWINSONDE and Surface Measurements	
11.0 Detailed Data Analyses	12
11.1 Ducting	13
11.2 Precipitation Scattering	13
11.3 Angle Dependent Guided Propagation	16
12.0 Conclusions	18
13.0 Acknowledgements	20
14.0 References	22

Appendix A - Correlation Procedure

Appendix B - Radio Refractive Index Computation

Index to Figures

Figure No.

1	POPSI Project System Design
2	Map of Propagation Path Area
3	View from Transmitter Site
4A	Transmitter Antenna Control Unit
4B	Chart Analyses Layout
5	Receiving Site Antenna Installations
6	Receiving Site Equipment Installations
7	Antenna Beam Definition Diagram
8	On-Path Common Volumes, Path to NAFEC
9	On-Path Common Volumes, Path to Wildwood
10	Off-Path Common Volume, Path to Wildwood, TX at 3°, RX at 6° & 1°
11	Off-Path Common Volume, Path to Wildwood, TX at 3°, RX at 3° & 1°
12	Off-Path Common Volume, Path to Wildwood, TX at 6°, RX at 3° & 1°
13	Off-Path Common Volume, Path to Wildwood, TX at 6°, RX at 6° & 1°
14	Off-Path Common Volume, Path to Wildwood, TX at 12°, RX at 3° & 2°
15	Off-Path Common Volume, Path to Wildwood, TX at 9°, RX at 6° & 2°
16	Off-Path Common Volume, Path to Wildwood, TX at 12°, RX at 6° & 2°
17	Off-Path Common Volume, Path to Wildwood, TX at 18°, RX at 3° & 2°
18	Off-Path Common Volume, Path to NAFEC, TX at 9°, RX at 6° & 2°
19	Off-Path Common Volume, Path to NAFEC, TX at 12°, RX at 6° & 2°

Probability Distributions

Figure No.	Location	Receiver	TX Ant. Az.	TX. Ant. Elev.	Date
20A	NAFEC	On-Path	0°	1/2°	Aggregate
20B	NAFEC	On	0°	1/2°	5/13/66-2/11/67
21A	Wildwood	On	0°	1/2°	Aggregate
21B	Wildwood	On	0°	1/2°	2/16/66-12/14/66
22	Wallops Island	On	0°	1/4°	1/24/67-2/16/67
23A	NAFEC	Off-Path	0°	1/2°, 5°, 10°	5/13/66-8/16/66
23B	NAFEC	Off	0°	1/4°, 3°, 15°	1/24/67-2/16/67
24A	Wildwood	Off	0°	1/2°, 10°	2/16/66-5/13/66
24B	Wildwood	Off	0°	1/2°, 1°, 2°	5/1/66-6/7/66
24C	Wildwood	Off	0°	1/2°, 1°, 4°, 10°	6/7/66-8/17/66
24D	Wildwood	Off	0°	1/2°, 2°, 20°	8/19/66-12/14/66
25A	NAFEC	On-Path	0°	5°, 10°, 20°	5/13/66-2/16/67
25B	NAFEC	On	0°	9°, 27°, 30°	1/24/67-2/16/67
26A	Wildwood	On	0°	1/2°, 1°, 2°, 3°, 4°, 5°	2/16/66-5/13/66
26B	Wildwood	On	0°	10°	2/16/66-5/13/66
27A	Wildwood	On	0°	1/2°, 1°, 2°, 3°, 4°, 5°	5/13/66-6/7/66
27B	Wildwood	On	0°	10°	5/13/66-6/7/66
28A	Wildwood	On	0°	1/2°, 1°, 2°, 3°, 4°, 5°	6/7/66-8/17/66
28B	Wildwood	On	0°	10°	6/7/66-8/17/66
29A	Wildwood	On	0°	1/2°, 2°, 4°, 6°	8/19/66-12/14/66
29B	Wallops Island	On	0°	20°	8/19/66-12/14/66

Probability Distributions (Cont'd)

<u>Figure No.</u>	<u>Location</u>	<u>Receiver</u>	<u>TX Ant. Az.</u>	<u>TX Ant. Elev.</u>	<u>Date</u>
30A	Wallops Island	Cn-Path	0°	1/4°, 24°	1/24/67-2/16/67
30B	Wallops Island	On	0°	3°, 21°	1/24/67-2/16/67
31A	NAFEC	On	3°	1/2°, 5°, 10°	5/13/66-6/7/66
31B	NAFEC	On	6°	1/2°, 7°, 10°	5/13/66-6/7/66
32A	NAFEC	On	9°	1/2°, 5°, 10°	6/7/66-8/16/66
32B	NAFEC	On	12°	1/2°, 9°	6/7/66-8/16/66
33A	NAFEC	On	12°	1/2°, 4°, 18°	8/19/66-11/25/66
33B	NAFEC	On	18°	1/2°, 18°	8/19/66-11/25/66
34A	NAFEC	On	3°	1/4°, 15°, 30°	1/24/67-2/16/67
34B	NAFEC	On	18°	1/4°, 15°	1/24/67-2/16/67
35	Wildwood	On	3°	9°, 10°	2/14/66-5/13/66
36	Wildwood	On	6°	10°	2/16/66-5/13/66
37	Wildwood	On	3°	9°, 10°	5/13/66-6/7/66
38	Wildwood	On	6°	10°	5/13/66-6/7/66
39	Wildwood	On	9°	5°, 10°	6/7/66-8/17/66
40	Wildwood	On	12°	1/2°, 10°	6/7/66-8/17/66
41	Wildwood	On	12°	1/2°, 20°	8/19/66-12/14/66
42	Wildwood	On	18°	1/2°, 2°, 20°	8/19/66-12/14/66
43A	NAFEC	Off-Path	9°	1/2°, 2°	6/7/66-8/16/66
43B	NAFEC	Off	9°	1°, 7°	6/7/66-8/16/66
43C	NAFEC	Off	9°	3°, 6°, 9°	6/7/66-8/16/66
43D	NAFEC	Off	9°	4°, 8°	6/7/66-8/16/66
44A	NAFEC	Off	12°	1/2°, 1°	6/7/66-8/16/66
44B	NAFEC	Off	12°	3°	6/7/66-8/16/66
44C	NAFEC	Off	12°	2°, 4°	6/7/66-8/16/66
44D	NAFEC	Off	12°	6°, 10°	6/7/66-8/16/66
45A	Wildwood	Off	3°	1/2°, 1°, 2°	2/16/66-5/13/66
45B	Wildwood	Off	3°	3°, 4°	2/16/66-5/13/66
45C	Wildwood	Off	3°	5°, 6°	2/16/66-5/13/66
45D	Wildwood	Off	3°	10°	2/16/66-5/13/66
46A	Wildwood	Off	9°	3°, 4°	6/7/66-8/17/66
46B	Wildwood	Off	9°	6°, 8°	6/7/66-8/17/66
47A	Wildwood	Off	12°	1/2°, 3°, 10°	6/7/66-8/17/66
47B	Wildwood	Off	12°	4°, 9°	6/7/66-8/17/66
48A	Wildwood	Off	18°	1/2°, 10°, 16°	8/19/66-12/14/66
48B	Wildwood	Off	18°	8°, 14°	8/19/66-12/14/66
49A	Wallops Island	Off	3°	1/4°, 3°	1/24/67-2/16/67
49B	Wallops Island	Off	18°	1/4°, 15°	1/24/67-2/16/67
50	Propagation Modes				
51A	Computer Derived Receiving Antenna Pattern - NAFEC				
51B	Computer Derived Receiving Antenna Pattern - Wildwood				
52A	through F Computer Derived Transmitting Antenna Patterns				
53A	& B Basic Data Charts, Wildwood, 6/16/66				
54A, B & C	Basic Data Charts, NAFEC, 6/28/66				
55A through F	Basic Data Charts, NAFEC & Wildwood, 10/15 and 10/16/66				
56	POPSI Meteorological Facilities				
57	Wildwood Recorder Charts, 6/16/66				
58A,	C NAFEC WX Radar PPI Scope Photographs, 6/15 & 6/16/66				

59 H vs N Refractivity Index Profile, JFK Airport, 6/16/66
60A,B, & C Wildwood and NAFEC Recorder Charts, 6/28/66
61A, B, & C NAFEC WX Radar PPI Scope Photographs, 6/28/66
62A & B Climatological Data, NAFEC June, 1966
63 H vs N Refractivity Index Profiles, NAFEC, 6/28/66
64A, B, C, & D Wildwood and NAFEC Recorder Charts, 10/15 & 10/16/66
65 Transmitter Site Backscatter Recorder Charts, 10/15 & 10/16/66
66A through L. NAFEC WX Radar PPI Scope Photographs, 10/15 & 10/16/66
67A, B & C H vs N Refractivity Index Profile, JFK Airport, 10/15 & 10/16/66

1.0

SUMMARY

From 15 February 1966 to 16 February 1967, the FCC and USAF, with the cooperation of the U. S. Coast Guard, the FAA, the U. S. Weather Bureau, and NASA, conducted an investigation known as the POPSI (Precipitation and Off-Path Scattered Interference) Project. The investigation involved studies of the scattered signal from precipitation and other mechanisms located in the common volumes established by the intersections of the beams from a transmitting antenna operating in a configuration simulating a satellite earth station, and receiving antennas configured in a manner typical of terrestrial microwave radio relay stations. The project was designed to obtain data at a frequency of 5.75 GHz for a statistical treatment to estimate the magnitude of the problem of both on and off-path scattered interference between microwave radio relay stations and satellite system earth stations sharing the same frequency bands. More than 3000 hours of field strength measurements were recorded. Propagation path lengths up to 300 km were examined. The common volumes given consideration were displaced as much as 18 degrees in azimuth and 30 degrees in elevation from the great circle path toward the receiving sites. Time probability curves have been derived for various path configurations from Highlands, N. J. to Pleasantville and Wildwood, New Jersey, and to Wallops Island, Virginia. Some attempt has been made to correlate the enhanced fields with meteorological phenomena, although the mechanisms have not been examined in great detail for this report.

2.0

INTRODUCTION

Since satellite communications systems are required to share frequency bands with terrestrial microwave systems, the utmost care must be exercised in station assignments if intolerable interference is to be avoided. The use of terrain shielding and minimum limits on the satellite earth station elevation angles are of considerable importance in the reduction of interference between terrestrial microwave and satellite system earth stations. However, the problems of interference scattered from precipitation and other off-path mechanisms cannot be avoided by these measures alone.

2.1 Past Research

Most past research has been directed toward an understanding of the mechanisms of the scattering problem.^{1,2,3,4/} These studies have associated the problem with certain meteorological phenomena (thunderstorms, hail, atmospheric discontinuities, etc.) and these phenomena have been studied in some detail. This approach has been useful in analyzing the physics of the phenomena, but has not resulted in a suitable model that can be theoretically extended to provide a basis for the prediction of interference where high service reliability is required. At present, the state of the art seems to admit only a statistical approach to the problem requiring considerably more data than has been obtained thus far.

2.2 POPSI, A Cooperative Project

From 15 February, 1966, to 16 February, 1967, the FCC and the USAF, with the cooperation of the U. S. Coast Guard, the FAA, the U. S. Weather Bureau, and NASA, conducted a precipitation and off-path scatter interference (POPSI) project to obtain data for a statistical treatment to get a better understanding of the magnitude of the problem. The project utilized an AN/FPS-26 height finder radar as a transmitter, left in place at a phased-out Air Defense Command site (Highlands, New Jersey), and was maintained and operated by a detachment of ADC personnel who remained there for the purpose. Most of the receivers were on loan from the U. S. Air Force. They were modified at the FCC Laboratory and installed by FCC personnel at locations supervised by the U. S. Coast Guard at Wildwood, New Jersey, the FAA at NAFEC near Pleasantville, New Jersey, and NASA at Wallops Island, Virginia. Coast Guard, FAA and NASA personnel provided field maintenance and calibration support of the receiver/recorder installations in addition to their regular duties. In this manner, the project was accomplished at a fraction of the usual cost of such a research project. Figure 1 provides a brief summary of the POPSI project system parameters.

3.0

TRANSMITTING SITE AND EQUIPMENT

3.1 Location

The transmitter was located near the top of a hill overlooking the Navesink River just south of Highlands, New Jersey. The supporting tower structure was such that the center of the antenna was slightly more than 90 meters above the terrain. For several kilometers in the direction of the propagation path, the terrain is only a few meters above mean sea level.

Figure 2 is a map of the propagation path area. Figure 3 is a view from the transmitter antenna tower in the general direction of the propagation path.

3.2 Transmitter and Transmitting Antenna Control

The AN/FPS-26 is a pulsed, C-band, height-finder radar with a peak effective radiated power on the order of that used by international communication satellite system earth stations. It normally operates in a nodding mode and is directed to the desired azimuth by electrical command from a remote location. If necessary, it can be directed manually from a local control unit. For POPSI operation the nodding mode was discontinued and an automatic antenna program control unit, designed and built by FCC personnel, was connected in place of the local manual control unit. This control unit automatically positioned the antenna in azimuth and elevation in accordance with a pre-programmed sequence, and furnished electrical readout to recorders to indicate the antenna position at all times. In addition, a recorder was interfaced with the radar receiver to furnish a backscatter indication. The programmer was controlled by a master timer synchronized to standard time signals and the recorders were driven by synchronous motors so their time bases could be synchronized with the recordings from the receiving sites for analysis. The programmer and chart analyses layout are shown in Figures 4A and 4B. The details of the design of the antenna programmer, its interface with the antenna control system, and the receiver modification and receiver/recorder interface, are expected to be the subject of a subsequent report.

4.0 RECEIVING SITES AND EQUIPMENT

Receiving sites were established at NAFEC* near Pleasantville, New Jersey, and at the U. S. Coast Guard Electronic Engineering Station at Wildwood, New Jersey. Near the conclusion of the project the receiving site at Wildwood was discontinued and a new site established at the NASA station at Wallops Island, Virginia. These sites were all on the same radial, bearing at approximately 205.4 degrees from the transmitter.

4.1 Antennas

Each site had two antennas of a type commonly used for microwave relay stations, with a receiver connected to each antenna. One antenna was directed along the great circle path toward the transmitter and oriented vertically for maximum field strength. The other antenna was oriented either 3 degrees or 6 degrees to the west of the great circle path and elevated slightly (1/2 to 2 degrees) above the horizon.

4.2 Receivers and Recorders

AN/APR-9 ECM receivers were installed at Wildwood and Wallops Island. At NAFEC an AN/APR-9 receiver and a Polarad Model R receiver were used.

*National Aeronautical Facilities Experimental Center (FAA)

The AN/APR-9 receivers were modified at the FCC Laboratory to decrease the bandwidth, increase the sensitivity, and permit recorder operation. When placed in service they had 6 dB bandwidths of about 16 MHz and usable sensitivities on the order of -75 to -80 dBm. The Polarad Model R had a bandwidth of about 4 MHz and a usable sensitivity of -70 dBm. Esterline-Angus chart recorders were connected to each receiver. These recorders and the transmitting site recorders were driven by synchronous motors at a chart speed of 12 inches per hour. The receiving recording equipment was calibrated at the same frequency and with the pulse width and repetition rate used by the transmitter. The receiving antenna installations at NAFEC, Wildwood, and Wallops Island are shown in Figure 5, and a typical receiver installation is shown in Figure 6.

5.0

PATH CONFIGURATIONS AND SAMPLING TECHNIQUE

The period during which the project was conducted was divided into several programs determined by path length, transmitting antenna azimuth and elevation configurations, and off-path receiving antenna orientation. During each program a maximum of 3 transmitting antenna azimuths and 12 transmitting antenna elevation angles, in conjunction with 1 off-path receiving antenna configuration, were examined. However, the calibration and time base synchronization techniques required that 1 of the azimuths and 2 of the elevation positions of the transmitting antenna be in the great circle path toward the receiving sites. Each azimuth was probed for 55 minutes during which each elevation was probed for 5 minutes for a total of 11 elevations per hour. For the last 5 minutes of each hour, the transmitting antenna was returned to the great circle path (maximum signal configuration) for calibration and time base synchronization purposes.

A normal complete transmitting antenna programming cycle required 3 hours and consisted of 4 samples of the great circle path configuration, plus 1 sample of each of 32 other azimuthal and elevation combinations.

5.1 Antenna Alignment

To establish the great circle or 0° azimuth, the transmitting and receiving antennas were aligned for maximum signal over a period of several hours during which the troposphere was considered to be well mixed. The antenna beamwidths were such that the positioning for maximum response did not appear to be critical as far as azimuth was concerned. The elevation angle positioning was somewhat more exacting, but there was no noticeable difference between elevation angles of 0° and $1/2^{\circ}$ above the horizon during well mixed troposphere conditions. The off-path transmitting antenna configurations were obtained by alignment to reference points on a vernier on the antenna pedestal. The off-path receiving antenna configurations were obtained by boresighting on optical reference points offset by surveying methods from the boresight reference point for the maximum signal position. The programmed transmitting antenna azimuthal positions correspond to true bearings from Highlands, New Jersey as follows:

TX Ant. Azimuth

True Bearing from highlands

0°	205.357°
3°	208.357°
6°	211.357°
9°	214.357°
12°	217.357°
18°	223.357°

5.2 Sample Intervals

The dynamic range and response time of the receiving/recording equipment eliminated the possibility of any evaluation of the short term (less than several seconds) signal variability. The recorder charts were analyzed by determining the median value for the 5 minute period of each transmitting antenna configuration. The data presentation represents the probability distributions of the 5 minute medians. Inasmuch as the great circle maximum signal positions were sampled 4 times every 3 hours, the probability distributions for these configurations are based upon several thousand samples. However, even the least investigated of the off-path positions were sampled 86 times in a period extending over more than 10 days. The number of samples in each configuration is given in Annex A.

6.0

MAIN BEAM COMMON VOLUMES

For purposes of analyses, the transmitting and receiving antenna main beams have been defined as bounded by surfaces coincident with the half-power points of the antenna vertical and horizontal patterns. In this manner, the transmitting antenna beam may be described as a pyramid with a rectangular cross-section having a maximum dimension in the horizontal plane equal to about 4 times its dimension in the vertical plane. The receiving antenna beam may be described as a cone having a cross-sectional diameter that subtends approximately the same angle as do the long sides of the transmitting antenna beam cross-section. The main beam common volume is that part of the propagation medium bounded by the above described surfaces and common to both antenna beams as shown in Figure 7.

6.1 On-Path Common Volumes

In the absence of shielding by the earth's bulge or by terrain features, an intersection of the transmitting antenna main beam and the on-path receiving antenna main beam always occurs and a common volume is established regardless of the transmitting antenna azimuth and elevation configurations. The size of this common volume is quite dependent upon the transmitting antenna elevation angle, especially in the 0° azimuthal position. Reference to Figures 8 and 9 shows that, for both the paths to Wildwood and to NAFEC, the common volumes at a transmitting antenna elevation angle of 1/2° are 3 orders of magnitude greater than the common volumes at a transmitting antenna elevation angle of 30°.

6.2 Off-Path Common Volumes

The common volumes for the various off-path combinations of receiving and transmitting antenna configurations are shown in Figures 10 through 19. It is quite obvious that the locations, sizes, and altitudes of these common volumes are dependent upon the antenna azimuth and elevation configurations. In many of the off-path antenna configurations examined during the project no main beam to main beam intersections were achieved and, therefore, no main beam common volumes were established. Even when such volumes did occur, their sizes varied considerably. These variations may have considerable influence on the received signal strength since, if the scattering is considered to be isotropic in nature and the scatterers are uniformly distributed, the received power is directly related to the size of the common volume. For example, with the off-path receiving antenna at Wildwood pointed at an azimuth of 30° , the maximum size of the common volume occurring with a transmitting antenna azimuth of 30° is nearly 20 times that occurring with a transmitting antenna azimuth of 180° . This alone could account for a 13 dB ratio in the received powers during such configurations. A comparison of the off-path common volume for the Highlands to Wildwood path with that for the Highlands to NAFEC path for the same antenna configurations indicates that the longer path results in common volumes about 5 times the size of those set up by the shorter path geometry. Assuming uniformly distributed isotropic scatterers, this would result in a 7 dB ratio in the volume-scattered powers. Since the ratio of the free space losses due to the difference in path lengths is only about 4 dB, the off-path scattered signal received at Wildwood may equal or exceed that received at NAFEC even though the off-path receiving antennas at both sites are looking at essentially the same scattering cell.

7.0

BASIC PROPAGATION EQUATION

For simplicity in the data analyses, the basic propagation equation was used in the following form:

$$(1) \quad P_R = P_t + G_t + G_r - L_b$$

P_t = transmitter peak power (dBW)

G_t = free space isotropic gain of the transmitting antenna (dB)

G_r = free space gain of receiving antenna less
transmission line losses (dB)

L_b = basic transmission loss (dB)

P_R = power at receiver input (dBW)

P_t was continuously monitored at the transmitter.

G_t and G_r were obtained from the equipment manufacturers' specifications. P_r was obtained by direct measurement at each receiving installation and appears as the ordinate value of the probability distribution curves. Assuming that the significant propagation mode involved only main beam to main beam coupling, the basic transmission loss L_b may be obtained from the measured value of P_r by conversion factors based upon P_t , G_t , and G_r for each path as follows:

Highlands to NAFEC 137 - P_r (dB)

Highlands to Wildwood 140 - P_r (dB)

Highlands to Wallops Island 138 - P_r (dB)

The great circle path free space loss was calculated by

$$(2) L_{fs} = 20 \log \left(\frac{4\pi d}{\lambda} \right) \quad (\text{dB})$$

L_{fs} to NAFEC: 148 dB

L_{fs} to Wildwood: 152 dB

L_{fs} to Wallops Island: 157 dB

7.1 Interference Criteria

Using the criteria set forth in CCIR Report 382 (Oslo, 1966) for the determination of coordination distance between satellite system earth stations and terrestrial stations sharing the same frequency band, the basic transmission loss is given by the following general formula:

$$(3) L_b = (P_t + G_t) - F_s - (P_r - G_r)$$

where

P_t = power, in dBW, supplied by the interfering transmitter to the input to the transmitting antenna;

G_t = isotropic gain, in dB, of the transmitting antenna of the interfering station in the pertinent direction;

F_s = earth station site shielding factor, in dB;

P_r = maximum permissible interfering carrier power, in dBW, at the input to the receiver subject to interference;

G_r = isotropic gain, in dB, in the pertinent direction, of the receiving antenna of the station subject to interference, less feeder losses and polarization discrimination, if applicable.

The minimum permissible basic transmission loss from an earth station to an angle-modulated, radio-relay station is as follows:

$$(4) \quad L_b (0.005\%) = (P_t + G_t) - F_s + 173$$

Substituting (4) in (3) and solving for P_r with G_r set equal to 42 dB (assumed G_r in CCIR Report 382) yields

$$P_r = -131 \text{ dBW (allowable level of interfering signal)}$$

But the POPSI transmitter peak power exceeded the CCIR assumed P_t by 24 dB and the value of G_r for the POPSI operation was 33 dB instead of 42 dB. Therefore, for a typical radio relay station installation the equivalent permissible level of the undesired signal (equating the POPSI operation to the CCIR criteria) becomes $P_r = -131 + 24 - 9 = -116 \text{ dBW}$.

8.0 PROBABILITY DISTRIBUTION CURVES

Since there were a large number of antenna configurations involved in the investigation, there are a large number of probability distribution curves. Only those considered to be of primary importance have been included in the text of this report. The remainder of the distribution curves have been included in Annex A.

8.1 Transmitting Antenna On-Path

Figures 20, 21 and 22 show the distribution of the received powers at the input terminals of the on-path receivers during the periods the transmitting antenna was directed along the great circle path in the maximum signal configuration. A theoretical distribution, obtained by applying the prediction techniques of NBS Technical Note 101, Volume II, Fig. 1.12, 5 is also shown on each figure. The distributions for the NAFEC and Wildwood sites are given for time frames corresponding to specific antenna pointing programs. Figures 23A and B may be compared with the corresponding curves on Figure 20B to arrive at the NAFEC off-path receiving antenna side lobe response. In this manner, it can be seen that the median value of the off-axis response of the off-path receiving antenna to a great circle path signal varied between -12 and -24 dB below the on-path receiving antenna response to the same signal. Figures 25 through 30B represent the distributions of the powers at the input terminals of the on-path receivers when the transmitting antenna was directed along the great circle path at various elevation angles.

8.2 Transmitting Antenna Off-Path

Figures 31 through 42 show the distributions of the powers at the input terminals of the on-path receivers when the transmitting antenna was directed in various off-path configurations. In most cases, the extreme limit reached during each pointing program is represented. However, some configurations did not result in enough measurements to permit the establishment of a distribution.

Figures 43 through 49B are the distributions of the powers at the input terminals of the off-path receivers for various off-path transmitting antenna configurations. CV on the legend means that, theoretically, a common volume was established by the antenna main beam intersection. NCV indicates that the main beams did not intersect and no common volume was established.

A comparison of the charts shown in Figure 57 with those shown in Figures 60A, B and C, indicates some difference in the short term signal variations. Although this may provide the clue to an obviously dominant propagation mechanism many of the enhanced signal periods seemed to involve a "mixing" of envelope amplitude variations in such a manner as to make mode identification difficult without a detailed analysis of the short term variability. Therefore, the principal problem confronting any effort to determine the contribution of off-path scattered energy to the received power at any given location is the difficulty in isolating the dominant propagation mode at any given time. Figure 50 is a somewhat simplified presentation of the possible propagation paths and modes. The great circle paths are indicated by the letters A, B, C, and D, with the usually dominant path indicated by the main beam to main beam coupling at A. Of secondary importance are the main beam to side lobe couplings identified as B and C. The side lobe to side lobe coupling represented by D must be given tertiary consideration. The off-path modes are indicated by the numbers 1 through 10 with the theoretically dominant mode consisting of main beam to main beam coupling in a common scattering volume indicated by the number 1. During anomalous propagation conditions, the great circle modes may be effective to such an extent that they contribute substantially to the power at the off-path receiver input terminals, even though the transmitting antenna is also directed off-path. It is also possible that off-path modes other than main beam to main beam scattering contribute significantly to the off-path received power. There have been a number of attempts to overcome the difficulties in propagation mode separation by using beam swinging or frequency sweeping techniques and determining short term frequency (phase) correlation or time auto correlation.^{6,7} Such techniques require extremely sophisticated equipment and generally present formidable data processing problems if an extended operation is to be conducted.

Limited success in identifying the dominant propagation mode may be achieved by comparing the received power in an off-path configuration with the received power in a juxtaposed on-path configuration and considering the probable order of magnitudes of the amplitudes of the two signals based upon comparative common volume sizes and effective antenna gains across the common volume integrals. This approach requires certain gross assumptions but they are not unique in classical tropospheric electromagnetic wave propagation theory. The assumptions are:

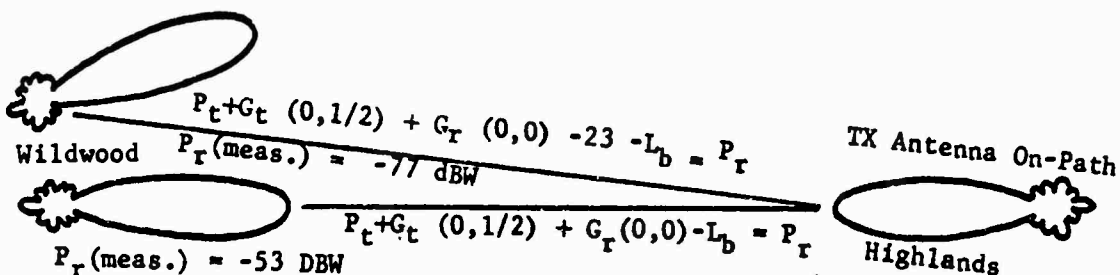
1. The antenna patterns are considered to be discretely defined in a manner similar to the commonly used keyhole pattern concept (Figures 51A through 52F).
2. The scattering medium is homogeneous over the entire volume under consideration. (This appears to be a contradiction in terms because some widely-accepted scattering theories depend upon inhomogeneities in the troposphere.^{8,9,10} Perhaps a better way of stating this assumption would be to say that the inhomogeneities are assumed to be uniformly distributed.)

3. The scatterers are implied to be isotropic. 9/
4. The propagation conditions have remained stable over the comparison period.

9.1 Mode Separation Technique

The propagation mode separation technique is exemplified in the basic data forms shown in Figures 53A through 55F. Beginning at 0100 hours on June 16, 1966, the transmitting antenna began the 3-hour pointing sequence in the great circle configuration. During the 5 minute period from 0100 to 0105 the median power input to the on-path receiver at Wildwood was -80 dBW and the median power input to the off-path receiver was -100 dBW. Aside from the two mildly enhanced on-path signals in the periods from 0105 to 0110 and 0110 to 0115, both the on-path and off-path signals were below the receiver noise level until the end of the hour. When the transmitting antenna returned to the great circle path between 0155 and 0200, the signal was considerably enhanced; the on-path receiver input was -53 dBW and the off-path receiver input was -77 dBW. The ratios of the on-path to the off-path receiver inputs represents essentially the receiving antenna side lobe response, so the same propagation mode is probably working into both antennas.

RX Antenna Off-Path



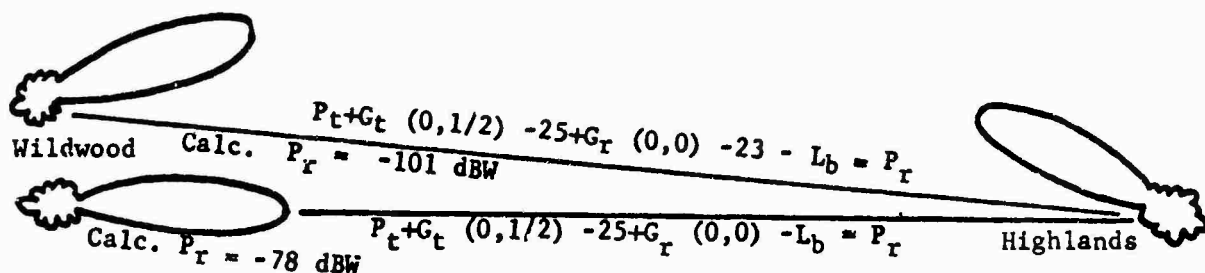
RX Antenna On-Path

Horizontal Plane Diagram

At 0200 hours, the transmitting antenna was directed into the 9° off-path azimuth at the minimum elevation angle. From Figure 52D, the transmitting antenna pattern response in the direction of the great circle path should be down 25 dB from the maximum. If the propagation conditions had not changed and both antennas were responding to only the great circle path signal, the median on-path receiver input should have been $-53 + (-25)$ or -78 dBW and the off-path input should have been $-53 + (-25) + (-23)$ or -101 dBW .

RX Antenna Off-Path

TX Antenna Off-Path



RX Antenna On-Path

Horizontal Plane Pattern

The actual measured value was 11 dB less than predicted into the on-path receiver. Unfortunately, the receiver noise level was too high for an off-path measurement, but the signal was not greater than -101 dBW. Between 0205 and 0210 hours, the transmitting antenna was at 9° off-path azimuth and elevated to 1° . From Figure 52D, the transmitting antenna pattern response is 30 dB below the maximum. Therefore, the on-path receiver input due to a great circle path signal could be expected to be $-53 + (-30)$ or -83 dBW and the off-path receiver input could be expected to be $-53 + (-30) + (-23)$ or -106 dBW. The measured values were 6 and 8 dB higher than expected. In the 2° elevation configuration, the measured values were 10 and 8 dB higher than expected; in the 3° elevation configuration, the measured values were 4 and 5 dB higher than expected. Continuing in this manner, it will be noted that, when the measured on-path signal is higher than expected, the measured off-path signal is also higher than expected and, furthermore, the differences agree within 3 dB. This can best be interpreted as an indication that when the transmitting antenna was in the great circle path configuration either the optimum antenna position was not being achieved or the on-path receiver was being saturated and the true signal level could not be measured. Attention is invited to the period during which the transmitting antenna was in the 9° azimuth and 6° to 10° elevation positions. Although both the on-path and off-path signals were considerably higher than expected, the correlation between the differences broke down. In the 7° elevation configuration the differences were 9 dB apart. This is a probable indication that the off-path antenna was receiving a signal component propagated by some mode other than the great circle path. The same situation apparently occurred when the transmitting antenna was in the 12° azimuth and 5° elevation position at 0325 hours. From 0300 to 0400 there was some change in the great circle path propagation conditions. During this period the estimated receiver input powers for the elevation steps through 5° were based upon the measured median value at 0255 and the estimated values for the 6° through 10° steps were based upon the value measured at 0355 hours. Because the measured values were 11 to 19 dB lower than calculated, it is obvious that the received power of -31 dBW measured at 0355 should not have been used for the 6° to 10° calculations. However, when the values measured at the beginning and end of each hour differed, the division for computation purposes was arbitrarily made on the half hour.

10.0

METEOROLOGICAL DATA

Although the facilities for the collection of meteorological data for the propagation path were not ideal for good correlation of radio propagation characteristics with meteorological conditions, they were probably as complete as could be obtained anywhere in the United States without introducing techniques, equipment and procedures considerably more sophisticated than are now being used.

10.1 Weather Radar

Figure 56 is an overlay chart for the WSR-57 weather radar located at NAFEC. For analysis purposes this radar can be considered to be co-located with the receiving site at NAFEC. This radar has a precision attenuator input but this capability was activated only during periods of increased weather watch in connection with the MESONET operation.

10.2 RAWINSONDE and Surface Measurements

In addition to the weather radar there were also a RAWINSONDE facility at NAFEC and a RAWINSONDE facility at JFK International Airport situated about 39 kilometers north of the transmitter site. Hourly surface meteorological data were also available for stations at New York City, Philadelphia, Atlantic City, and Salisbury. The RAWINSONDE data from JFK were normally for 4 releases per day at 0015, 0615, 1215 and 1815 local time. The RAWINSONDE releases at NAFEC were usually made only during activation of the MESONET. The MESONET data consisted of surface data (temperature, dew point, precipitation and average cloud height) every 30 minutes from each of 13 stations in the area surrounding NAFEC.

11.0

DETAILED DATA ANALYSES

As previously mentioned, one of the greatest obstacles to a detailed propagation mechanism analysis is the difficulty in the separation of the propagation modes. The power received at the input terminals of the off-path receiver when the transmitting antenna is also directed off-path consists of off-path scattered components arriving by way of one or more of the numbered paths in the simplified diagram shown in Figure 50 and an on-path component arriving by way of the great circle path indicated by the intersection marked "D" in Figure 50. During "normal" propagation conditions the great circle path component is of little significance since the highly directive transmitting and receiving antennas result in very little power radiated along the great circle path. However, during these same "normal" conditions the off-path scattered components give no cause for alarm because, although the power illuminating the common volume is quite high, the power transfer or coupling mechanism between the antenna main beams and/or significant side lobes is extremely inefficient. During abnormal conditions one or more of the signal components may be greatly enhanced due to the increased efficiency of the coupling mechanisms. Although present theories concerning the mechanisms are not universally accepted it is generally agreed that the on-path and off-path components are principally affected by different mechanisms. Therefore, any successful mechanism study involves the separation of the signal into components, the

assignment of a likely value to the most easily identified component, and the vector manipulation of this value to obtain possible values for the other component(s). Using this approach, analysis has been attempted for 3 representative enhanced signal periods.

11.1 Ducting

Highlands to Wildwood, 16 June 1966, 0100 - 0700 hours.

Figure 57 shows photographs of the Wildwood on and off-path receiver/recorder charts for the period covered by the basic data charts in Figures 53A and B. By application of the correlation technique described in Section 9.0 and formulated in Appendix A, the unusually high signal power into the off-path receiver can be attributed to an on-path component due to a super-refractive or ducting condition except for the possibilities of weak off-path scattered components at 0235 when the transmitting antenna was in the 90° azimuth and 70° elevation position and at 0325 when the transmitting antenna was in the 120° azimuth and 50° elevation position. By considering the error component in the measured power into the on-path receiver at 0225, the approximate magnitude of the median (5 min.) optimum great circle path signal may be determined by the procedure of Appendix A:

$$P_{rt} = P_{rm} (0^\circ, 1/2^\circ) - E$$

$$P_{rt} = -53 - (-14) = -39 \text{ dBW}$$

The basic transmission loss for this level of receiver input power is 27 dB greater than that for free space.

There are other indications that the signal into the off-path receiver was due to ducting or superrefraction. A comparison of the envelopes of the input power levels recorded on the on and off-path charts shown in Figure 57 discloses good correlation. The photographs in Figures 58A, B & C show presentations on the PPI scope of the WSR-57 weather radar at NAFEC. The display at 2250 on 6/15/66 indicates long range ground returns from the coastal area as far south as Norfolk, Virginia. The display at 0600 on 6/16/66 indicates long range ground returns from the coastal area to the north of NAFEC. Vertical radio refractive index profiles calculated from RAWINSONDE data at JFK International Airport are shown in Figure 59. These profiles were determined in accordance with the procedure set forth in Appendix B. The profile based upon the release at 0015 on 6/16/66 shows nothing unusual. The profile for the data from the release at 0615 on 6/16/66 indicates strong negative refractive index gradients near the earth's surface. These gradients exceeded the slope associated with ducting (-157 N units/km) according to at least one dissertation on the subject. 11/

11.2 Precipitation Scattering

Highlands to NAFEC and Wildwood, 28 June 1966, 1500 - 2100 hours.

Figures 60A, B and C are photographs of the NAFEC on and off-path receiver/recorder charts and the Wildwood off-path chart for the period covered by the basic data charts in Figures 54A, B, and C.

The correlation technique described in Appendix A indicated no on-path (great circle) component of significance in the off-path receiver input at NAFEC. The correlation technique could not be applied at Wildwood because only one receiver was in operation. It is obvious that the enhanced signal into the off-path receiver was due to off-path scattering, alone. With the transmitting antenna at an azimuth offset of 9° , the highest median value for the off-path receiver input at NAFEC occurred at a transmitting antenna elevation angle of 3° . From Figure 18 it may be seen that this represents the maximum common volume configuration. For the same receiver, with the transmitting antenna offset to an azimuth of 12° , the highest median values occurred at elevation angles of 5° , 6° , 7° and 8° . Figure 19 indicates that the maximum common volume was at 4° . However, that at 5° was only slightly less. For the Highlands to Wildwood path the maximum receiver power input levels occurred for transmitting antenna configurations of 9° azimuth with 2° elevation and 12° azimuth with 3° elevation. Figures 15 and 16 indicate maximum common volumes at 3° and 4° respectively. The fact that the highest signal levels were occasionally received in common volume configurations other than the theoretical maximum only attest to the non-homogeneous character of the scattering medium. The conclusion that the enhanced off-path signal during this period was due to off-path scattering is incontrovertible. However, the identification of the responsible mechanism is open to question. Figures 61A through L are photographs of the NAFEC weather radar PPI scope during this period. The points labeled WR = 6° are the locations of the Highlands to Wildwood common volumes, and those labeled NR = 6° are the locations of the Highlands to NAFEC common volumes. The time and the amount of precision attenuation inserted in the weather radar receiver are indicated on each photograph. The interpretations of the weather radar echoes during this period were entered on WB Form 610-3 by the radar operator at NAFEC. The decoding of this form resulted in the following information:

Time: 1544 E.S.T.
Echo area boundaries: 288° - 81 miles
 41° - 58 miles
 30 miles wide
Movement: from 270° at 15 knots
Echo character: Broken area
Precipitation symbol: Thunderstorms, rain showers
Intensity: Heavy
Radar tops: 270° - 64 miles - 52 K ft.
 324° - 50 miles - 54 K ft.
 39° - 46 miles - 47 K ft.

Time: 1646 E.S.T

Echo area boundaries: 216° - 83 miles
276° - 56 miles
59° - 74 miles

Movement: from 270° at 18 knots

Echo character: Broken

Precipitation: Thunderstorms, rain showers

Intensity: Heavy

Radar tops: 26° - 40 miles - 51 K ft.
346° - 36 miles - 50 K ft.

Time: 1747 E.S.T.

Echo area boundaries: 349° - 84 miles
73° - 94 miles
291° - 34 miles

Movement: from 270° at 20 knots

Echo character: Broken

Precipitation: Thunderstorms, rain showers

Intensity: Heavy to light

Radar tops: 358° - 65 miles - 47 K ft.
numerous tops - 45 K ft.

Echo area boundaries: 345° - 45 miles
244° - 187 miles

Echo character: Scattered

Precipitation: Thunderstorms, rain showers

Intensity: Heavy to light

Radar tops: 269° - 83 miles - 52 K ft.
293° - 80 miles - 46 K ft.

Time: 2120 E.S.T.

Echo area boundaries: 359° - 48 miles
Hook echo - diameter of 20 miles

Precipitation: Thunderstorm

Intensity: Heavy

Radar top: 46 K ft.

Time: 2147 E.S.T.

Echo area boundaries: 354° - 128 miles
57° - 187 miles
225° - 206 miles
287° - 127 miles

Movement: from 270° at 18 knots

Echo character: Broken

Precipitation: Thunderstorms, rain showers

Intensity: Heavy to very light

Radar tops: 256° - 44 miles - 49 K ft.
6° - 48 miles - 39 K ft.
disintegrating hook observed.

Time: 2243 E.S.T.
Echo area boundaries: 2° - 135 miles
32° - 111 miles
210° - 215 miles
278° - 123 miles

Movement: from 270° at 18 knots
Echo character: South - broken
North - scattered
Precipitation: South - thunderstorms
North - rain showers
Intensity: South - heavy
North - light
Radar tops: 240° - 22 miles - 42 K ft.

Time: 2345 E.S.T.
Echo area boundaries: 4° - 150 miles
213° - 173 miles
140 miles wide

Movement: from 270° at 22 knots
Echo character: Broken
Precipitation: Thunderstorms, rain showers, rain
Intensity: Heavy to light
Radar tops: 5° - near station - 42 K ft.

It is difficult to correlate the radar operator's interpretation with surface weather during this period. The surface weather reported at NAFEC was obtained by reference to Figures 62A and B. Only a trace of precipitation was recorded and the cloud cover varied from 4/10 at 1600 E.S.T. to 10/10 at 1900 E.S.T. and 2200 E.S.T. No precipitation was recorded at Philadelphia during the 24 hours preceding the end of this period and only traces were reported at New York and Salisbury; Washington, D. C., however, reported 1.03 inches of precipitation. Figure 63 shows radio refractive index profiles calculated from NAFEC RADIOSONDE releases at 1410 and 2235 E.S.T. The maximum negative N gradient detected at 1410 E.S.T. was -133 N units/km. Above an altitude of 300 meters no negative gradient in excess of -75 N units/km was detected. The profile at 2235 E.S.T. seems to indicate pronounced stratification. There were no negative gradients in excess of -73 N units/km. Three positive-slope N gradients were apparent. Two of these were below 300 meters and the third appeared between 5300 and 5500 meters. They all appear to be due to humidity inversions.

11.3 Angle Dependent Guided Propagation

Highlands to NAFEC and Wildwood, 2200 hours, 15 October to 0700 hours, 16 October 1966.

Figures 64A through 64D are photographs of the NAFEC and Wildwood receiver/recorder charts for the period covered by the basic data charts in Figures 55A through 55F. From 2300 on 10/15/66 to 0200 on 10/16/66, the power levels of the on-path receiver inputs at both NAFEC and Wildwood were considerably higher than normal. This indicated the existence of an abnormal propagation mechanism. The technique of Appendix A resulted in very poor correlation between the on and off-path receiver power inputs at both NAFEC and Wildwood. The criterion of equation (10) was not met at any antenna configuration where the receiver sensitivities permitted

measurements. An examination of the charts in Figure 64A indicated no envelope correlation between the on and off-path recordings at either NAFEC or Wildwood from 2300 on 10/15/66 to 0100 on 10/16/66. During this period sampling recorders were in operation at Wildwood. These recorders were interfaced in such a manner that the on and off-path receiver power input levels were simultaneously sampled for 3 seconds out of every 20 seconds. Correlation coefficients were computed by comparing the on and off-path samples for each azimuthal setting during the period from 2200 on 10/15/66 to 0100 on 10/16/66.

<u>Time</u>	<u>TX Ant. Azimuth</u>	<u>Correlation Coefficient</u>
2200-2300	0°	.92
2300-2355	12°	.54
0000-0055	18°	.58

Although these correlation coefficients are not too significant because of the bias introduced by receiver sensitivity-limiting at one end and receiver/recorder saturation at the other, it can be seen that the azimuthal offset significantly reduces the correlation coefficient. It appears that the on-path antennas at both sites were receptive to a signal propagated by a different path than the signal received on the great-circle-path-oriented side lobes of the off-path antennas.

During the period from 2200 to 2300, the signal into the NAFEC on-path receiving antenna seems to be dependent upon the transmitting antenna elevation in a manner not consistent with the differences in common volume sizes or the transmitting antenna vertical side lobe radiation. This indicates the existence of incident-angle-dependent reflection or scattering that could be explained by the hypothesis of an elevated layer or elevated duct. During the period from 2300 to 2355, the transmitting antenna was aligned with a 12° azimuth offset. The signal into the Wildwood on-path receiver increased substantially at nearly all elevation angles while the NAFEC signal decreased. This indicates some change in the path geometry introduced by the transmitting antenna azimuthal offset. By using ray-tracing techniques it can be hypothesized that the plane including the incident and reflected rays was not vertical and therefore, the reflecting or refracting layer(s) were not horizontal. Such a layer or layers would result in scatter-angle-sensitive forward propagation without correlated backscatter. During the interval from 0500 to 0600 on 10/16/66, the on and off-path receivers at both sites indicated scattering from a mechanism located in an area near the transmitter site. This scattering had the same short term variation and common volume dependence exhibited during the period on 6/28/66 which was previously analyzed.

In Figure 65 are photographs of the backscatter recorder charts from the radar receiver at Highlands taken during this period. Although the forward-scattered signal was significant during the interval from 2200 to 0000, there was no backscatter other than that caused by the ground return into the side lobes at low elevation angles. On the other hand, there was considerable backscatter from the cell located in the transmitter antenna beam during the period from 0500 to 0600.

Figures 66A through 66L are photographs of the NAFEC weather radar PPI scope during this period. During the interval between 2300 hours, 15 October, and 0000 hours, 16 October, 1966, the weather radar indicated no returns from the area of the common volumes or the great circle path near the transmitter site. A return from this area is indicated during the period from 0500 to 0600 hours on 16 October, 1966. Figures 67A through 67C are radio refractive index profiles calculated with the data from RADIOSONDE releases from JFK International Airport at 1815 on 15 October, and at 0015 and 0700 on 16 October, 1966. These profiles clearly indicate the existence of elevated layers. The surface weather in the area as taken from the local climatological summaries indicated no precipitation at NAFEC during the interval between 2200 and 0600 and .04 inch between 0600 and 0700. At JFK International Airport there was no precipitation during the 24 hour period ending at 0100 on 16 October, 1966 and .19 inch during the next 24 hours. At Philadelphia there was no precipitation during the 24 hour period ending at 0100 on 16 October, 1966 and .18 inch during the next 24 hours.

12.0

CONCLUSIONS

In an area exhibiting meteorological conditions similar to those of the Atlantic Coastal Region from New York City to Norfolk, Virginia, anomalous microwave propagation modes must be considered if severe interference to radio relay stations from satellite communications system earth stations in the same frequency band is to be avoided. During the POPSI Project, common volumes established by the intersection of transmitting and receiving antenna beams below the tropopause resulted in off-path scattering at interfering power levels for significant percentages of the time. Enhanced great circle path propagation due to ducting and both on and off-path guided propagation attributed to mechanisms associated with elevated tropospheric discontinuities resulted in interfering power levels at the receivers for time percentiles far in excess of the allowance of existing allocation criteria. All of these effects were noted with great circle path distances of 112 and 177 kilometers between the simulated earth station transmitter and the radio relay station receivers and persisted to antenna bearings offset by 18° in azimuth and more than 20° in elevation from the great circle path.

Off-path and high-angle on-path scattering from precipitation cells were definitely identified as significantly contributory to the interference problem. However, there appeared to be other mechanisms involved during some of the off-path anomalous propagation. These mechanisms seem to exhibit scatter-angle dependencies not related to the relative common volume sizes. The correlation of the backscatter and forward-sector scatter from such cells appears to be possible in many instances only if the backscatter and forward-scatter investigation facilities are interfaced to achieve common volume coherency and detect angle dependency. The correlation of off-path scattering with nearby surface rain fall rates appears to be very questionable.

Inasmuch as the phenomena resulted in significant signal levels with all of the path configurations and at nearly every antenna orientation examined during the POPSI Project, the limits of the problem have not yet been defined. Further investigation should be conducted over greater path distances and with transmitting antenna elevation angles up to 50 or 60 degrees. Propagation paths affording terrain shielding should be used to determine the effectiveness of such measures against interference due to enhanced great circle path propagation. If the mechanisms contributing to the enhanced signal conditions are to be understood sufficiently for modeling purposes, the meteorological input must be greatly enlarged for future investigations. In the meantime, further detailed analyses of the POPSI data is being pushed in an effort to gain more insight into the problem.

ACKNOWLEDGMENTS

The POPSI Project could not have been undertaken without assistance from a great number of people some of whom were not even known to the authors. Acknowledgment is made of significant contributions to the effort as follows:

Coordination

U. S. Air Force, The Pentagon

Lt. Col. Maurice W. Gouchoe - AFXOP
Lt. Col. A. Sager - AFSME
Lt. Col. Selmanovitz - AFSME
Capt. J. A. Gibson - AFXOPA

U. S. Coast Guard, Washington, D. C.

Mr. F. B. Duncan

Federal Aviation Administration, Washington, D. C.

Mr. William B. Hawthorne

NASA Headquarters, Washington, D. C.

Lt. Col. Wayne Matthews

Transmitter Operation and Technical Assistance

Highlands Air Force Station

M/Sgt. Charles D. Foster, Jr.
T/Sgt. Wilbert S. Baker
T/Sgt. William G. Redfield
Airmen J. E. Koons, W. S. Van Benthuyzen, P. J. Tribles,
W. E. Jewell, L. J. Buss, J. J. Wright, D. C. Thorp,
K. R. Cole and J. R. Blodgett

AVCO Corporation, Cincinnati, Ohio

Mr. Robert Bartow
Mr. Robert S. Weirich

Receiving Sites

NAFEC, Pleasantville, New Jersey

Mr. H. C. Williamson
Mr. William Young
Electronic Technicians Bert Simeone, John Dempsy
and Charles Flack

U.S.C.G. Electronic Engineering Station, Wildwood, N. Jersey

Commander R. Parkhurst
Lt. Comm. Glass
CPO Ronald Kornbluth
Electronic Technicians Kraft, Richardson, Greenway and Hunter

NASA, Wallops Station, Virginia

Mr. William Lord
Mr. Dick Gladding

Meteorological Data and Technical Assistance

U.S. Weather Bureau, DATAC Division, Silver Spring, Md.

Mr. Stuart Bigler
Mr. Paul Hexter

Receiving Antennas and Technical Assistance

Bell Telephone Laboratories, Holmdel, N. Jersey

Mr. W. T. Barnett
Mr. Lee Gussler

Laboratory Facilities and Receiver Maintenance and Calibration

FCC Field Bureau

Mr. Floyd W. Wickenkamp
Mr. Alfred Kleist

FCC Laboratory Division

Mr. Edward W. Chapin
Mr. Willmar K. Roberts
Mr. Milton C. Mobley
Mr. Joseph Hanyok
Mr. Benjamin Harrison
Mr. Andrew R. Gabor

Technical Advice, Review, Typing, Duplication, etc.

Mr. Arnold G. Skrivseth
Mr. Harry Fine
Mr. Eugene D. Harris
Mrs. Margaret B. Fox
Mrs. Pauline C. Barr
Mr. Russell G. Wilkins

Computer Programming

Mr. Phillip G. Tremper

REFERENCES

1. Dennis, A. S., "Forward Scatter from Precipitation as an Interference Source at Stations Monitoring Satellites," Stanford Research Institute Memorandum 2, November 1961.
2. Dennis, A. S., "Measurements of Forward Scatter from Rain at 9.05 Gc.," Research Memorandum 4, Stanford Research Institute 14 May 1962.
3. Dennis, A. S. and Fernald, F. G., "A Preliminary Analysis of Forward Scatter Signals from Showers," Research Memorandum 5, Stanford Research Institute, October 1963.
4. Doherty, L. H. and Stone, S. A., "Forward Scatter from Rain," Trans. IRE, PGAP-8, July 1960.
5. Rice, F. L., et al, "Transmission Loss Predictions for Tropospheric Communication Circuits, NBS Technical Note 101, Vol. II, Revised, May 1, 1966.
6. Strobehn, J. W., "Transhorizon-Propagation Measurements and Simulated Angular-Response Patterns," Stanford Electronics Laboratories, October 1963.
7. Barrow, B. B., et al, "Tropospheric Scatter Propagation Tests Using a RAKE Receiver," Applied Research Lab., Sylvania Electronic Systems, Conference Record, IEEE Annual Communications Convention, Boulder, Colorado, June 7-9, 1965.
8. Booker, H. G. and Gordon, W. E., "A Theory of Radio Scattering in the Troposphere," Proc. IRE, Vol. 38, April 1950.
9. Villars, F. and Weisskopf, V. F., "On the Scattering of Radio Waves By Turbulent Fluctuations of the Atmosphere," Proc. IRE, Vol. 43, October 1955.
10. Du Castel, Francois, "Tropospheric Radiowave Propagation Beyond the Horizon, Pergamon Press English Translation, 1966.
11. Bean, B. R. and Dutton, E. J., "Radio Meteorology, NBS Monograph 92, March 1, 1966.
12. Gringarten, I. I., et al, "Atmospheric Humidity Atlas-Northern Hemisphere," Air Force Cambridge Research Laboratories.
13. Crane, R. K., "Microwave Scattering Parameters for New England Rain," M.I.T. Lincoln Laboratory Technical Report No. 426 (October, 1966).
14. Altman, F. J., "Precipitation Scatter Interference Between Space and Terrestrial Communications Systems," Communications Systems, Inc., Report No. 453340, October, 1967.

Appendix A

Correlation Procedure

List of Symbols

P_{rt}	Power at on-path receiver input due to optimum path component, alone (dBW)
P_{rs}	Power at off-path receiver input due to off-path components (dBW)
P_{rm}	Measured power at on-path receiver input (dBW)
P_{rp}	Predicted power at on-path receiver input due to great circle component, alone (dBW)
P_{rp}	Predicted power at off-path receiver input due to great circle component, alone (dBW)
P_{rm}	Measured power at off-path receiver input (dBW)
θ	Transmitting antenna azimuth offset angle (degrees)
ϕ	Transmitting antenna elevation angle (degrees)
α	Off-path receiving antenna azimuth offset (degrees)
β	Off-path receiving antenna elevation angle (degrees)
G_t	Free space isotropic gain of transmitting antenna (dB) (Transmission line loss insignificant)
G_r	Free space gain of receiving antenna less transmission line losses (dB)
P_t	Peak transmitter power (dBW)
$G_t (\theta, \phi)$	Pattern response factor of transmitting antenna at horizontal angle θ and vertical angle ϕ from main beam maximum (dB)
$G_r (\alpha, \beta)$	Pattern response factor of receiving antenna at horizontal angle α and vertical angle β from main beam maximum (dB)
E	Error component (dB)
	Predicted power from on-path component into on-path receiver may be calculated from:

$$(5) \quad P_{rp} (\theta, \phi) = P_{rm} (0^\circ, 1/2^\circ) + G_t (\theta, \phi) \quad (\text{dBW})$$

Predicted power from on-path component into off-path receiver is given by:

$$(6) P_{rp}(\theta, \phi) = P_{rm}(0^\circ, 1/2^\circ) + G_t(\theta, \phi) + G_r(\alpha, \beta) \quad (\text{dBW})$$

The quantity $P_{rm}(0^\circ, 1/2^\circ)$ may not represent the power received via the optimum path because the transmitting elevation angle $\phi \approx 1/2^\circ$ may not be the alignment for optimum transmission.

In such cases:

$$(7) P_{rm}(0^\circ, 1/2^\circ) = P_{rt} + E \quad (\text{dBW})$$

where E is the error component. The error component is the ratio of the predicted power to the measured power into the on-path receiver, or

$$(8) E = P_{rp}(\theta, \phi) - P_{rm}(\theta, \phi) \quad (\text{dB})$$

E is also the ratio of the predicted power to the measured power into the off-path receiver if the signal into that receiver is solely due to a great circle path component, then

$$(9) E = P'_{rp}(\theta, \phi) - P'_{rm}(\theta, \phi) \quad (\text{dB})$$

If only the great circle path component is involved in both receivers,

$$(10) P_{rp}(\theta, \phi) - P_{rm}(\theta, \phi) - 3 \geq P'_{rp}(\theta, \phi) - P'_{rm}(\theta, \phi)$$

where ± 1.5 dB is considered to be the measurement accuracy of the equipment. The test in (10) is an indication of whether or not off-path propagation signal components are significant in the off-path receiver input.

Appendix 3

Radio Refractive Index Computation

If the troposphere is considered to be a pure dielectric with a permeability (μ) equal to unity, its refractive index, n , may be related to its dielectric constant, ϵ , as follows:

$$(11) \quad n = \sqrt{\epsilon}$$

It is the usual procedure to identify the radio refractive index as N ,

where

$$(12) \quad N = (n - 1) 10^6$$

The radio refractive index is calculated from ordinary meteorological data by using the equation

$$(13) \quad N = \frac{77.6}{T} \left(P + \frac{4810 e}{T} \right)$$

where

T is the absolute temperature (degrees Kelvin)

P is the pressure of the atmosphere in millibars

e is the partial pressure of the water vapor in millibars

The value of e is determined from the equation

$$(14) \quad \log e = - \frac{2937.4}{T_d} - 4.9283 \log T_d + 23.5518$$

where

T_d is the dew point temperature in degrees Kelvin

The refractive index was calculated for each discrete height appearing in the radiosonde data, viz. H_1 , H_2 , H_3 , etc. where H is the height above sea level in kilometers. The N gradients were calculated for the intervals between the discrete heights in the following manner:

$$(15) \quad \frac{dN}{dH} = \frac{N_2 - N_1}{H_2 - H_1}$$

where N_1 , N_2 , N_3 , etc. are the refractive indices at heights H_1 , H_2 , H_3 , etc.

POPSI PROJECT

WALLOPS ISLAND	WILDWOOD	NAFEC	TRANSMITTER																																				
Two 1.83 m Parabolas $H_T = 7.62$ m Two AN/APR-9 Receivers	Two 1.83 m (6 Ft.) Parabolas or One 1.83 m Parabola and One 1.22 m (4 Ft.) Bell Horn $H_T = 10.06$ m Two AN/APR-9 Receivers	Two 1.83 m Parabolas Vert. Polarized $BW = 20$ Gain : 38 db $H_T = 9.6$ m Polarad Model R Receiver AN/APR-9 Receiver	AN/FPS - 26 Freq. : 5.75 Ghz. ERP = +107 dbw $H_T = 91.44$ m																																				
<table><tr><th>Az.</th><th>Elev.</th></tr><tr><td>0°</td><td>0°</td></tr><tr><td>30°</td><td>10°</td></tr></table>	Az.	Elev.	0°	0°	30°	10°	<table><tr><th>Az.</th><th>Elev.</th></tr><tr><td>0°</td><td>0°</td></tr><tr><td>30°</td><td>10°</td></tr><tr><td>60°</td><td>20°</td></tr><tr><td>90°</td><td>20°</td></tr></table>	Az.	Elev.	0°	0°	30°	10°	60°	20°	90°	20°	<table><tr><th>Az.</th><th>Elev.</th></tr><tr><td>0°</td><td>172° to 175°</td></tr><tr><td>30°</td><td>"</td></tr><tr><td>60°</td><td>"</td></tr><tr><td>90°</td><td>"</td></tr><tr><td>120°</td><td>172° to 200°</td></tr><tr><td>180°</td><td>"</td></tr><tr><td>0°</td><td>140° to 300°</td></tr><tr><td>30°</td><td>"</td></tr><tr><td>180°</td><td>"</td></tr></table>	Az.	Elev.	0°	172° to 175°	30°	"	60°	"	90°	"	120°	172° to 200°	180°	"	0°	140° to 300°	30°	"	180°	"	
Az.	Elev.																																						
0°	0°																																						
30°	10°																																						
Az.	Elev.																																						
0°	0°																																						
30°	10°																																						
60°	20°																																						
90°	20°																																						
Az.	Elev.																																						
0°	172° to 175°																																						
30°	"																																						
60°	"																																						
90°	"																																						
120°	172° to 200°																																						
180°	"																																						
0°	140° to 300°																																						
30°	"																																						
180°	"																																						

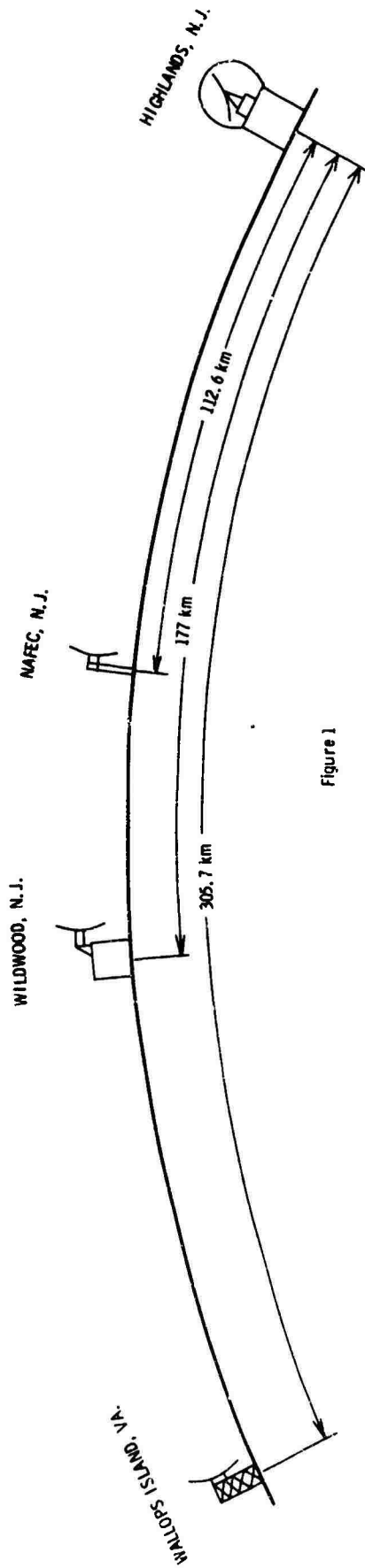
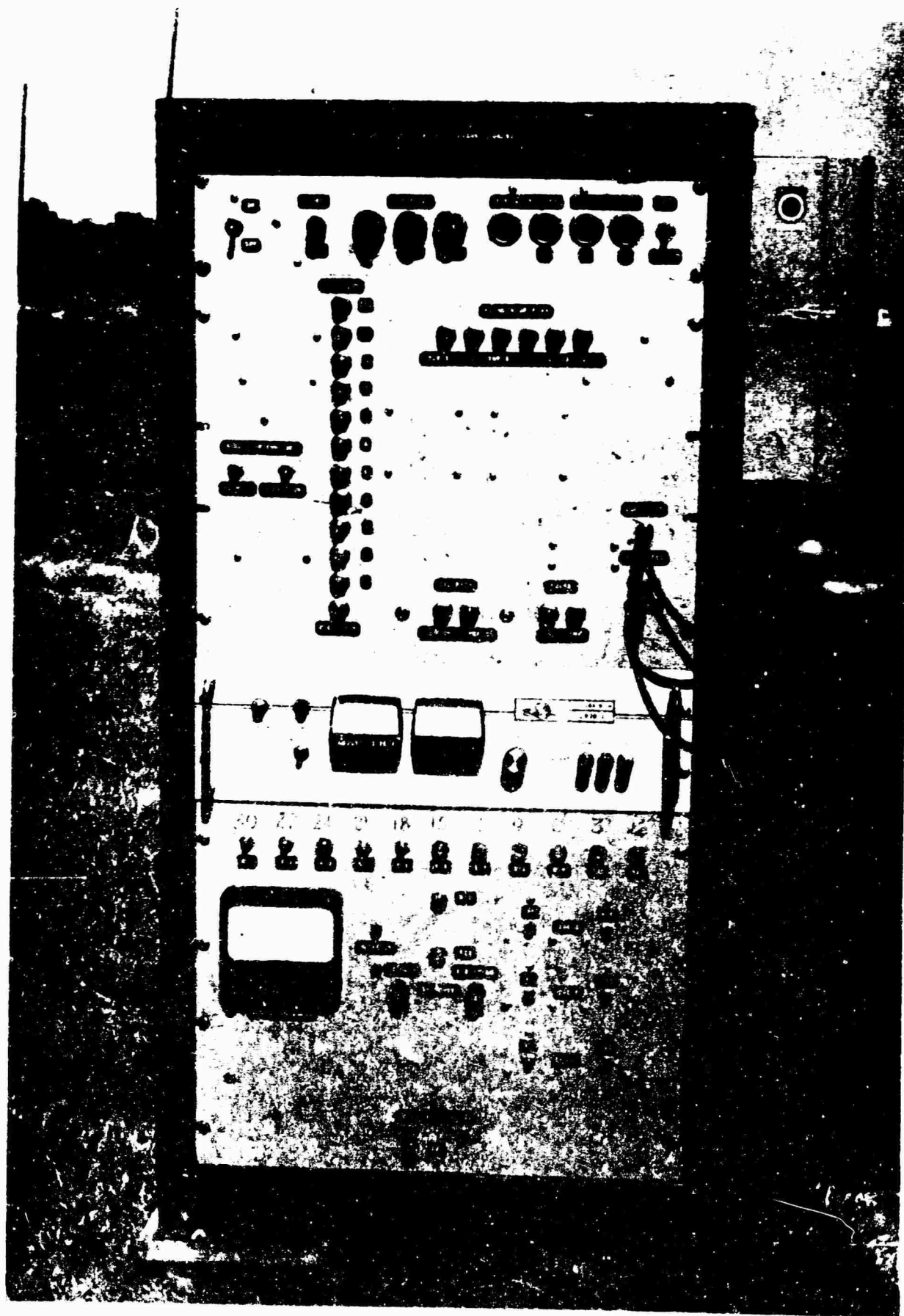


Figure 1



Figure 3



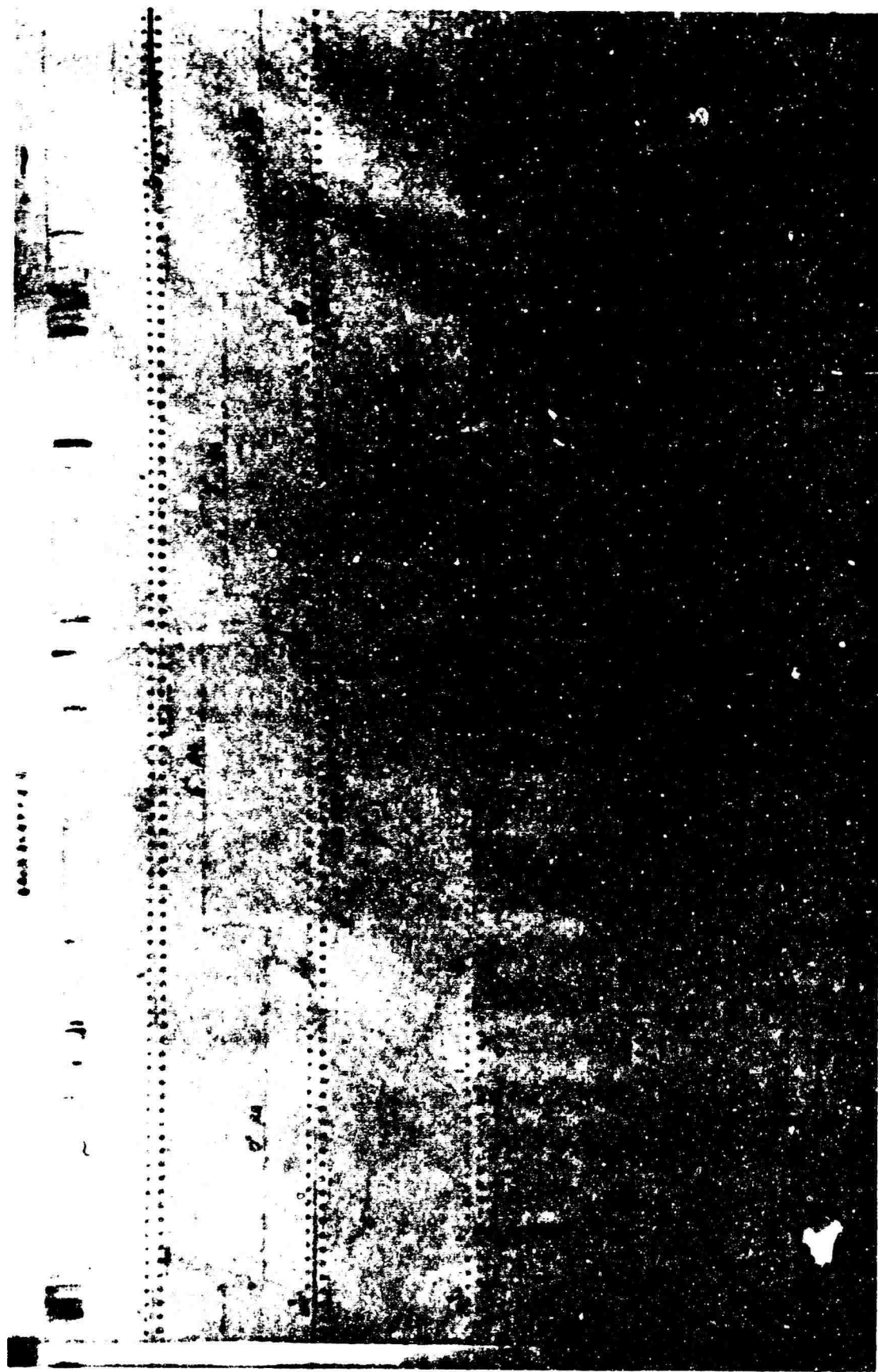
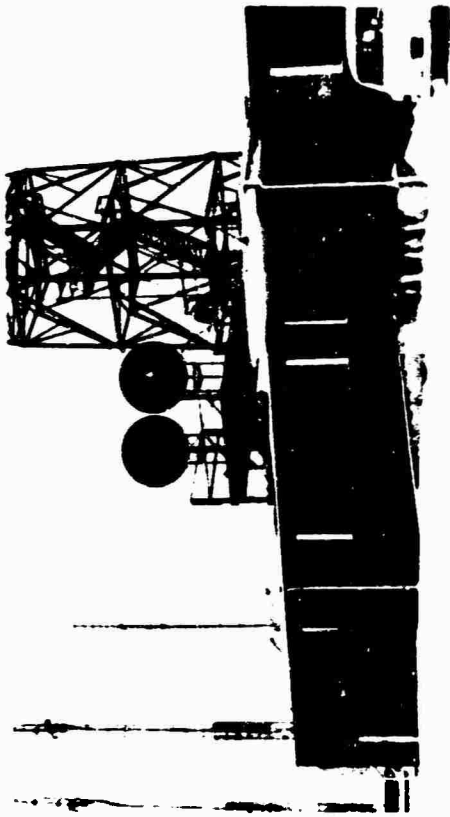
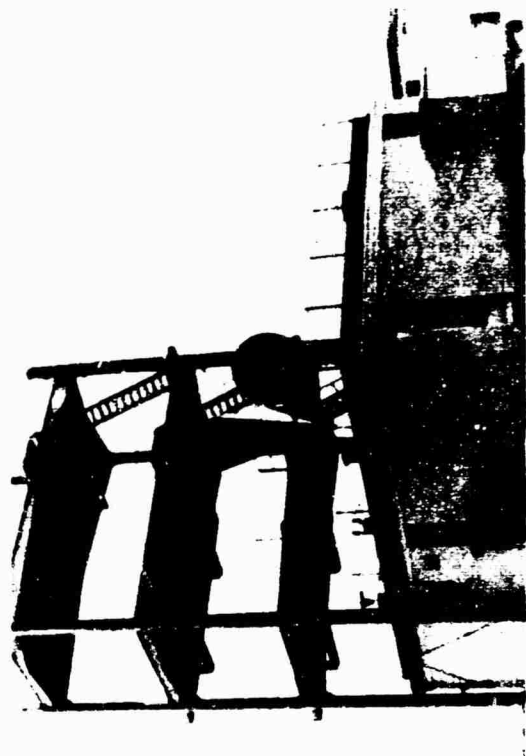


Chart Analysis Layout
Figure 4B



Wallops Island Rec. Site



Wildwood Site with Horn Ant.

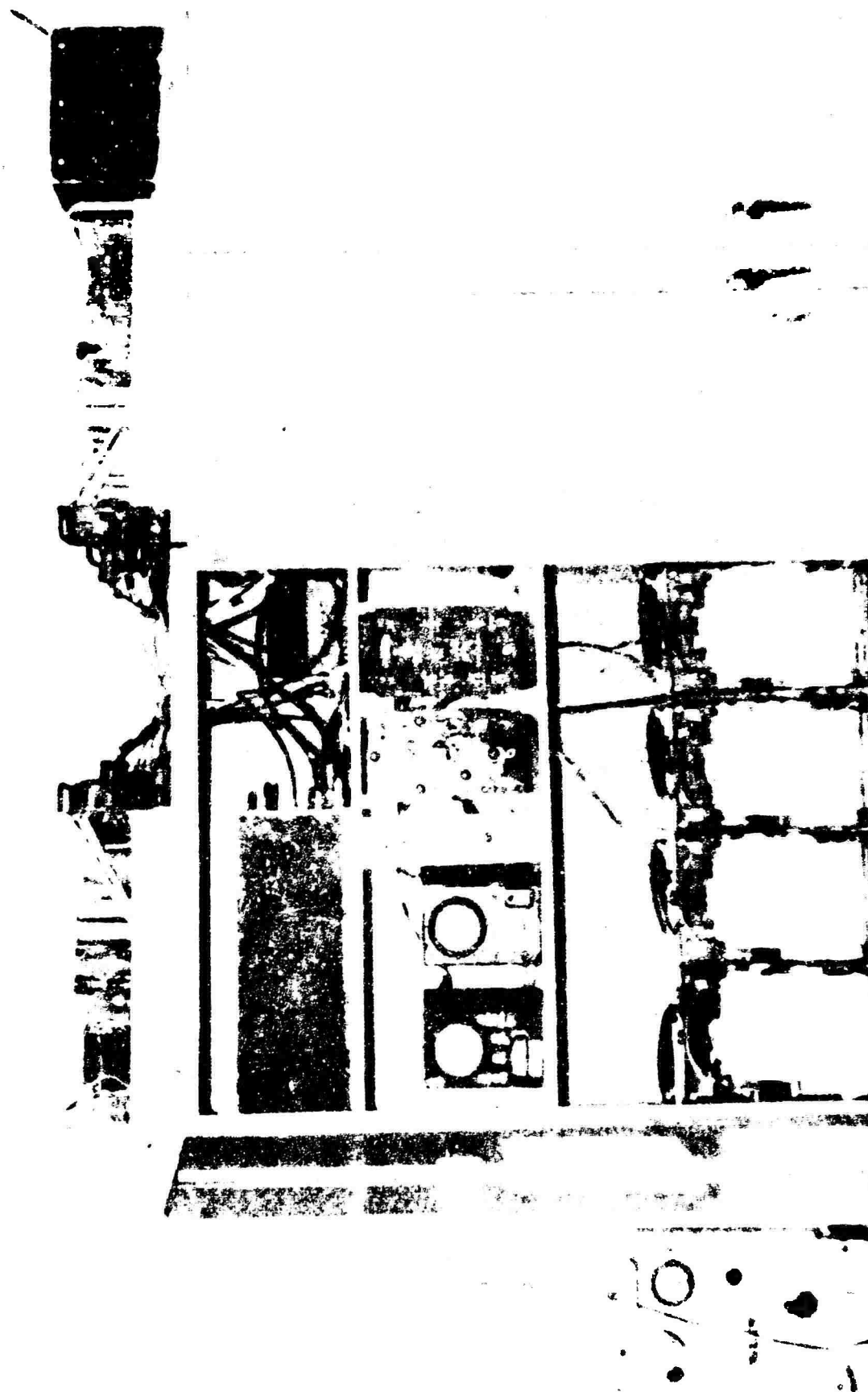


NAFEC Rec. Site



Wildwood Rec. Site

Figure 5



Typical Receiver Site Equipment

Figure 6

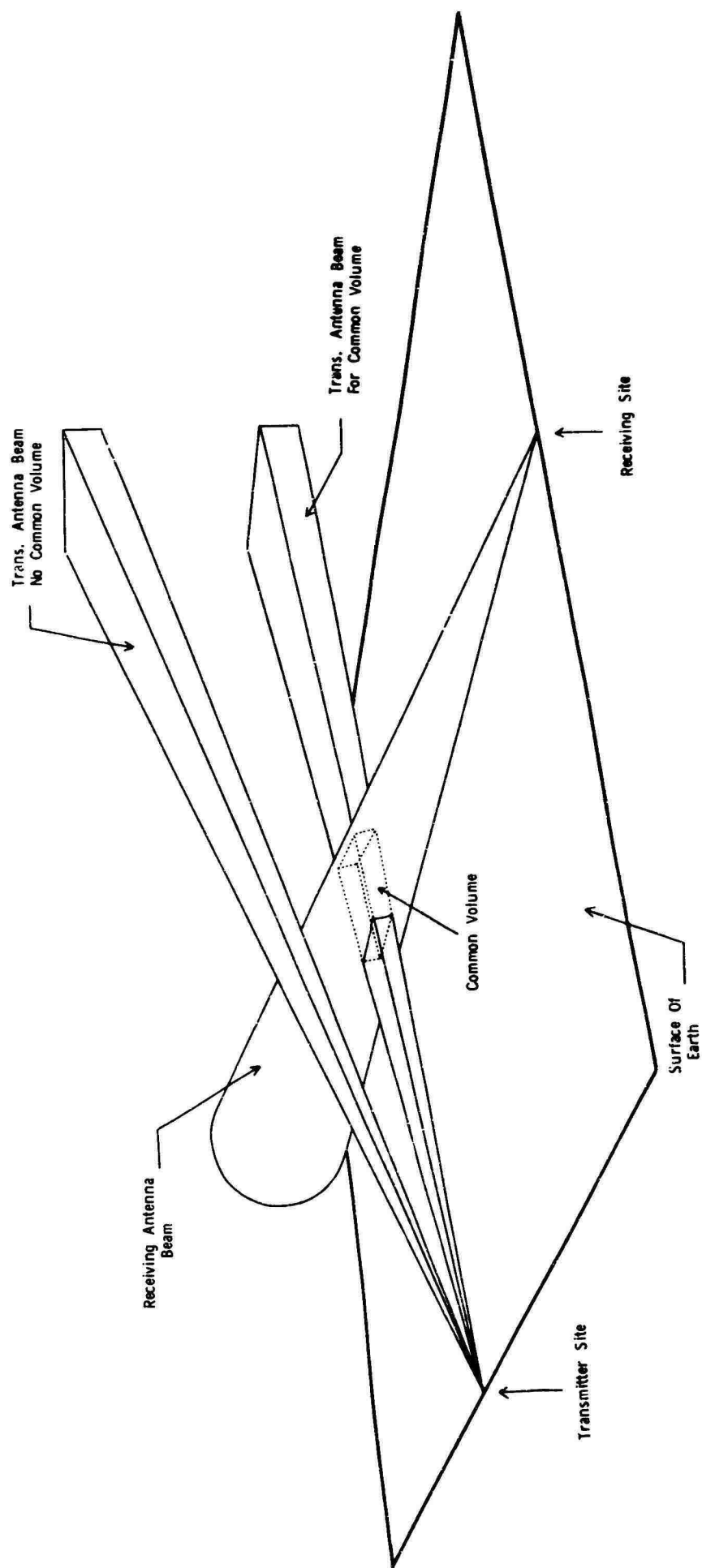


Figure 7

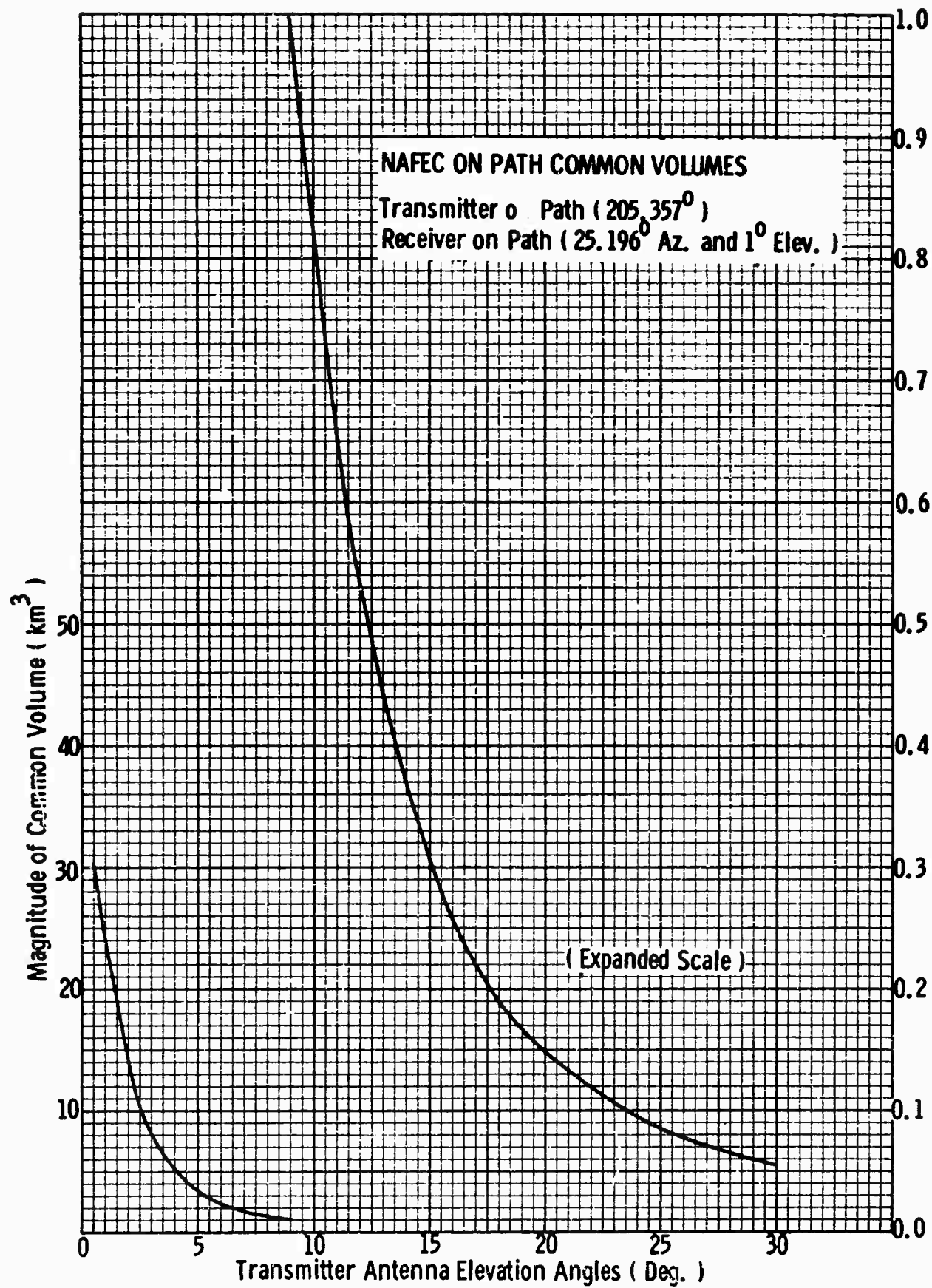


Figure 8

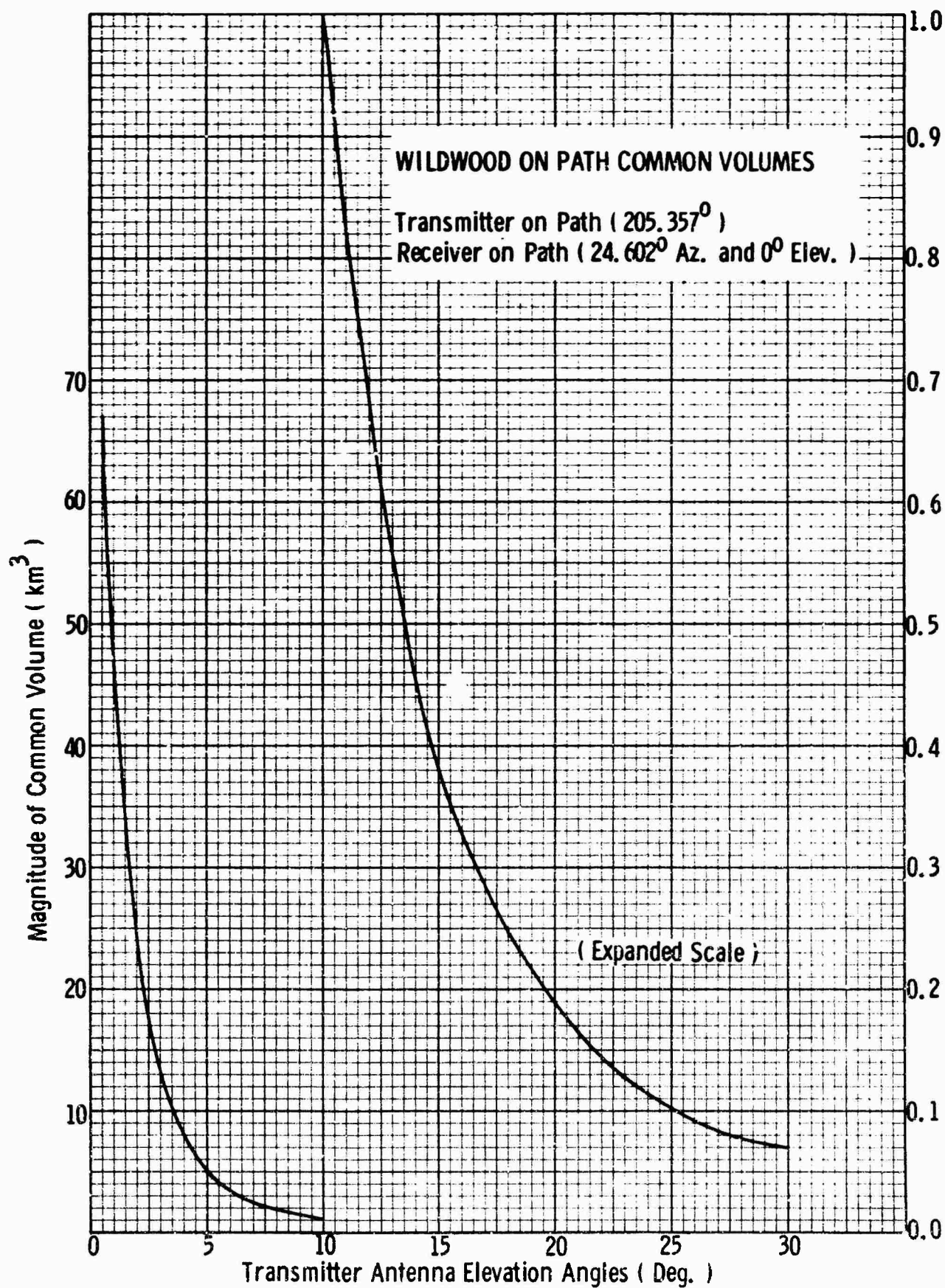
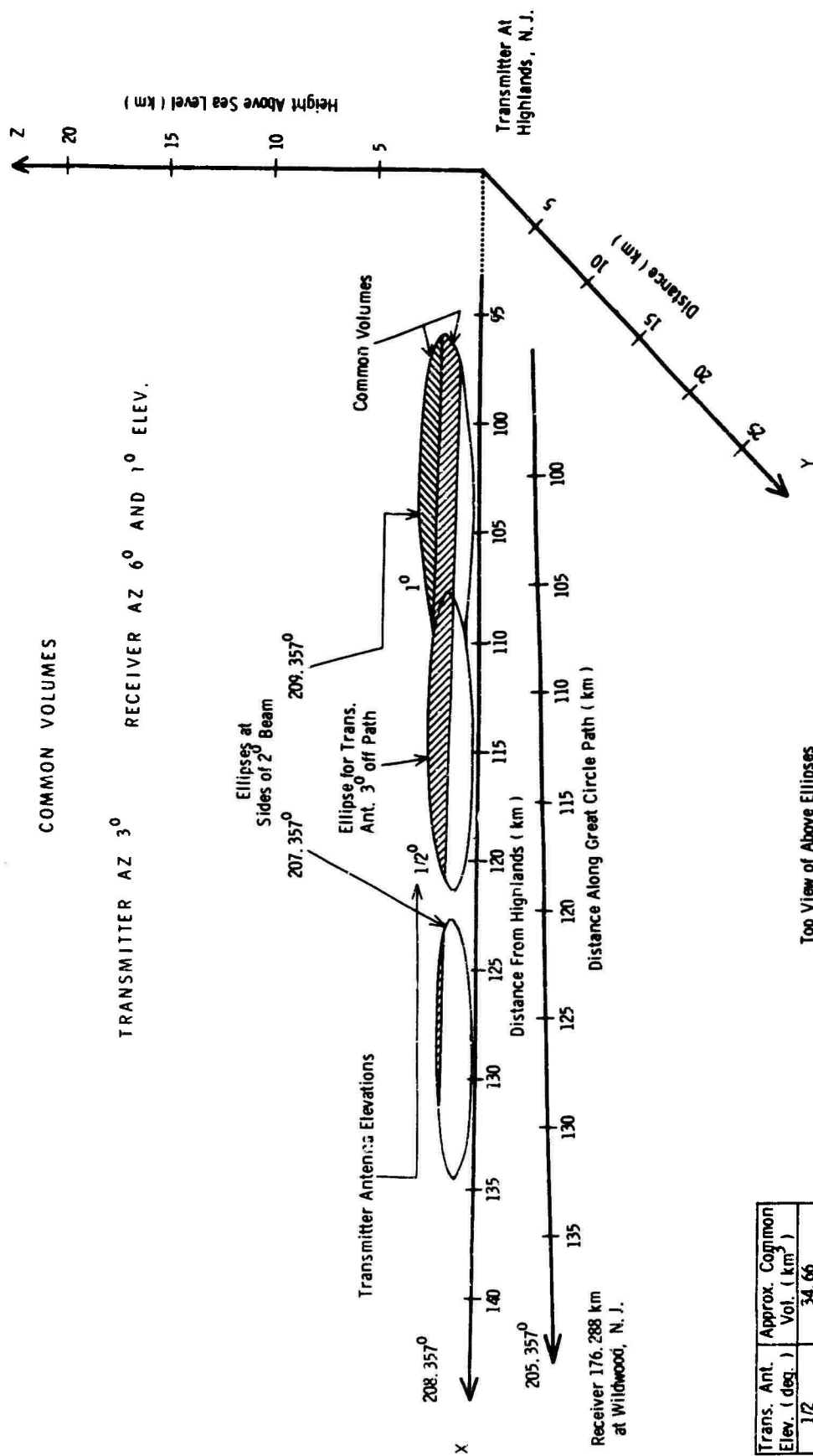


Figure 9

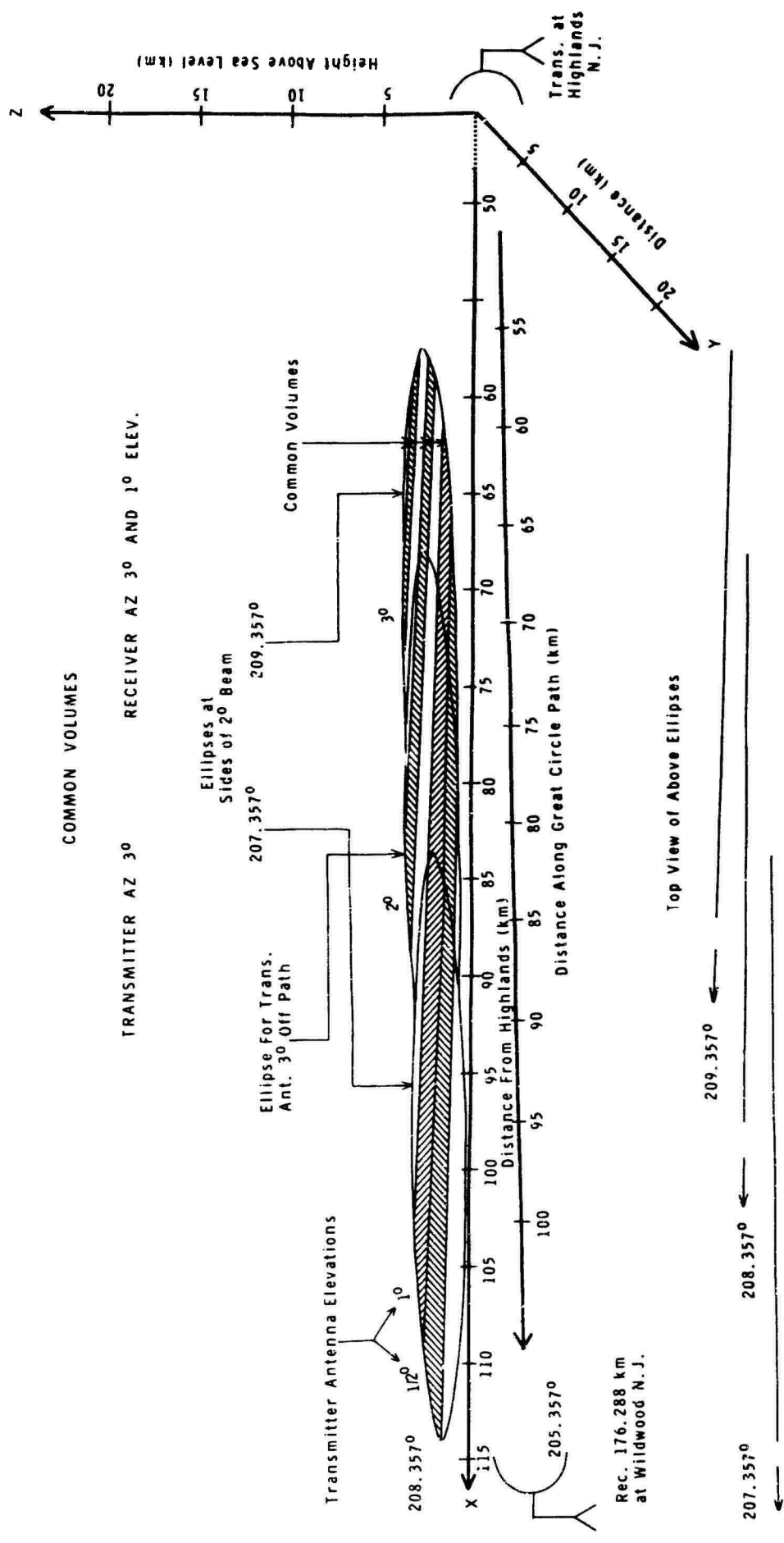


207.357°

208.357°

209.357°

Figure 10

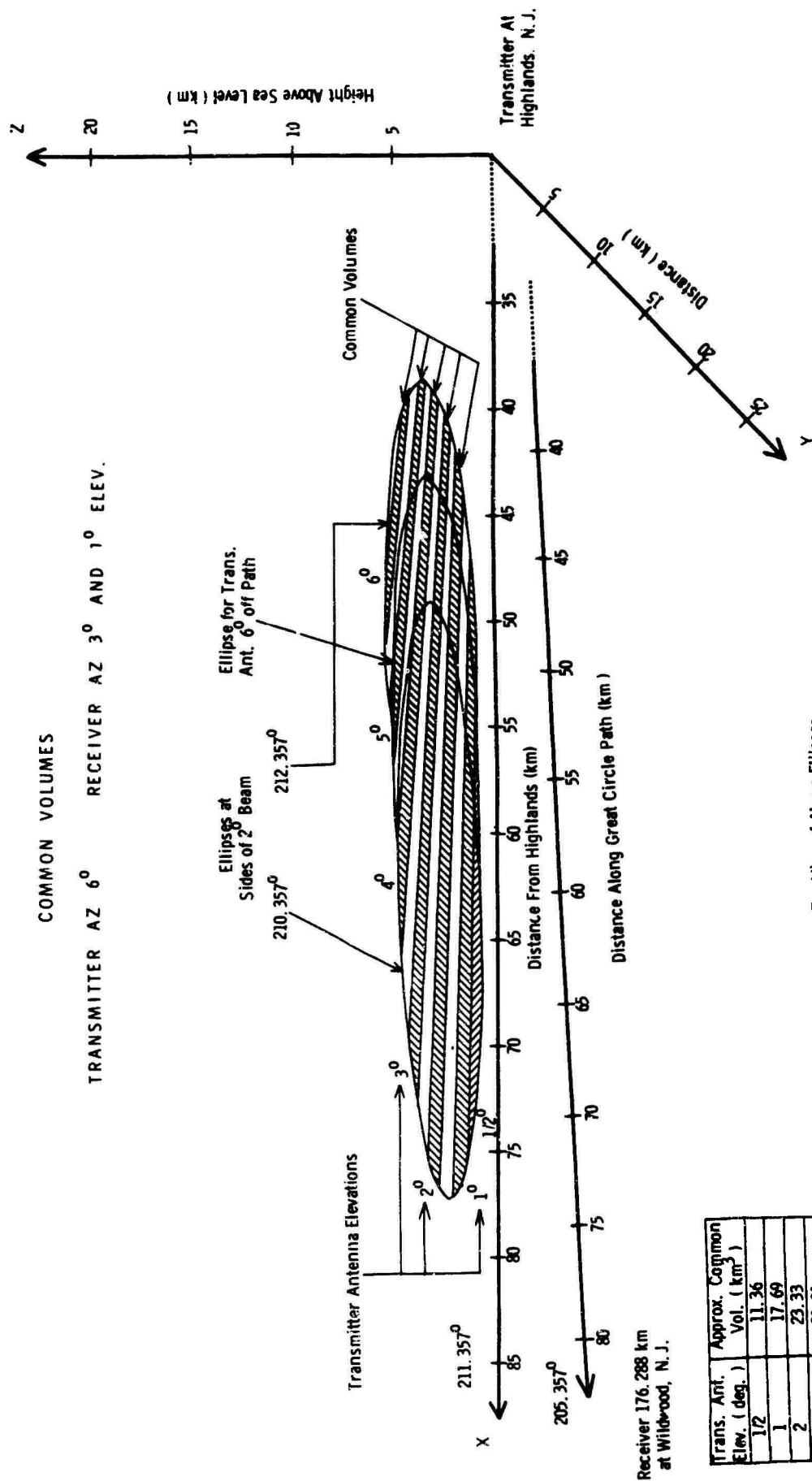


Trans. Ant. Elev. (Deg.)	Approx. Common Volume (km ³)
1/2	46.72
1	54.54
2	18.66
3	5.90

Figure 11

COMMON VOLUMES

TRANSMITTER AZ 6° RECEIVER AZ 3° AND 1° ELEV.



Trans. Ant. Elev. (deg.)	Approx. Common Vol. (km ³)
1/2	11.36
1	17.69
2	23.33
3	21.01
4	14.92
5	5.29
6	1.30

Top View of Above Ellipses

212.357°

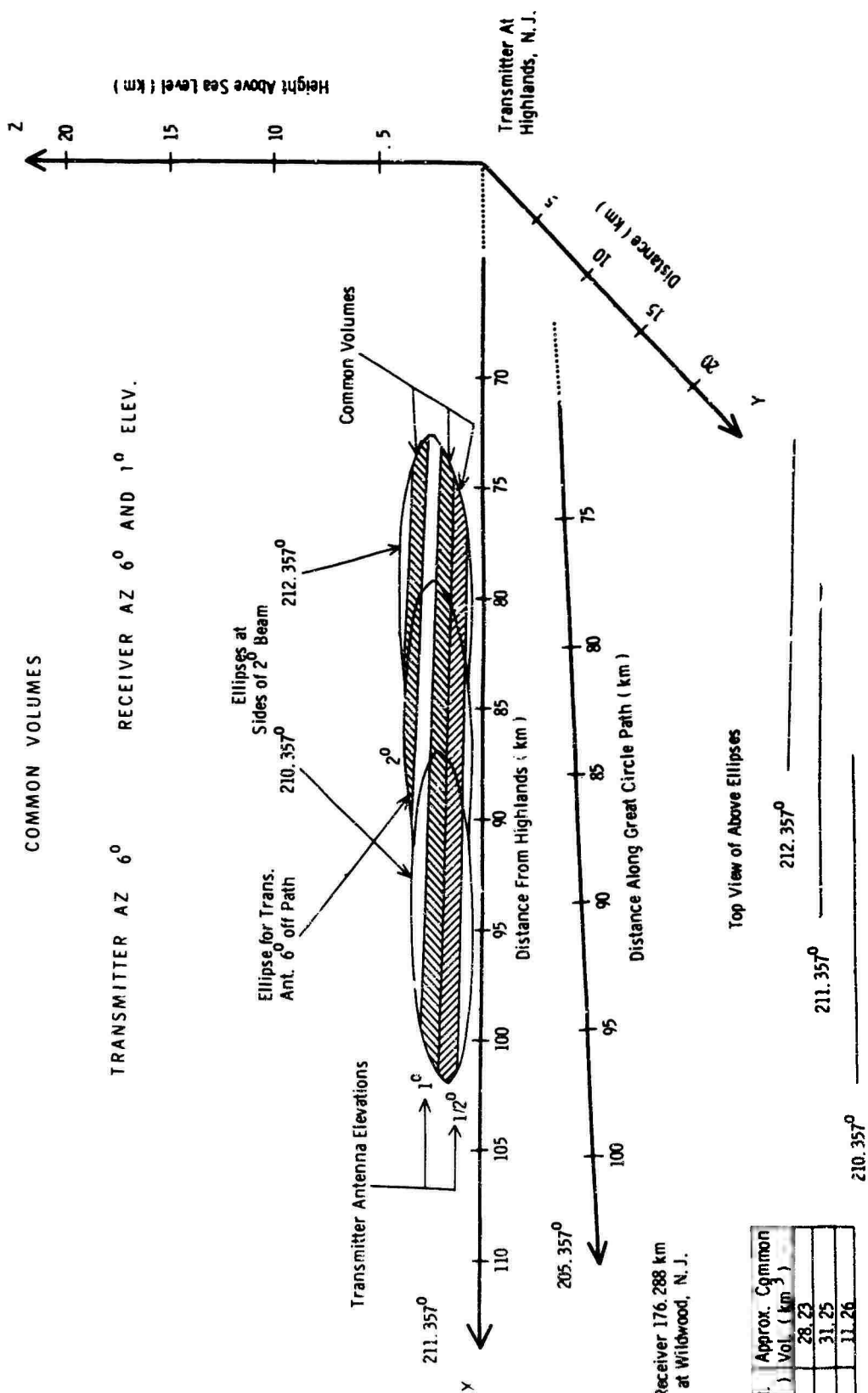
211.357°

210.357°

Figure 12

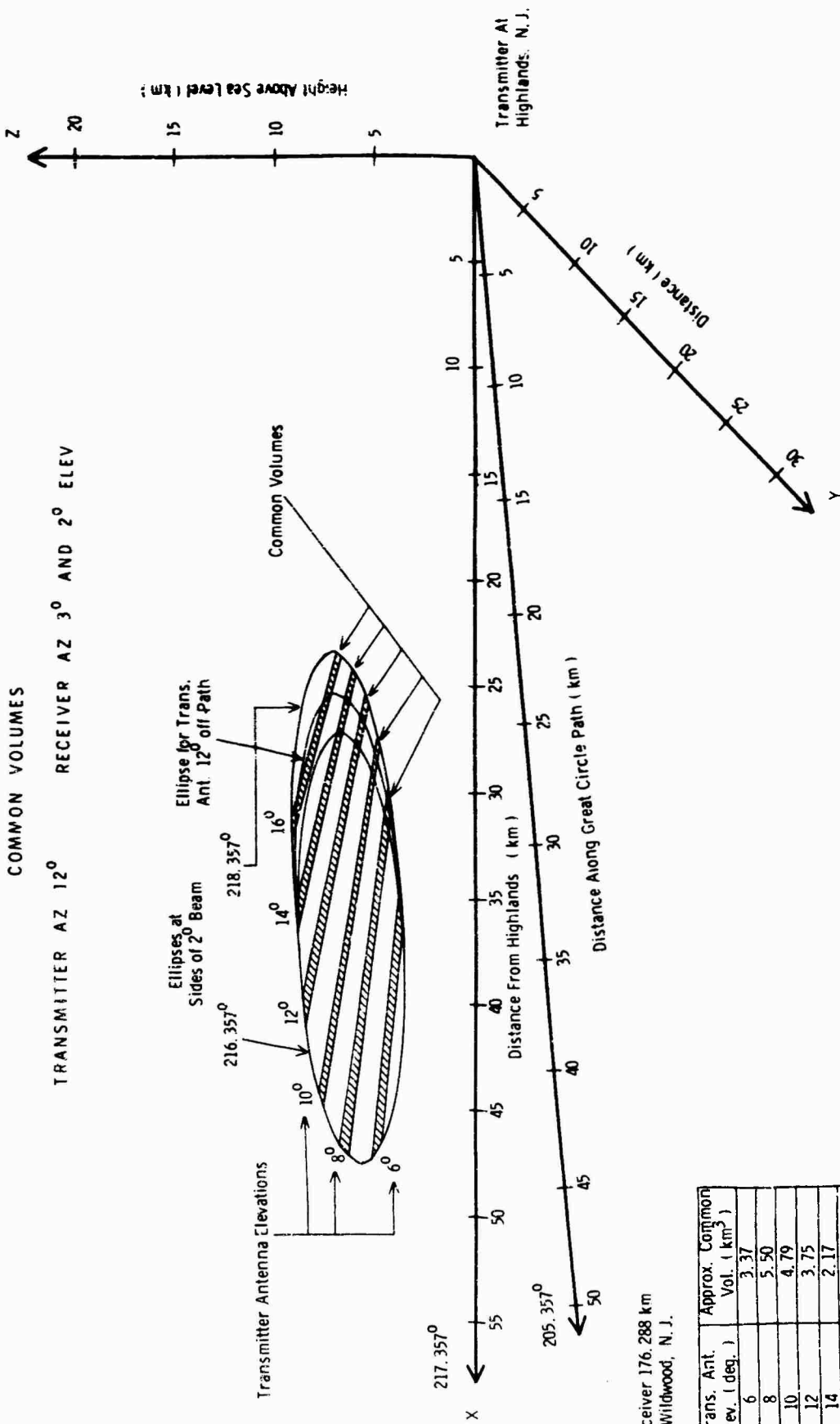
COMMON VOLUMES

TRANSMITTER AZ 6° RECEIVER AZ 6° AND 1° ELEV.



Trans. Ant. Elev. (deg.)	Approx. Common Vol. (km ³)
1/2	28.23
1	31.25
2	11.26

Figure 13



Receiver 176.288 km
at Wildwood, N. J.

217.357°

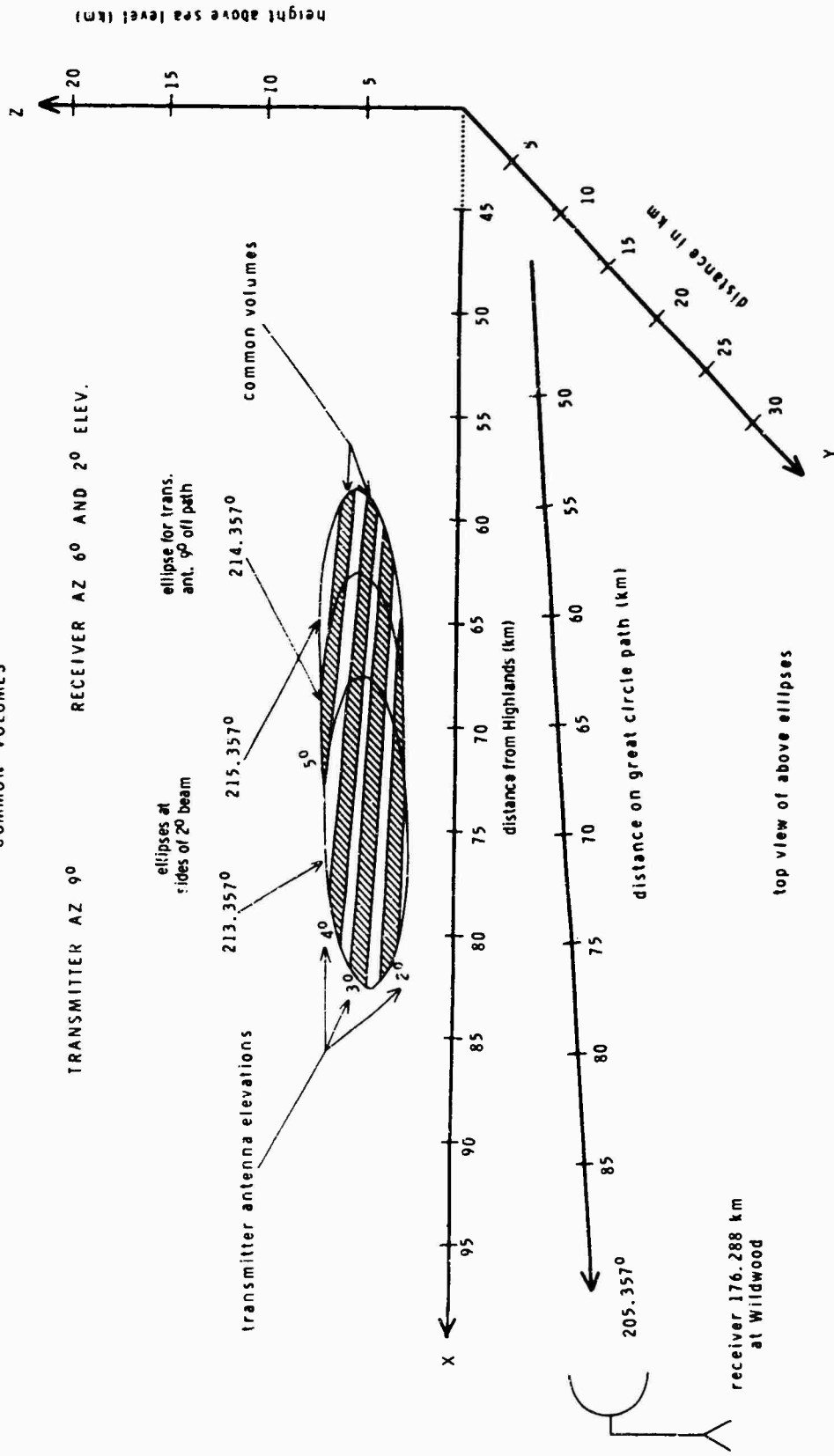
218.357°

216.357°

Figure 14

COMMON VOLUMES

TRANSMITTER AZ 90° RECEIVER AZ 60° AND 20° ELEV.



trans. ant. elev. (deg.)	approx. common vol. (km ³)
2	17.32
3	25.32
4	22.65
5	8.08

215.3570

214.3570

213.3570

Figure 15

COMMON VOLUMES

TRANSMITTER AZ. 12° RECEIVER AZ. 6° AND ELEV. 2°

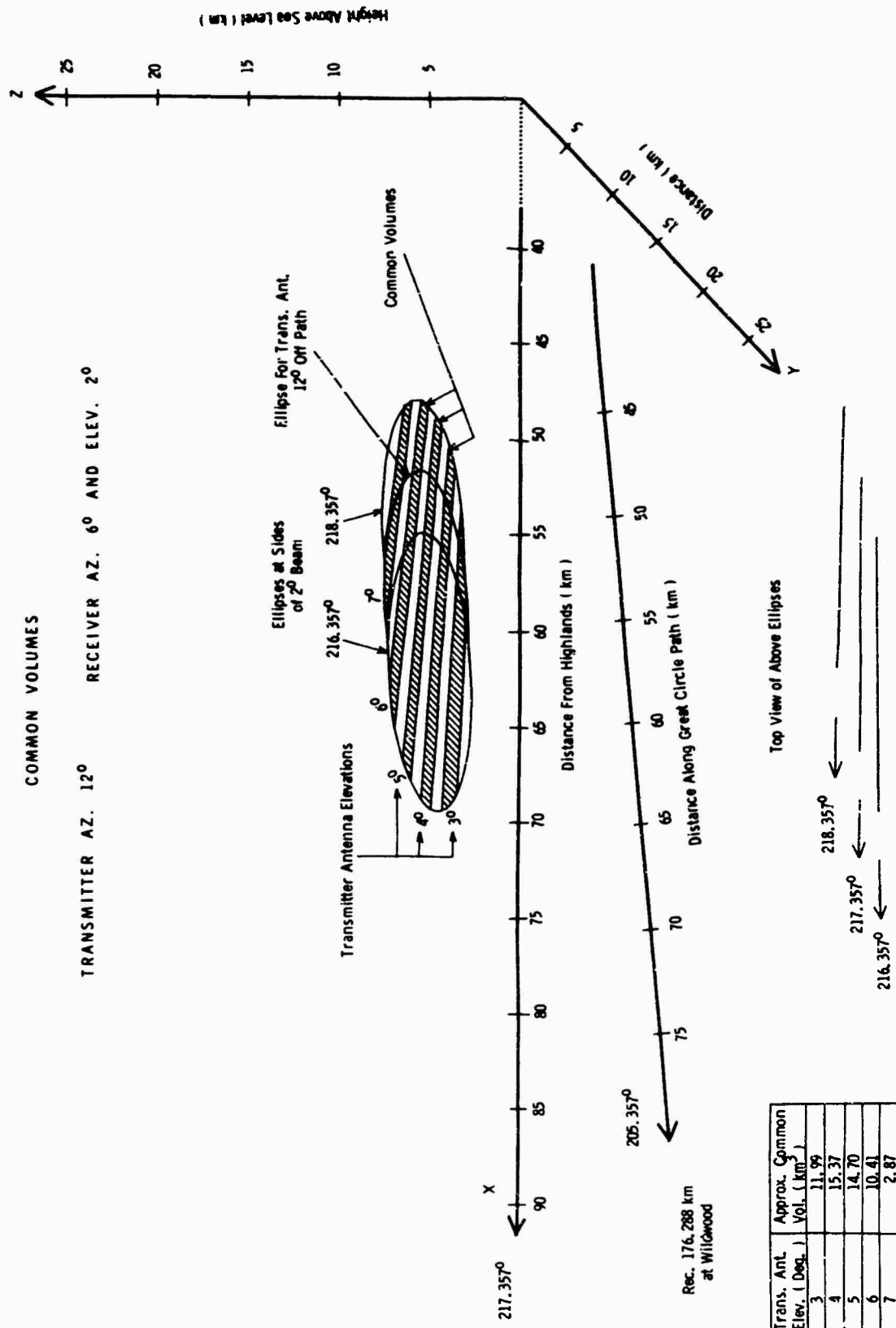
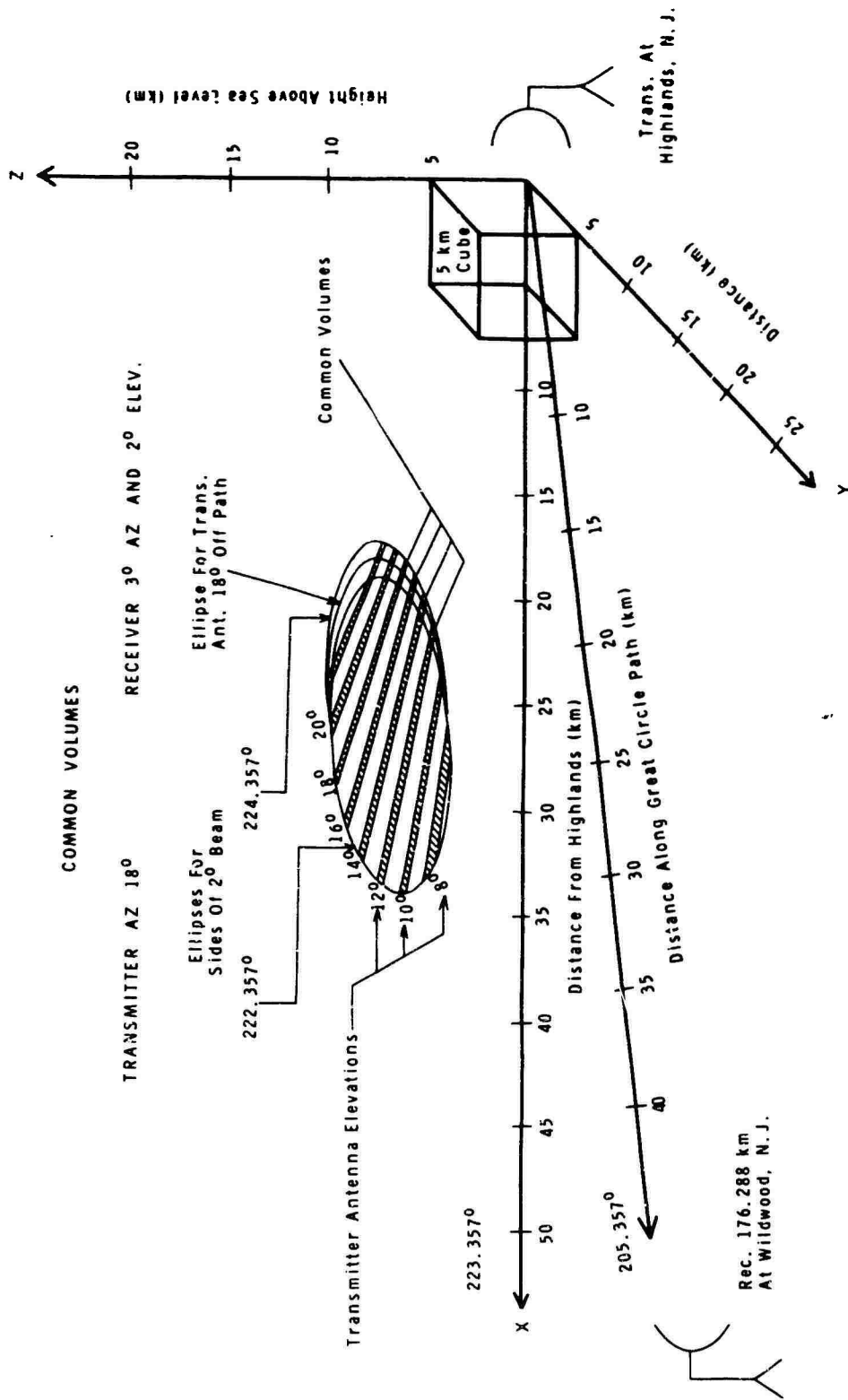


Figure 16



Trans. Ant. Elev. (Deg.)	Approx. Common Volume (km ³)
8	5.4
10	2.17
12	2.33
14	2.37
16	2.00
18	1.50
20	1.21

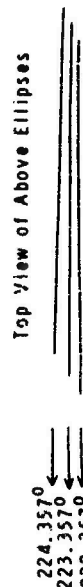
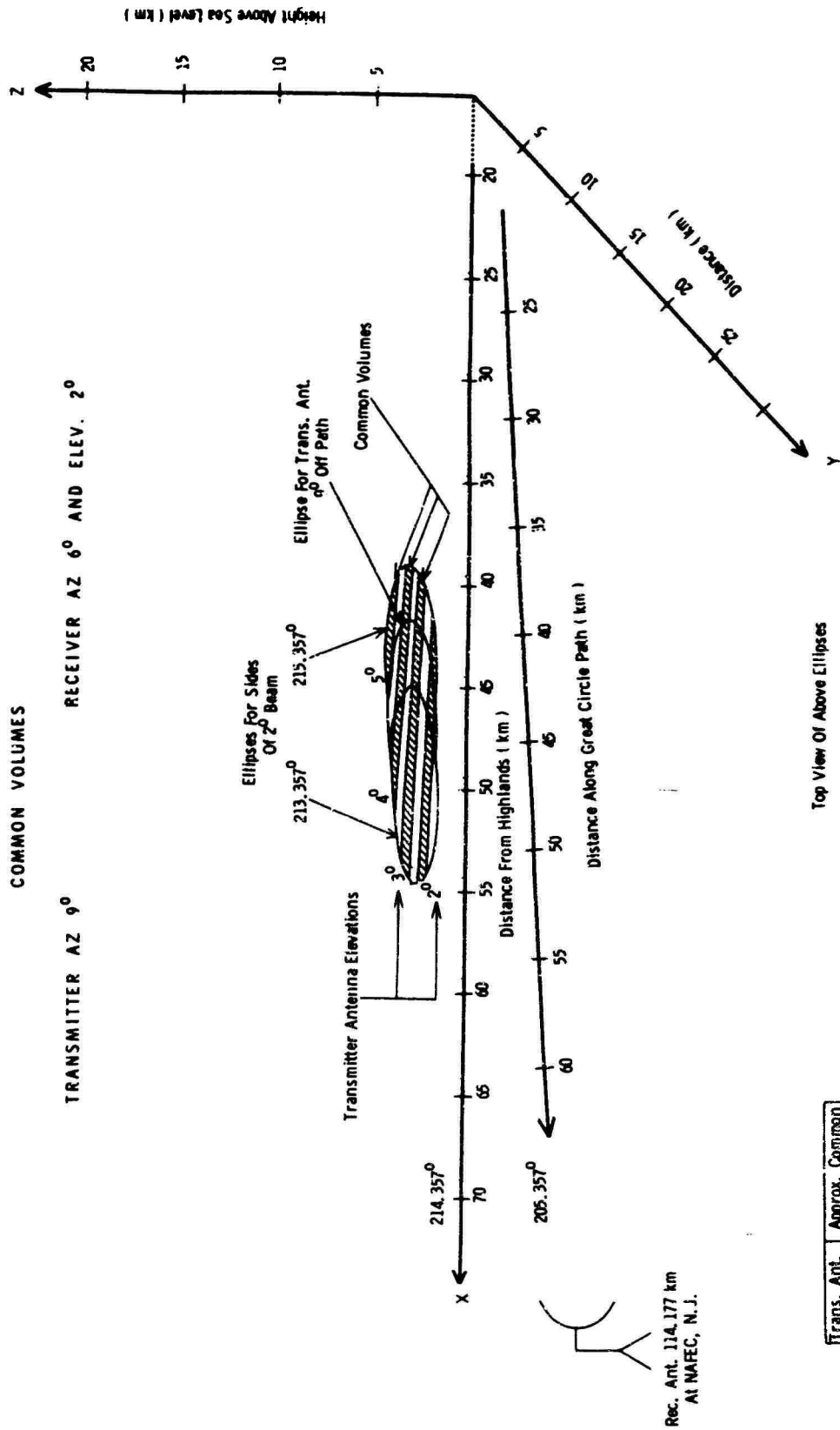


Figure 17



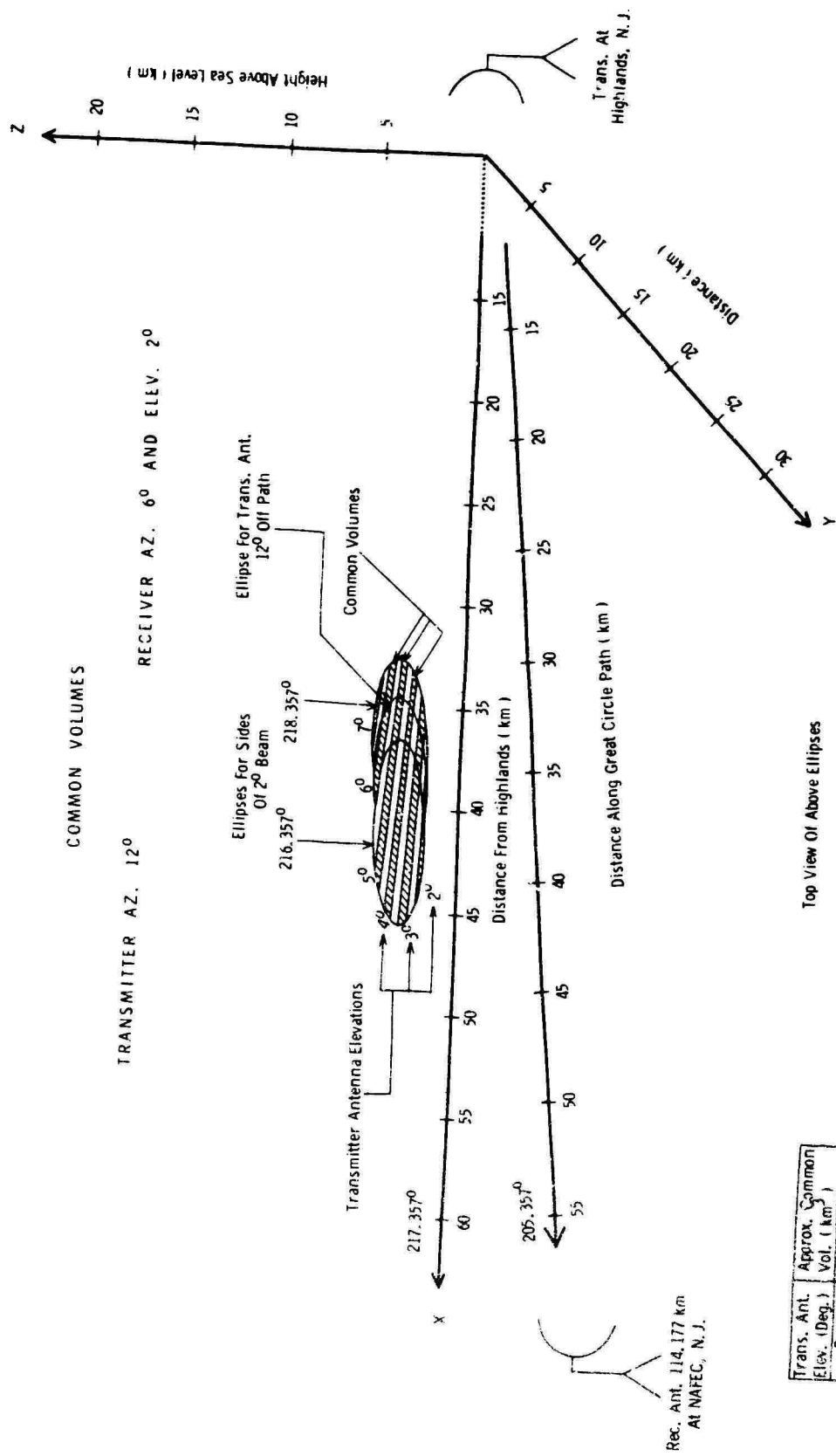
Top View Of Above Ellipses

214.357 $^\circ$ 215.357 $^\circ$

213.357 $^\circ$

Trans. Ant. Elev. (Deg.)	Approx. Common Vol. (km ³)
2	4.17
3	5.61
4	3.91
5	.56

Figure 18



Trans. Ant. Elev. (Deg.)	Approx. Common Vol. (km ³)
2	.24
3	3.16
4	3.71
5	3.19
6	1.84
7	.07

Top View Of Above Ellipses

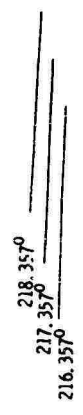
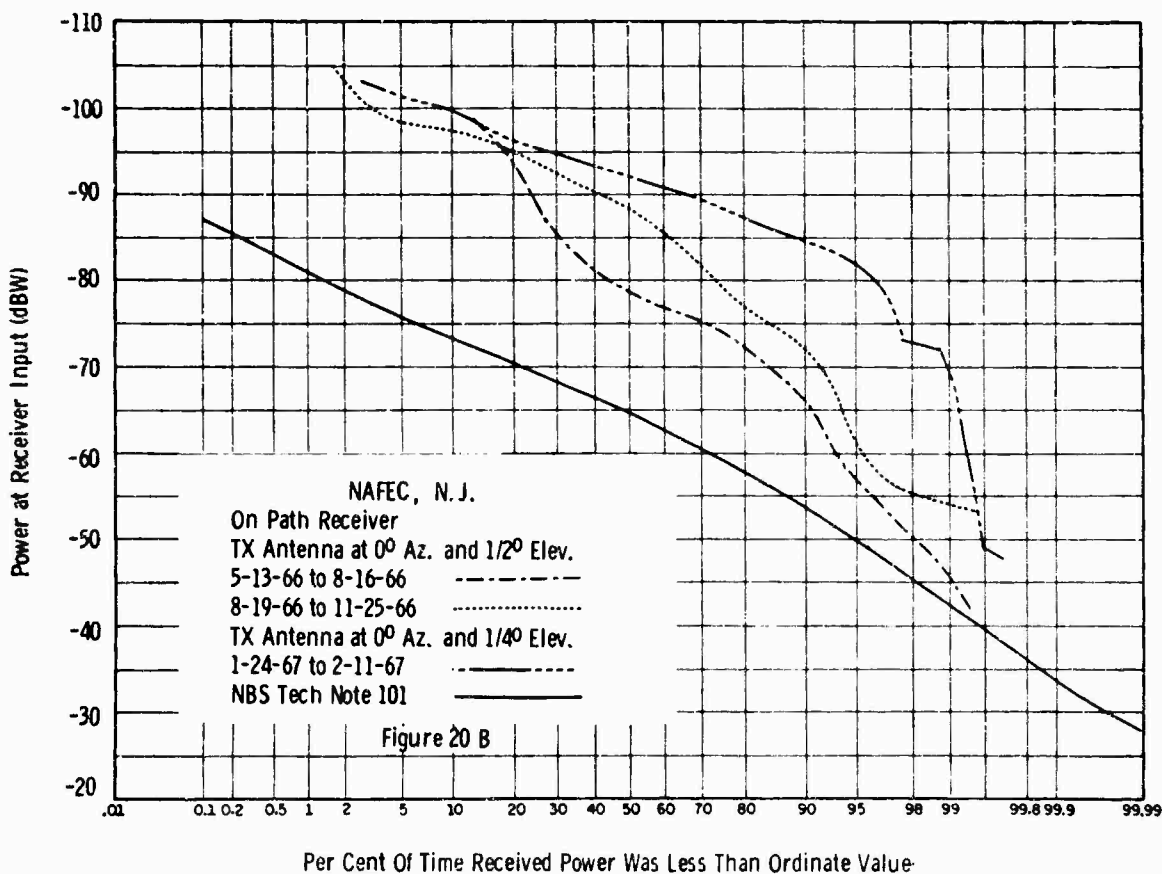
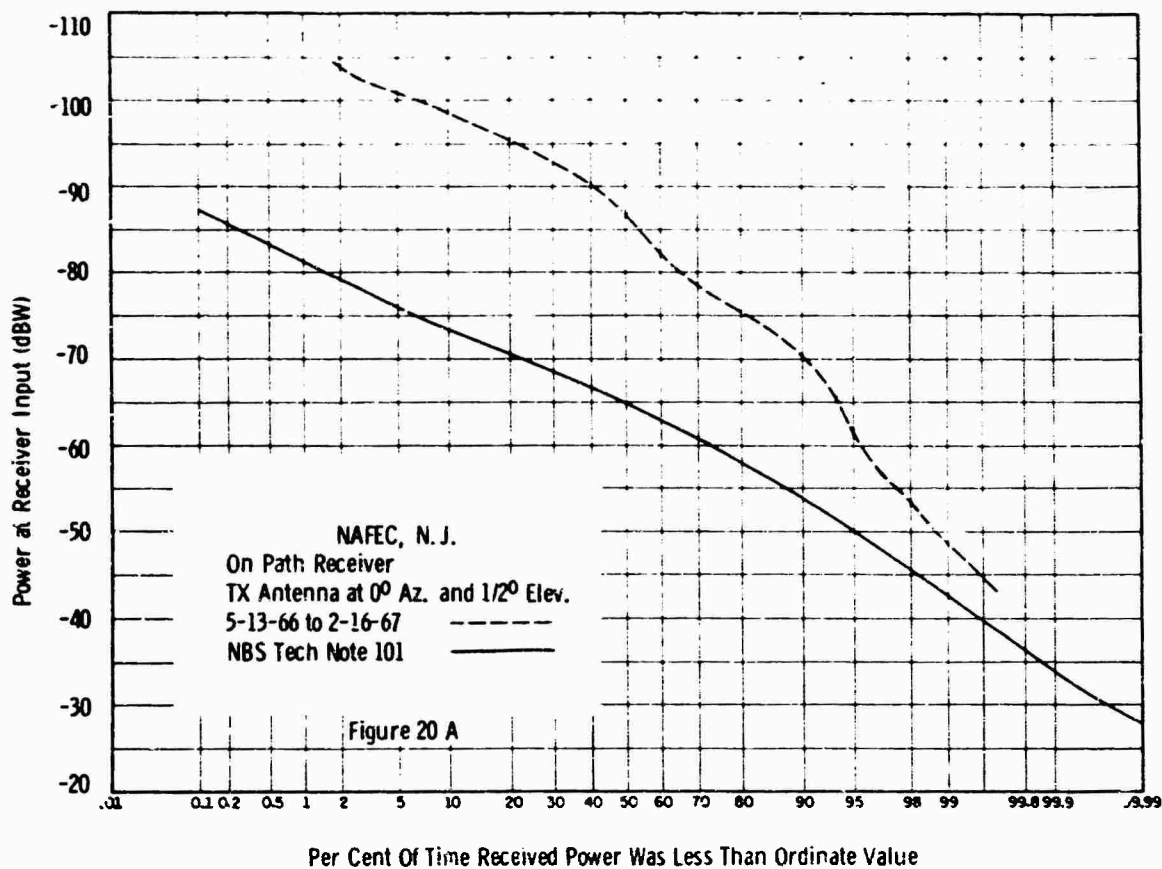
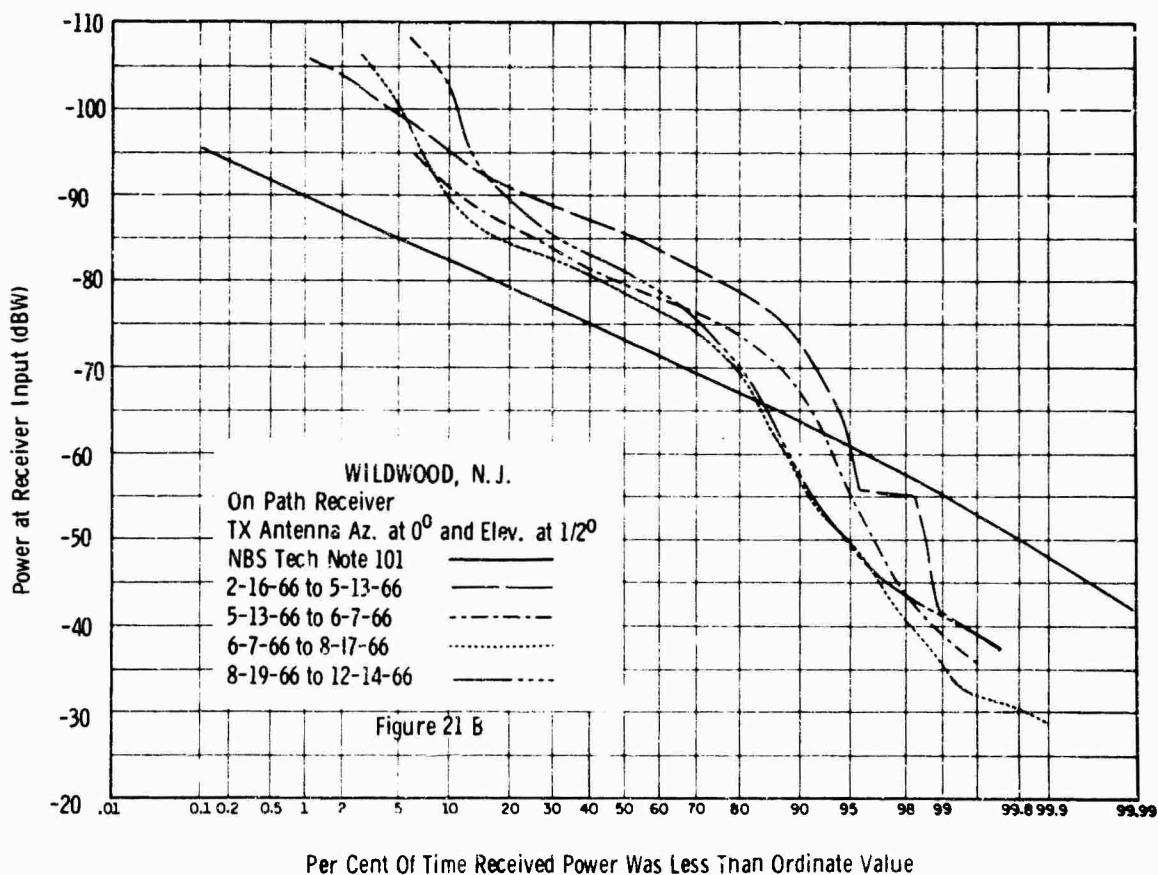
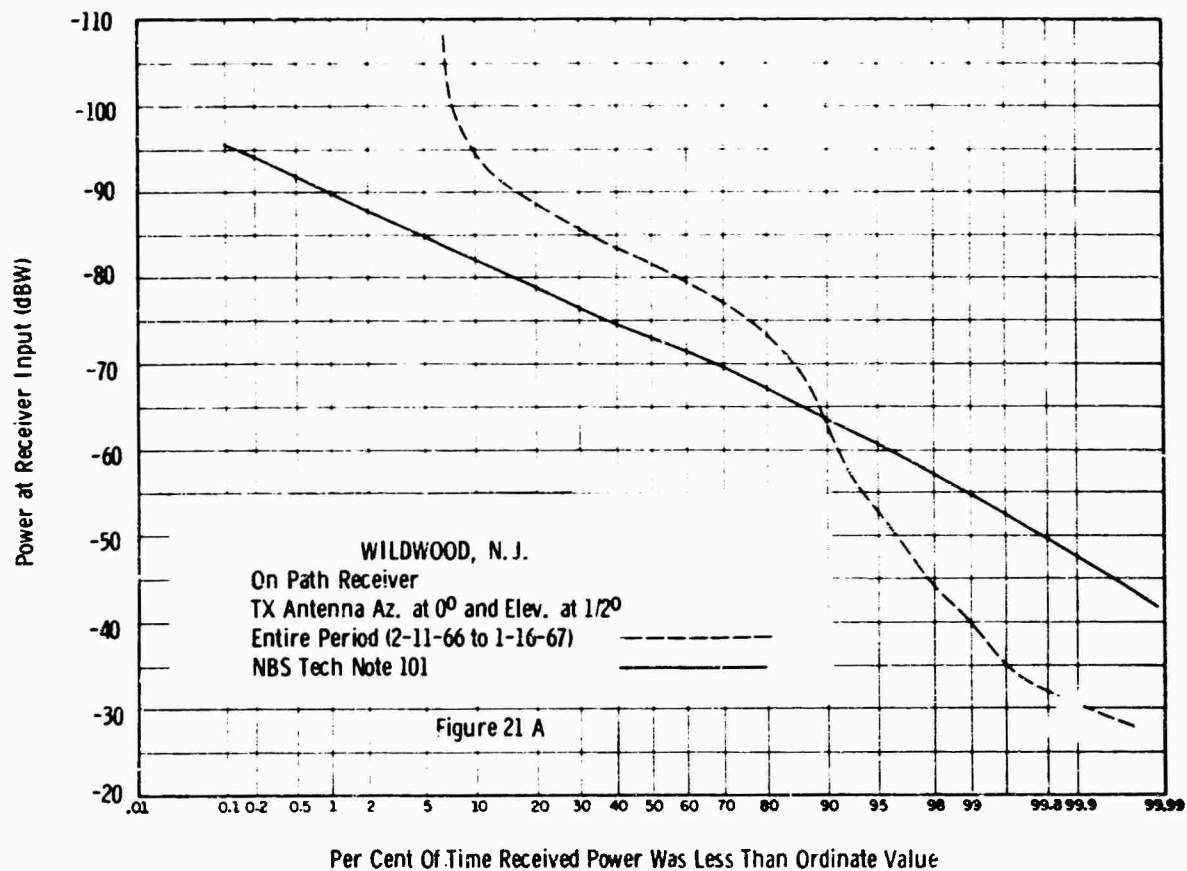
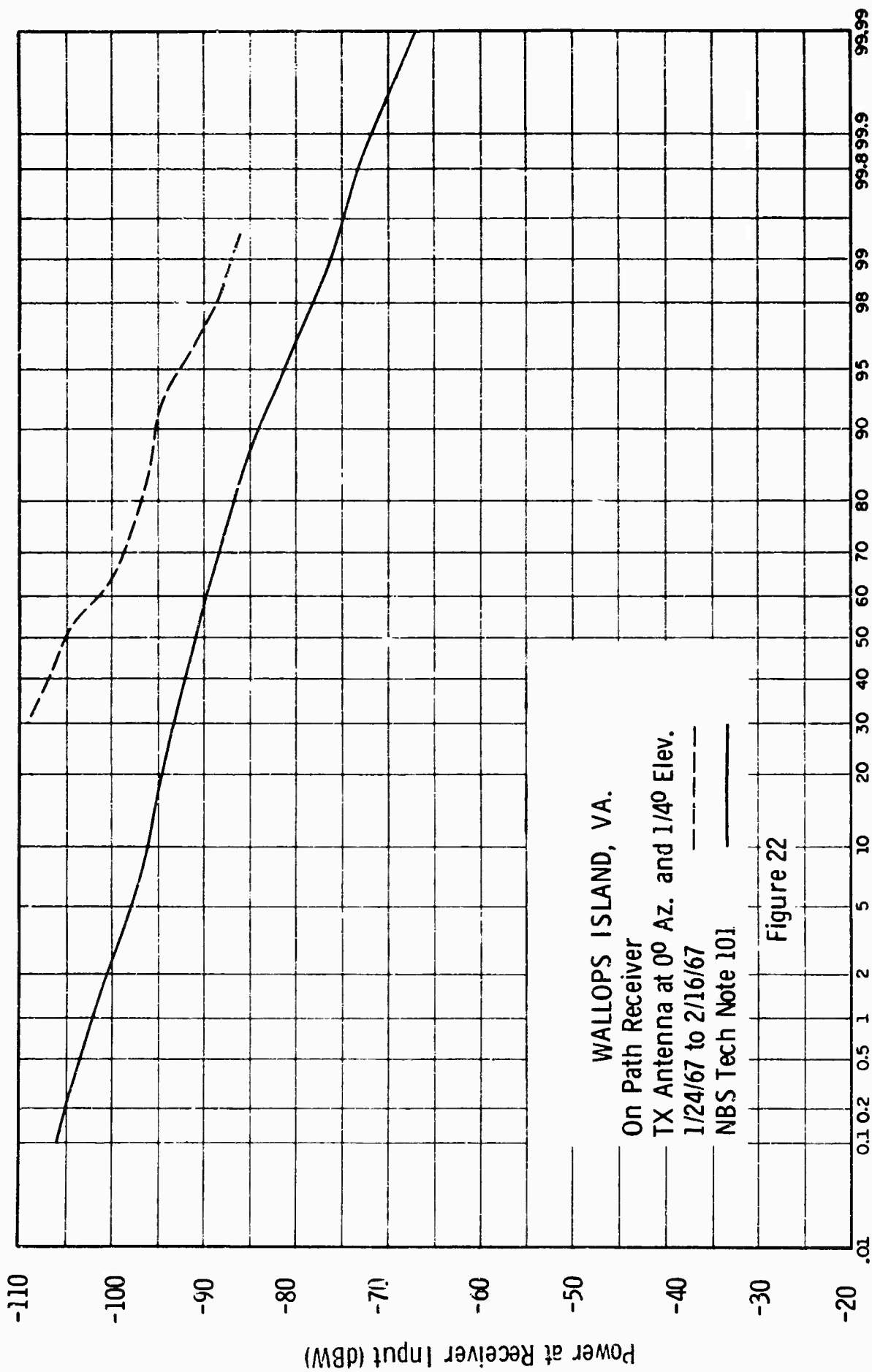
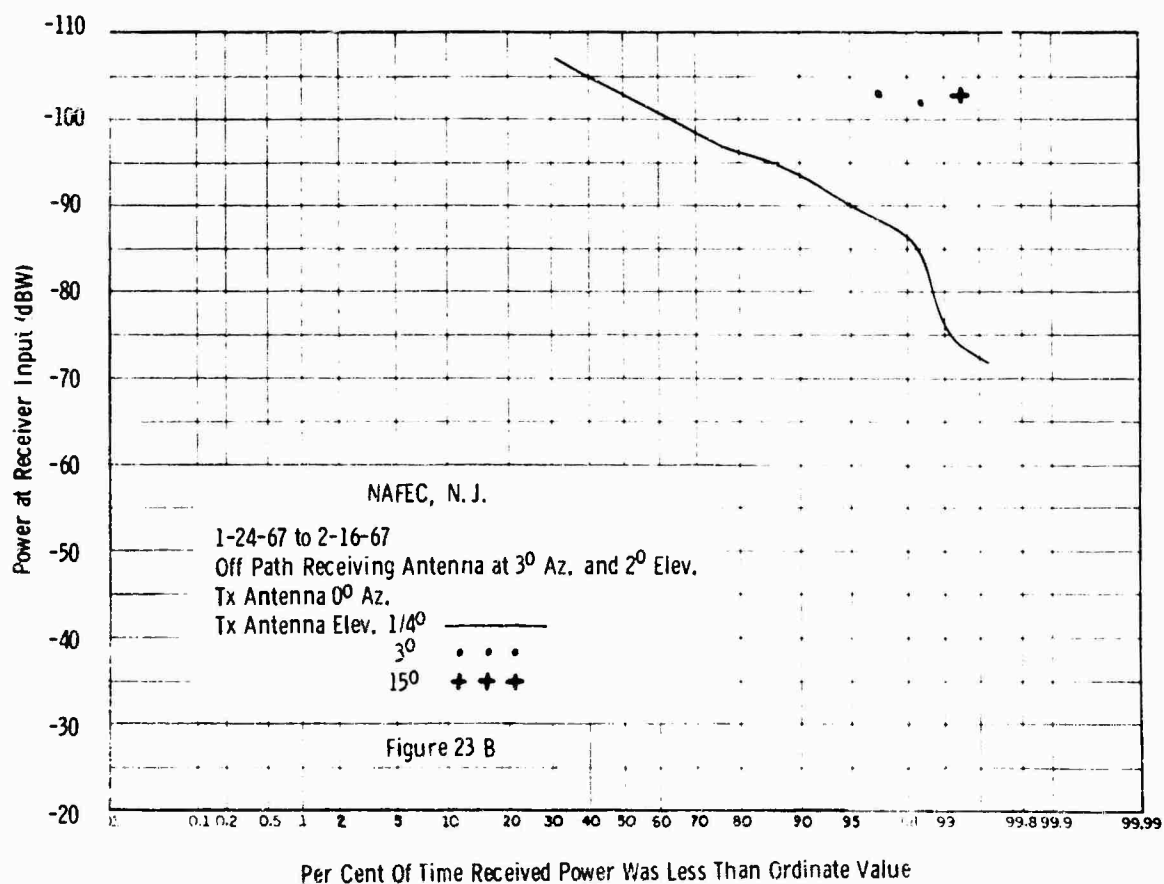
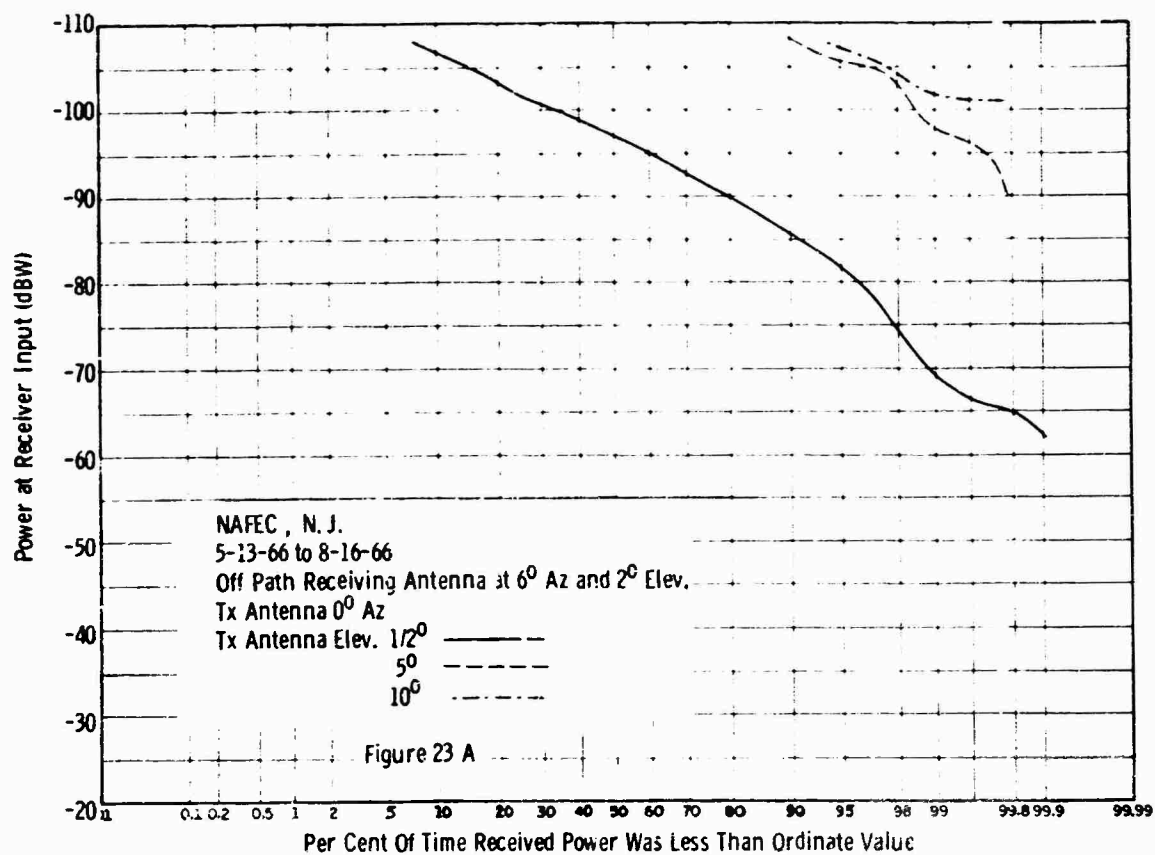


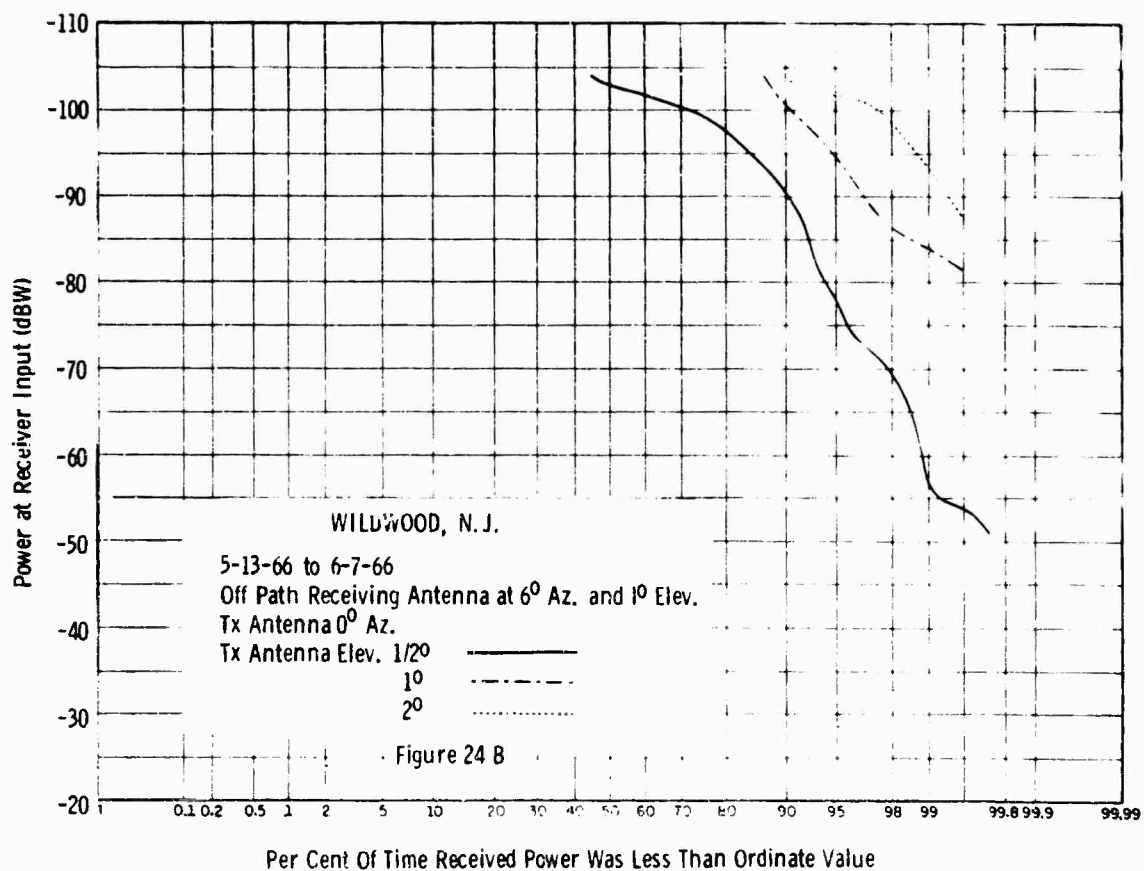
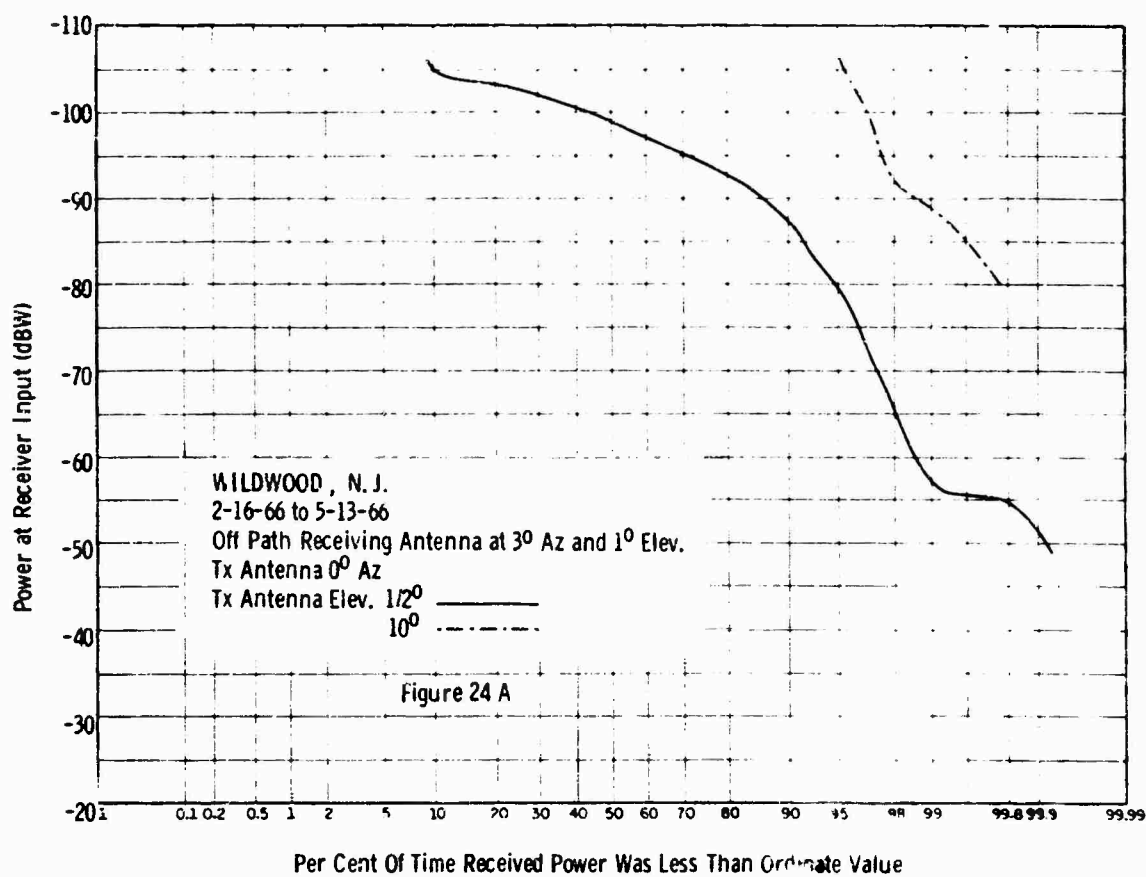
Figure 19

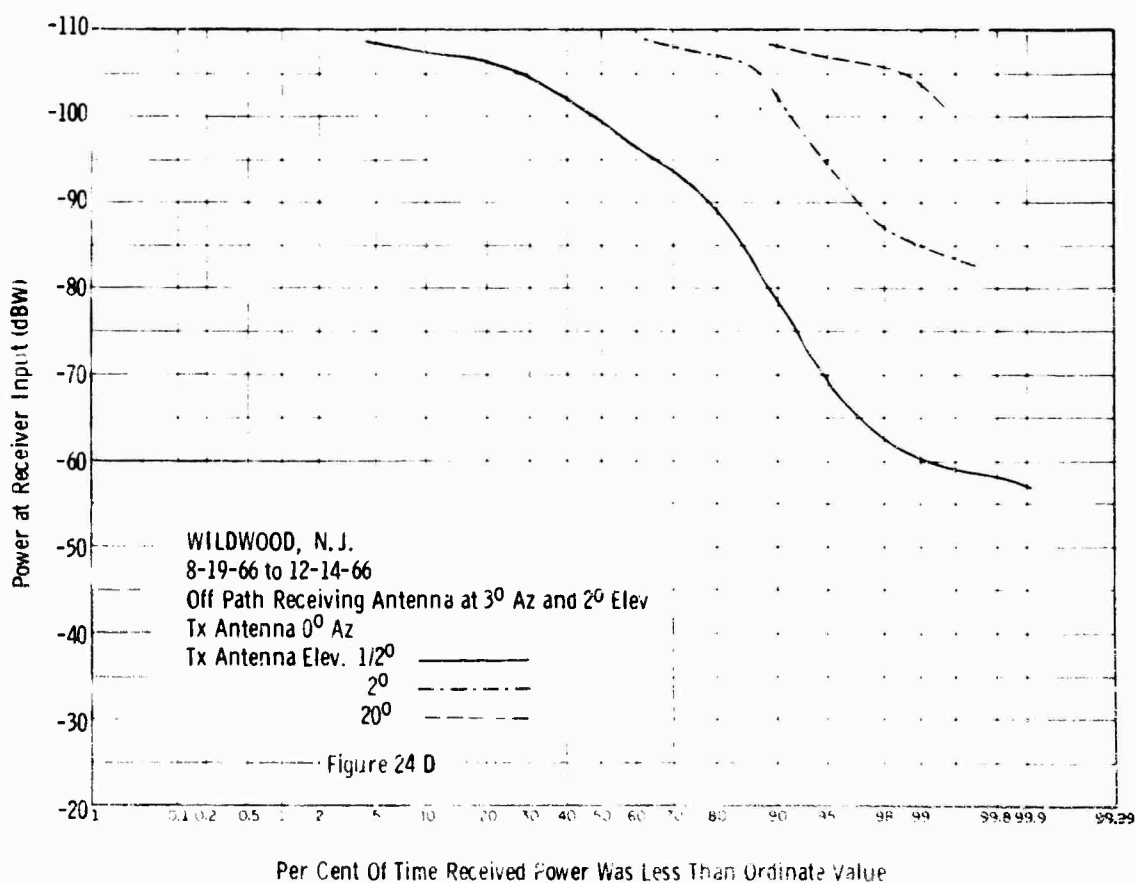
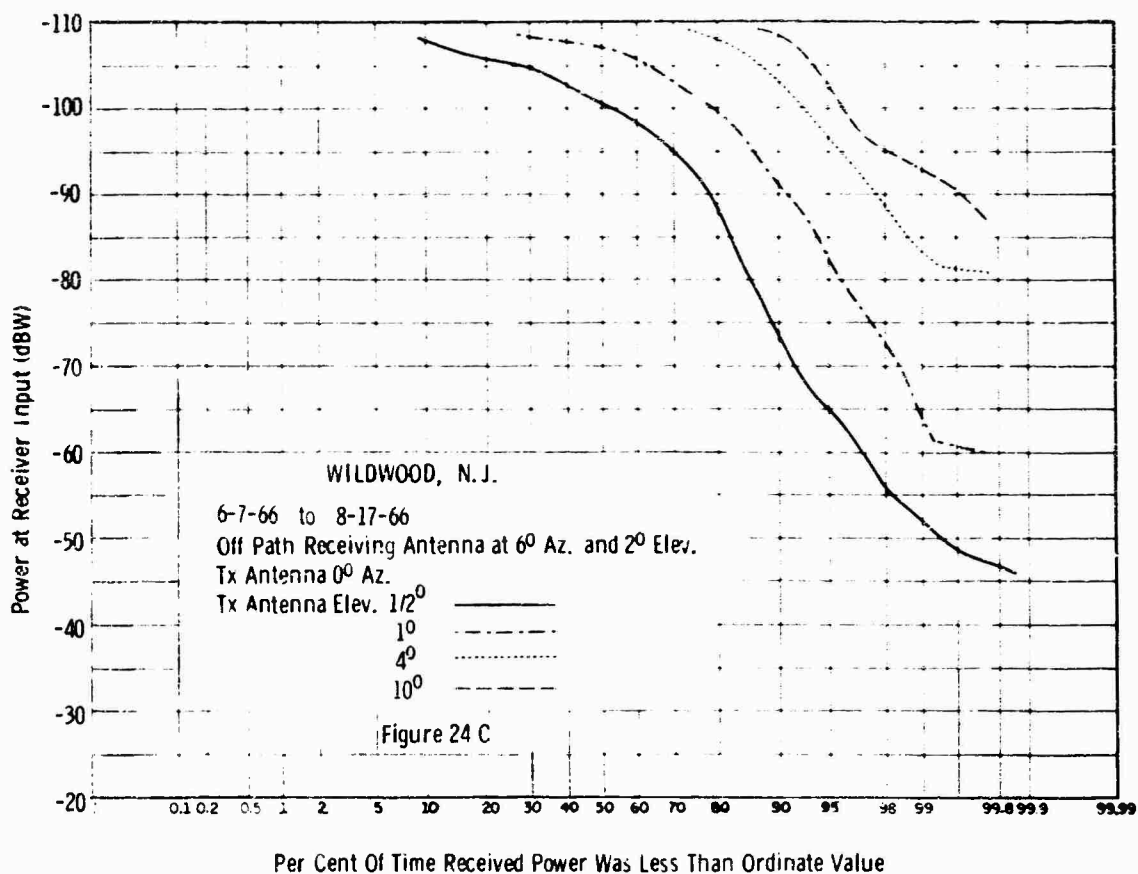


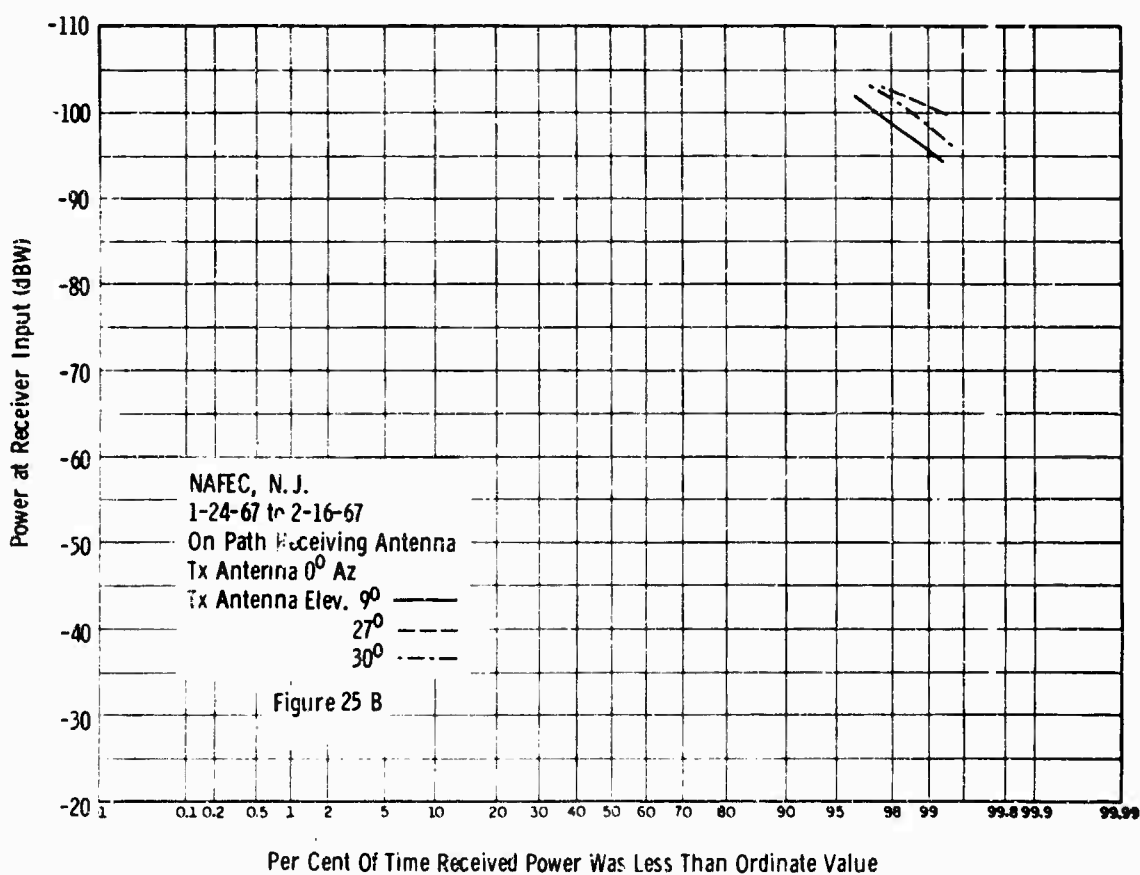
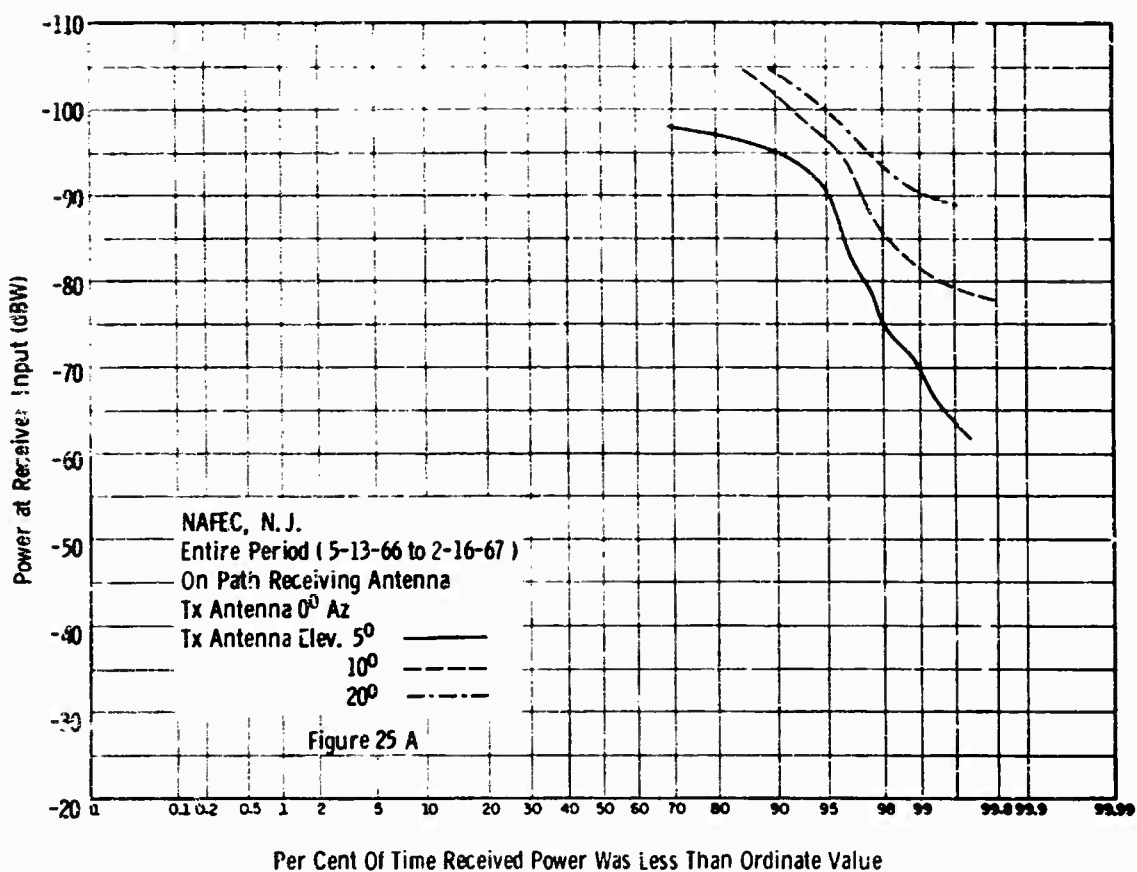


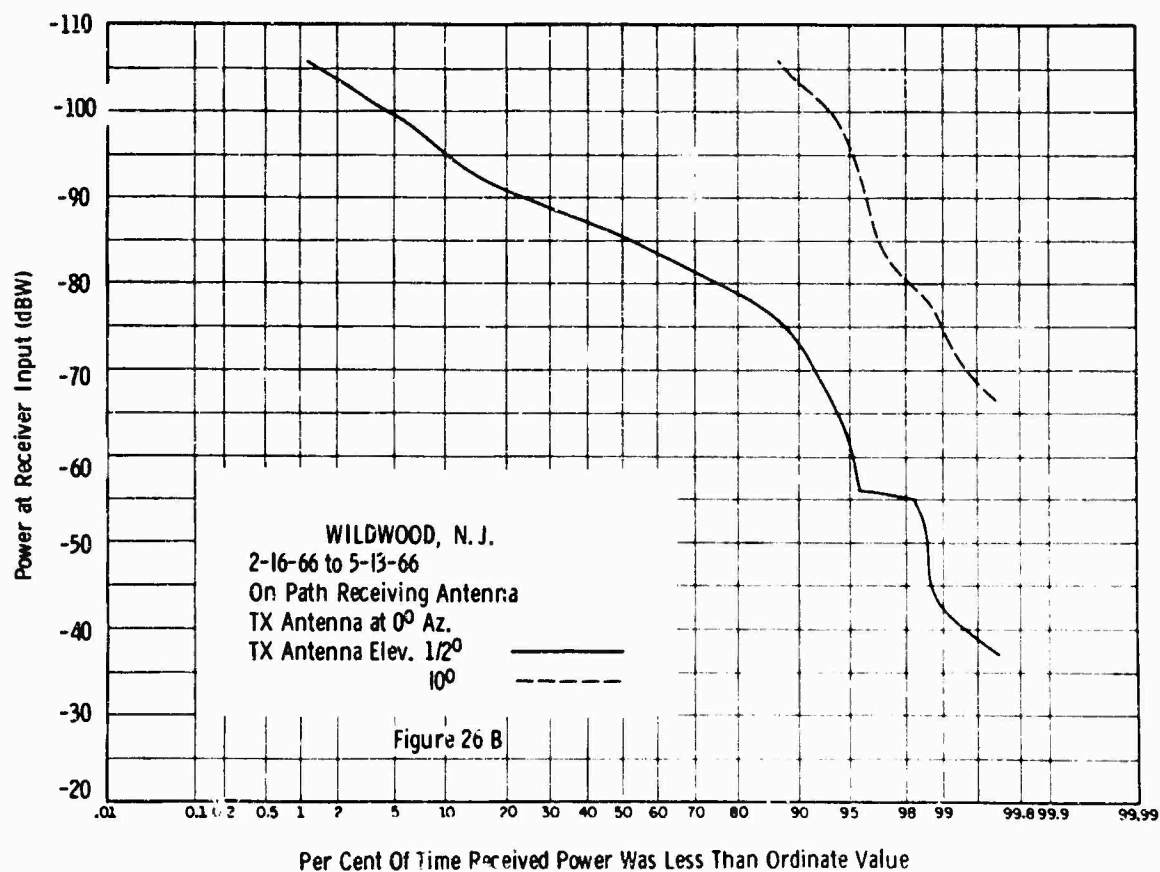
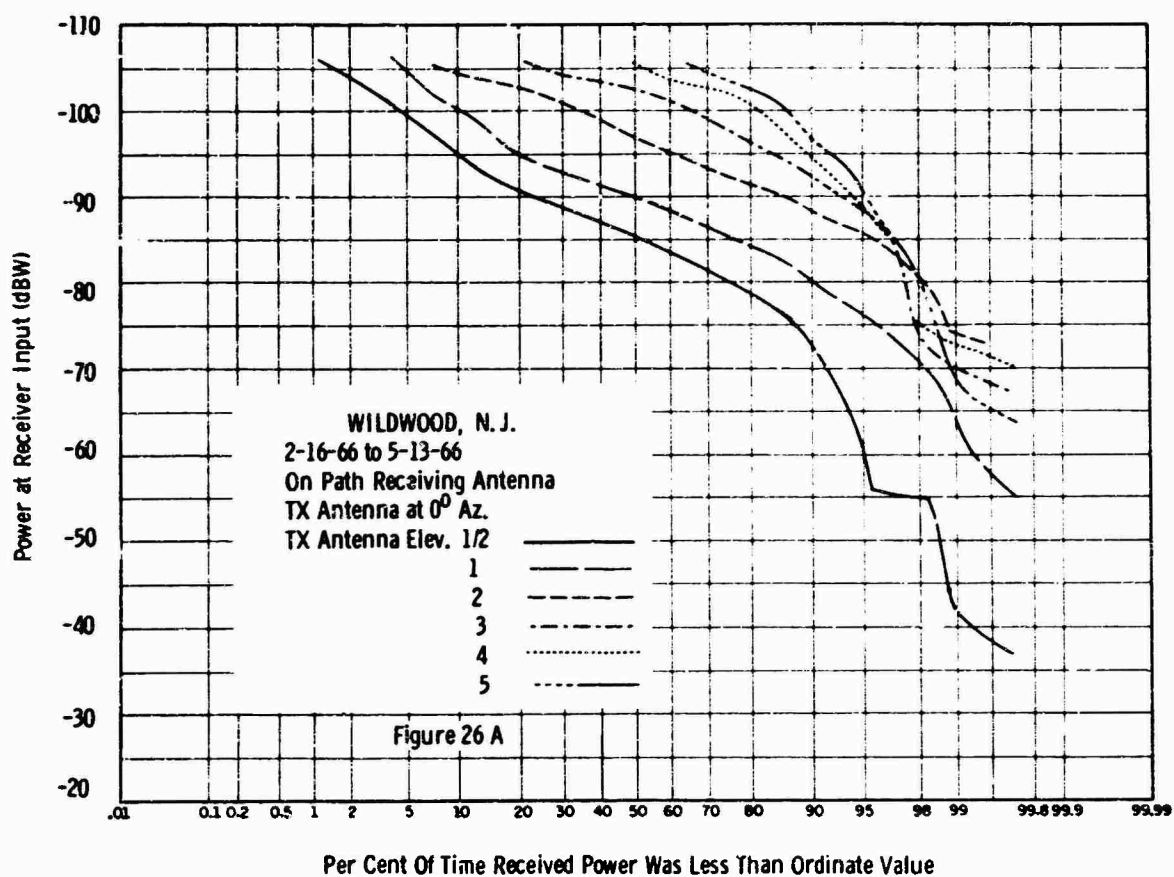


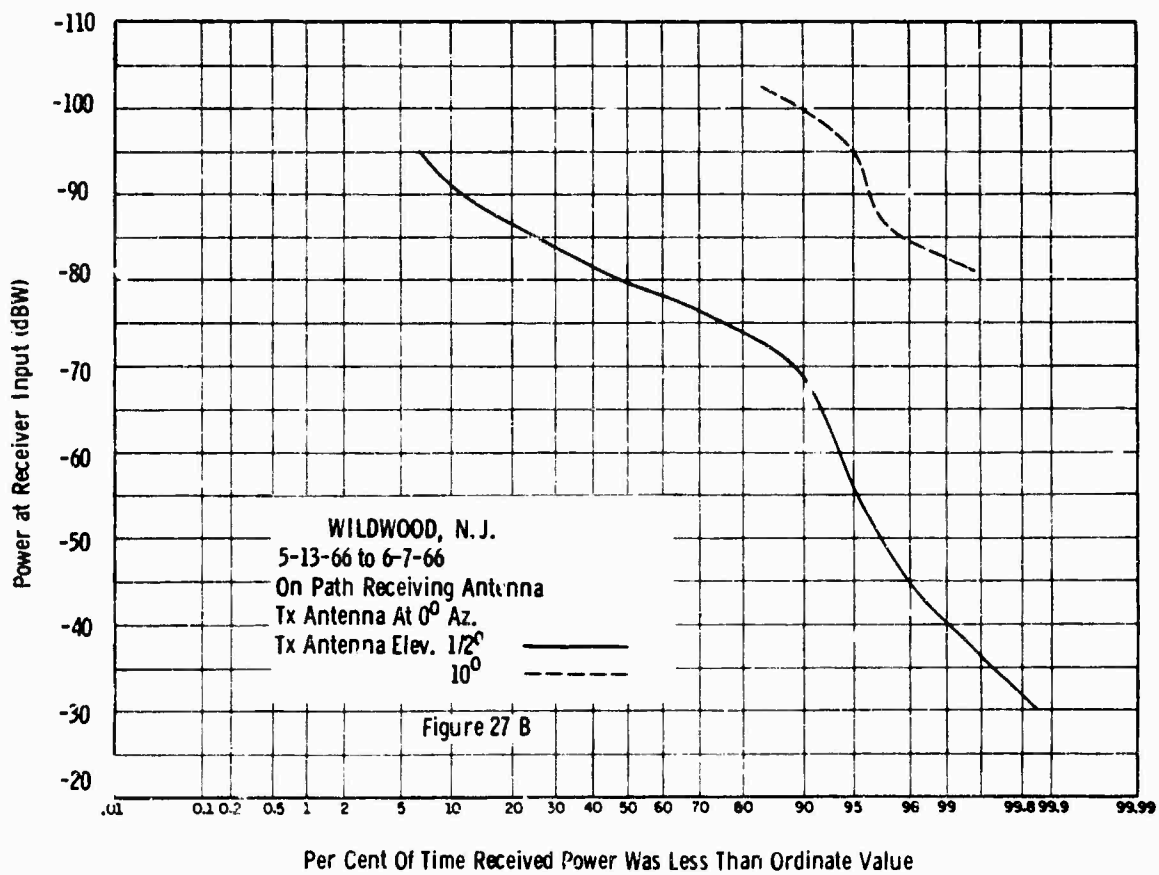
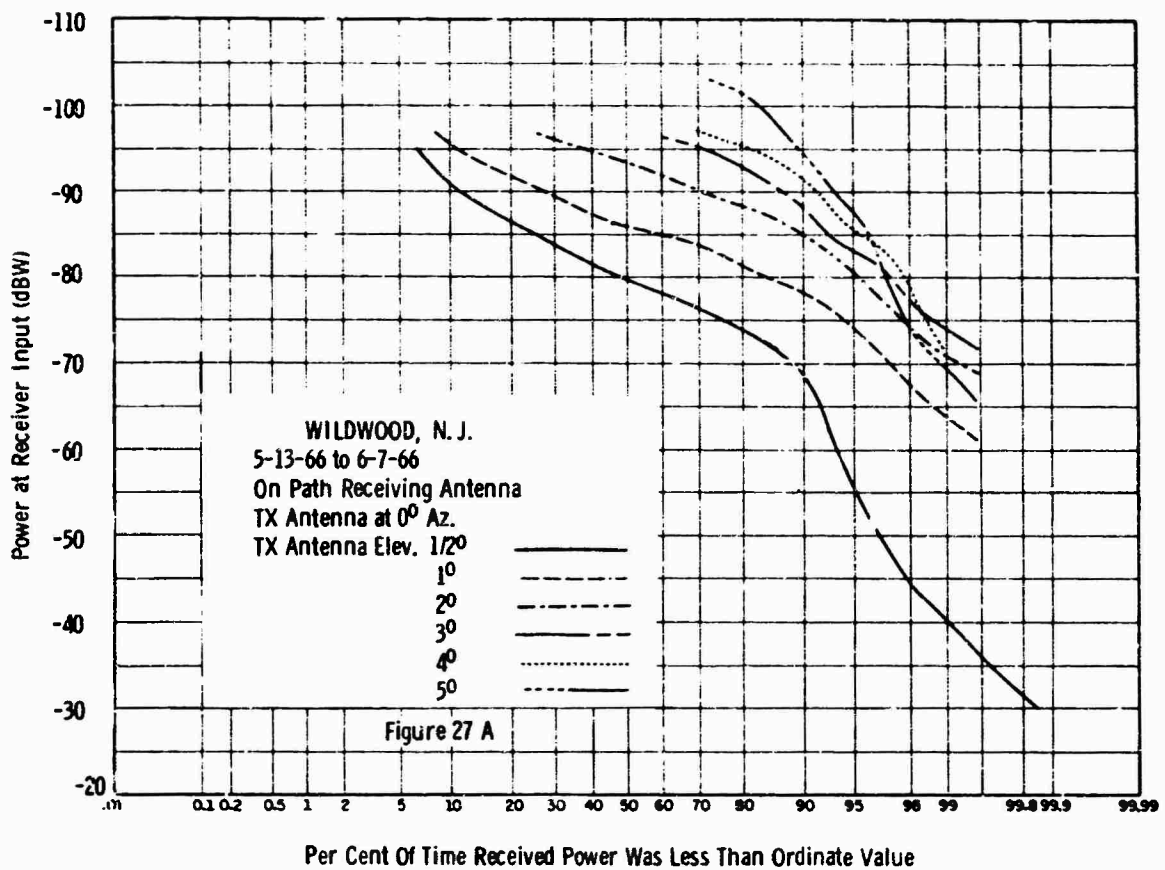


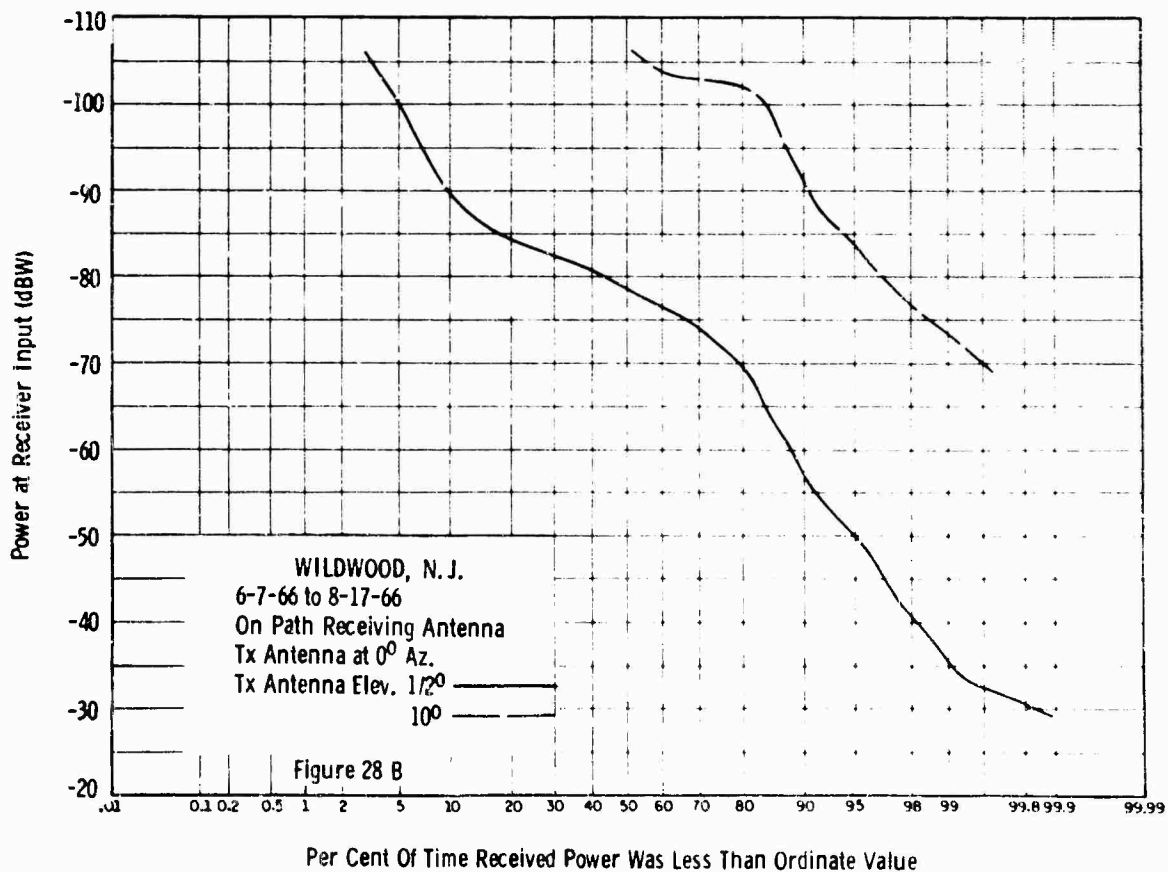
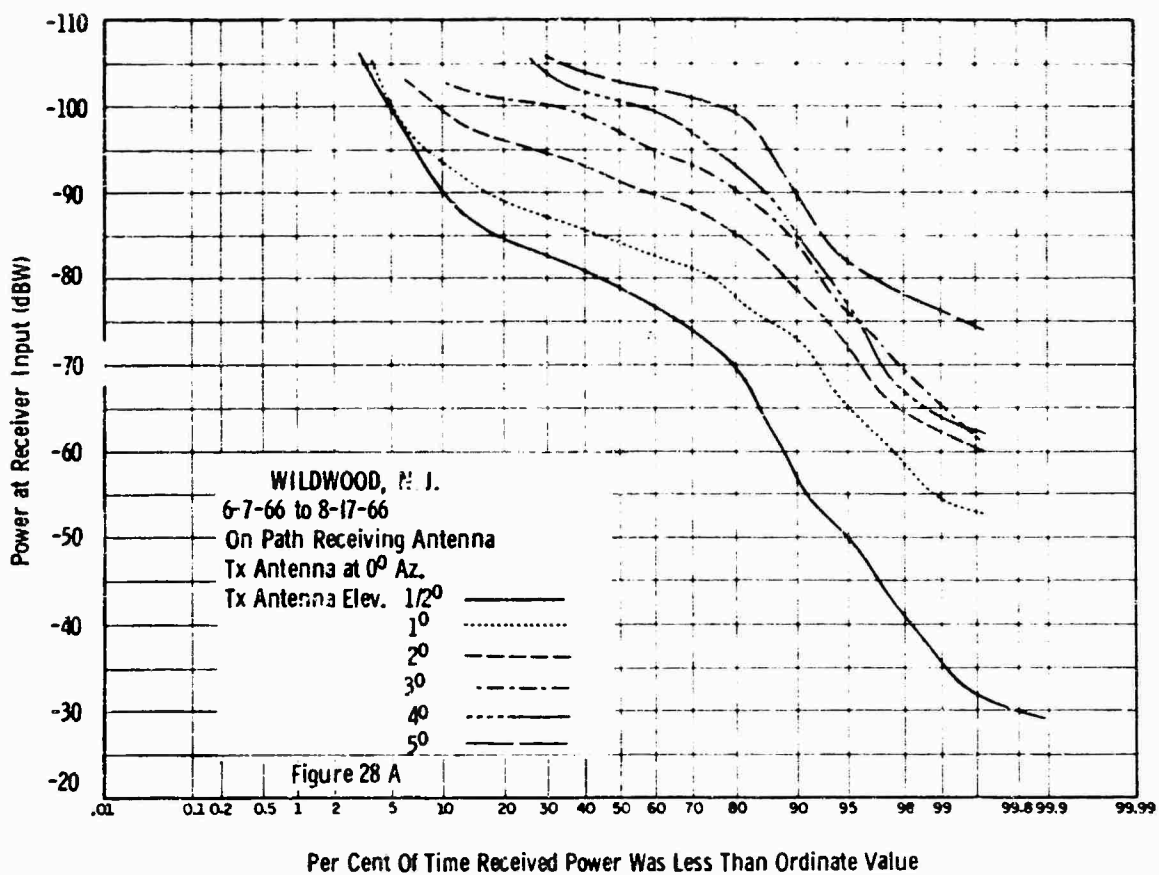


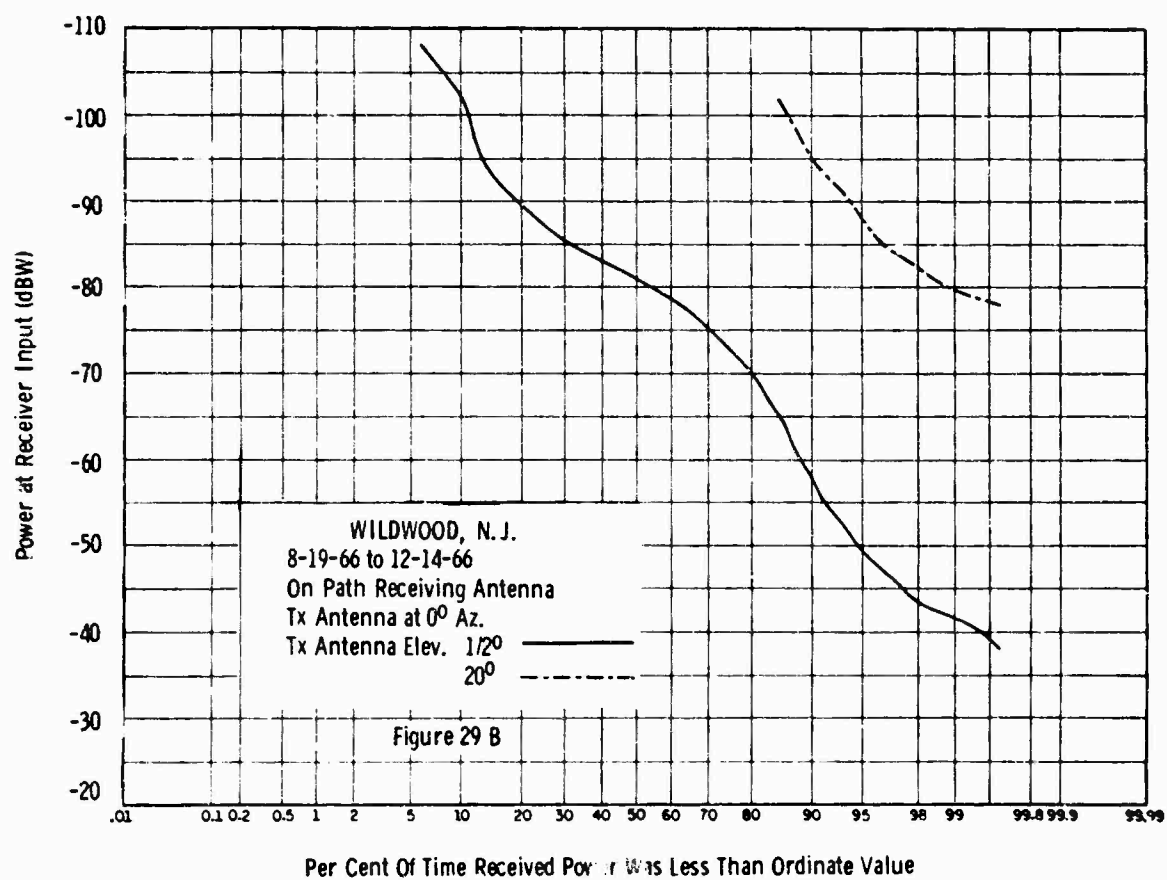
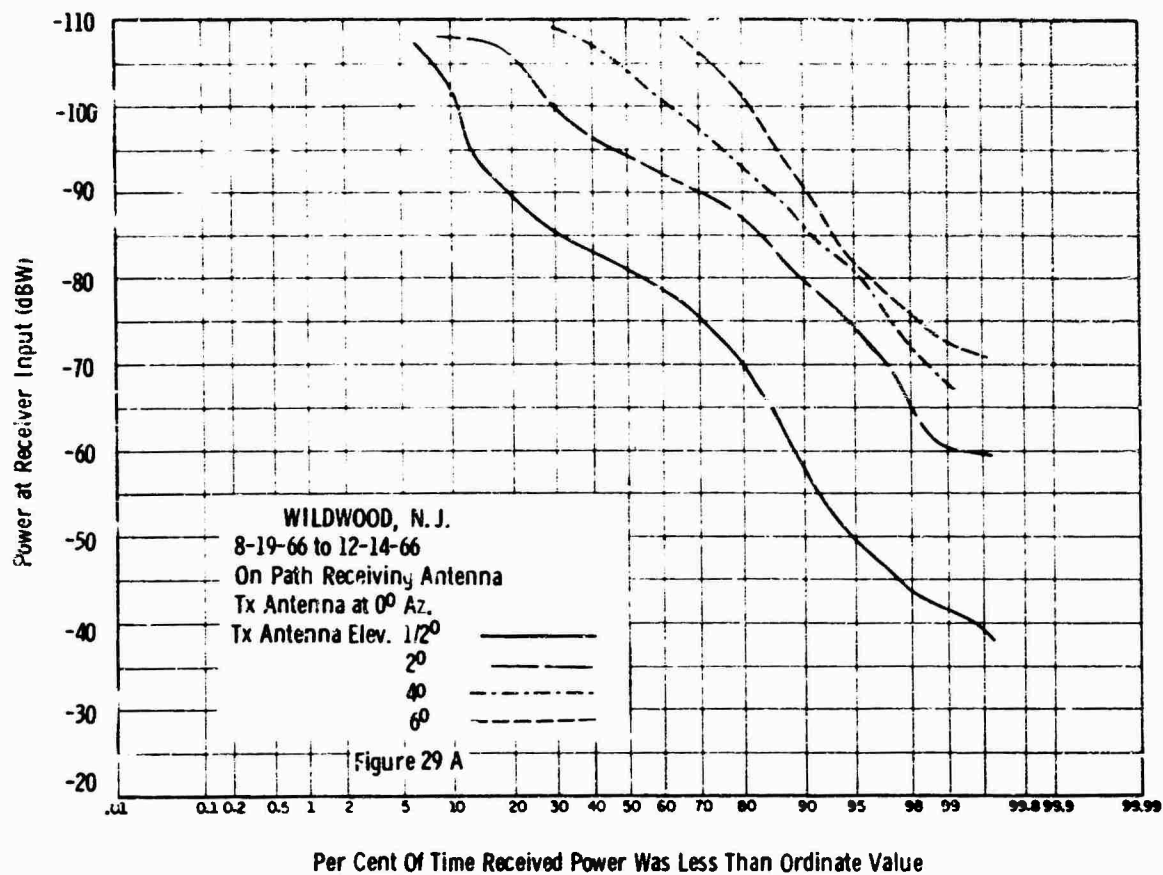


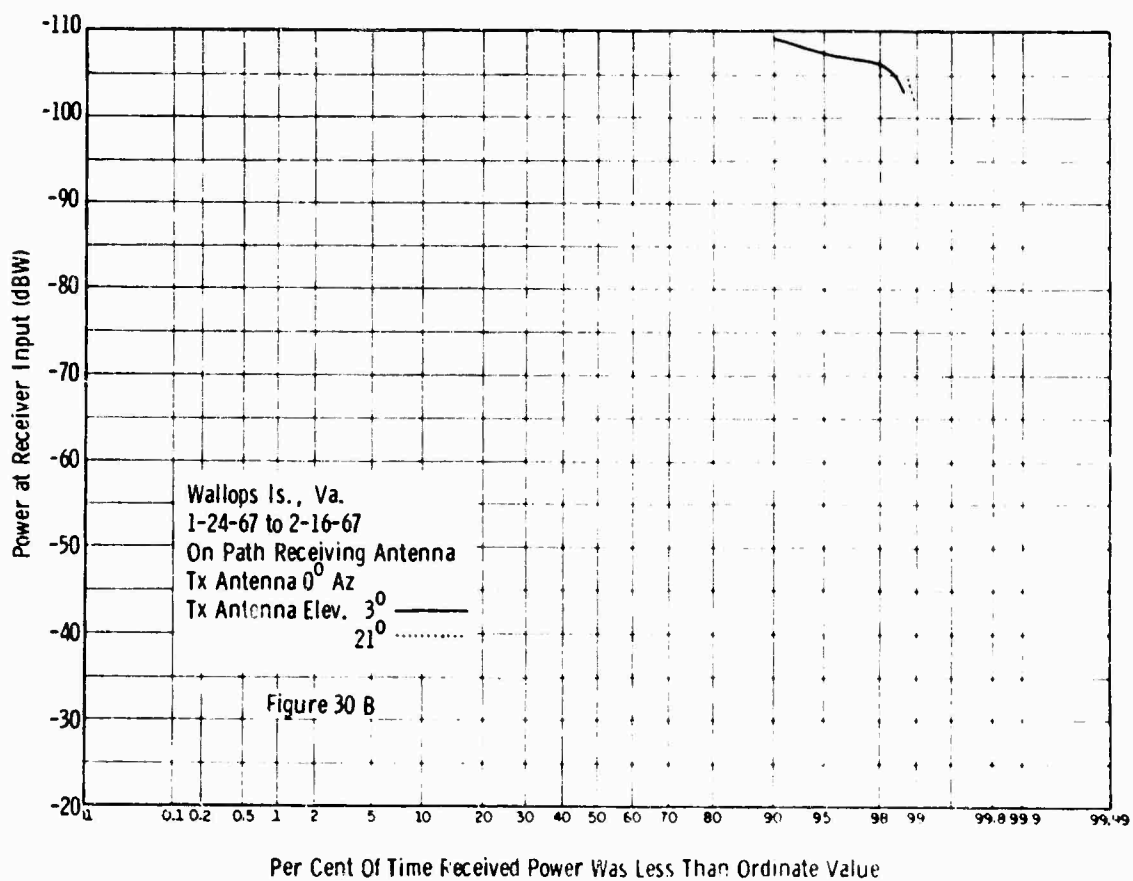
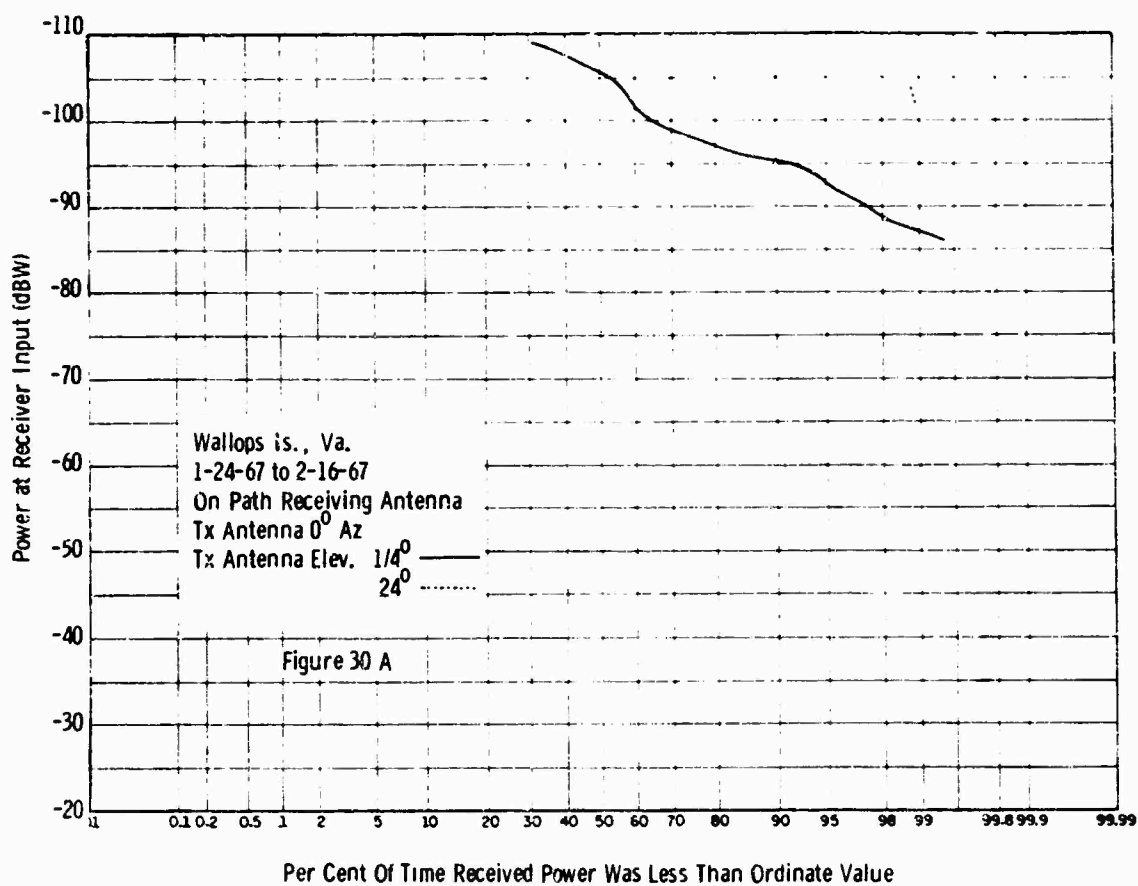


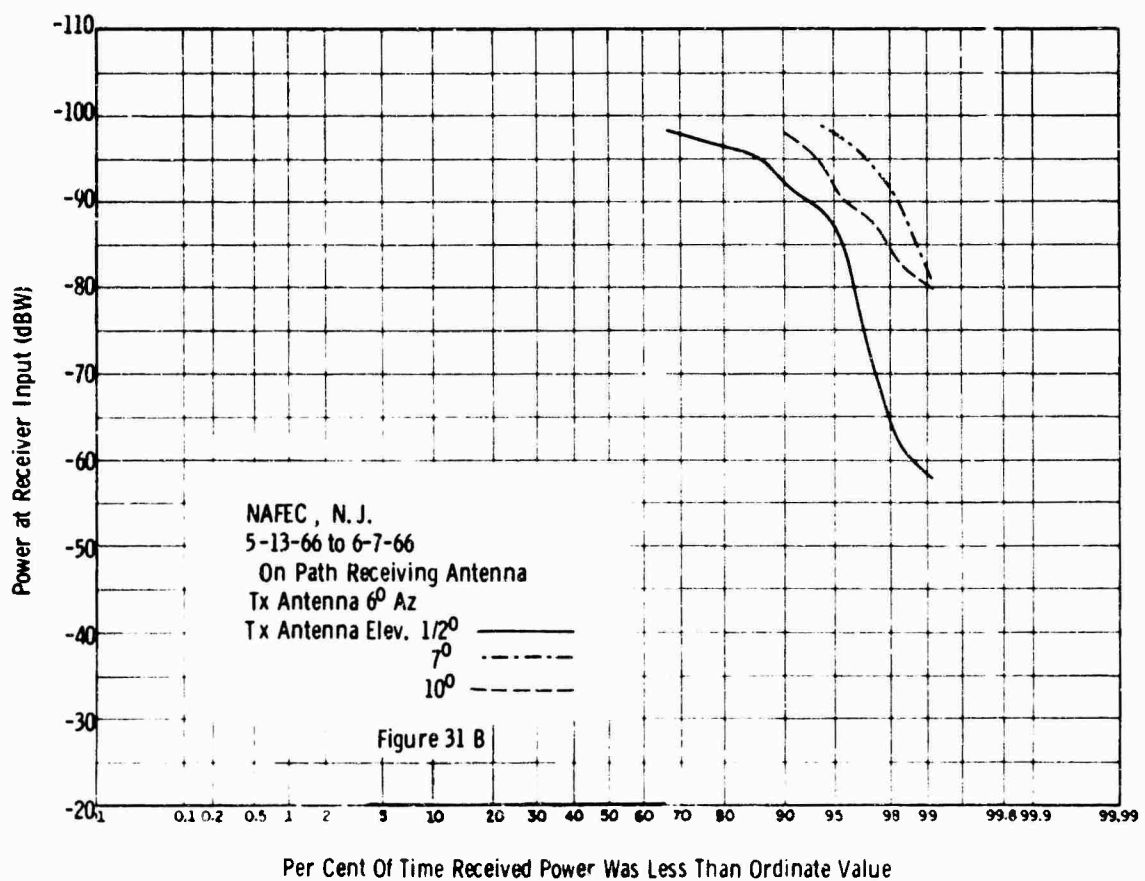
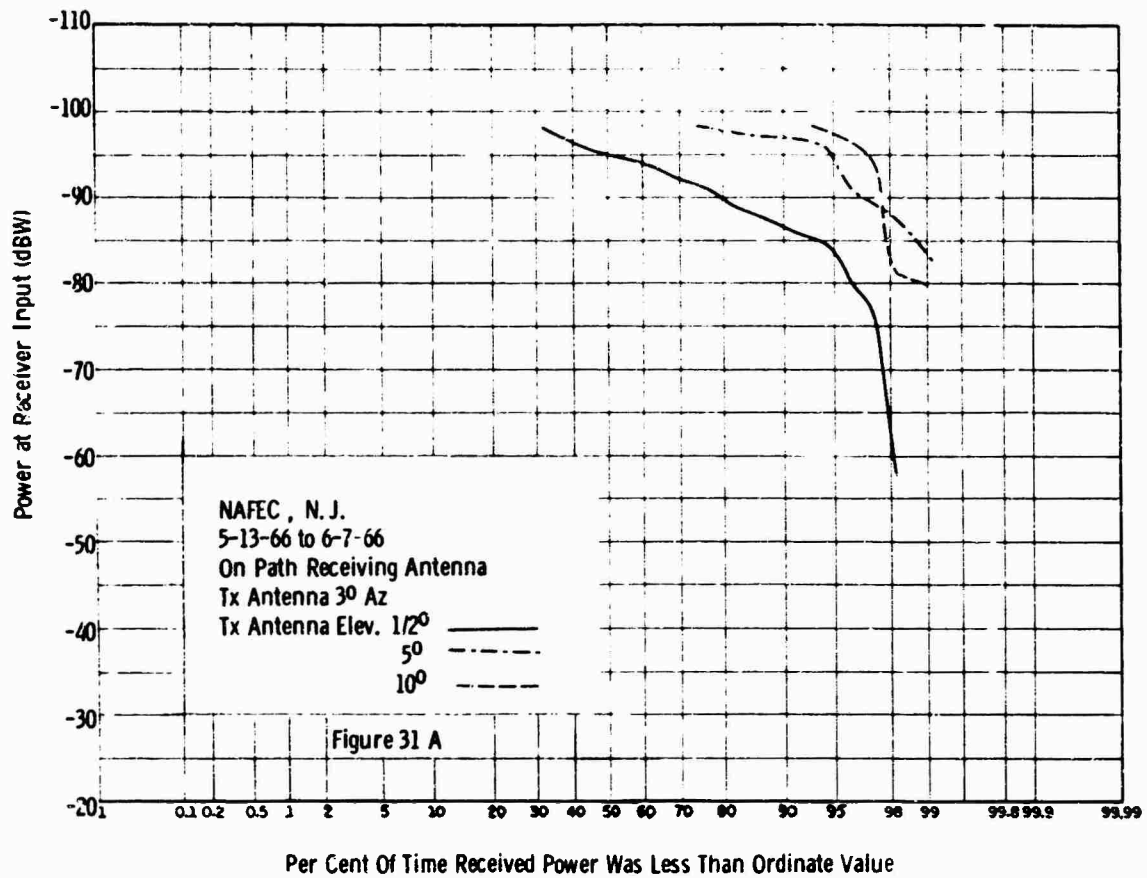


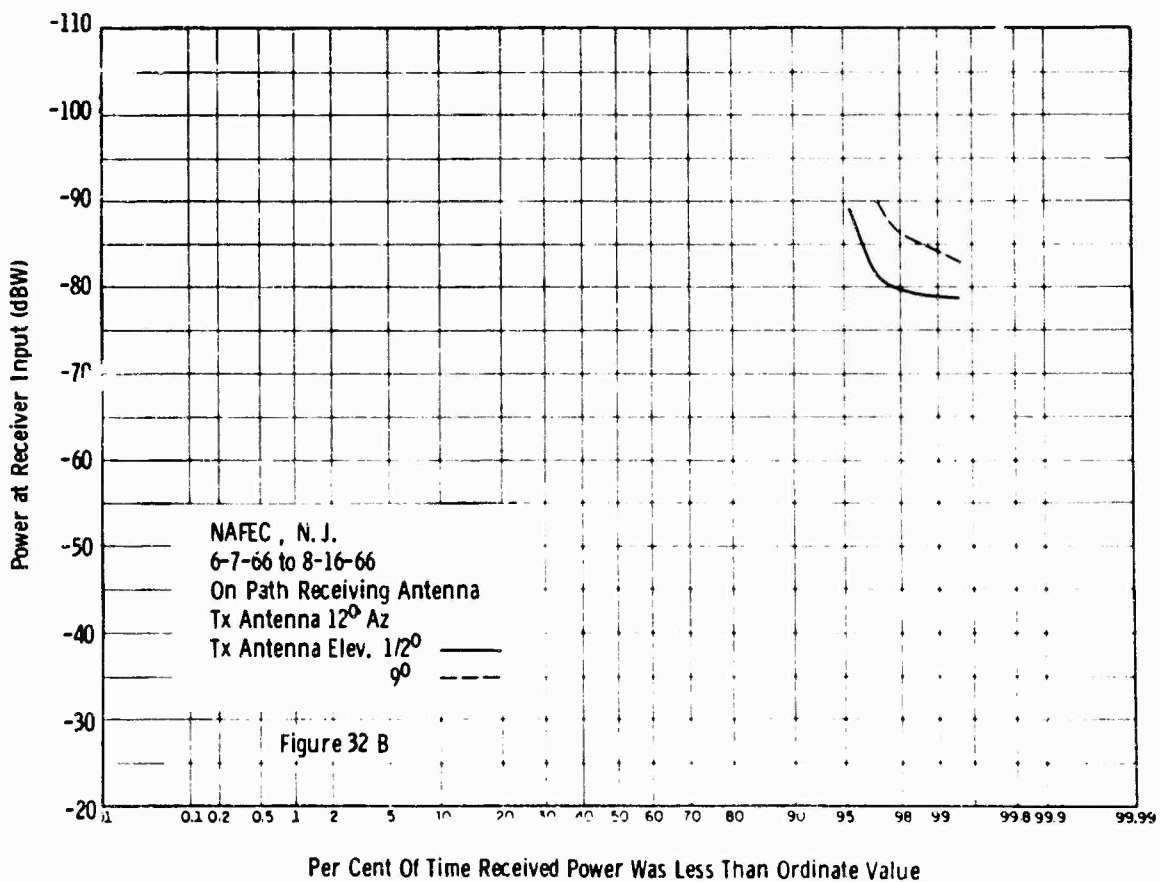
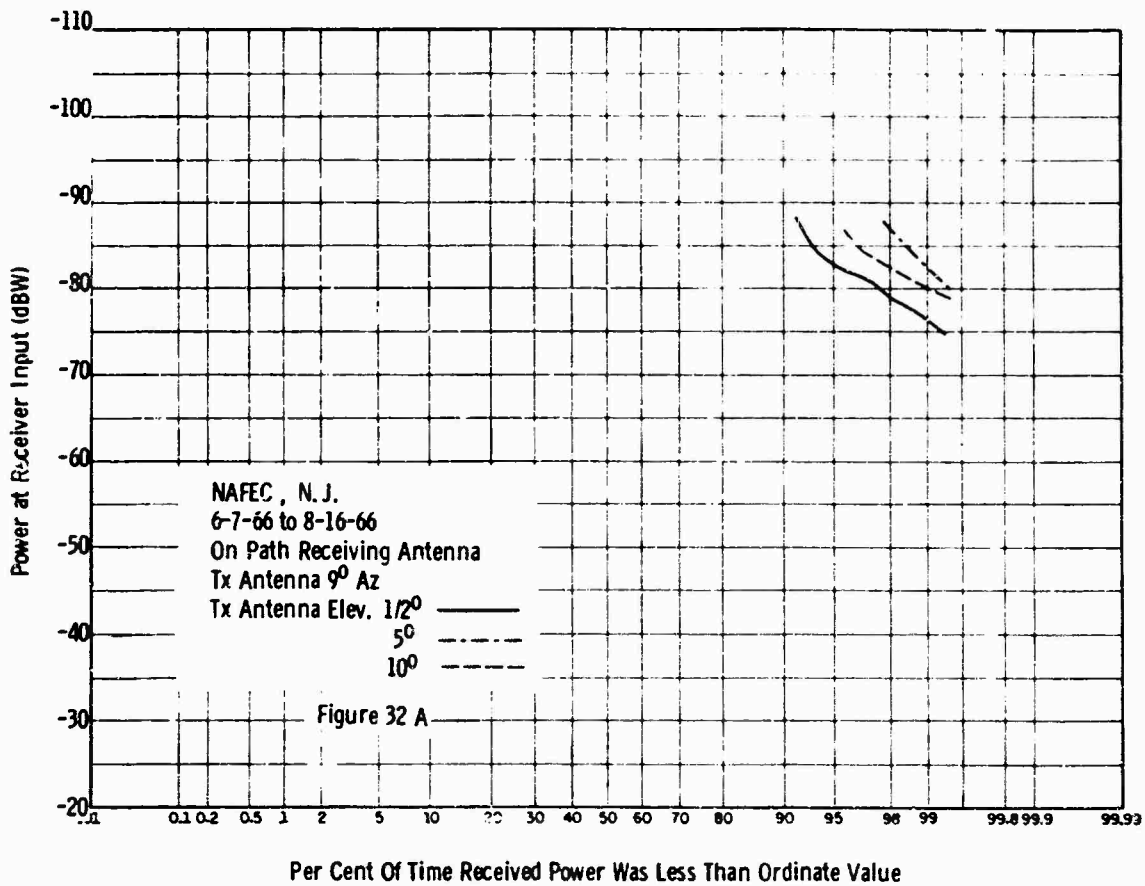


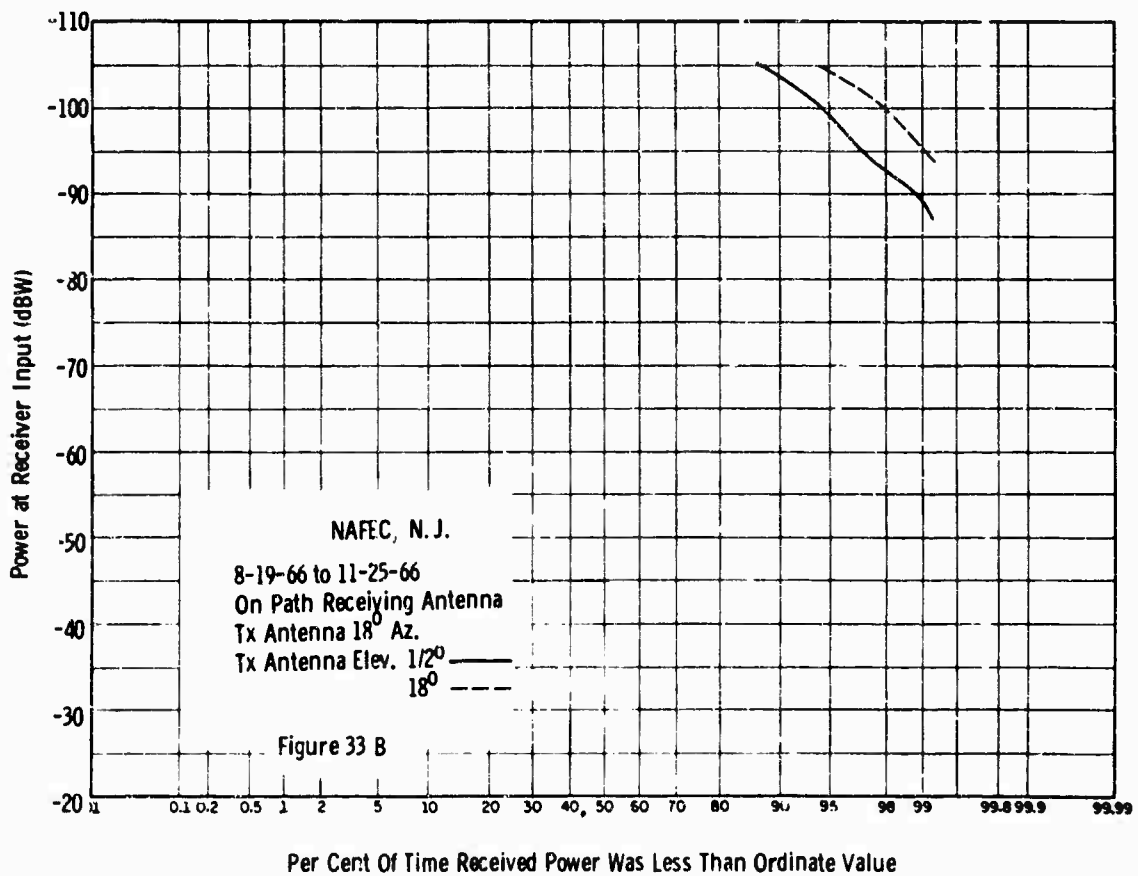
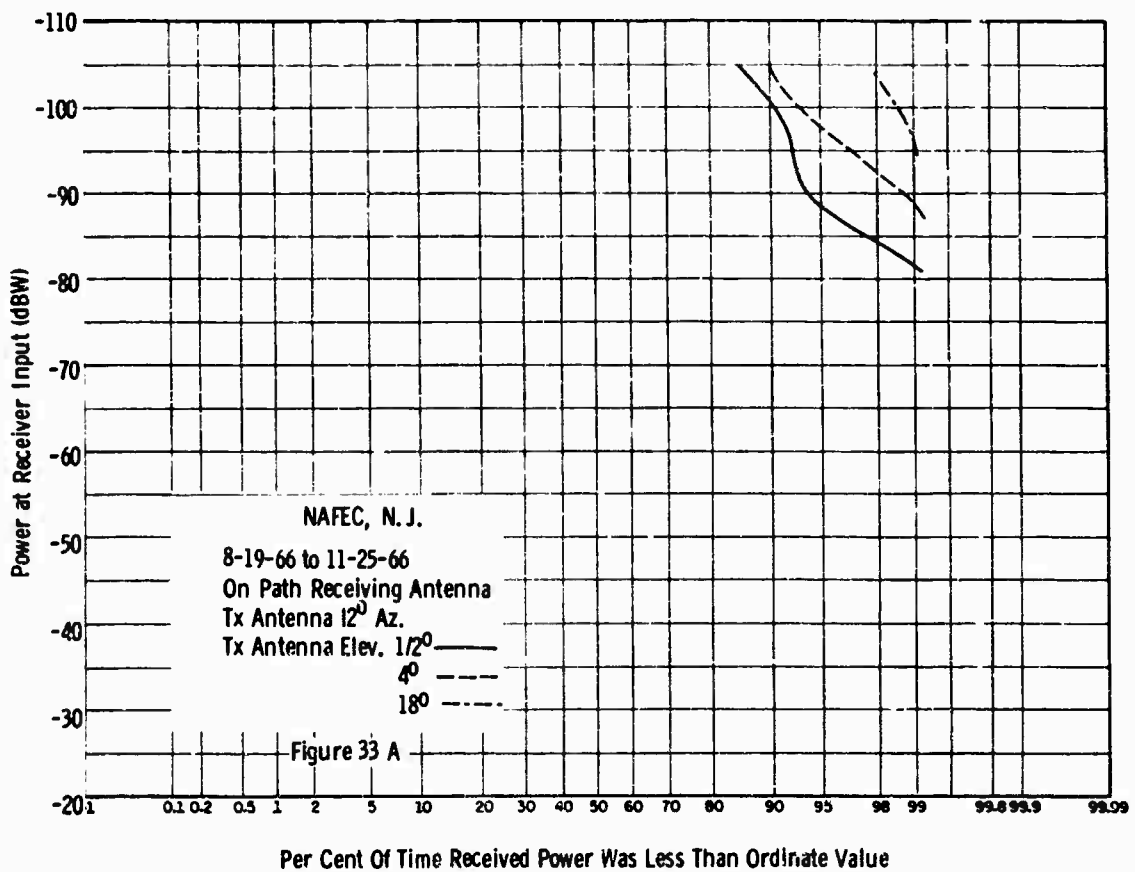


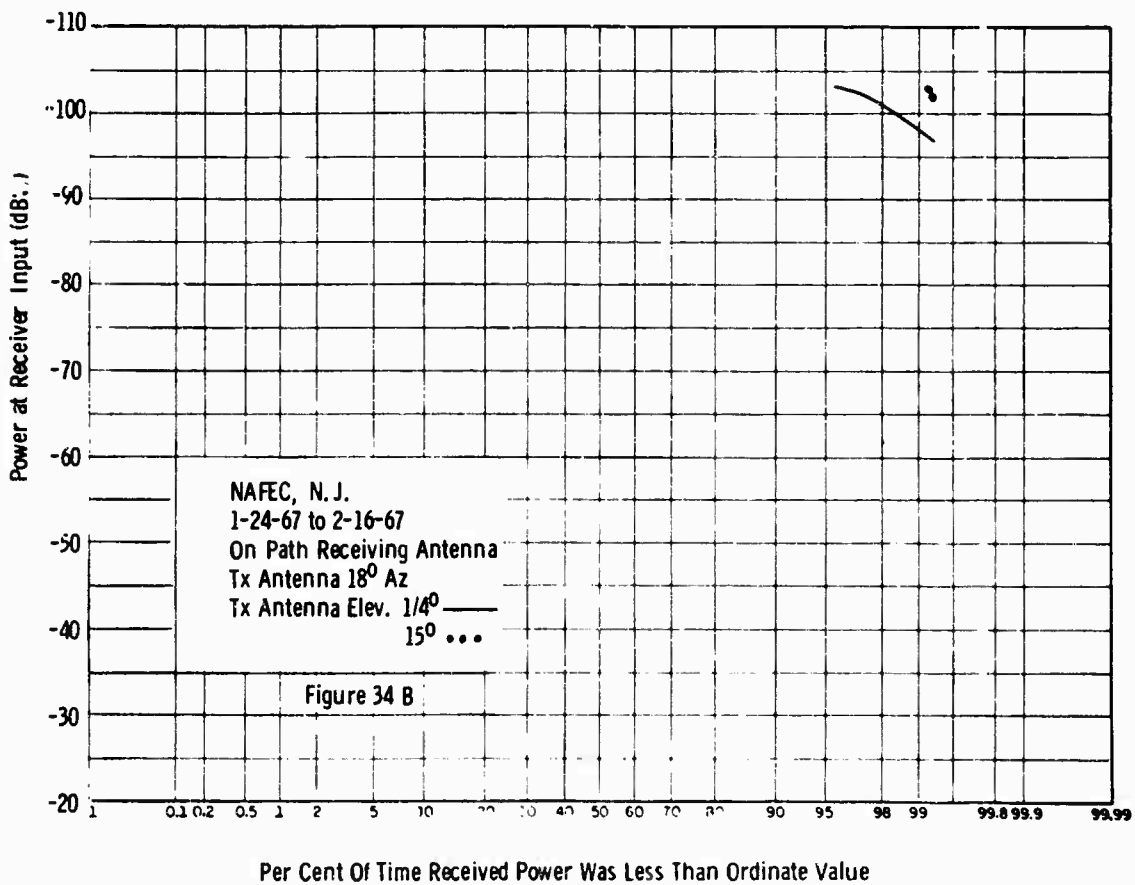
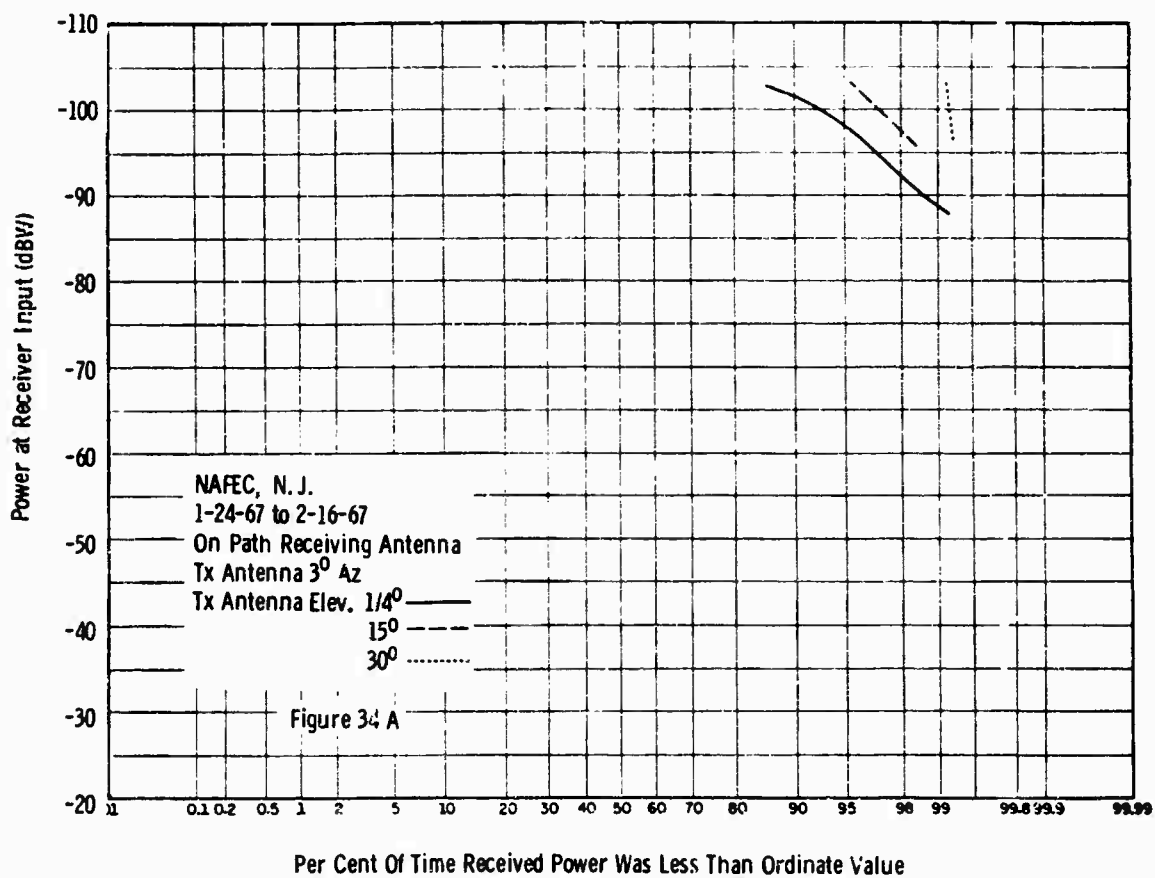


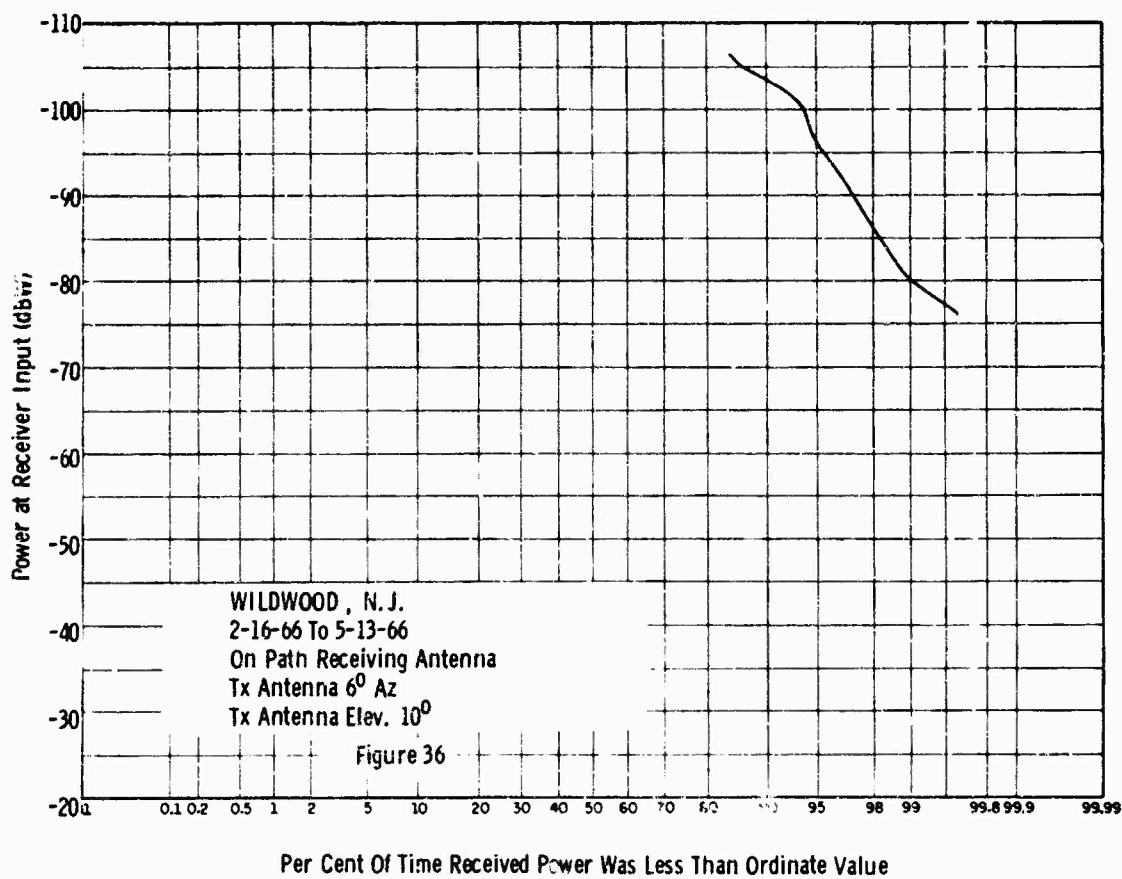
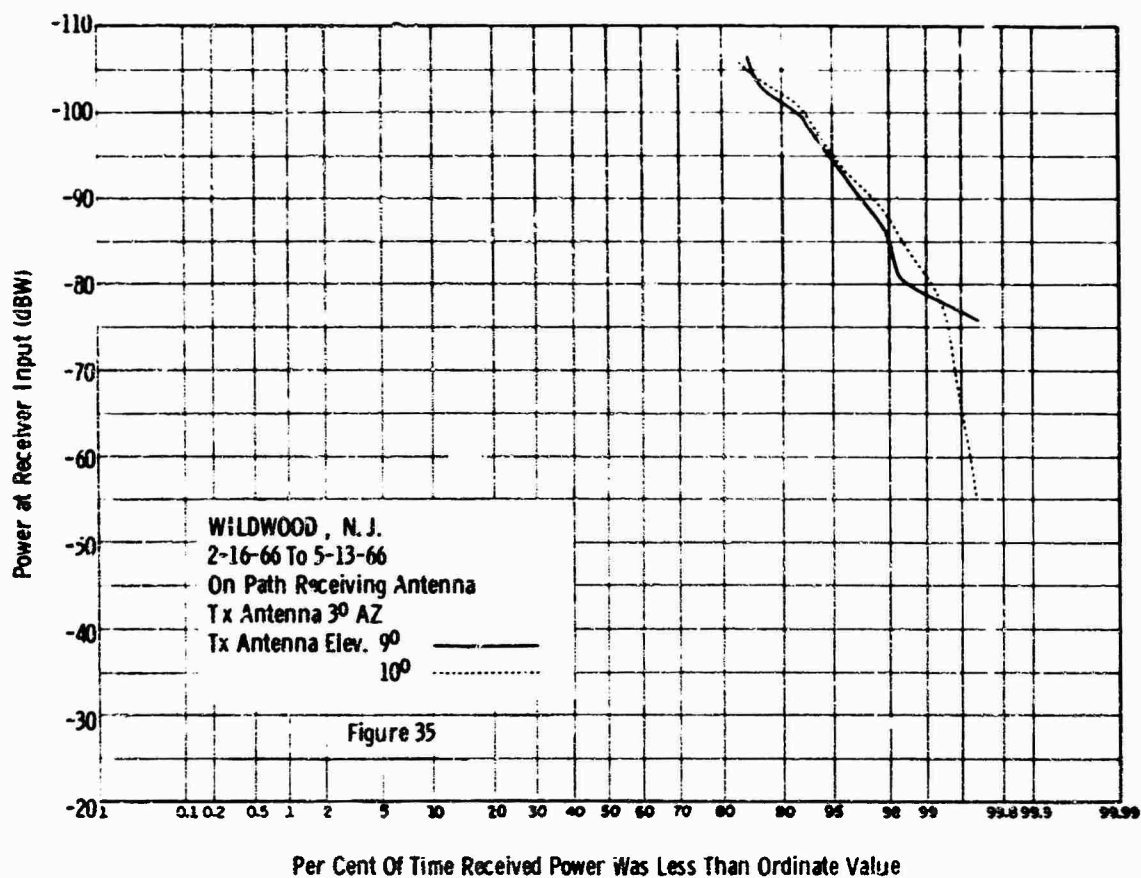


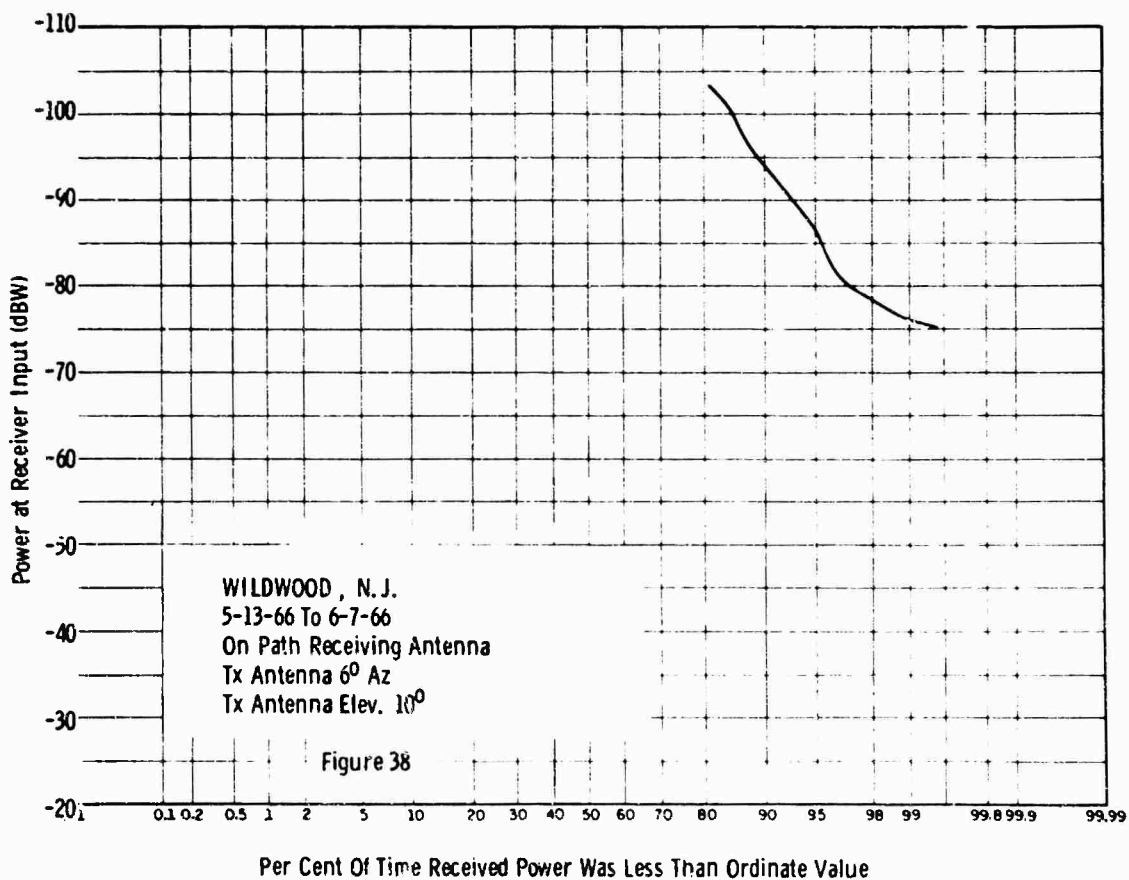
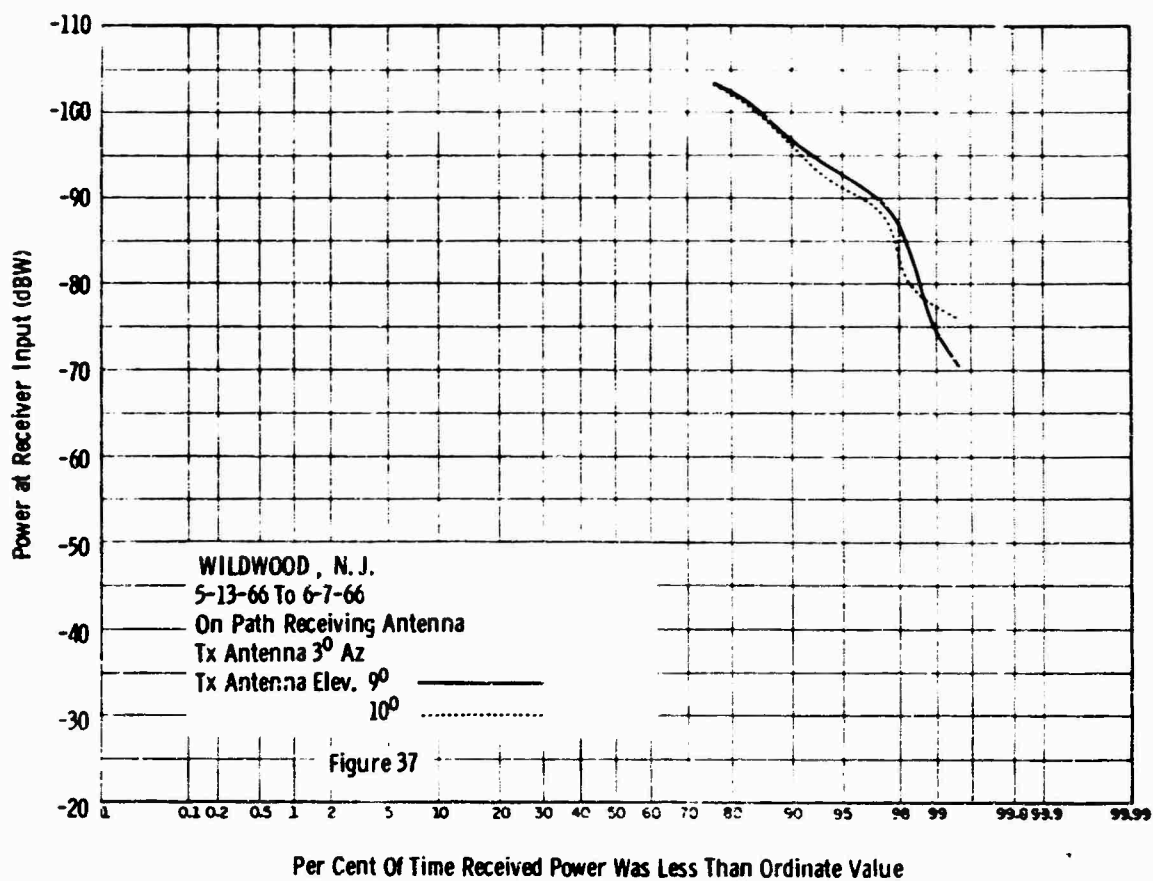


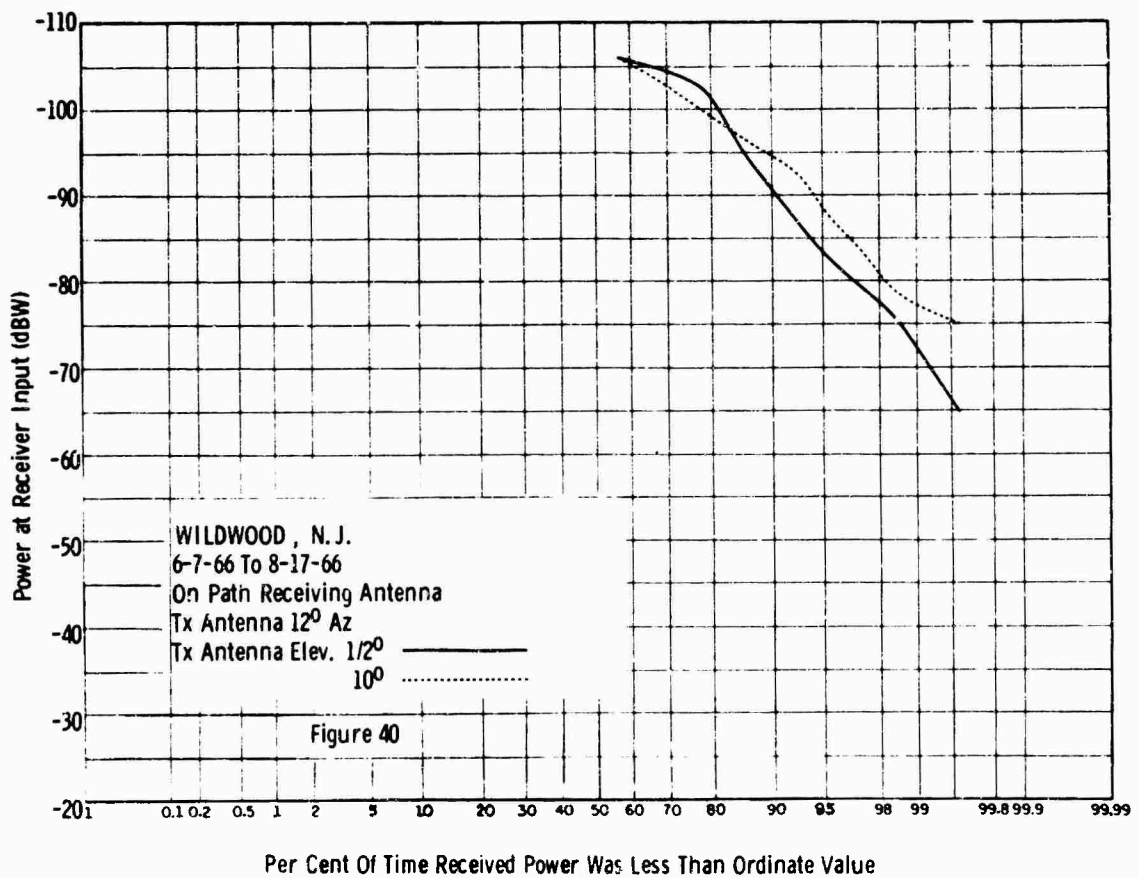
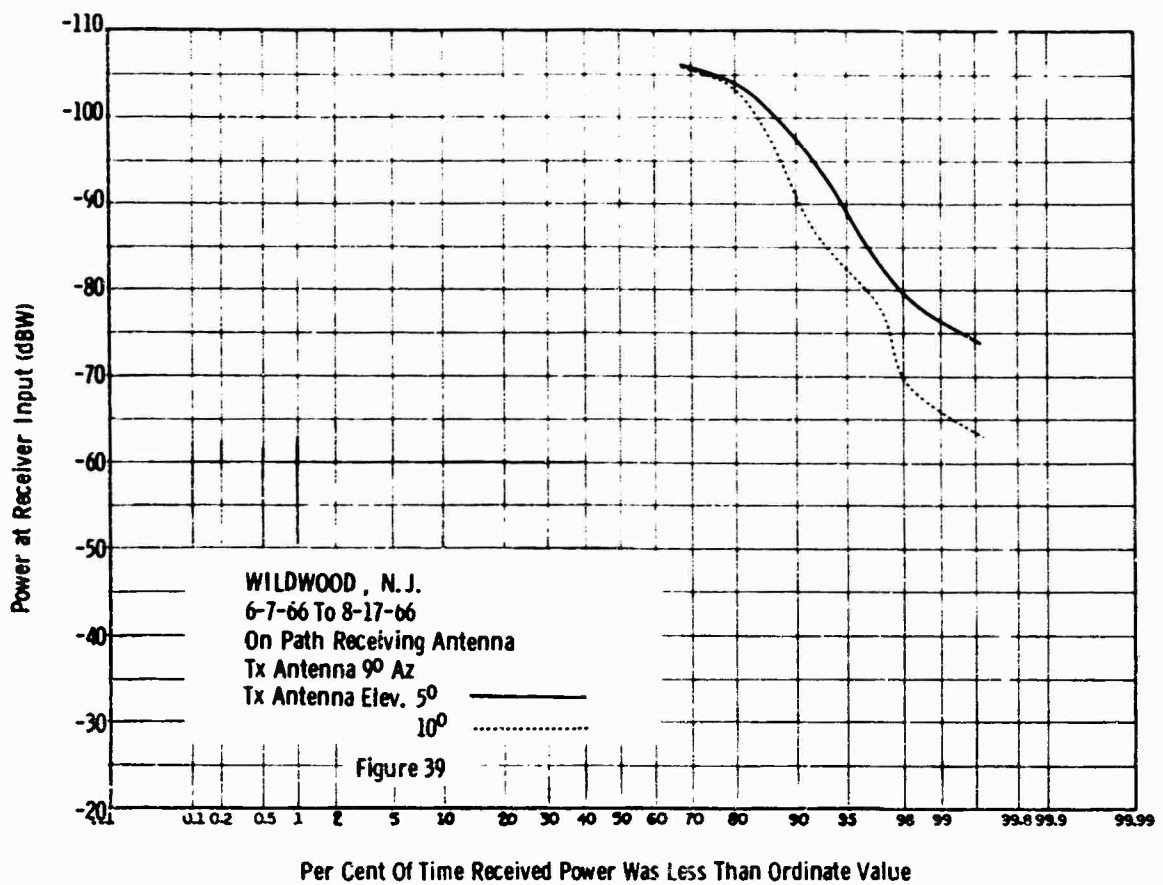


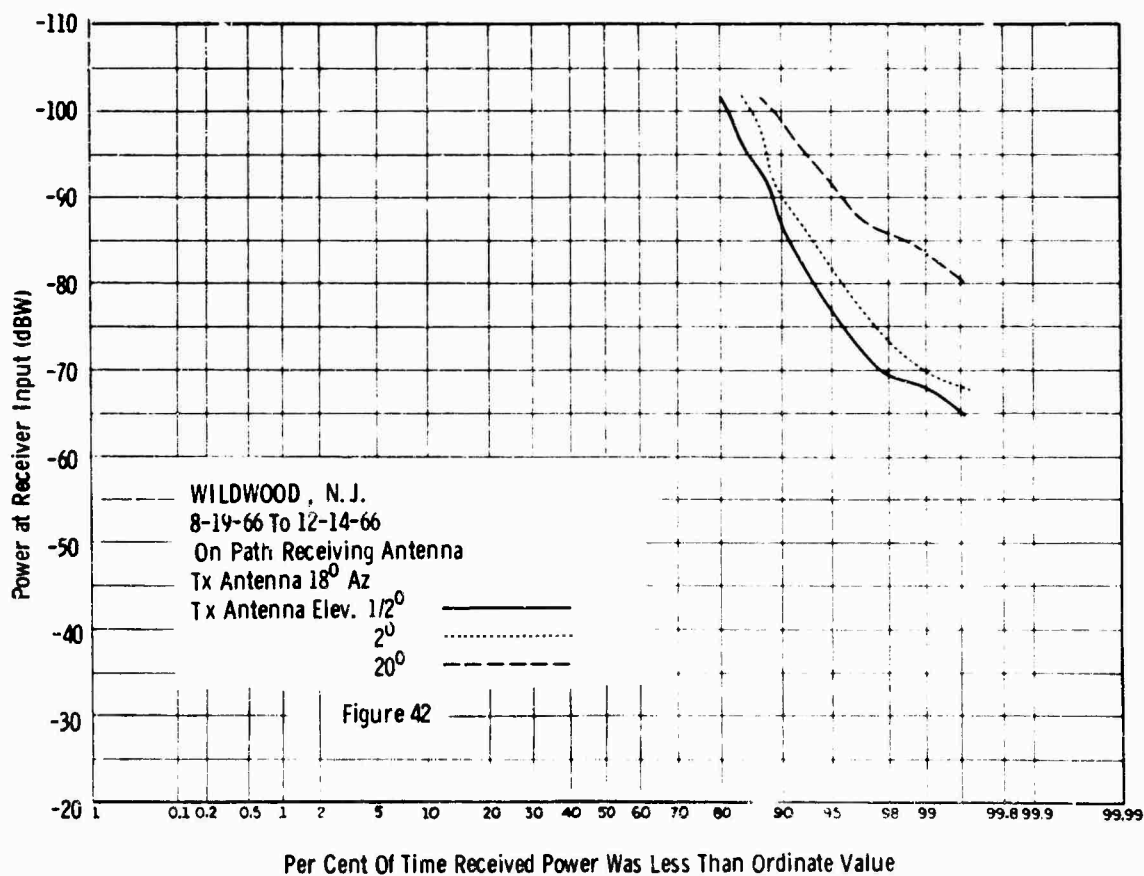
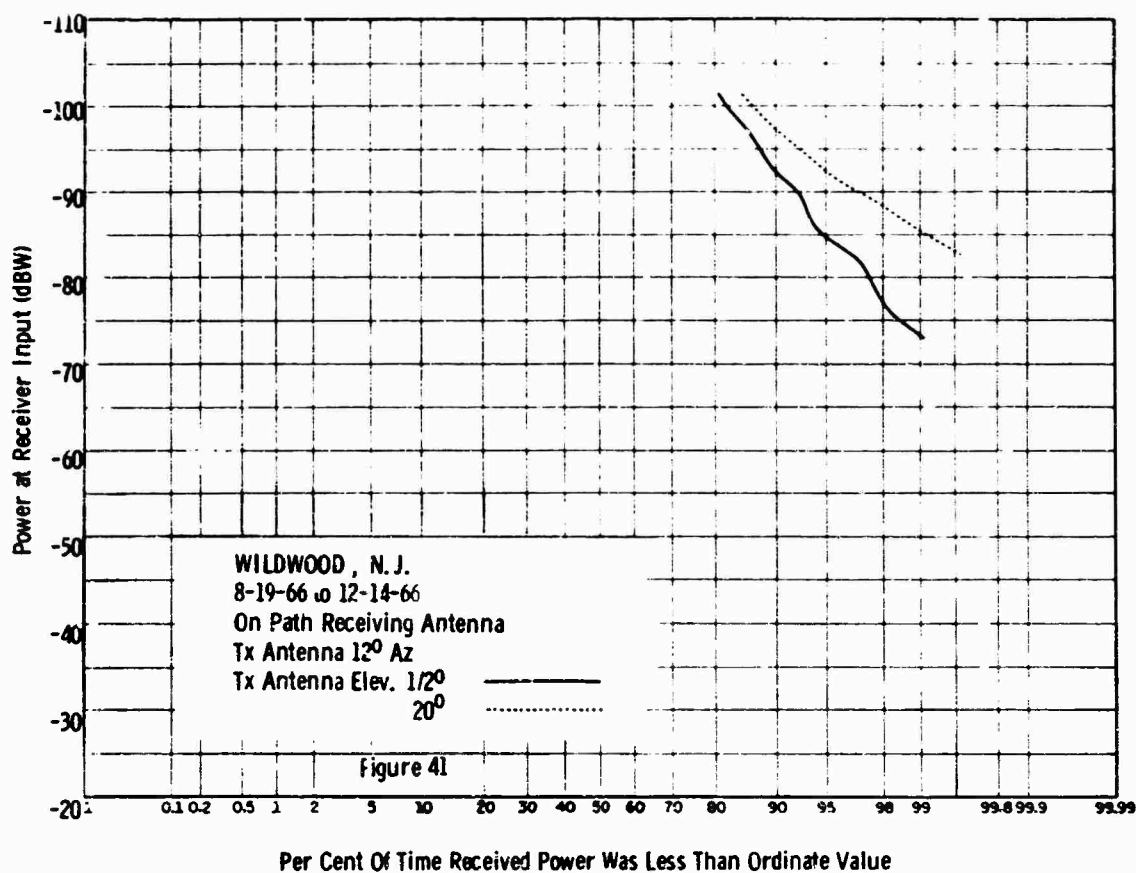


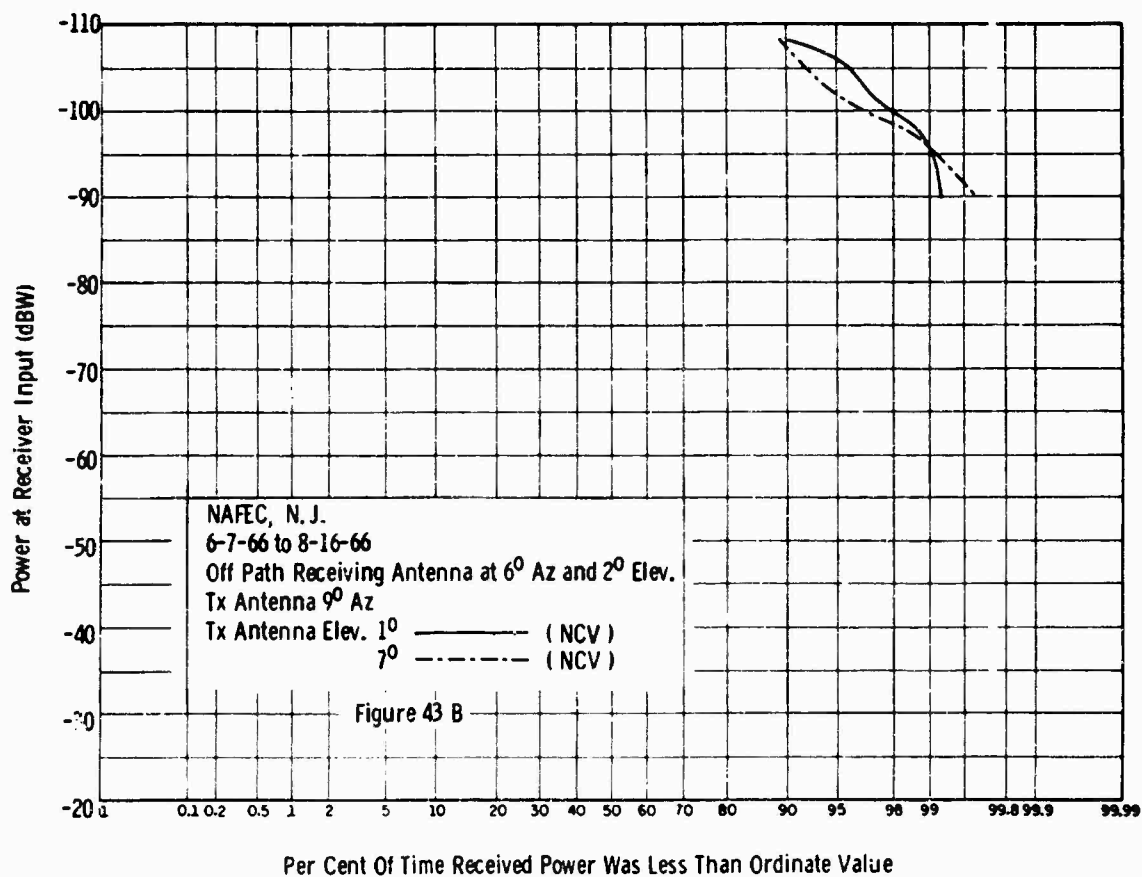
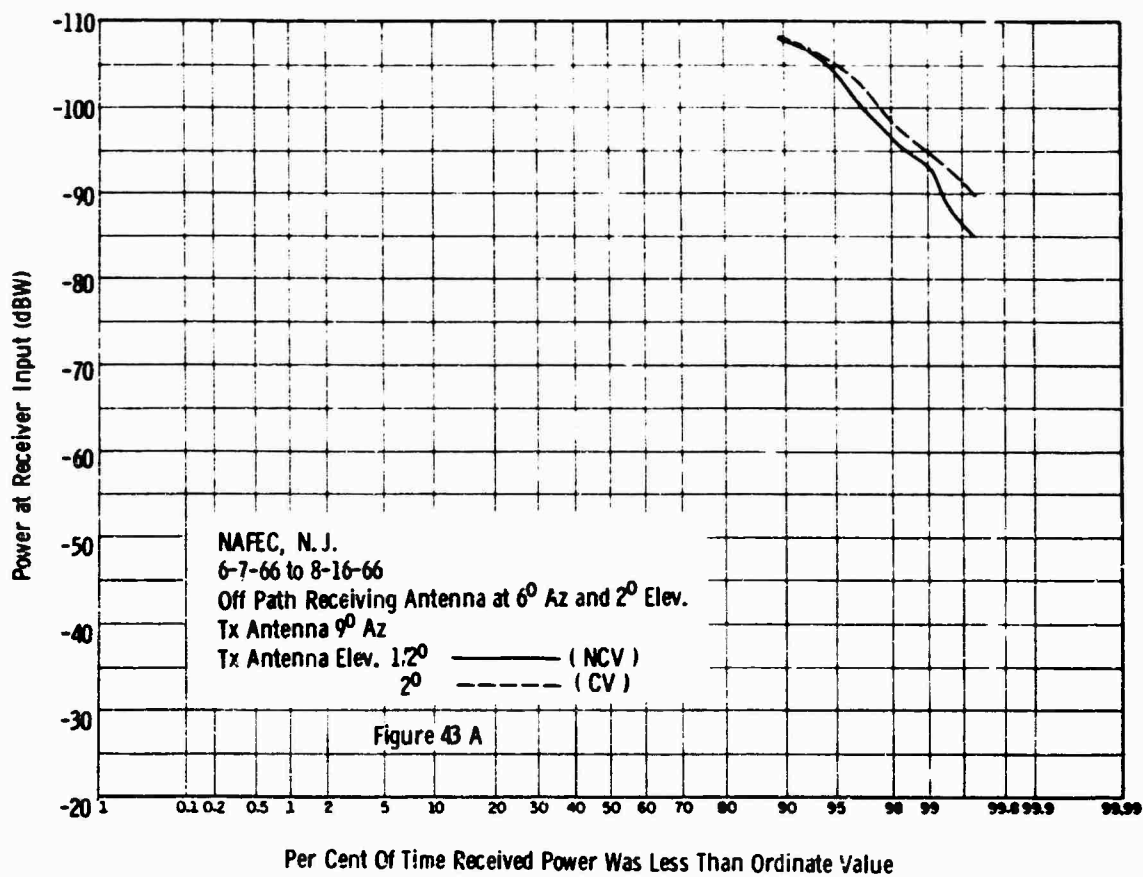


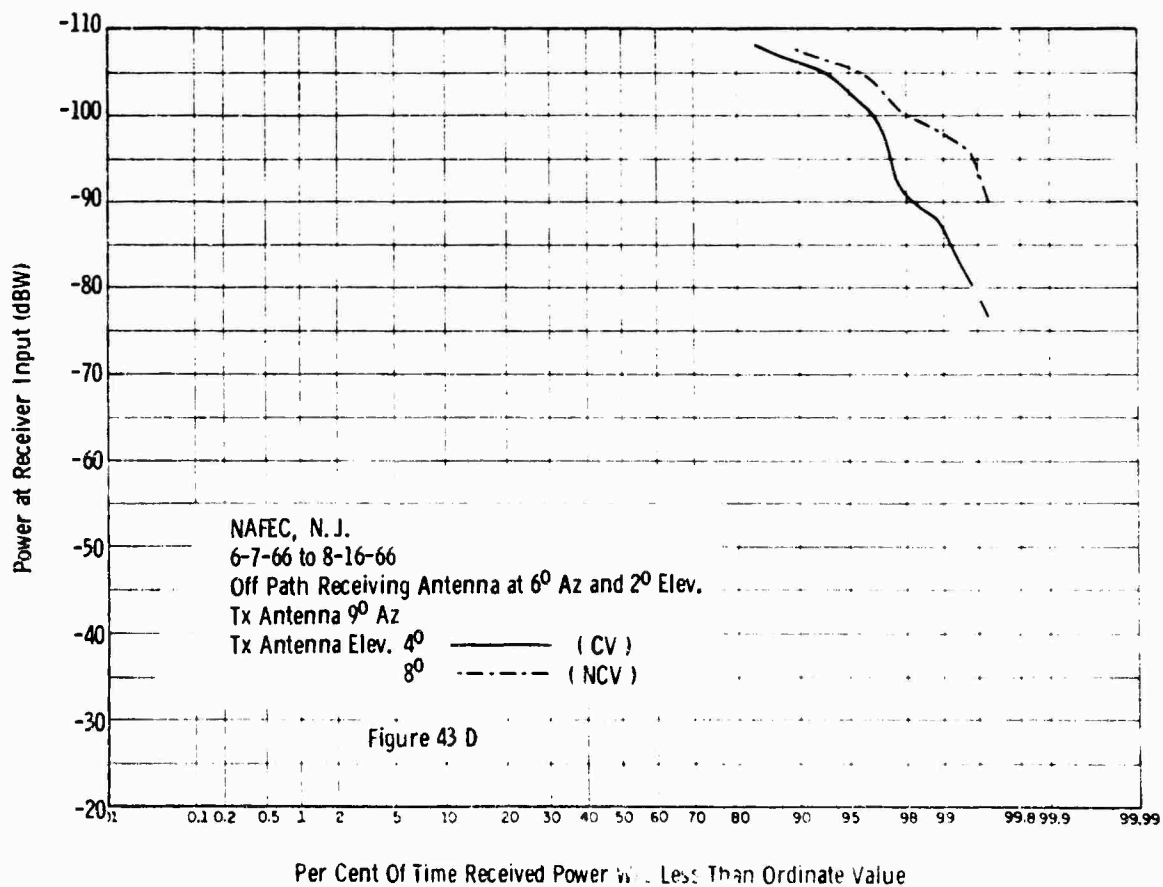
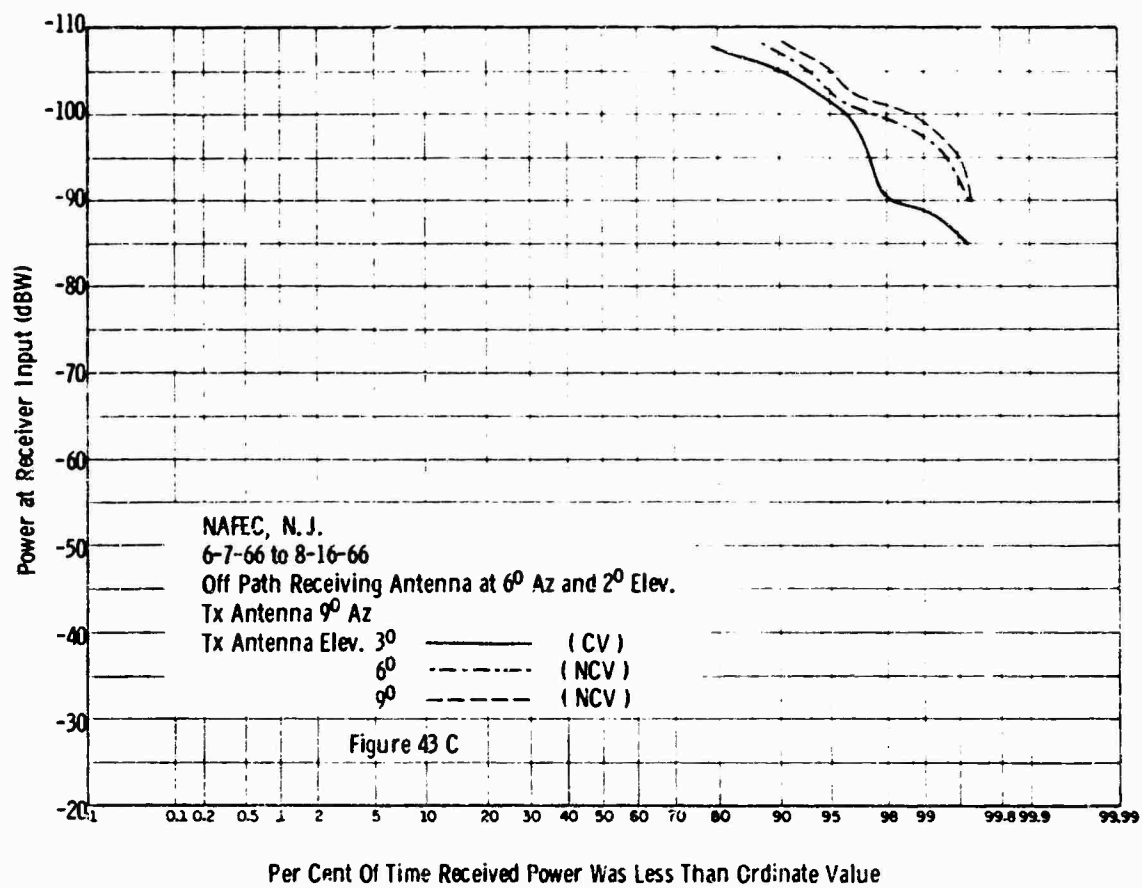


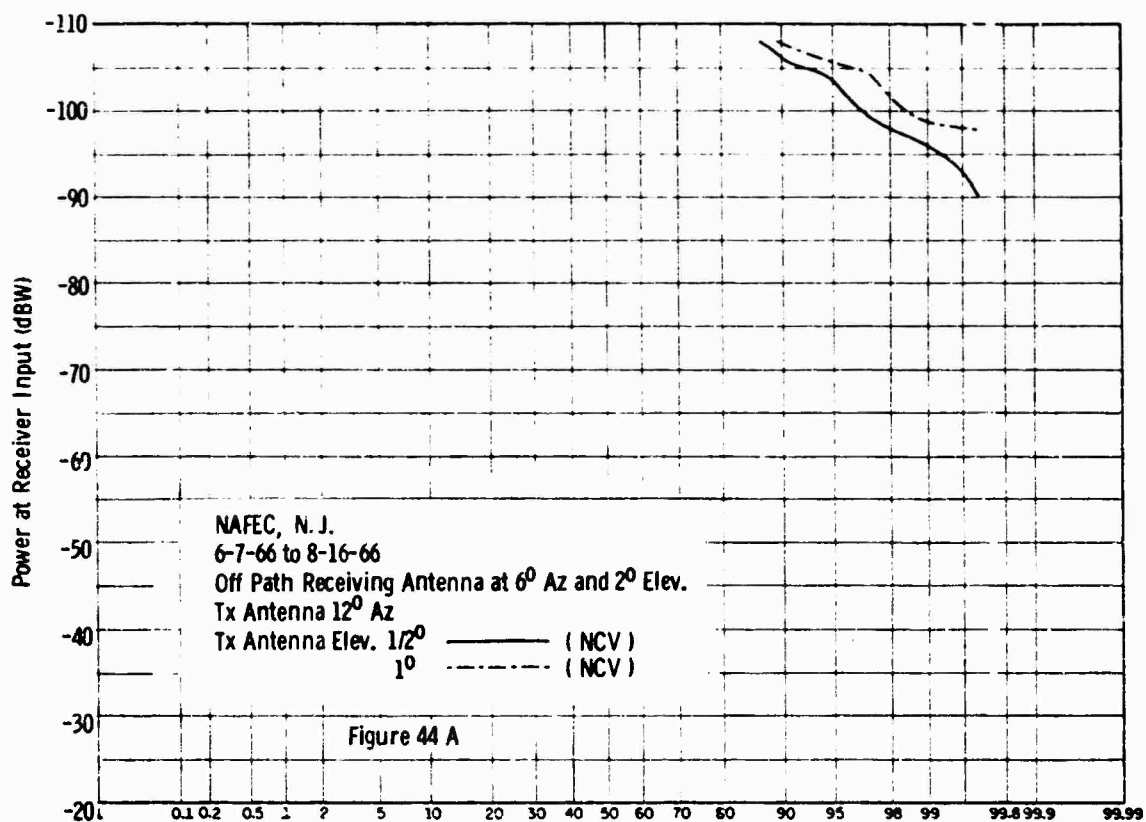




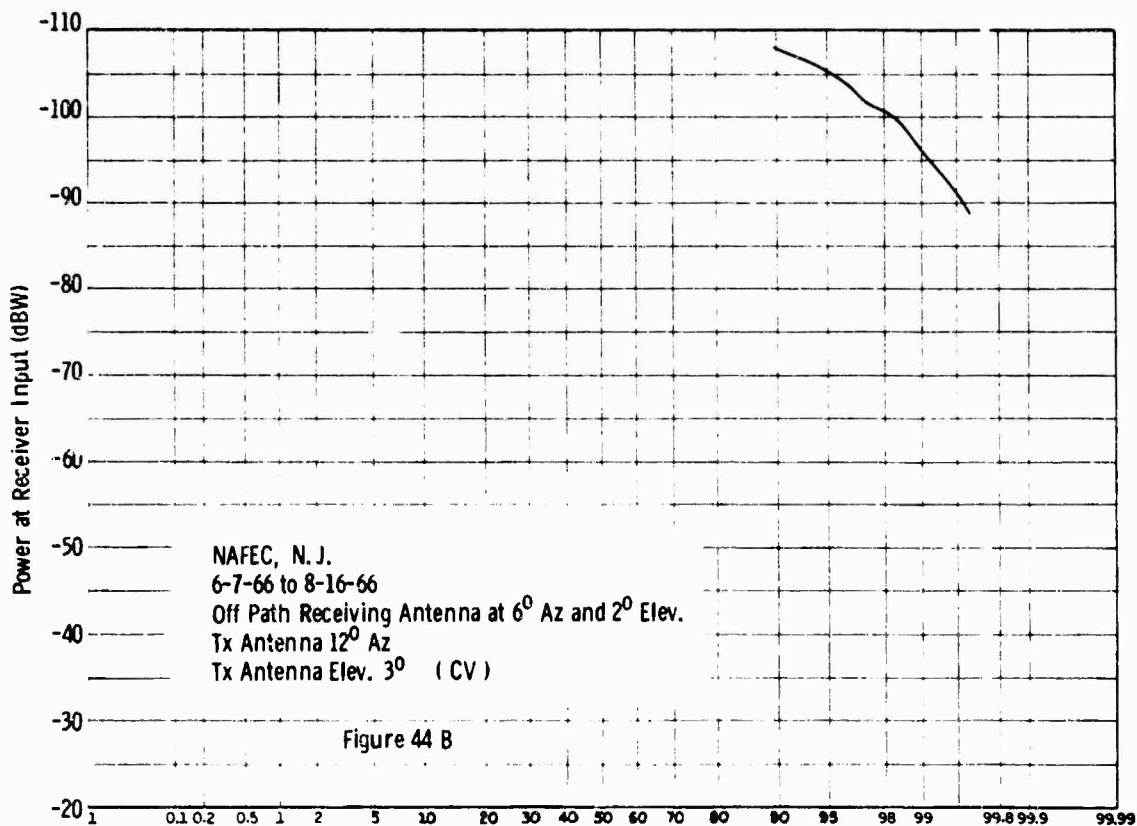




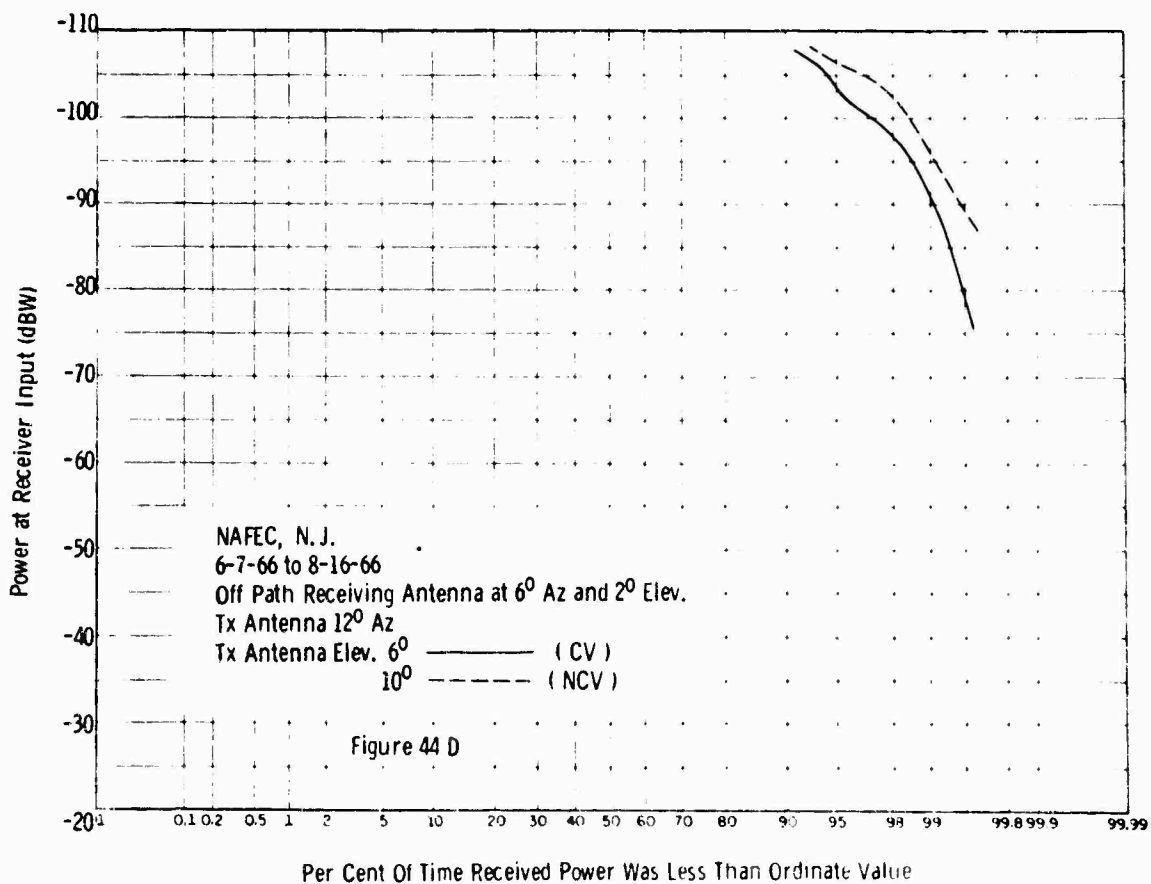
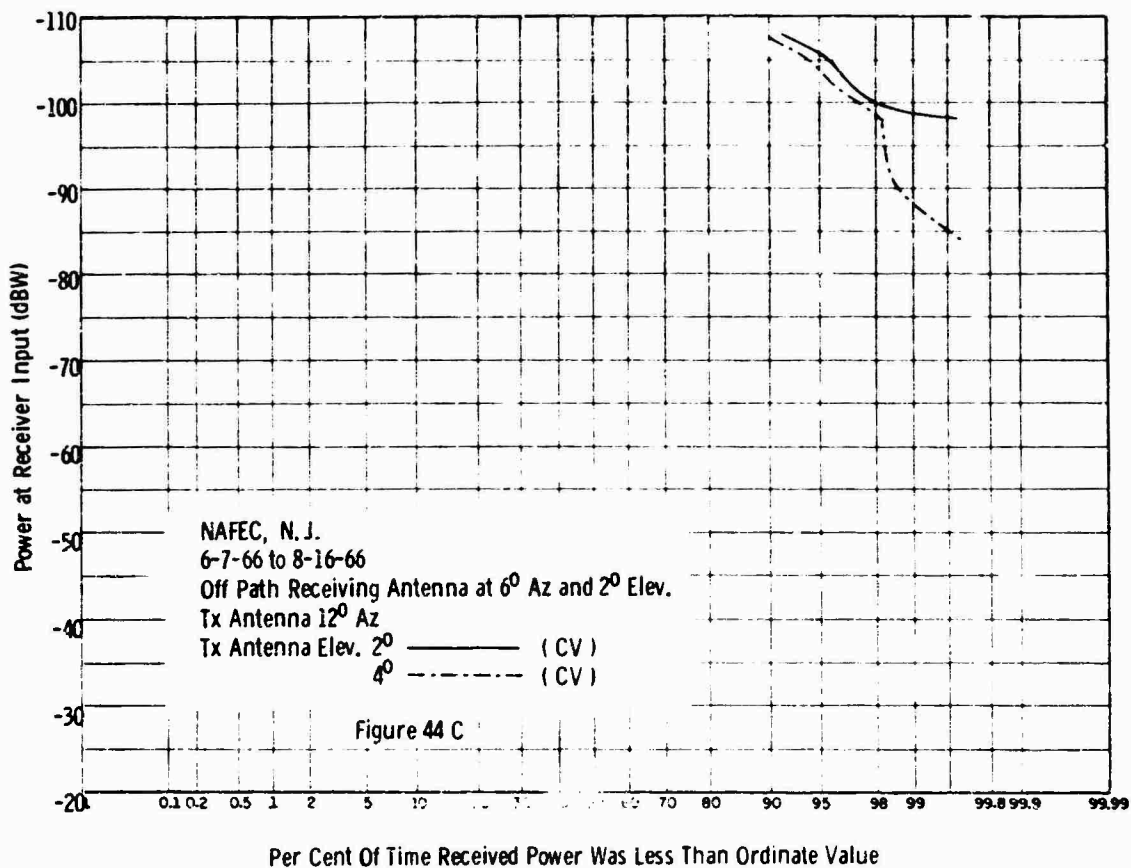


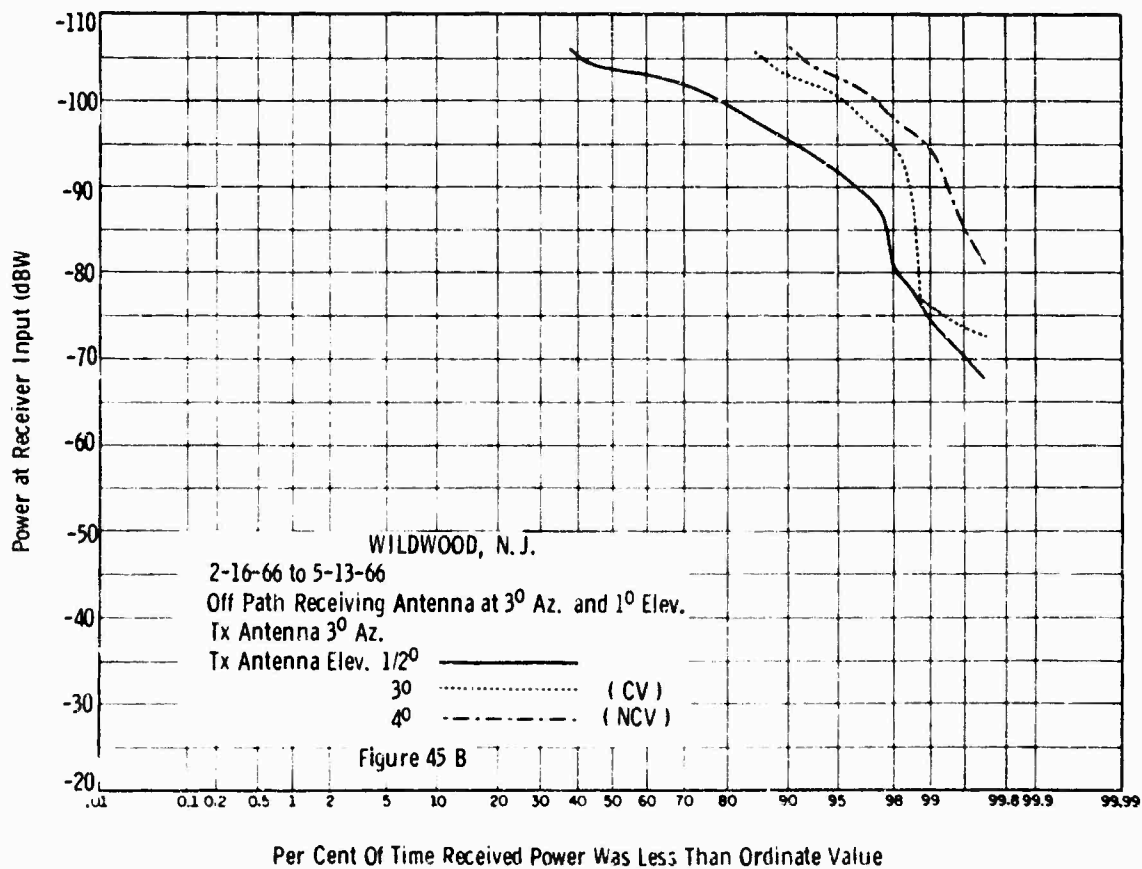
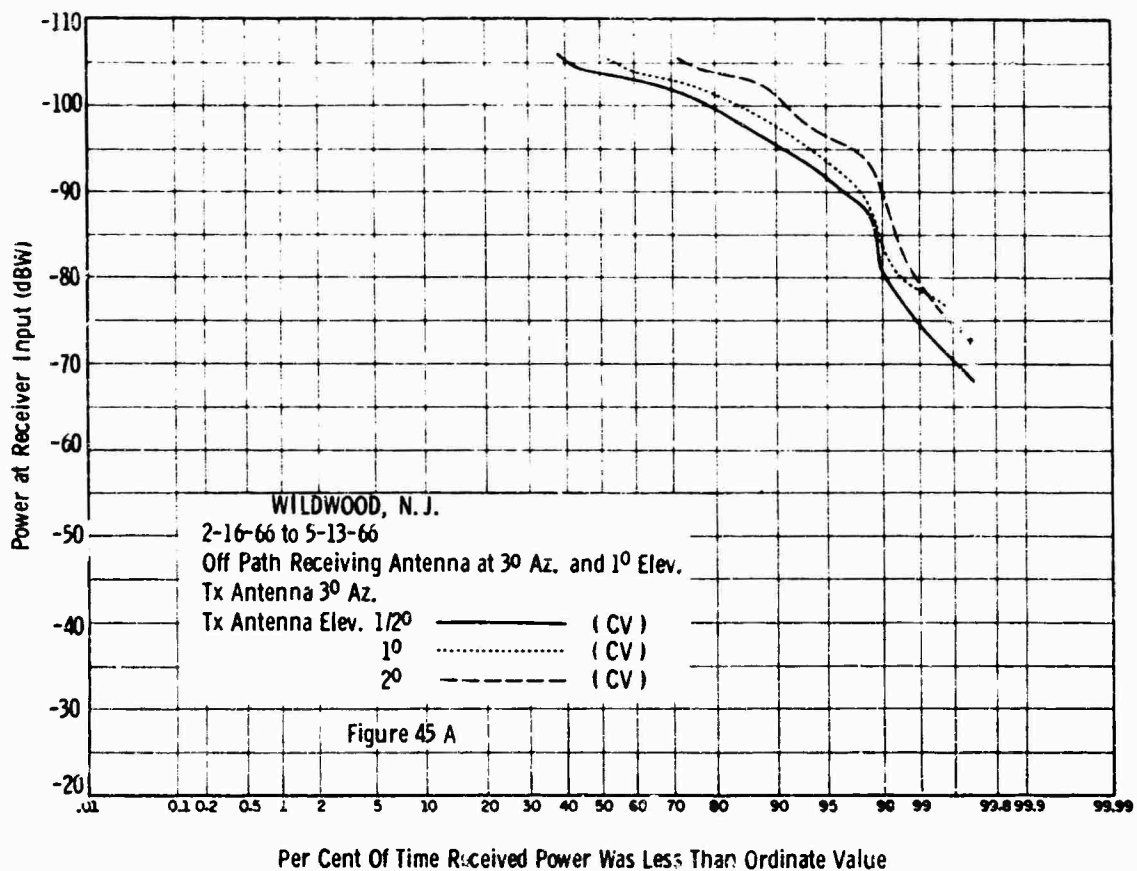


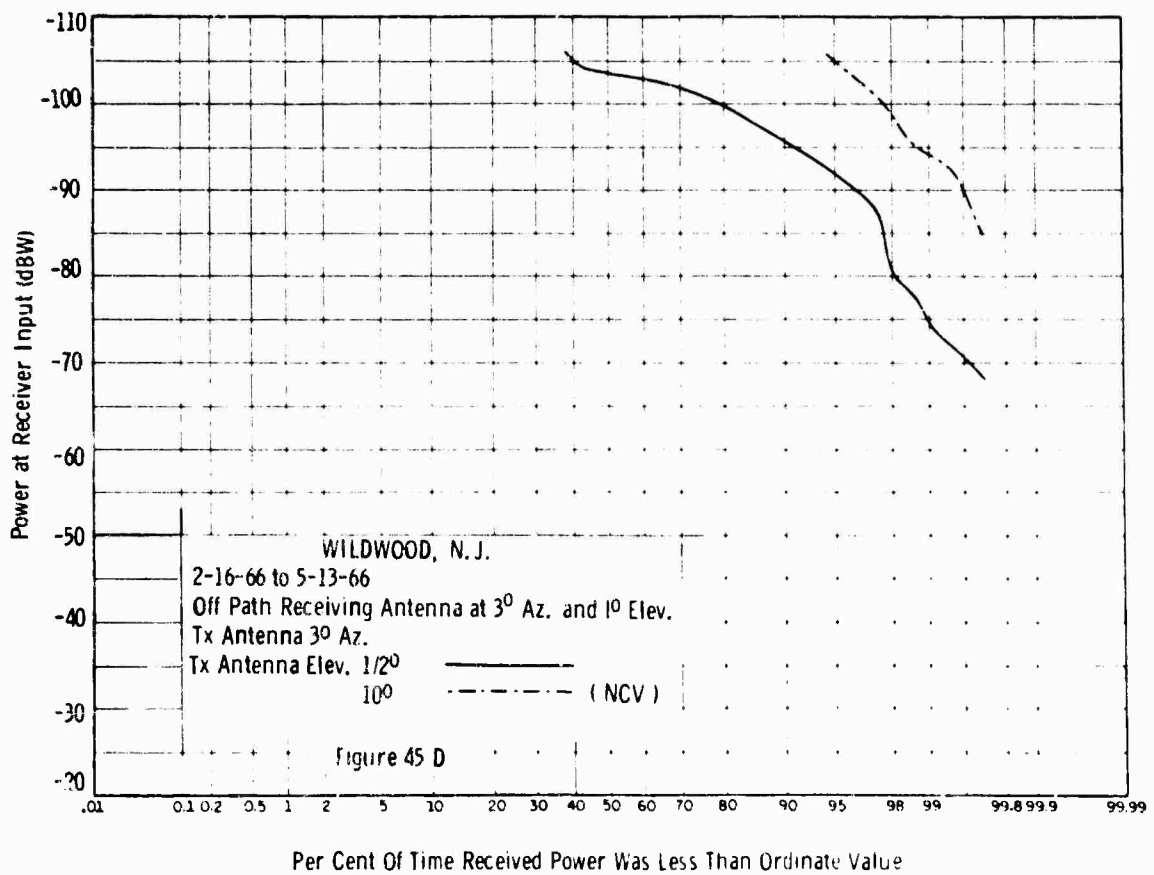
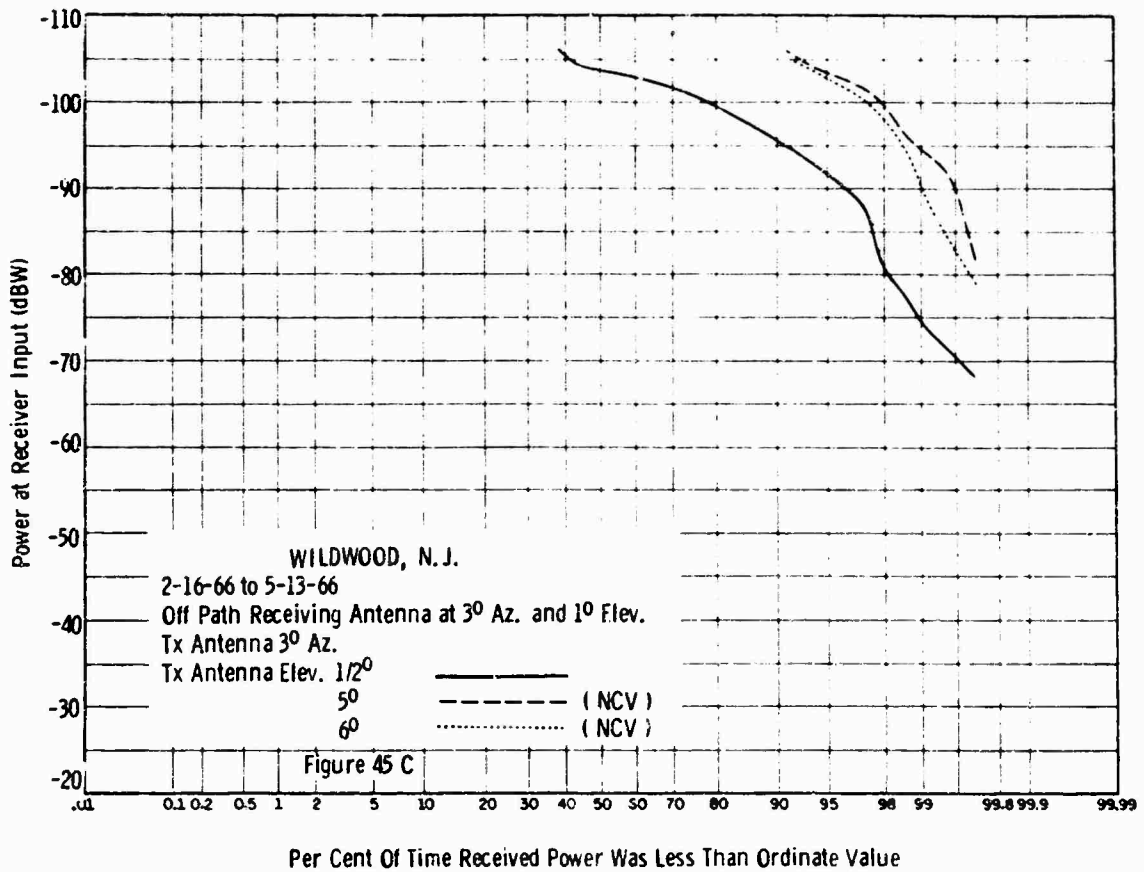
Per Cent Of Time Received Power Was Less Than Ordinate Value

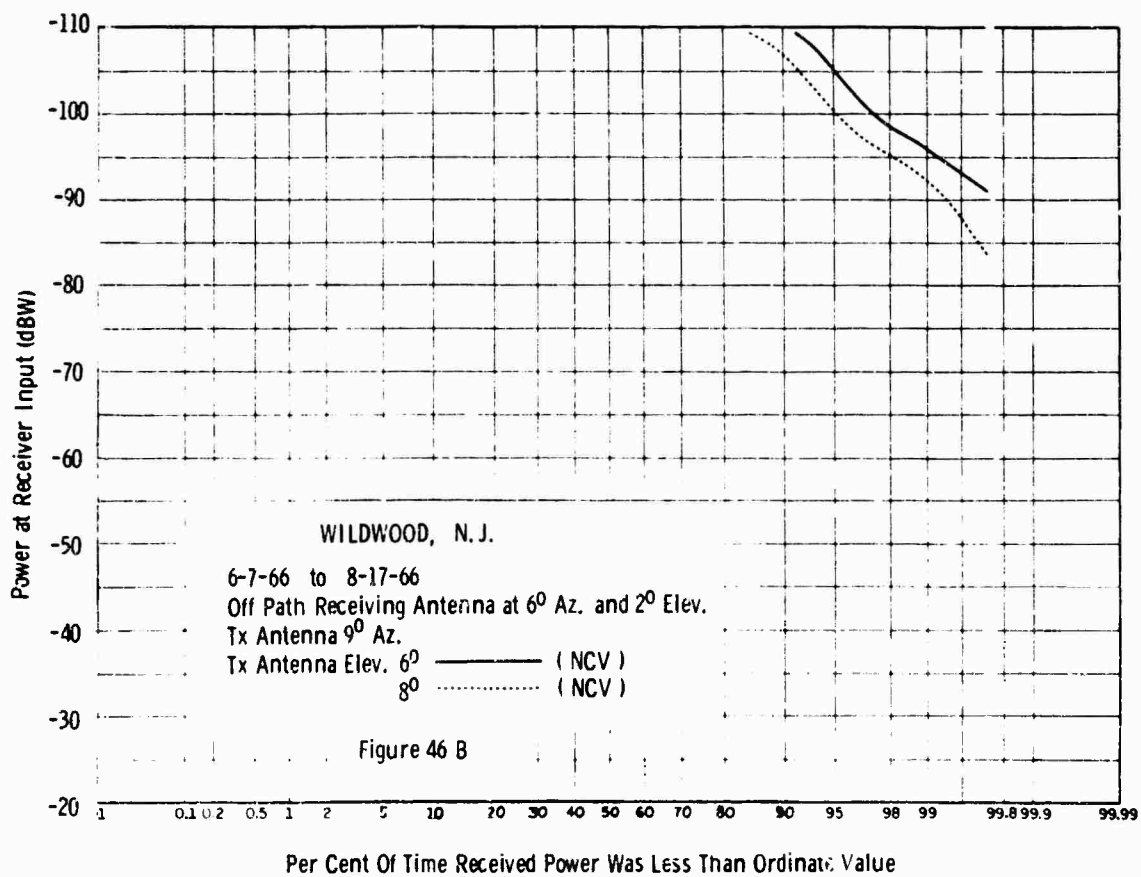
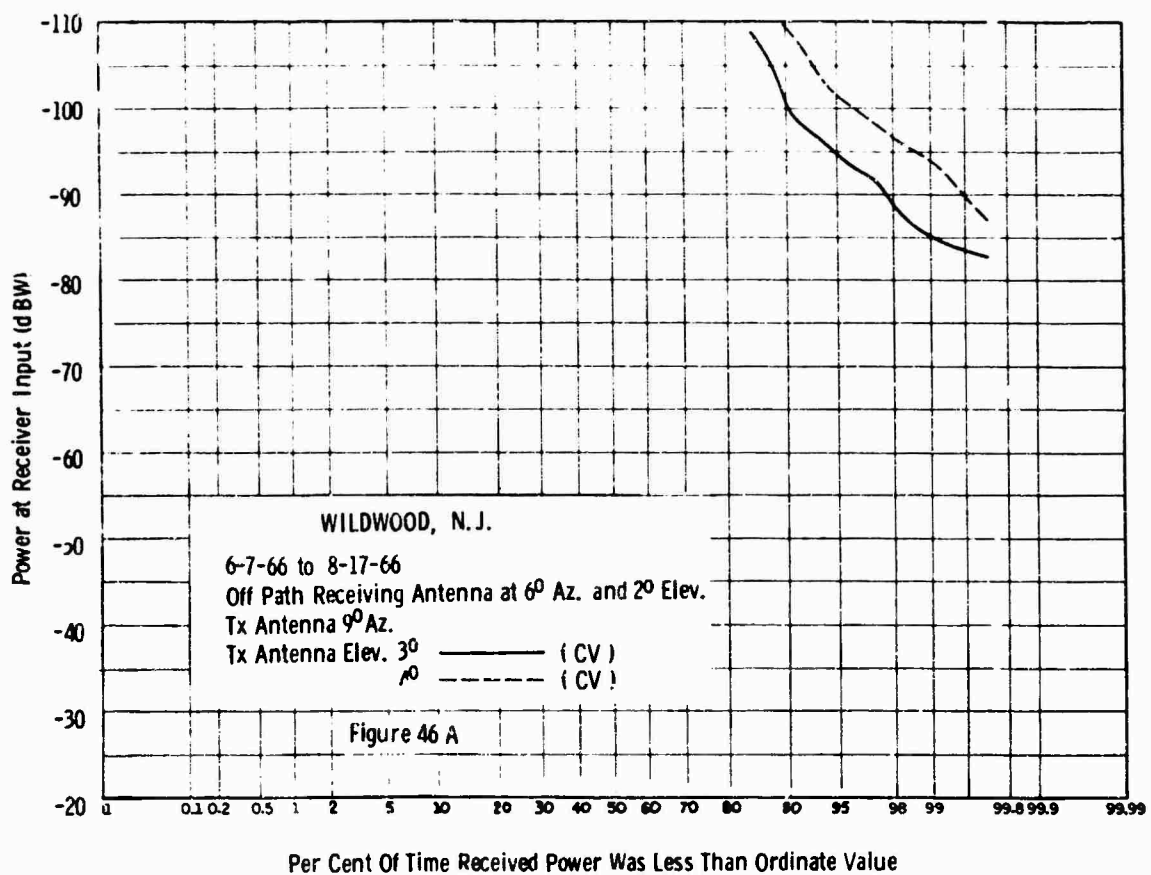


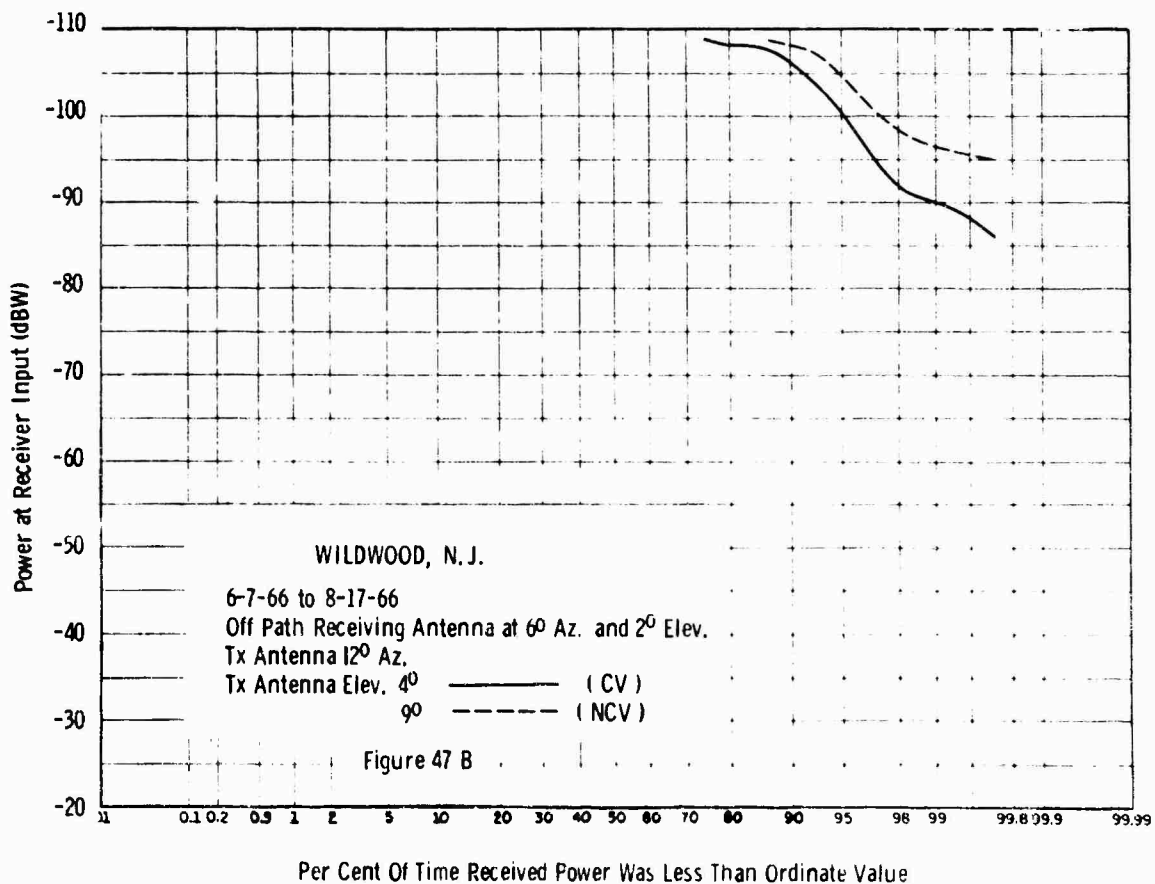
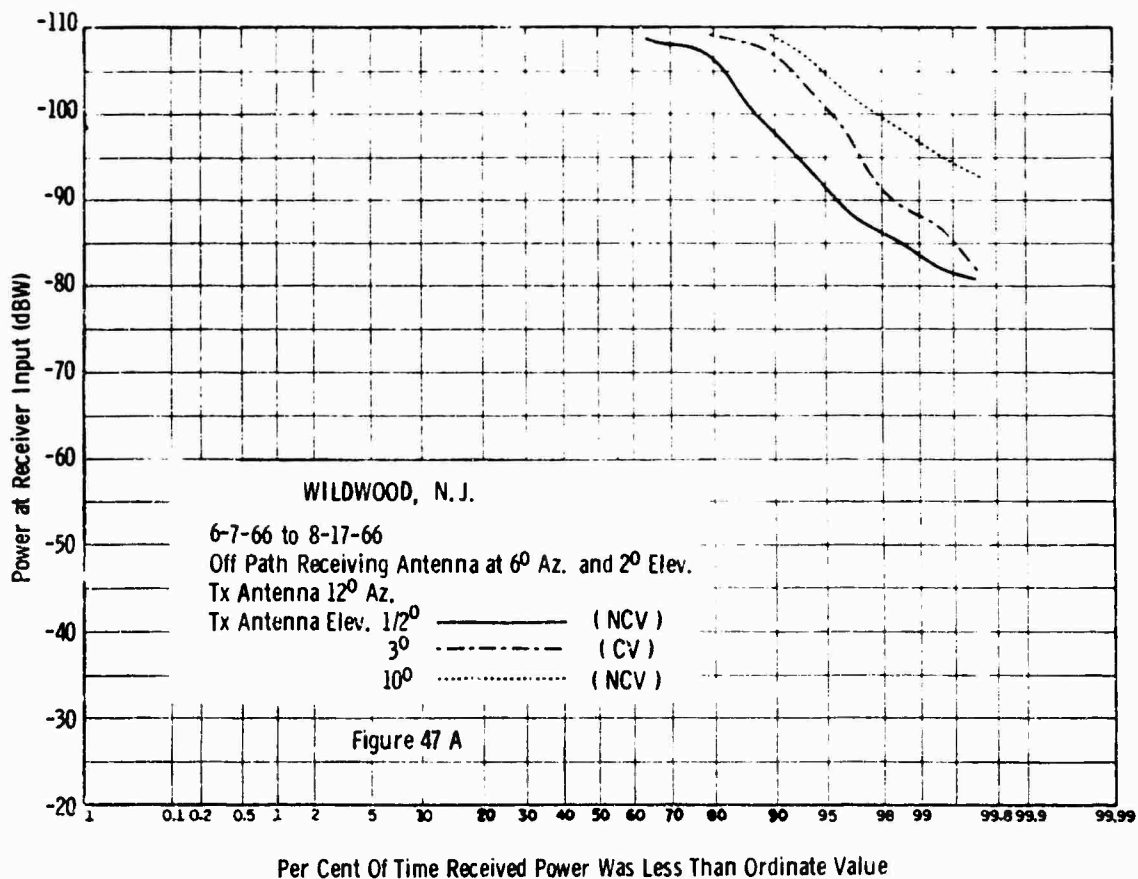
Per Cent Of Time Received Power Was Less Than Ordinate Value

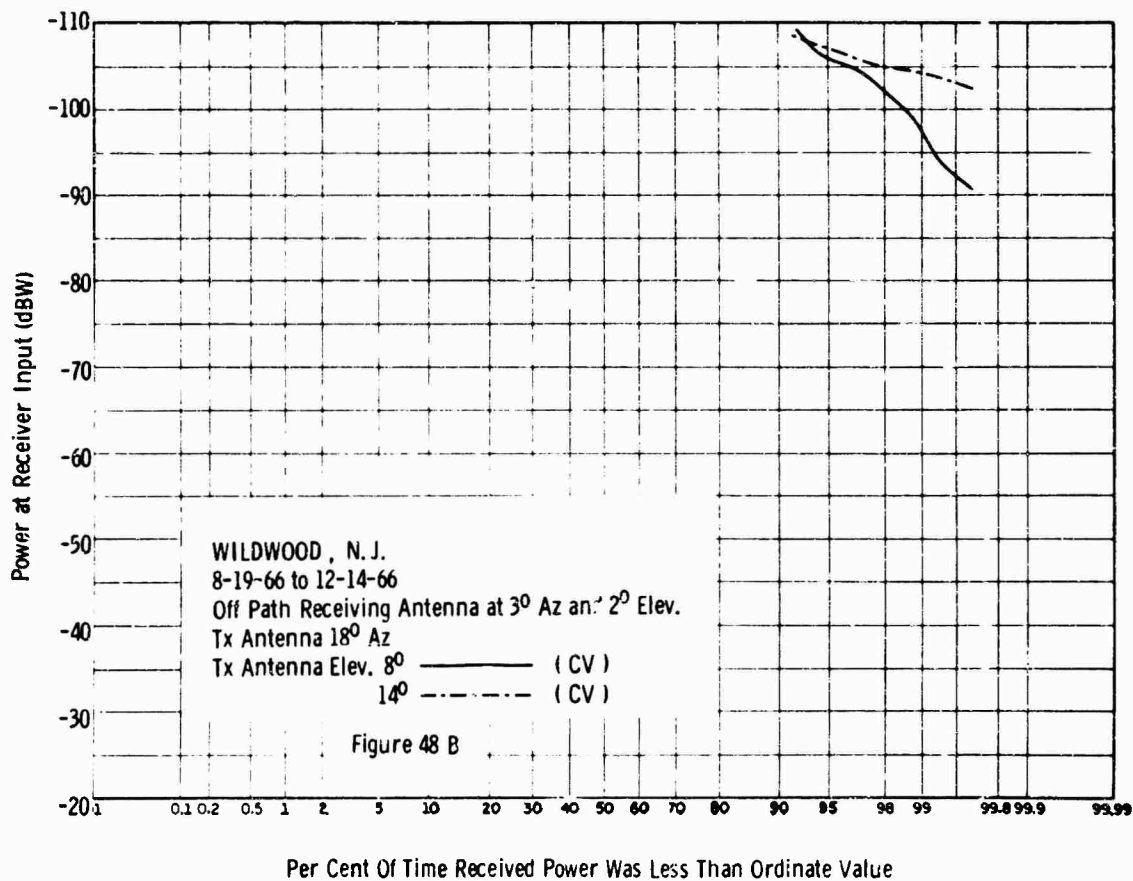
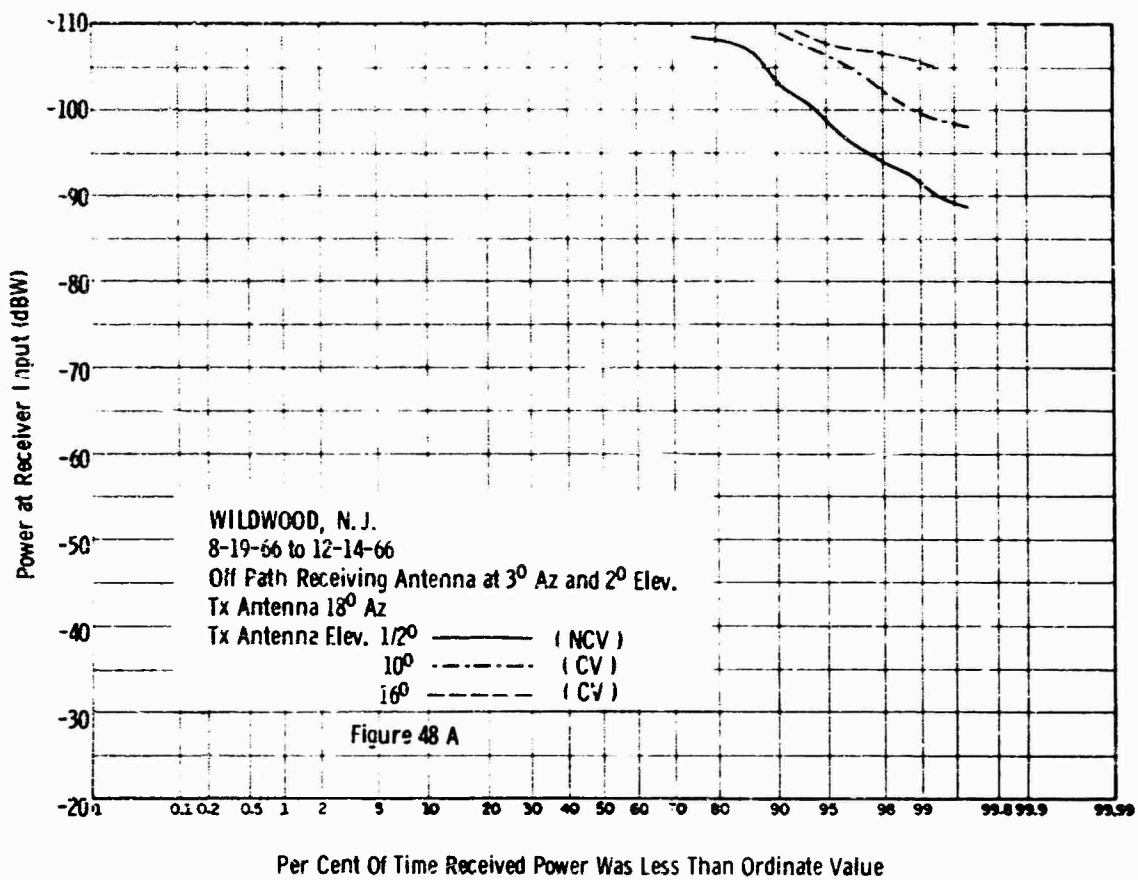


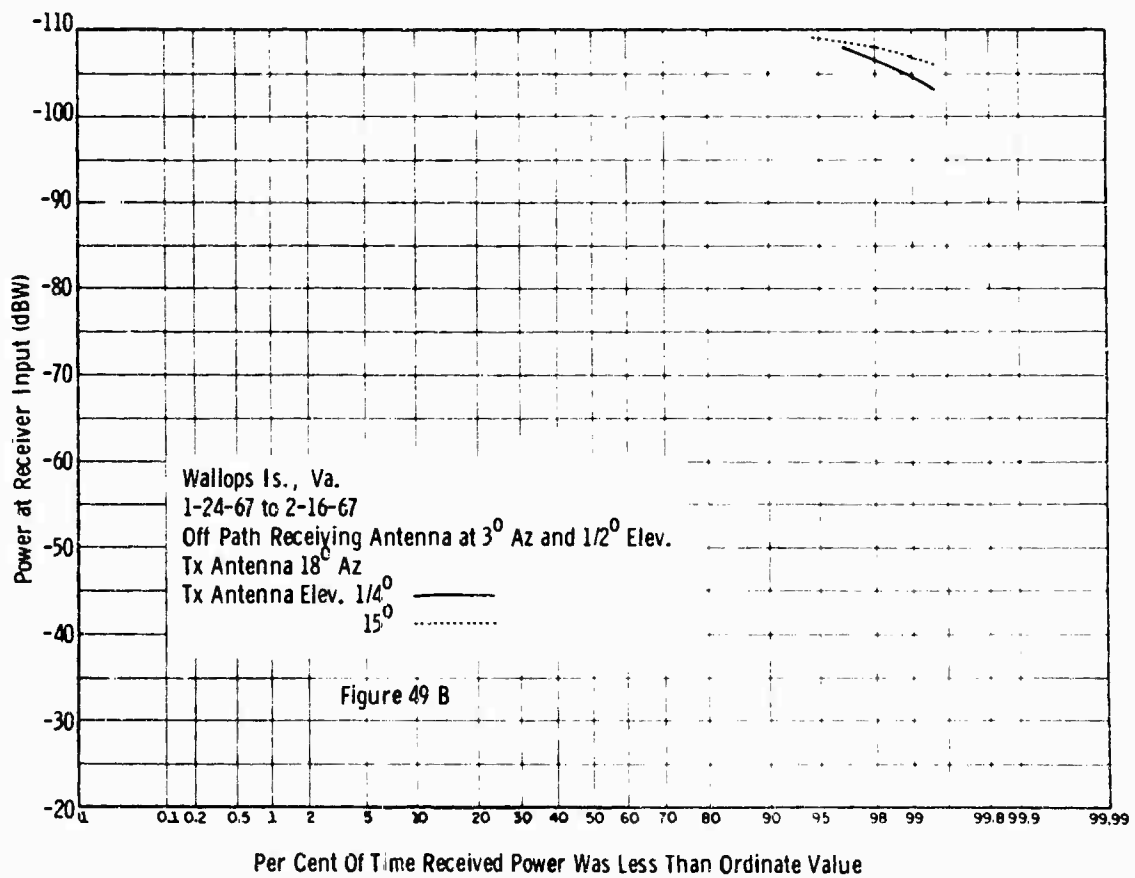
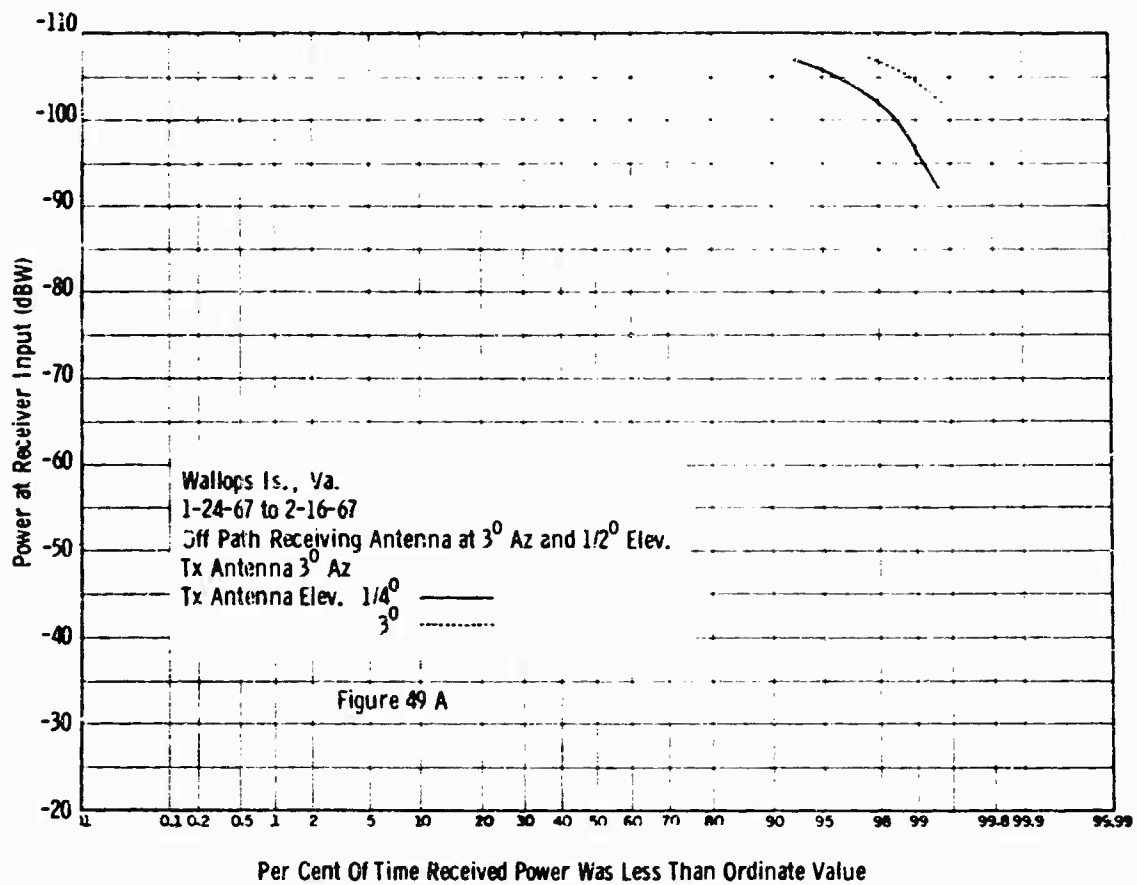












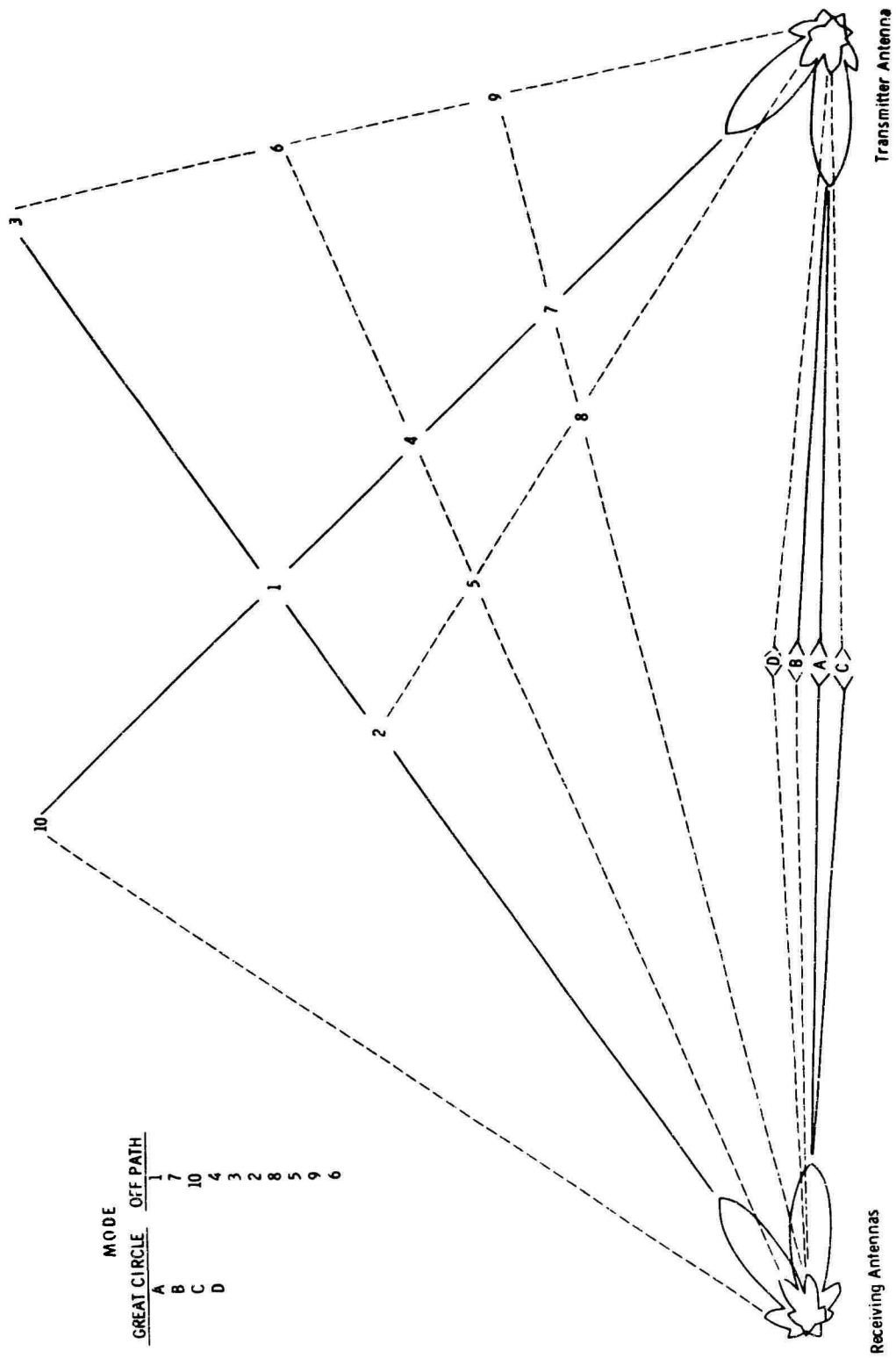
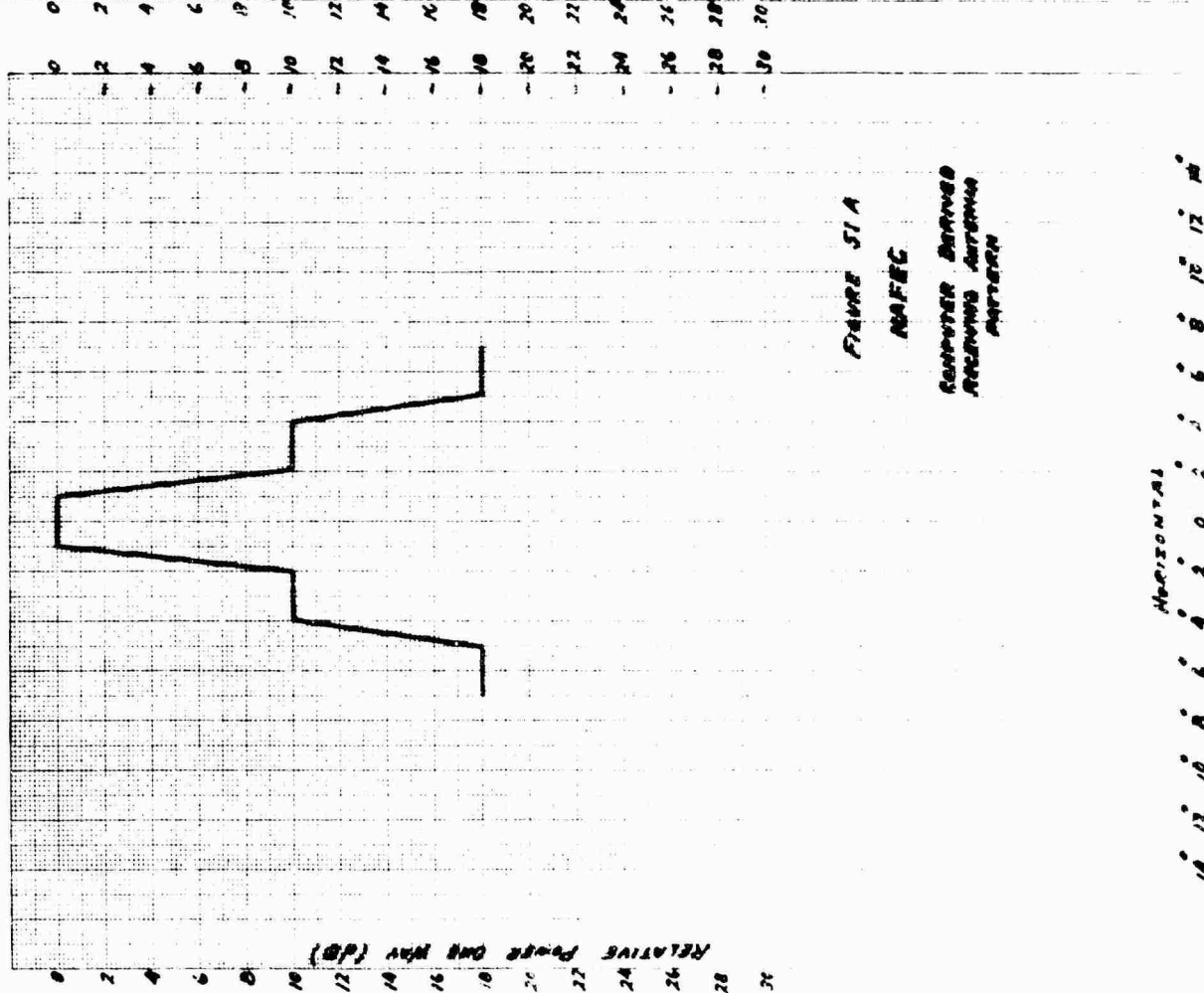
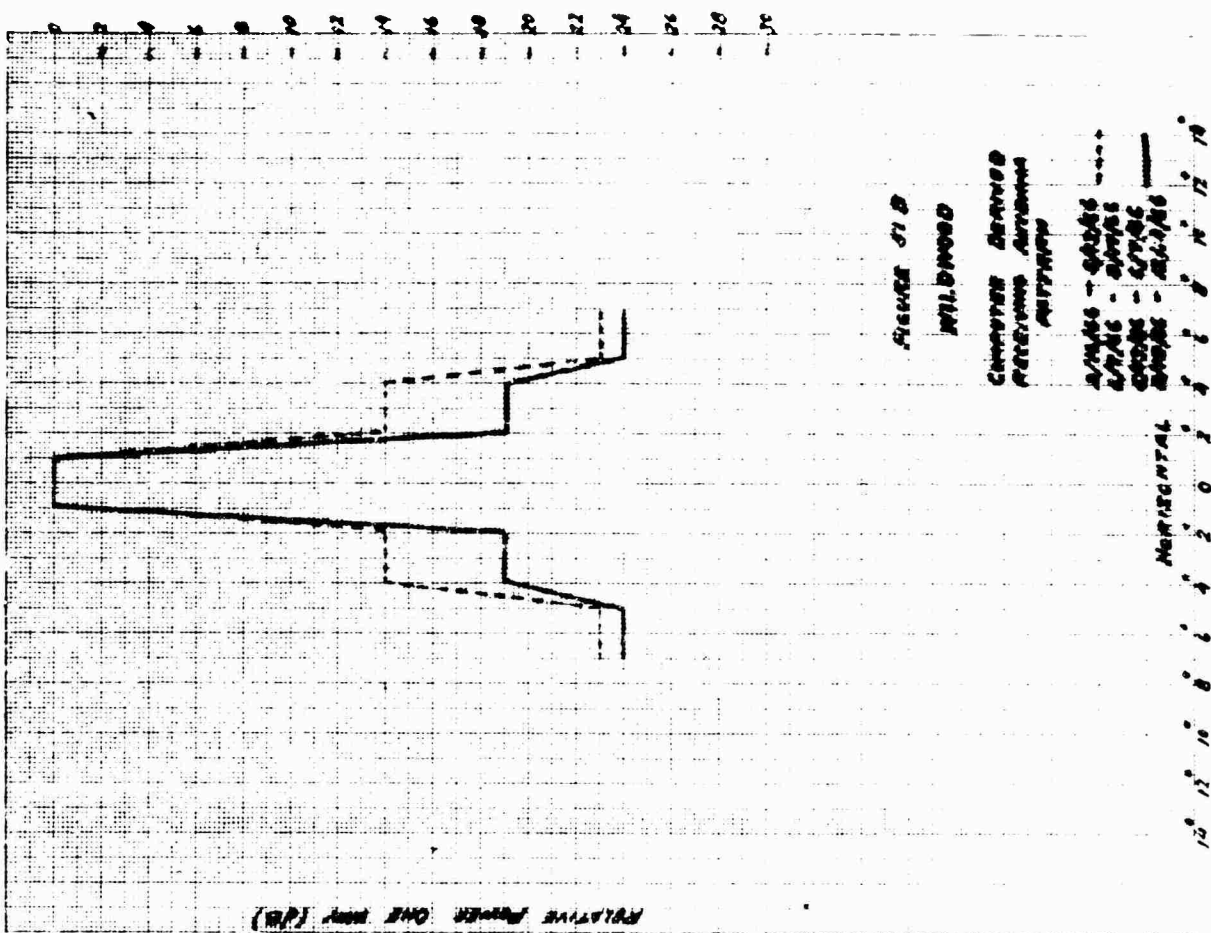
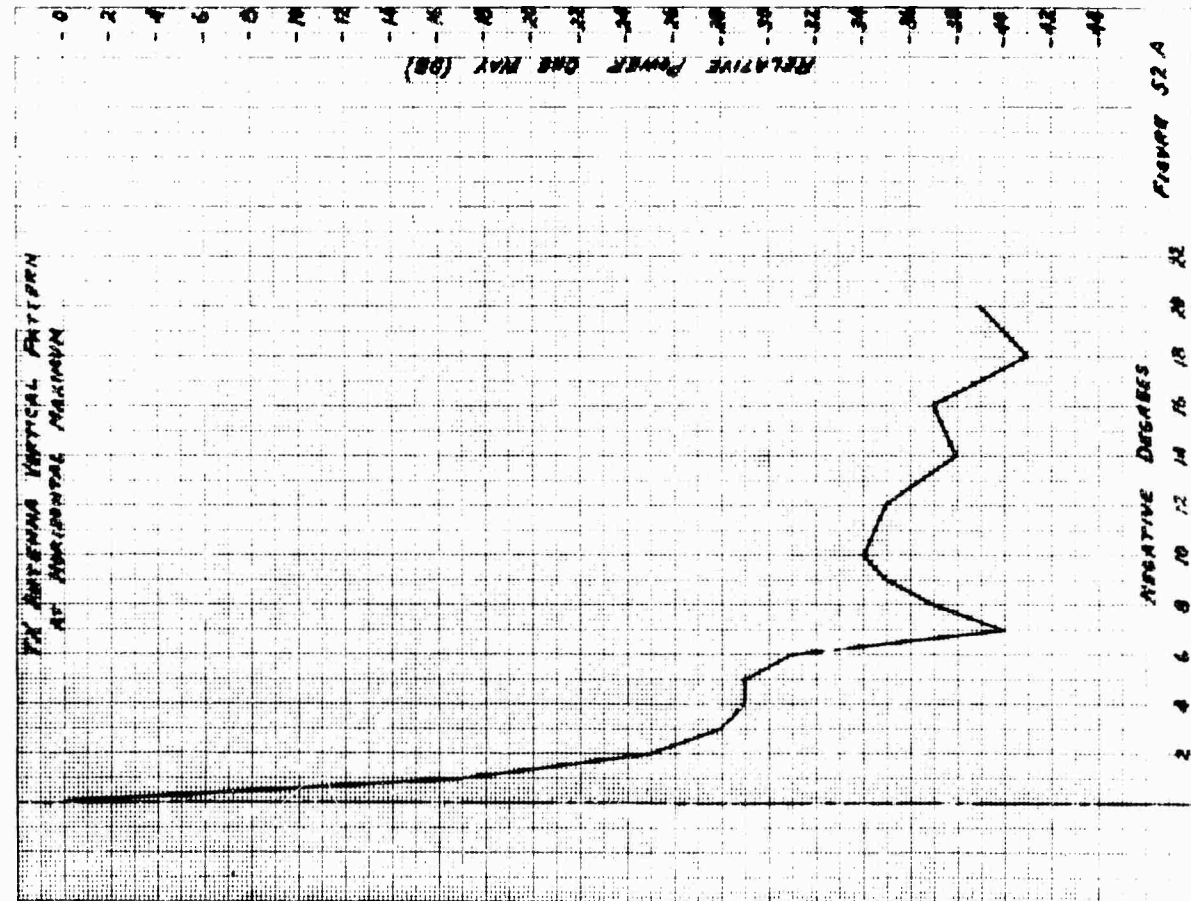
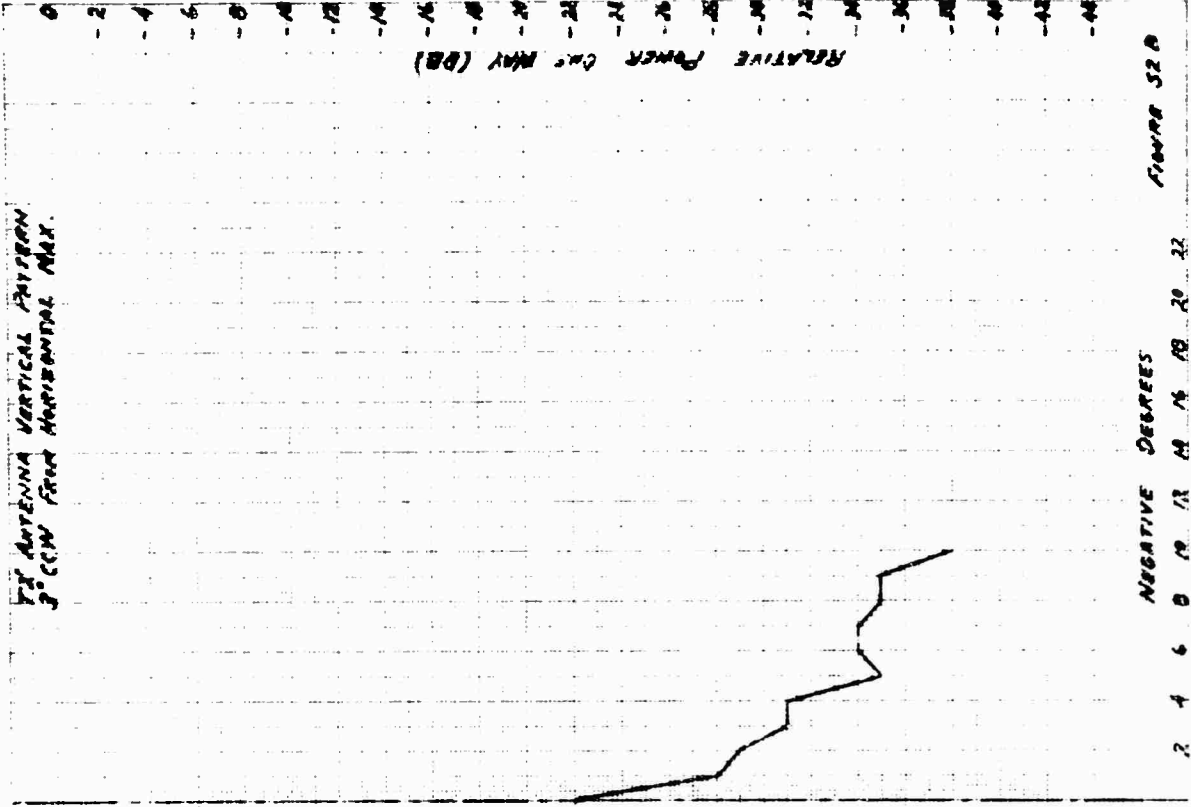


Figure 50





TX ANTENNA VERTICAL PATTERN
9° CW FROM HORIZONTAL MAX.

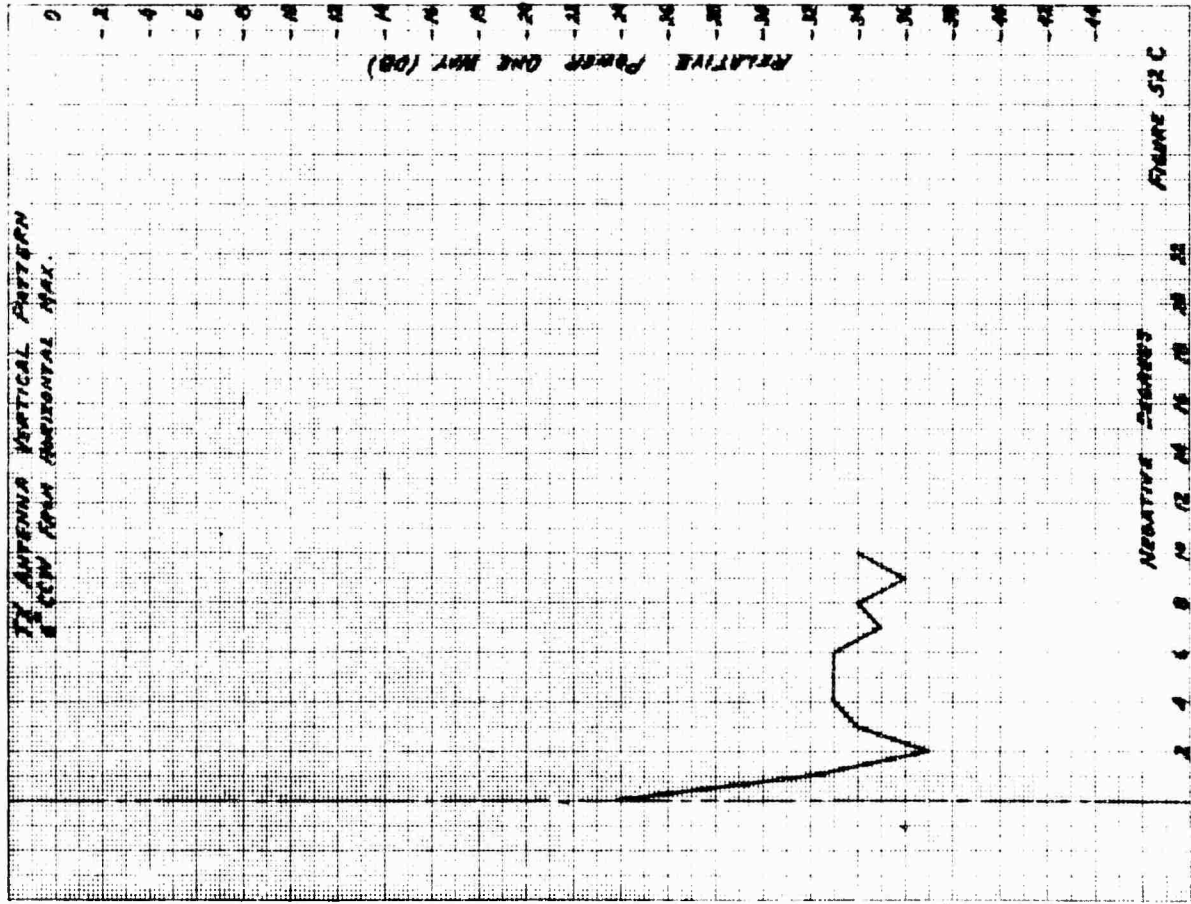


FIGURE 51C

TX ANTENNA VERTICAL PATTERN
9° CW FROM HORIZONTAL MAX.

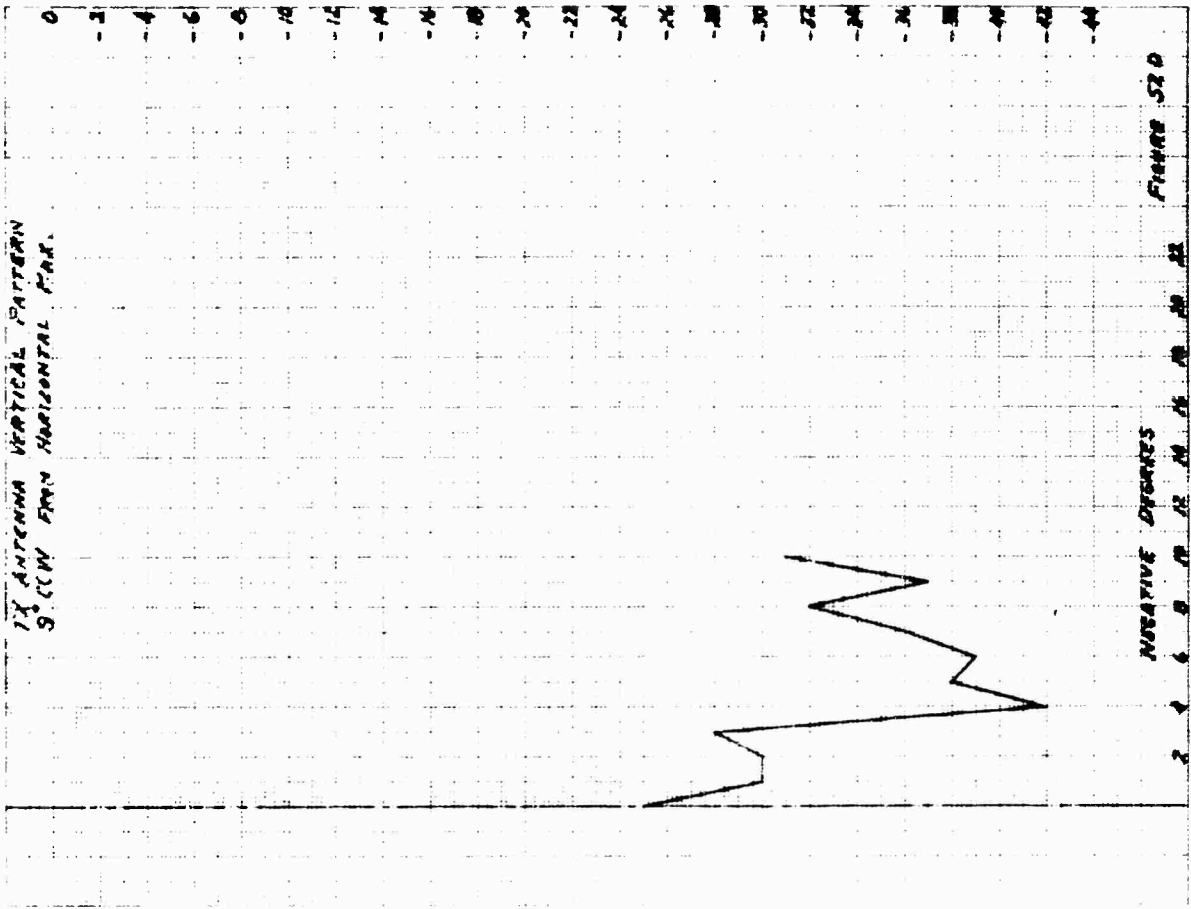
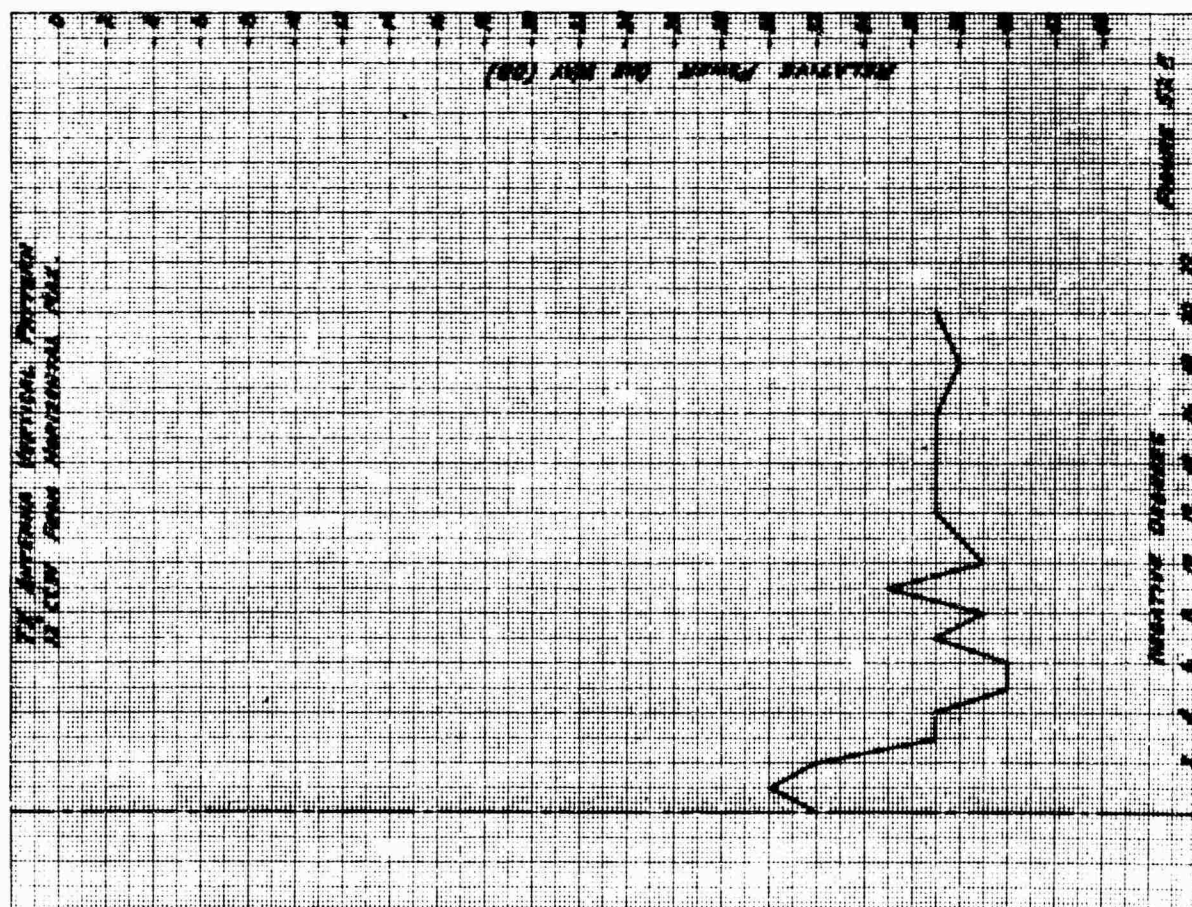
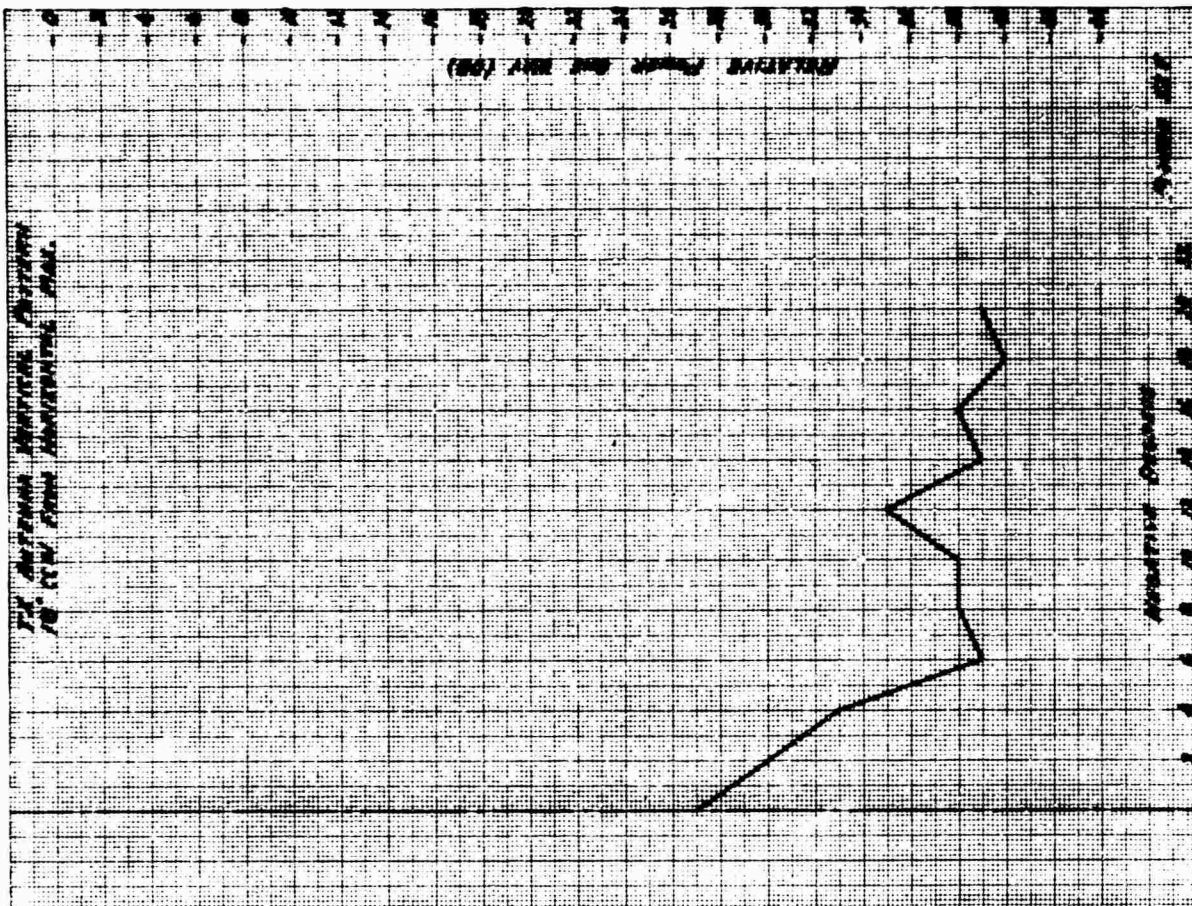


FIGURE 51D



WILDWOOD Receiving Antenna at 6° Az. & 2° Elev.

Time	TX Ant.	AZ	Elev	Measured Antenna		Predicted Antenna		Measured
				On Rth Side Libe	On Rth Side Libe	On Rth Side Libe	On Rth Side Libe	
0400	0°	12	1	-17	-23	-17	-23	-55
			2	-25	-	-25	-	-
			3	-28	-	-28	-	-
			4	-29	-	-29	-	-
			5	-29	-	-29	-	-
			6	-31	-	-31	-	-
			7	-40	-	-40	-	-
			8	-27	-	-27	-	-
			9	-35	-	-35	-	-
			10	-34	-	-34	-	-
0500	0°	12	1	-25	-	-25	-	-
			2	-30	-	-30	-	-
			3	-38	-	-38	-	-
			4	-42	-	-42	-	-
			5	-38	-	-38	-	-
			6	-39	-	-39	-	-
			7	-36	-	-36	-	-
			8	-32	-	-32	-	-
			9	-37	-	-37	-	-
			10	-31	-	-31	-	-
0600	0°	12	1	-32	-	-32	-	-89
			2	-30	-	-30	-	-87
			3	-32	-	-32	-	-89
			4	-37	-	-37	-	-84
			5	-37	-	-37	-	-94
			6	-40	-	-40	-	-97
			7	-40	-	-40	-	-97
			8	-37	-	-37	-	-96
			9	-35	-	-35	-	-97
			10	-39	-	-39	-	-94
0655	0°	12	1	-32	-	-32	-	-97
			2	-30	-	-30	-	-100
			3	-32	-	-32	-	-100
			4	-37	-	-37	-	-96
			5	-37	-	-37	-	-97
			6	-40	-	-40	-	-97
			7	-37	-	-37	-	-96
			8	-35	-	-35	-	-97
			9	-35	-	-35	-	-94
			10	-39	-	-39	-	-96

FIGURE 53 B

NAFEC Receiving Antenna at 6° Az. & 2° Elev.

Time	TX Ant.	Az	Elev.	Measured Antenna On Path Side Lobe	Predicted Path On Path	Measured Antenna On Path Side Lobe	Predicted Path On Path	Measured Antenna On Path Side Lobe	Predicted Path On Path
6/20/55	12°	0°	2°	TX	RX	TX	RX	TX	RX
1500	12°	0°	2°	-32	-102	-32	-102	-32	-102
	12°	0°	2°	-30	-100	-30	-100	-30	-100
	12°	0°	2°	-32	-102	-32	-102	-32	-102
	12°	0°	2°	-37	-107	-37	-107	-37	-107
	12°	0°	2°	-37	-107	-37	-107	-37	-107
	12°	0°	2°	-40	-110	-40	-110	-40	-110
	12°	0°	2°	-40	-114	-40	-114	-40	-114
	12°	0°	2°	-37	-111	-37	-111	-37	-111
	12°	0°	2°	-39	-113	-39	-113	-39	-113
	12°	0°	2°	-35	-109	-35	-109	-35	-109
	12°	0°	2°	-39	-113	-39	-113	-39	-113
1555	12°	0°	2°	-74	-74	-74	-74	-74	-74

Measured Antenna On Path Side Lobe	Predicted Path On Path	Measured Antenna On Path Side Lobe	Predicted Path On Path
-84	-88	-84	-88
-97	-120	-97	-120
-98	-120	-98	-120
-101	-120	-101	-120
-90	-125	-90	-125
-71	-125	-71	-125
-62	-128	-62	-128
-62	-132	-62	-132
-62	-129	-62	-129
-62	-131	-62	-131
-68	-127	-68	-127
-72	-131	-72	-131
-89	-92	-89	-92

-12
-11
-8
-19
-37
-47
-49
-47
-47
-41
-37

FIGURE 54 A

NAFEC Receiving Antenna at 6° Az. & 2° Elev.

[illegible]

FIGURE 3A B

NAFEC Receiving Antenna at 6° Az. & 2° Elev.

[illegible]

FIGURE 3A C

WILLOWOOD Receiving Ant. $\alpha:3^\circ \beta:2^\circ$

[illegible]

FIGURE 53A

WILLOWOOD

Receiving Ant. $\alpha = 2^\circ$ $\beta = 2^\circ$

TX Ant.	Measured On Ant	Antenna Side Lobe $\beta_m(0, \beta)$	β_m $\beta_m(0, \beta)$	$P_p - P_m$	Measured off Ant P_m	$\beta_m(0, \beta)$ $\beta_m(0, \beta)$	$P_p - P_m$
0°	0°	0°	0°				
0100	12	-58	-19	-1	-83	-77	+6
	2	-82	-25	+4	-107	-102	+5
	4	-91	-29	+7			
	6	-94	-39	+4			
	8	-99	-37	+3			
	10	-95	-24	-9			
	12	-87	-35	-6	-106	-115	-9
	14	-93	-38	-1			
	16	-97	-37	+4			
	18	-106	-41	+3			
	20	-103	-39				
	22	-61		+4	-85	-80	+5
0200	12	-97	-32	+3			
	2	-96	-32	+5			
	4	-103	-37	+8			
	6	-106	-40	+5			
	8	-106	-37	-14			
	10	-105	-39	-13			
	12	-105	-37				
	14	-106	-37				
	16	-106	-37				
	18		-38				
	20		-37				
	22	-82			-104	-101	+3
0300	18	-106	-27				
	2		-30				
	4		-33				
	6		-34				
	8		-38				
	10		-38				
	12		-35				
	14		-39				
	16		-38				
	18		-40				
	20		-39				
	22	-79			-103	-98	+5

FIGURE 55B

WILDWOOD									
Receiving Ant. $\alpha = 3^\circ \beta = 2^\circ$									
TX Ant.	Measured On Ant.	Antenna Side Lobe (θ, ϕ)	P_m	P_m	P_m	P_m	P_m	P_m	P_m
0°	0°	0°	-80	-19	-105	-16	-103	-99	-4
	2°	2°	-89	-25	-109	-14			
	4°	4°	-95	-29	-109	-6			
	6°	6°	-103	-33	-117	-11			
	8°	8°	-106	-34	-114				
	10°	10°	-106	-35					
	12°	12°		-38					
	14°	14°		-37					
	16°	16°		-41	-121	-15			
	18°	18°	-106	-39	-119	-14			
	20°	20°	-105						
	12°	12°	-80						
0°	12°	12°	-106	-32	-112	-6	-95	-99	-4
	2°	2°		-32	-112	-6	-106	-131	-25
	4°	4°	-104	-37	-117	-13	-92	-131	-39
	6°	6°	-94	-40	-120	-26	-86	-136	-50
	8°	8°	-91	-37	-119	-26	-92	-139	-47
	10°	10°	-88	-39	-117	-31	-87	-136	-39
	12°	12°	-86	-37	-117	-31	-101	-138	-37
	14°	14°	-88	-37	-117	-29	-106	-136	-30
	16°	16°	-95	-37	-117	-22			
	18°	18°		-38	-118				
	20°	20°		-37	-117				
0°	18°	18°	-106	-27	-109				
	2°	2°		-20	-112				
	4°	4°		-33	-115				
	6°	6°		-39					
	8°	8°		-38					
	10°	10°		-38					
	12°	12°		-25					
	14°	14°		-39					
	16°	16°		-38					
	18°	18°		-40					
	20°	20°		-39					
0°	20°	20°	-82				-92	-101	-9

FIGURE 55C

NAFEC		Receiving Ant.		Ant. $\alpha = 3^\circ$		$\beta = 2^\circ$	
Time	θ	ϕ	TX Ant.	Measured Antenna Side Lobe $R_m(\theta, \phi)$	$R_p(\theta, \phi) +$ $R_m(\theta, \phi)$	Measured Off Axis R_m	$R_p(\theta, \phi) +$ $R_m(\theta, \phi)$
10/15 2200	0°	2	10	-52	-77	-68	-62
		4	25	-75	-81	-96	-87
		6	29	-76	-81	-100	-91
		8	37	-75	-86	-101	-91
		10	34	-83	-86	-105	-91
		12	35	-76	-90	-103	-100
		14	38	-92	-93	-105	-105
		16	37	-85	-92	-105	-105
		18	41	-94	-96	-105	-105
		20	39	-85	-94	-105	-105
10/15 2200	12°	2	22	-87	-87	-82	-65
		4	32	-96	-87	-105	-65
		6	37	-91	-92	-105	-65
		8	40	-97	-95	-105	-65
		10	37	-99	-92	-105	-65
		12	39	-96	-94	-105	-65
		14	37	-103	-95	-105	-65
		16	37	-101	-95	-105	-65
		18	38	-103	-96	-105	-65
		20	37	-101	-95	-105	-65
10/16 0000	18°	2	27	-58	-85	-79	-68
		4	30	-89	-88	-105	-68
		6	37	-85	-91	-105	-68
		8	39	-102	-97	-105	-68
		10	38	-101	-96	-105	-68
		12	35	-101	-96	-105	-68
		14	35	-96	-87	-105	-68
		16	39	-98	-91	-105	-68
		18	40	-97	-90	-105	-68
		20	39	-86	-92	-105	-68
10/16 0000	0°	2	27	-52	-77	-68	-62
		4	25	-75	-81	-96	-87
		6	29	-76	-81	-100	-91
		8	37	-75	-86	-101	-91
		10	34	-83	-86	-105	-91
		12	35	-76	-90	-103	-100
		14	38	-92	-93	-105	-105
		16	37	-85	-92	-105	-105
		18	41	-94	-96	-105	-105
		20	39	-85	-94	-105	-105

FIGURE 55D

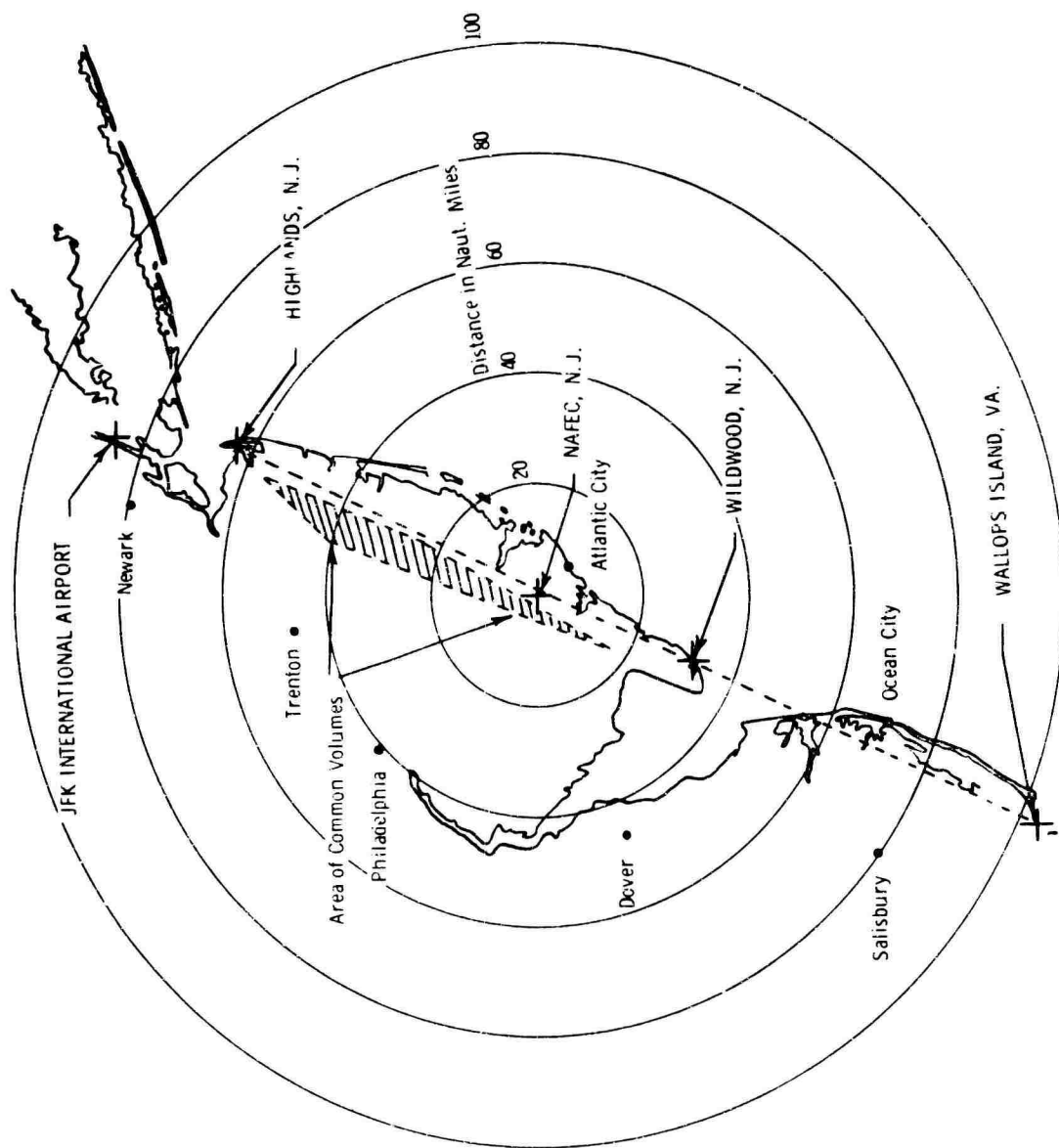
NAFEC Receiving Ant. $\alpha = 3^\circ \beta = 2^\circ$									
Time	TX Ant.	Measured On Ant.	Side Lobe S (dB)	P_p $P_p(0.5\%)$	$P_p - P_m$	Measured Off Ant.	$P_p(0.5\%)$ $P_p(0.5\%)$	$P_p - P_m$	
0100	0	-52	-10	-77	-5	-63	-62	+1	
	2	-72	-25	-81	-13	-83	-87	+6	
	4	-68	-29	-81	-3	-93	-91	+2	
	6	-79	-29	-89	0	-104	-91	+13	
	8	-89	-27	-86	+2	< -105			
	10	-88	-24	-87	-2				
	12	-85	-25	-93	0				
	14	-93	-27	-92	+1				
	16	-93	-27	-96	+4				
	18	-100	-41	-94	+2				
	20	-97	-39			-75	-65	+10	
	22	-55				< -105			
0200	0	-89	-22	-87	+2				
	2	-94	-22	-87	+7				
	4	-89	-27	-92	-3				
	6	-101	-40	-95	+6				
	8	-99	-37	-92	+7				
	10	-93	-29	-94	-1				
	12	-95	-27	-125	-20				
	14	< -103	-27	-125					
	16		-27	-125					
	18		-28	-126					
	20		-27	-125					
0300	0	-88	-27	-115		-100	-98	+2	
	2	< -103	-20	-118		< -105			
	4		-22	-121					
	6		-29	-127					
	8		-28	-126					
	10		-28	-126					
	12		-25	-122					
	14		-29	-126					
	16		-28	-125					
	18		-40	-127					
	20		-29	-126					
0400	0	-87				-93	-97	-4	

FIGURE 55E

NAFEC Receiving Ant. $\alpha = 3^\circ \beta = 2^\circ$									
Time	TX Ant.	Measured Antenna On Path Side Lobe	P_m $P_m(0.5)$ $P_m(0.4)$	P_p $P_p(0.5)$ $P_p(0.4)$	$P_p - P_m$	Measured on 1216 P_m $P_m(0.5)$ $P_m(0.4)$	P_p $P_p(0.5)$ $P_p(0.4)$	$P_p - P_m$	
104000	0°	ϕ							
		$\frac{1}{2}$	-85	-10	-19	-93	-95	-2	
		2	-91	-10	-15				
		4	-93	-10	-15				
		6	-103	-10	-15				
		8	-103	-10	-15				
		10	-103	-10	-15				
		12	-103	-10	-15				
		14	-103	-10	-15				
		16	-103	-10	-15				
0500	12°	ϕ							
		$\frac{1}{2}$	-87	-119	-16	-94	-97	-3	
		2	-103	-119	-16	-105	-105		
		4	-103	-119	-16	-103	-103		
		6	-103	-119	-16	-92	-92		
		8	-103	-119	-16	-87	-87		
		10	-103	-119	-16	-87	-87		
		12	-103	-119	-16	-88	-88		
		14	-103	-119	-16	-91	-91		
		16	-103	-119	-16	-102	-102		
0600	18°	ϕ							
		$\frac{1}{2}$	-102	-124	-22	-102	-102		
		2	-102	-124	-22	-102	-102		
		4	-102	-124	-22	-102	-102		
		6	-102	-124	-22	-102	-102		
		8	-102	-124	-22	-102	-102		
		10	-102	-124	-22	-102	-102		
		12	-102	-124	-22	-102	-102		
		14	-102	-124	-22	-102	-102		
		16	-102	-124	-22	-102	-102		
0655	0°	ϕ							
		$\frac{1}{2}$	-89	-119	-16	-90	-99	-9	
		2	-89	-119	-16	-90	-99	-9	
		4	-89	-119	-16	-90	-99	-9	
		6	-89	-119	-16	-90	-99	-9	
		8	-89	-119	-16	-90	-99	-9	
		10	-89	-119	-16	-90	-99	-9	
		12	-89	-119	-16	-90	-99	-9	
		14	-89	-119	-16	-90	-99	-9	
		16	-89	-119	-16	-90	-99	-9	

FIGURE 55F

POPSI METEOROLOGICAL FACILITIES



METEOROLOGICAL FACILITIES

JFK - RAWINSONDE, Surface Data

NAFEC - WSR - 57 Radar, RAWINSONDE, MESONET, Surface Data

Philadelphia - Surface Data

Salisbury - Surface Data

Figure 56

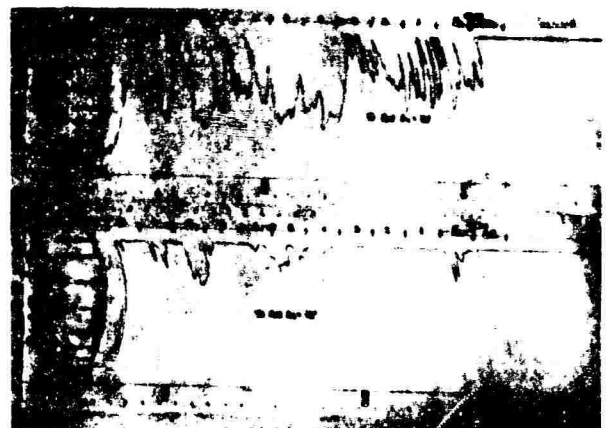
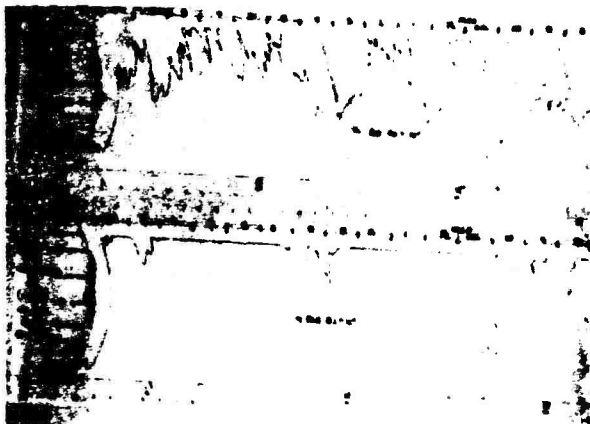
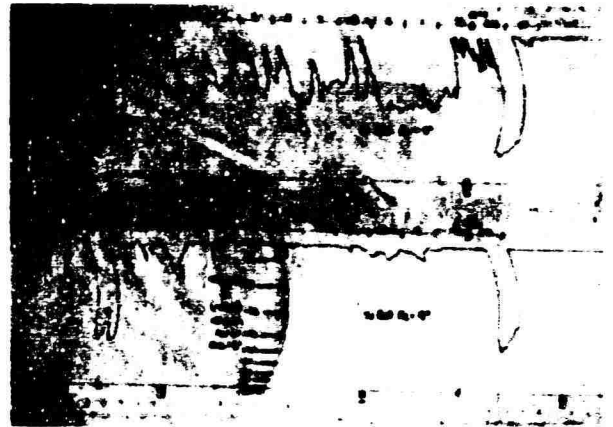


Figure 57

2250

6/15/66

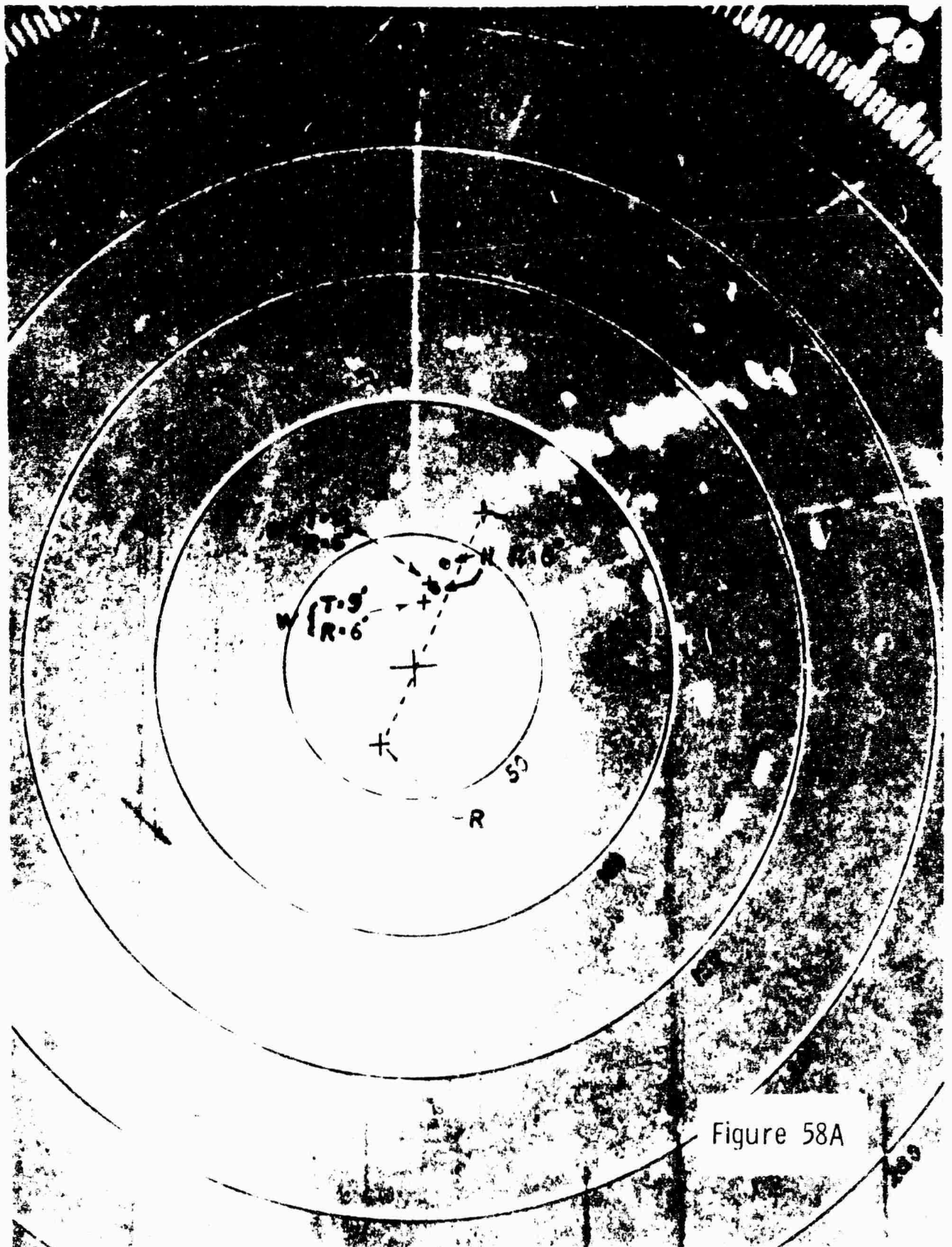


Figure 58A

0600

6/16/66

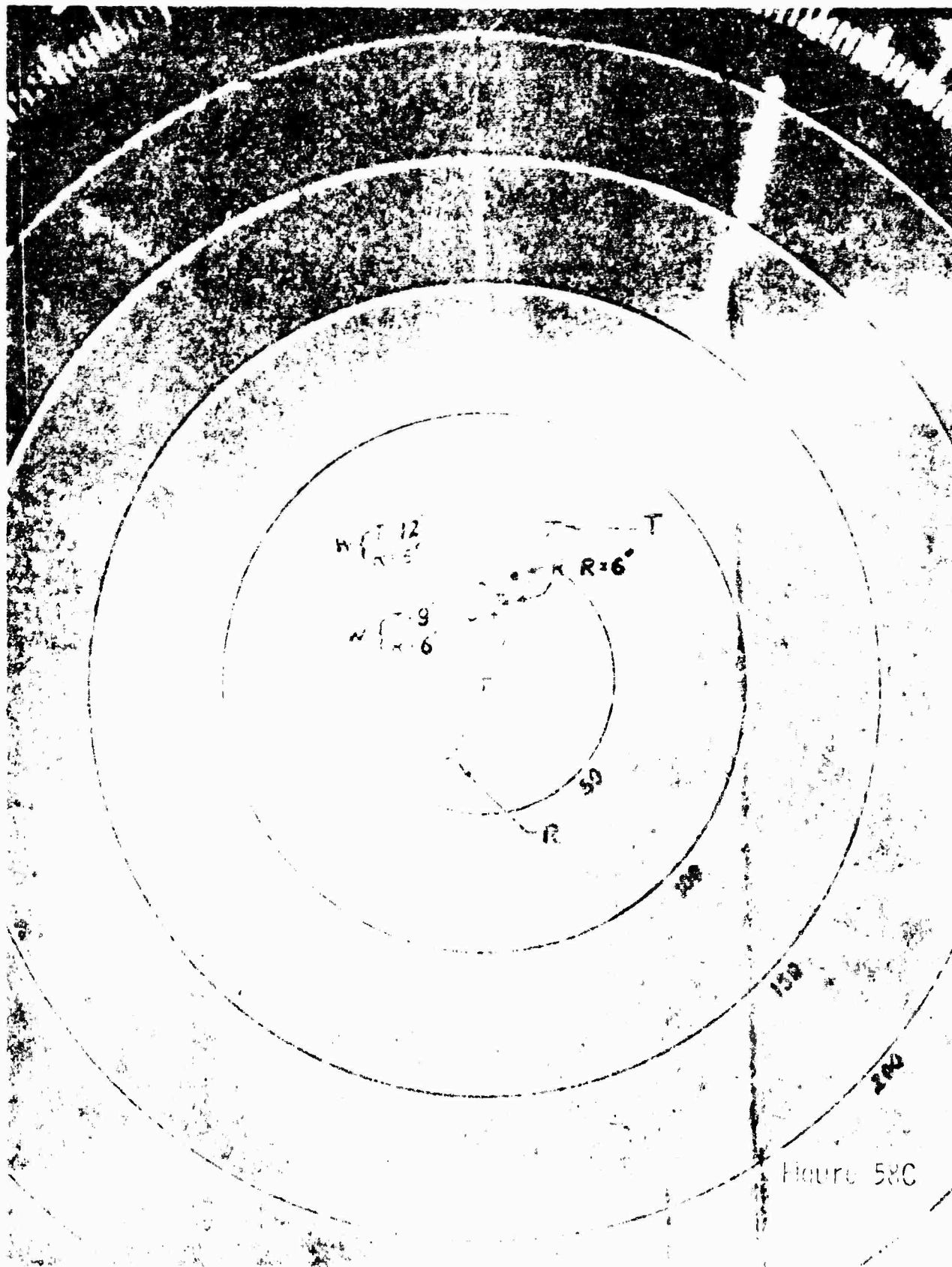


Figure 58C

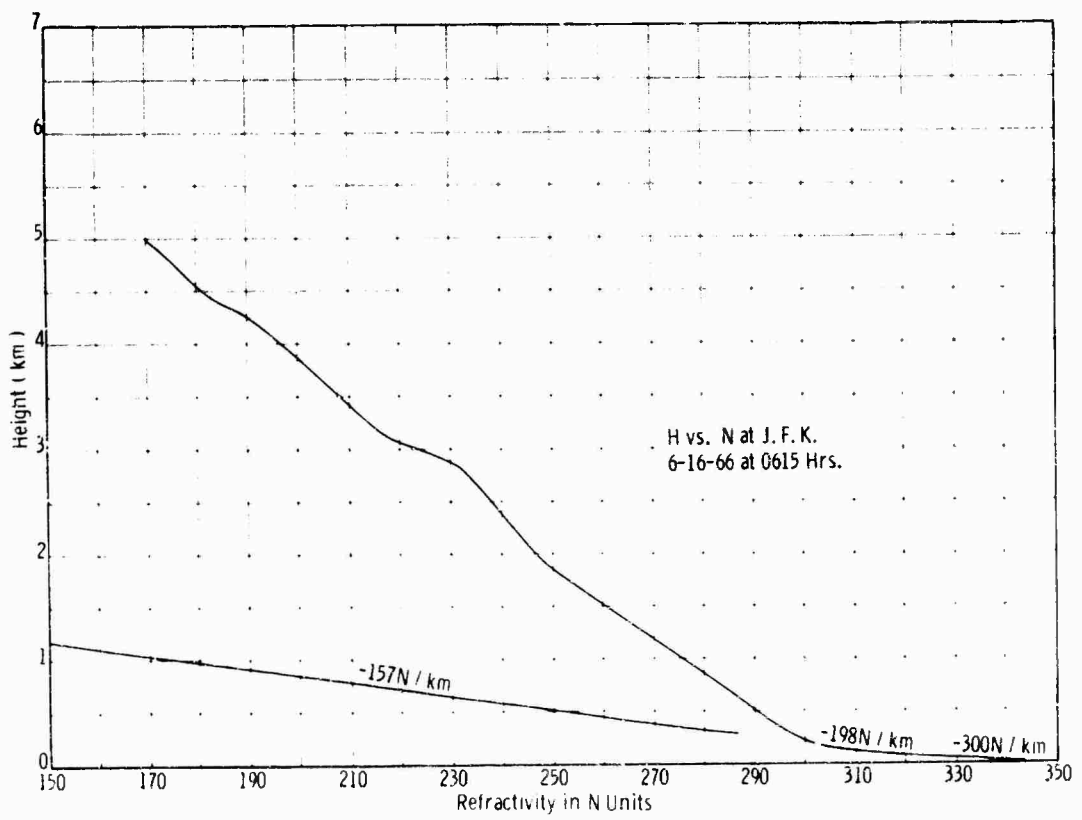
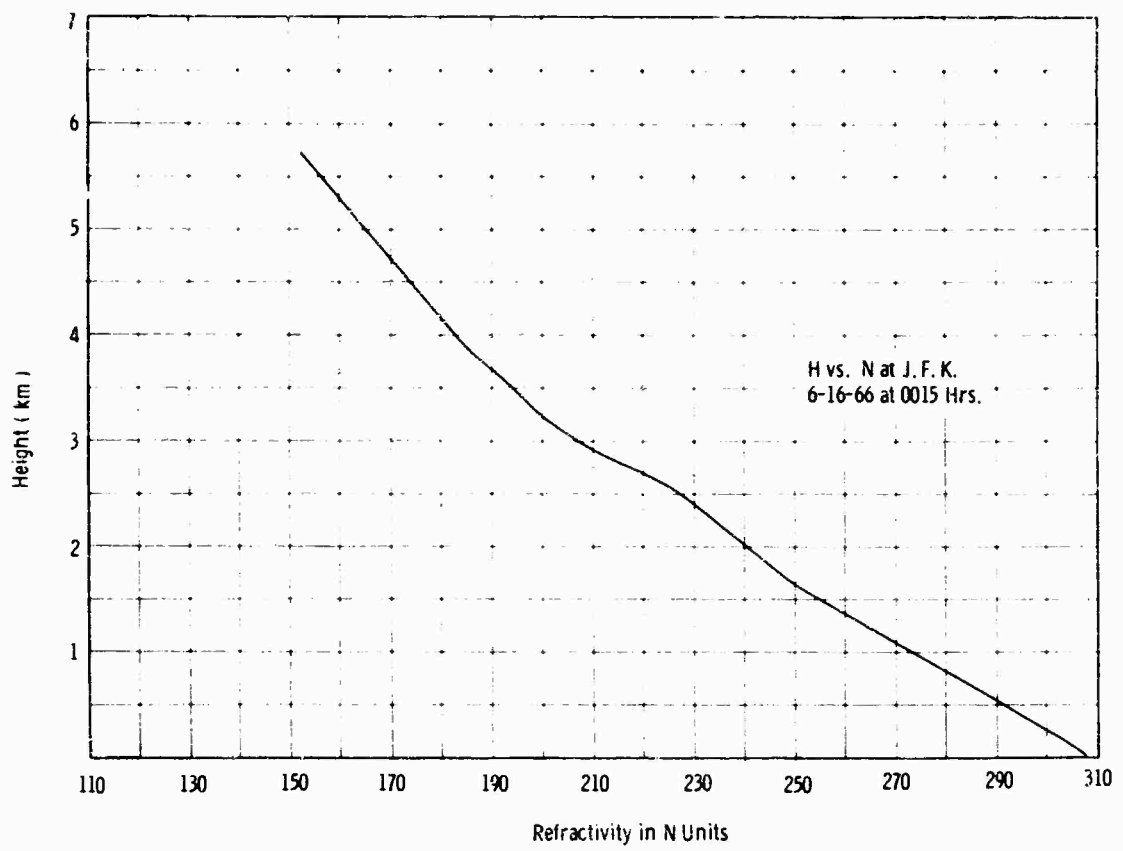


Figure 59



Figure 60 A

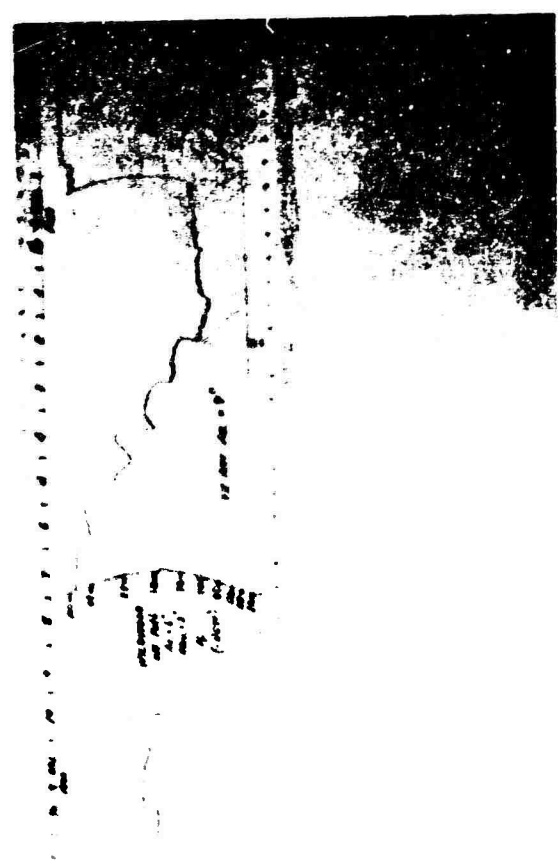
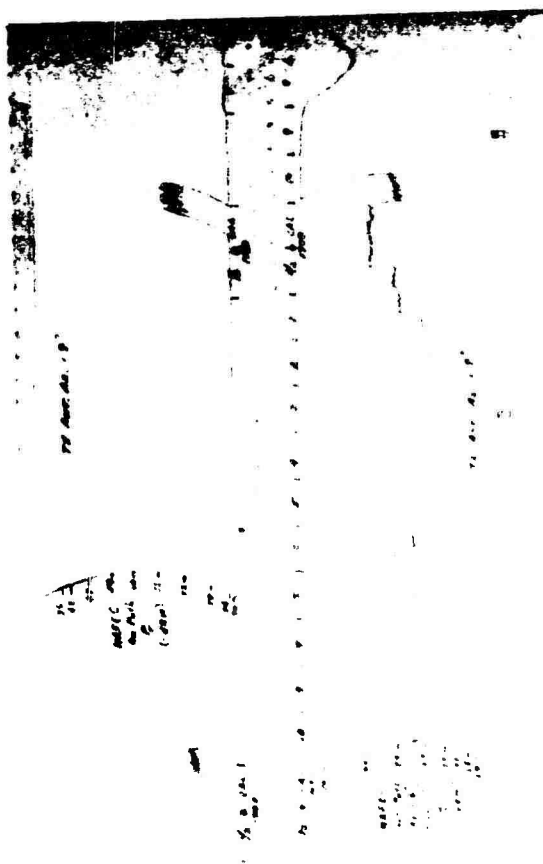
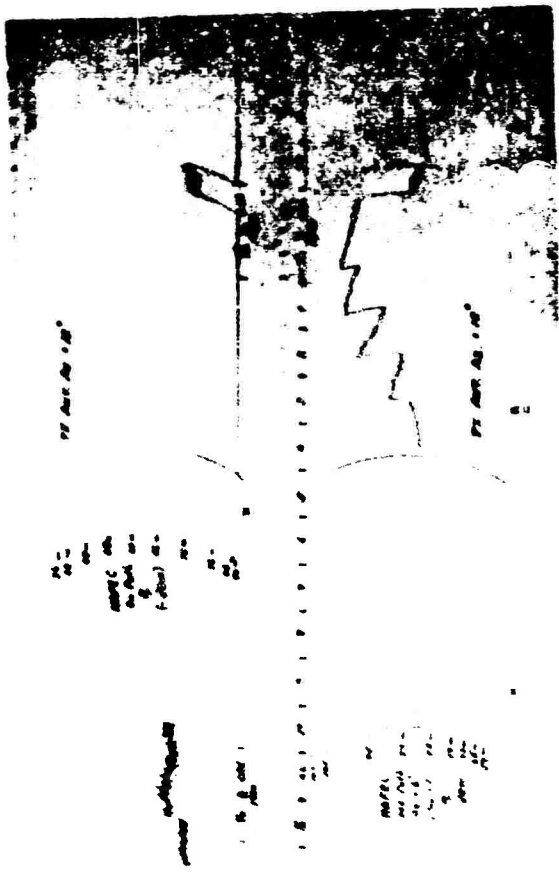


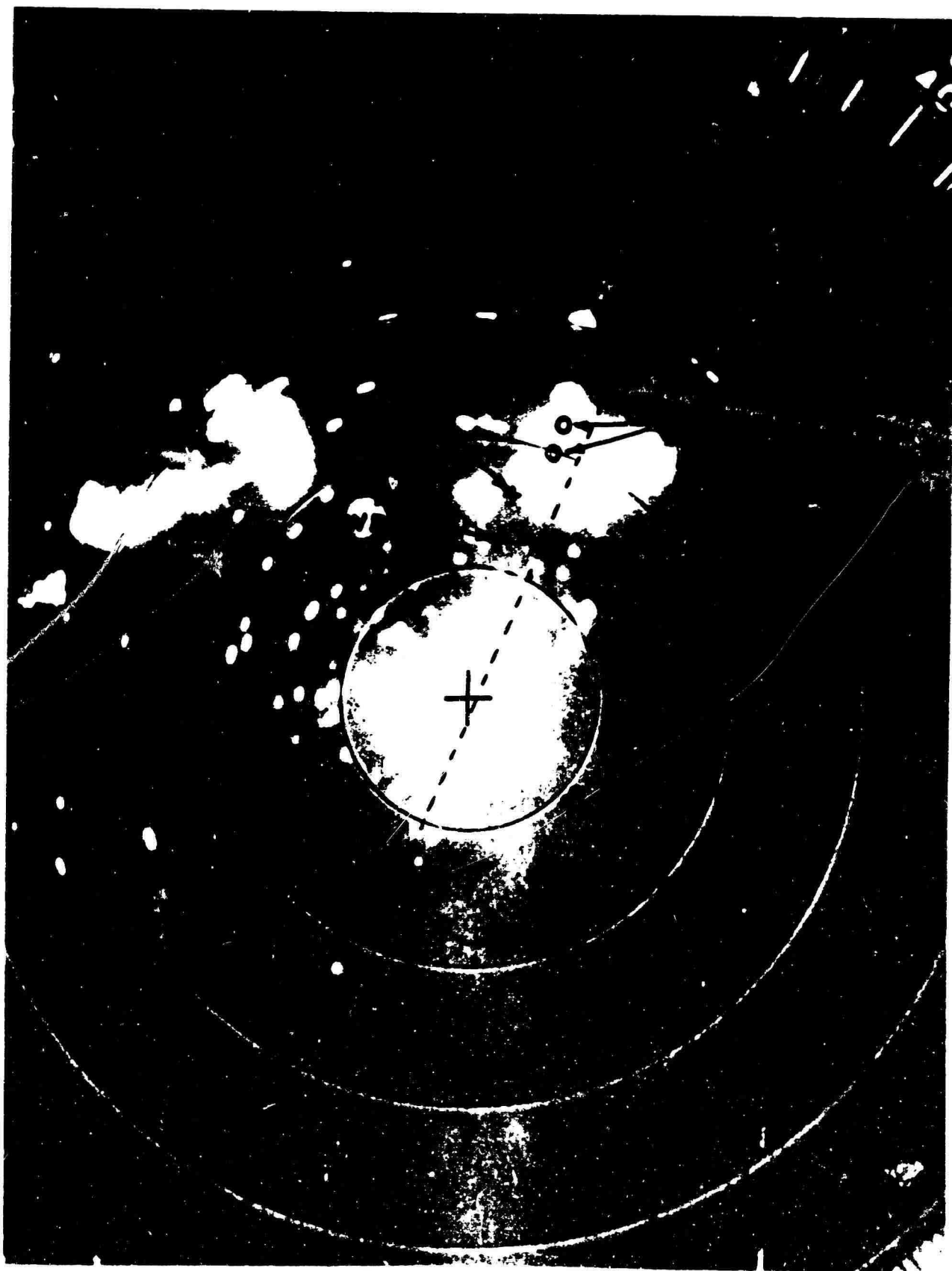
Figure 60 B



Figure 60 C



1532 6/28/66 No Att. Fig 61A



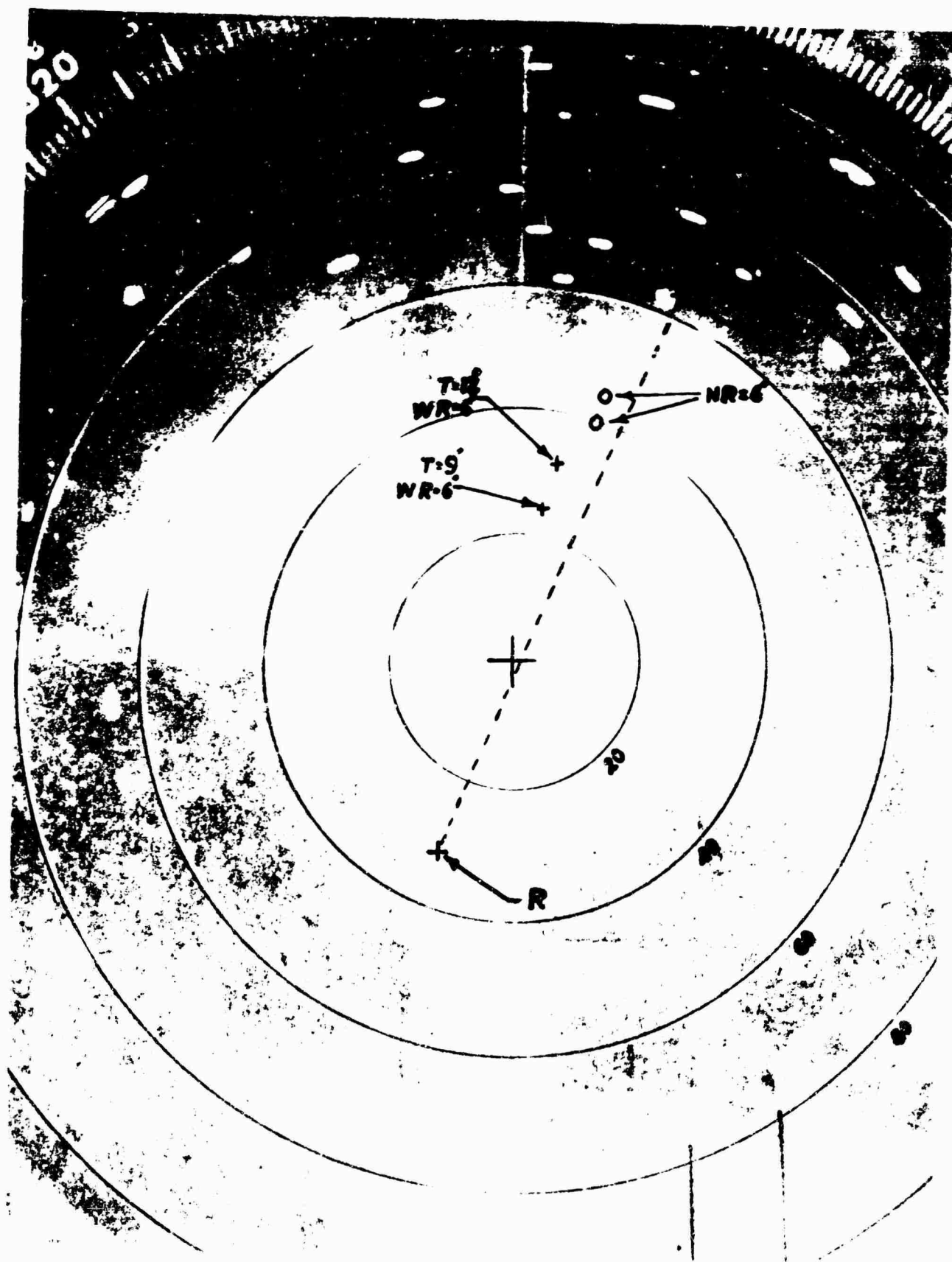
1532 6/28/66 18 dB Att.

Figure 61B



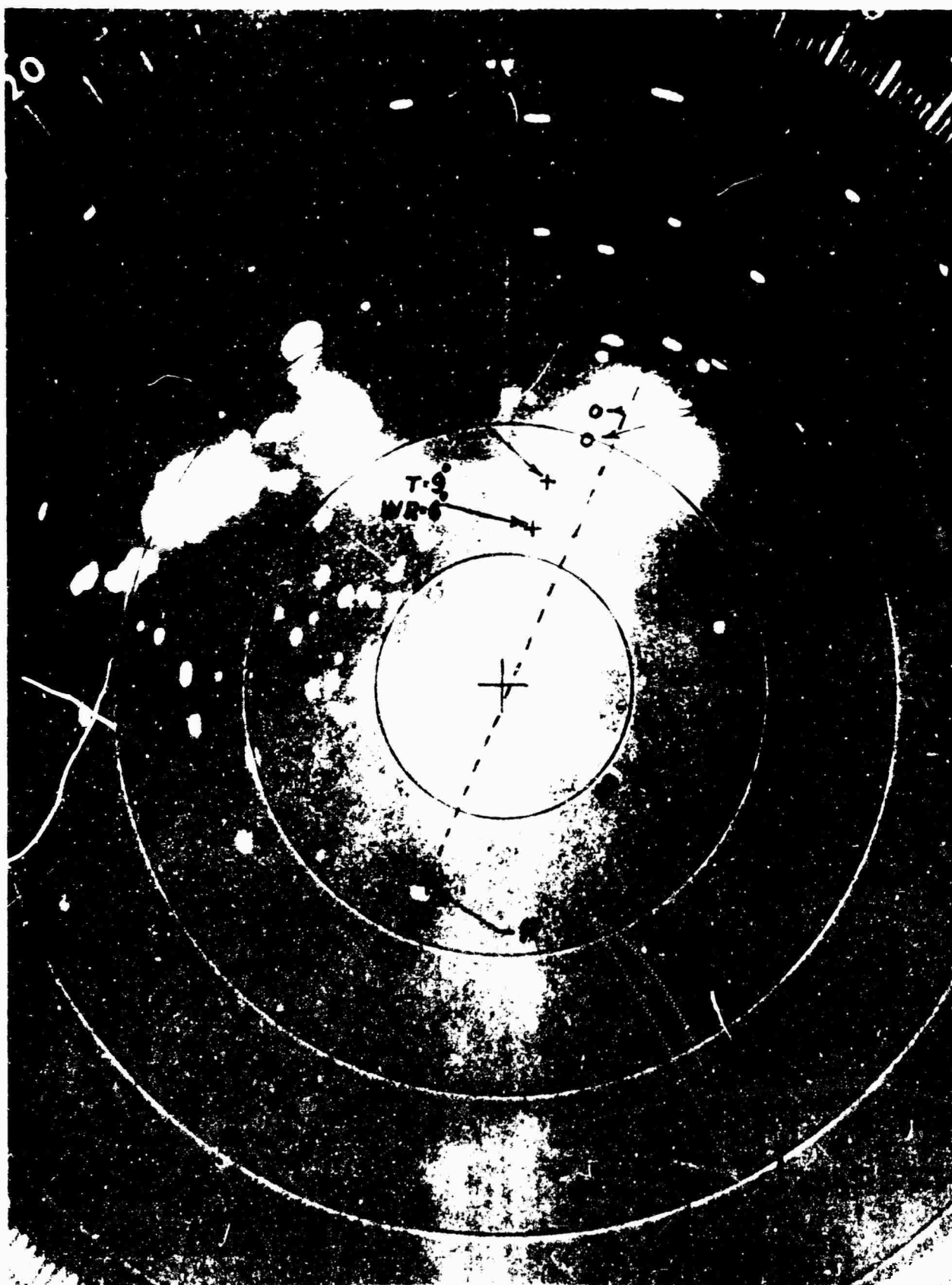
1532 6/28/66 36 dB Att.

Figure 61C



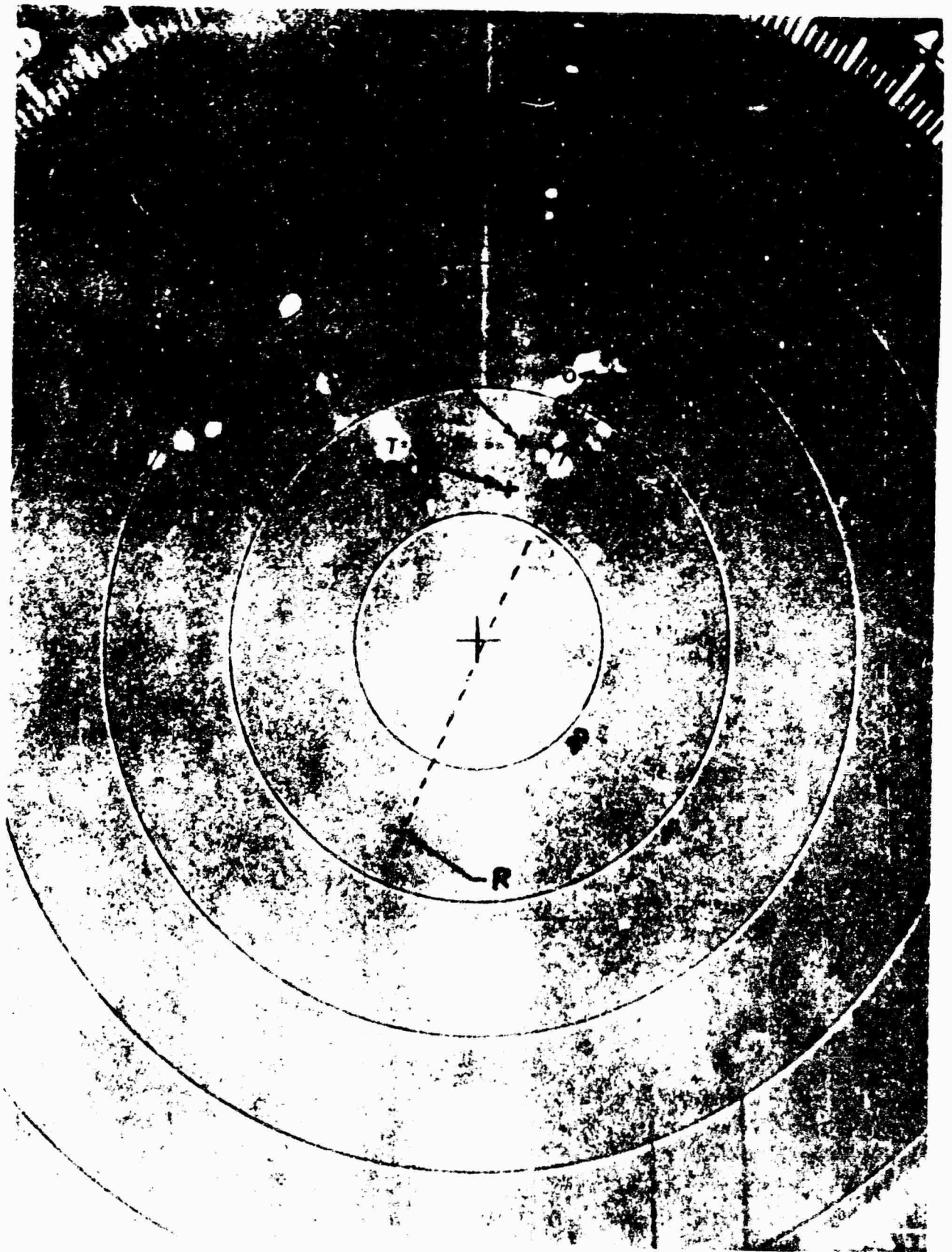
1551 6/28/66 No Att.

Figure 61D



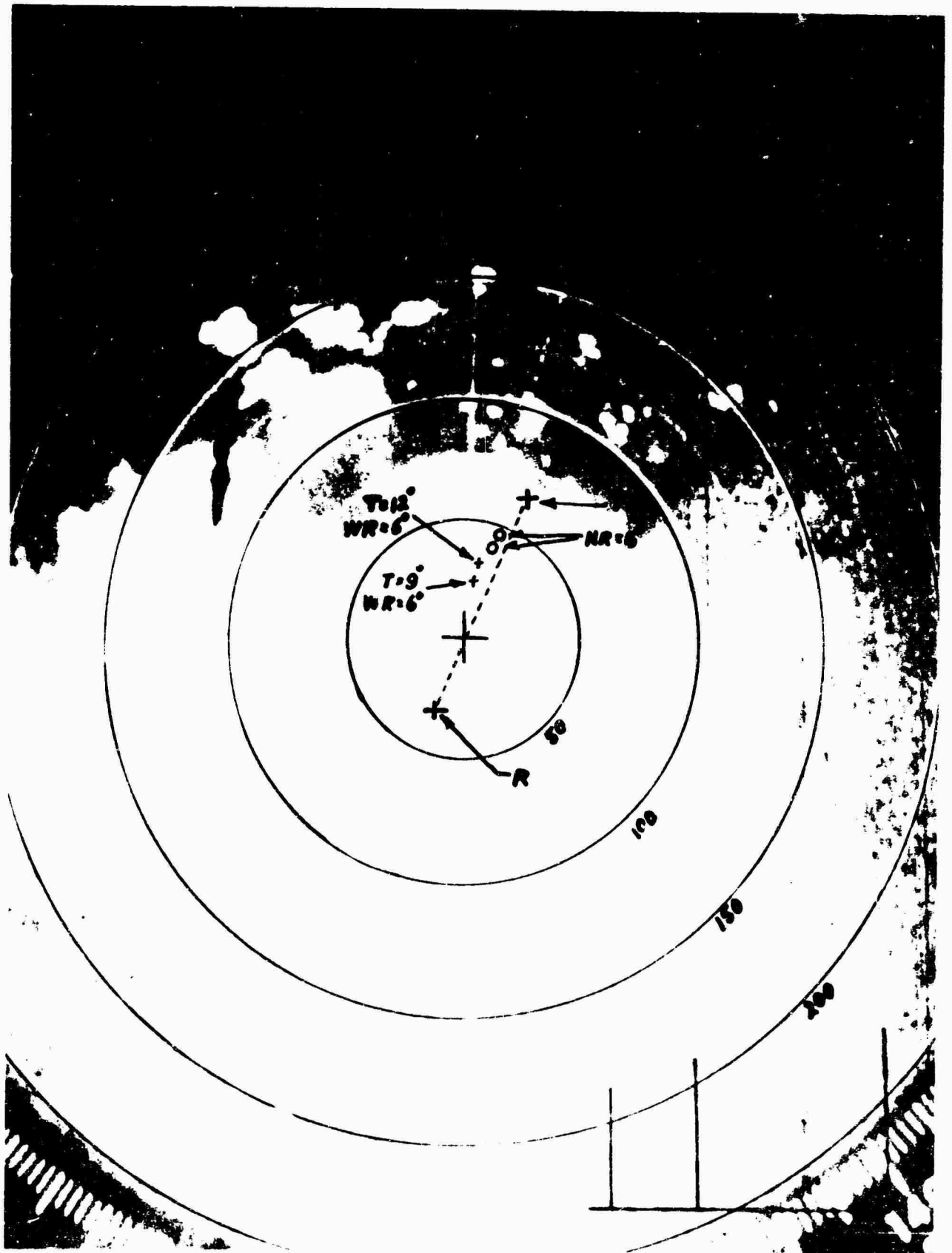
1551 6/28/66 12 dB Att.

Figure 61E



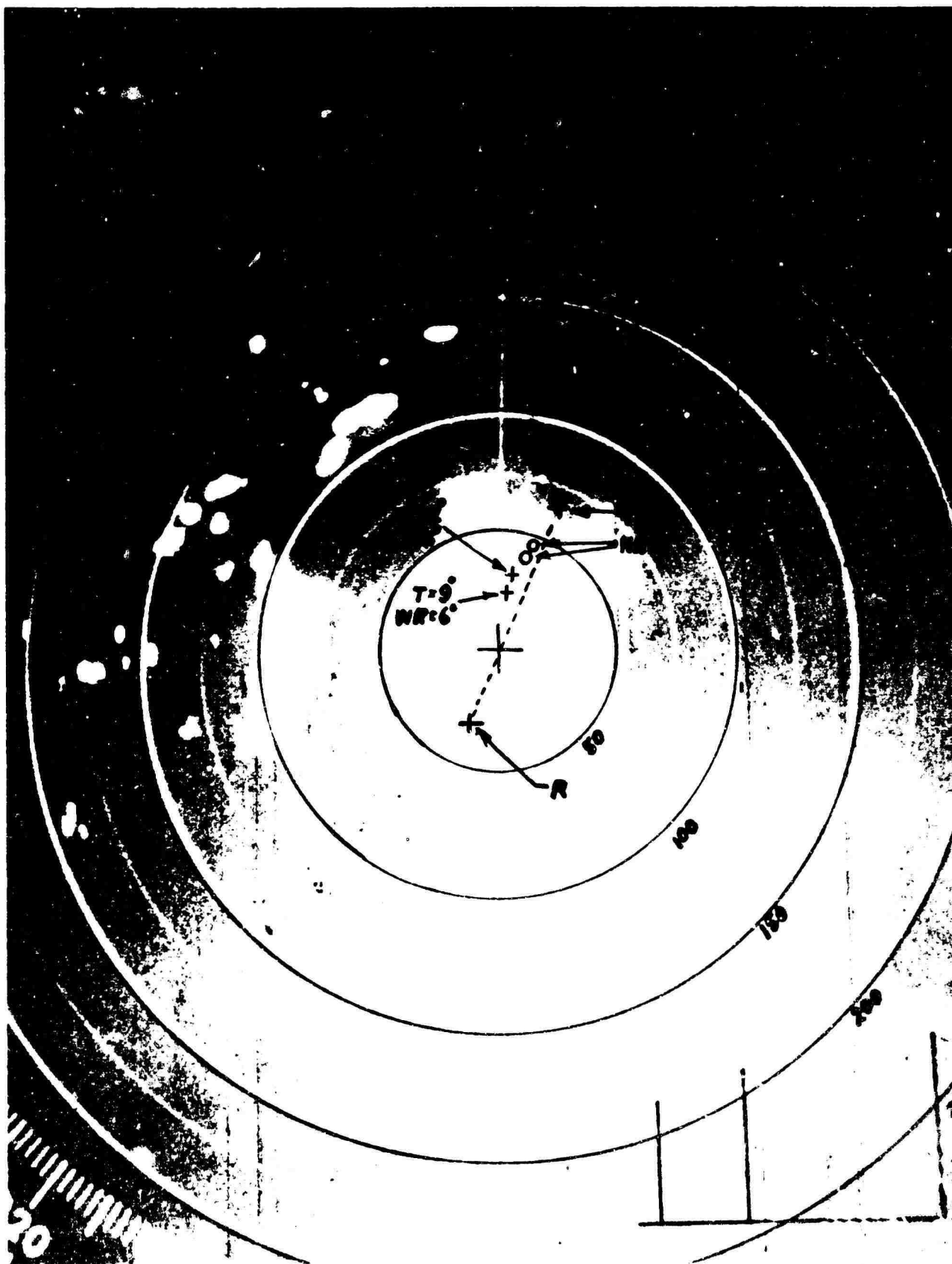
1551 6/28/66 42 dB Att.

Figure 61F



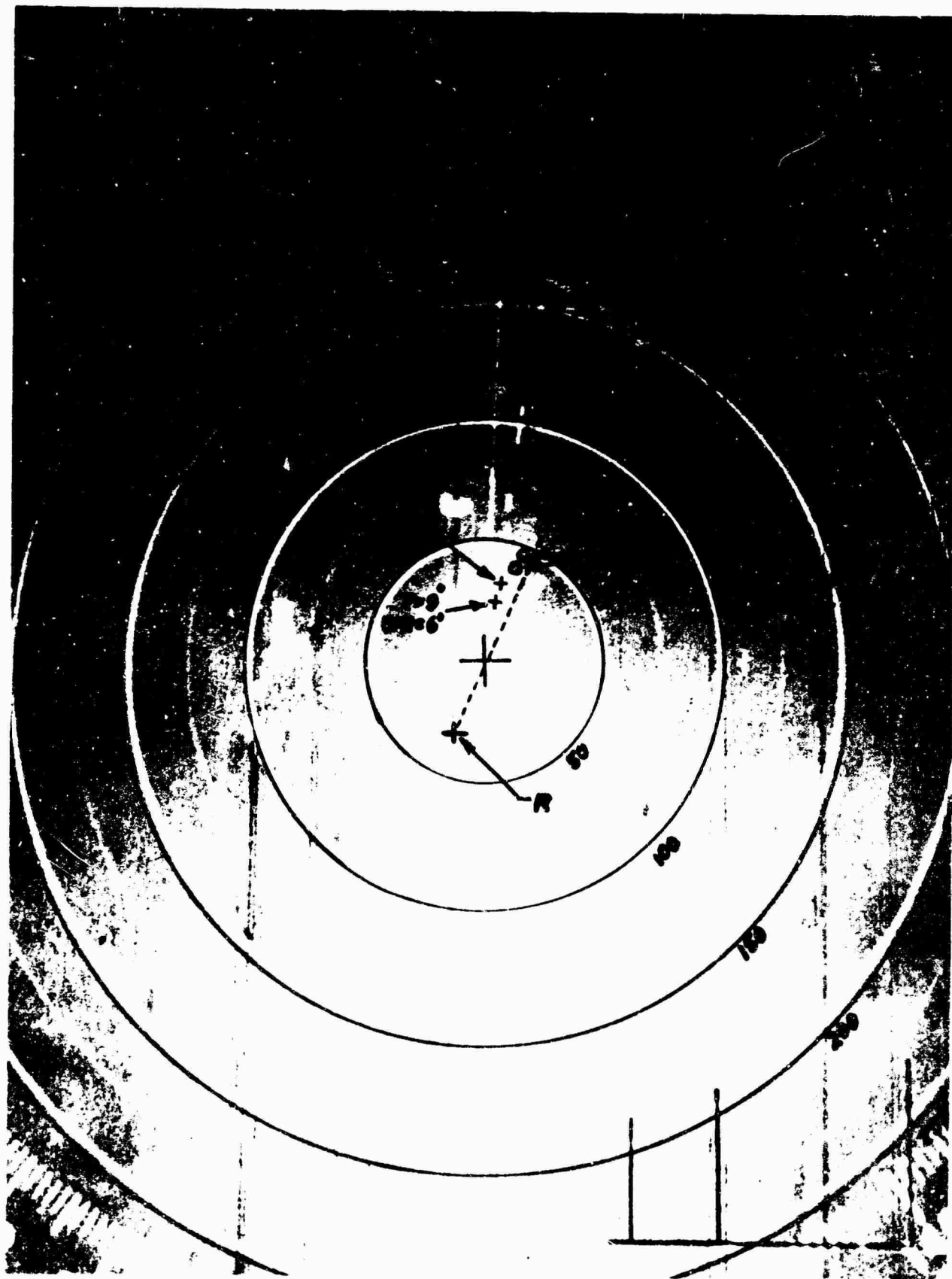
1716 6/28/66 No Att.

Figure 61G



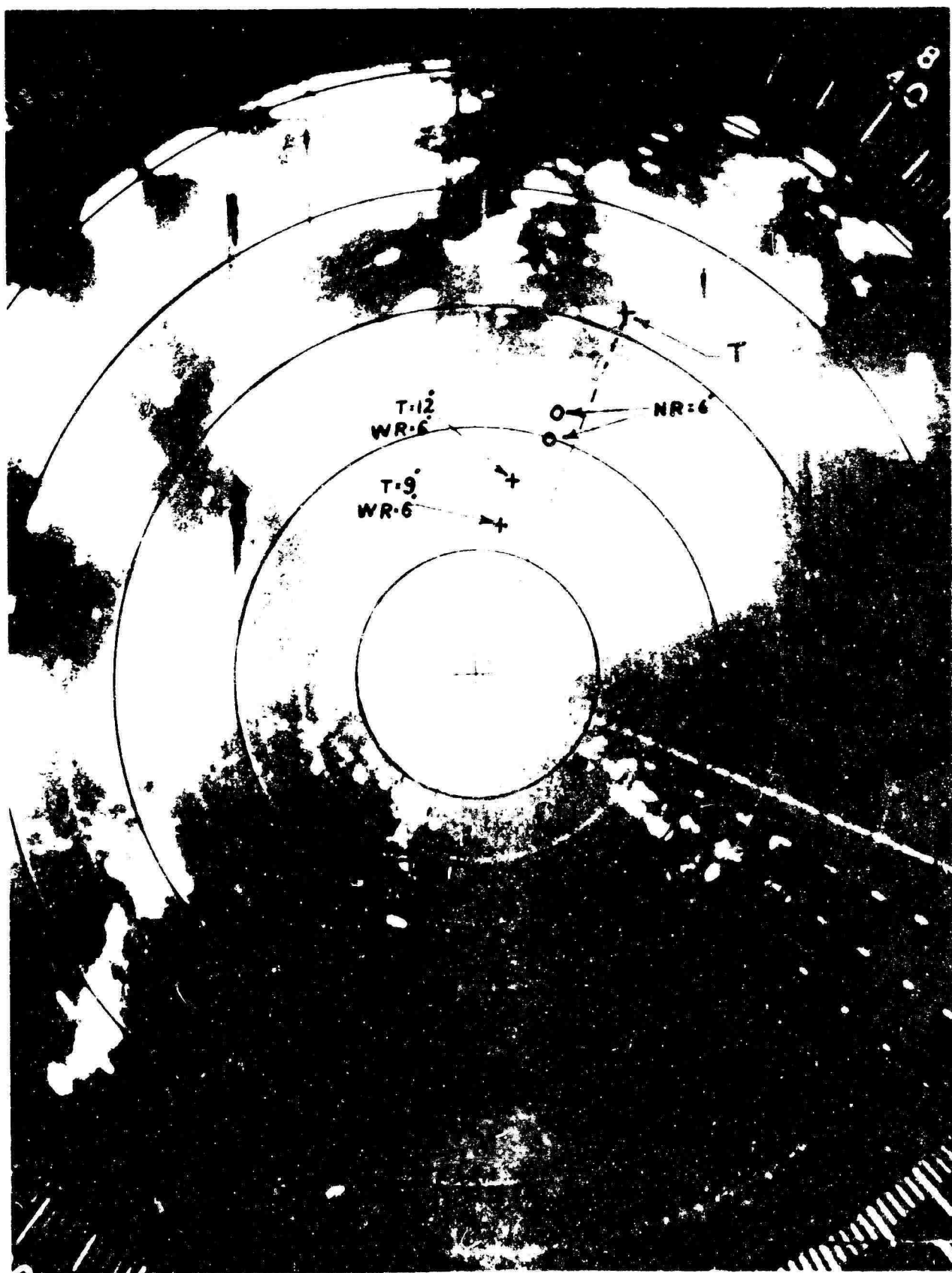
1716 6/28/66 10 dB Att.

Figure 61H



1716 6/28/66 42 dB Att.

Figure 611



2015 6/28/66 No Att.

Figure 61J



2015 6/28/66

18dB Att.

Figure 61K



2015 6/28/66 42 dB 411

Figure 61L



LOCAL CLIMATOLOGICAL DATA

U S DEPARTMENT OF COMMERCE -- JOHN T. CONNOR, Secretary

ATLANTIC CITY, NEW JERSEY
AVIATION FACILITIES EXPER CTR
JUNE 1966

ENVIRONMENTAL SCIENCE SERVICES ADMINISTRATION -- ENVIRONMENTAL DATA SERVICE

Latitude 39° 27' N			Longitude 74° 35' W			Elevation (ground) 64 ft.			Standard time used: EASTERN													
Temperature (°F)						Weather types shown by code 1-9 on dates of occurrence			Precipitation		Avg. station pressure (in.)		Wind			Sunshine		Sky cover (Tenths)				
Date	Maximum	Minimum	Average	Departure from normal	Average dew point	Degree days (base 65°)	Weather types shown by code 1-9 on dates of occurrence	Snow, sleet, or ice on ground at 07AM (in.)	Total (Water equivalent) (in.)	Snow, sleet (in.)	Exes feet m.s.l.	Resultant direction	Resultant speed (m.p.h.)	Average speed (m.p.h.)	Speed (m.p.h.)	Direction	Total (Hours and tenths)	Percent of possible	Sunrise to sunset	Midnight to midnight	Date	
1	65	40	53	14	44	12	1	0	0	0	0	29.99	04	3.1	6.5	12	17	7.1	48	5	4	1
2	67	39	53	14	37	12	1	0	0	0	0	30.07	33	8.9	9.2	17	34	10.7	72	5	3	2
3	78	45	62	6	44	1	0	0	0	0	0	30.17	25	8.2	10.9	16	22	13.1	88	3	4	3
4	87	64	71	3	54	0	0	0	0	0	0	30.11	22	8.2	11.2	20	16	10.0	93	4	4	4
5	90	60	75	7	60	0	0	0	0	0	0	30.06	41	9.3	9.9	18	22	14.8	100	0	0	5
6	86	61	74	5	49	0	0	0	0	0	0	30.02	19	10.9	11.2	18	19	13.5	91	1	1	6
7	85	61	73	5	62	0	0	0	.03	0	0	29.93	21	9.6	10.6	14	25	7.5	50	7	7	7
8	88	63	76	7	62	0	1	0	0	0	0	29.96	22	8.7	9.9	17	19	9.7	45	6	6	8
9	88	66	77	8	62	0	0	0	0	0	0	29.91	22	8.5	10.4	16	18	11.5	77	5	6	8
10	90	53	72	3	63	0	3	0	.20	0	0	29.74	23	9.6	15.0	23	23	3.2	21	10	9	10
11	66	48	59	10	46	4	1	0	0	0	0	30.01	09	9.4	11.4	18	09	11.1	74	8	7	11
12	65	52	59	11	50	4	1	0	.01	0	0	30.12	09	14.8	15.1	23	06	2.3	19	10	10	12
13	69	56	63	7	62	7	1	0	.14	0	0	29.99	02	12.1	13.1	17	01	0.0	0	10	10	13
14	65	62	74	4	65	0	1	0	.01	0	0	29.89	20	9.8	10.4	17	18	10.6	71	7	7	14
15	64	63	74	4	61	0	0	0	0	0	0	29.88	24	7.0	8.8	18	21	9.7	65	6	6	15
16	90	59	75	4	63	0	1	0	1.24	0	0	29.82	19	10.4	11.1	28	21	10.3	69	6	6	16
17	72	60	66	5	64	0	1	0	0	0	0	29.84	24	6.4	7.0	9	25	0.4	0	10	9	17
18	79	57	68	3	62	0	2	0	0	0	0	30.01	18	4.1	4.3	13	18	4.0	27	10	9	18
19	73	55	64	7	58	1	1	0	0	0	0	30.06	05	3.5	5.6	12	09	3.5	23	9	8	19
20	76	51	64	7	56	1	2	0	0	0	0	30.12	20	6.3	7.0	15	16	13.0	87	2	2	20
21	92	58	75	4	62	0	1	0	0	0	0	30.08	26	4.7	6.3	12	26	11.2	75	2	2	21
22	77	55	66	6	57	0	0	0	0	0	0	30.16	08	6.8	9.9	15	08	12.1	87	2	2	22
23	88	51	70	2	60	0	2	0	0	0	0	30.01	21	5.0	6.9	14	18	12.3	82	7	6	23
24	96	68	82	10	62	0	0	0	0	0	0	29.88	33	9.7	10.9	27	34	9.4	63	3	3	24
25	90	65	78	6	62	0	0	2	0	0	0	30.03	04	4.7	8.9	16	09	11.4	76	2	4	25
26	80	63	72	0	64	0	2	0	0	0	0	30.13	14	5.3	7.5	14	17	8.0	54	5	7	26
27	95	65	80	8	65	0	0	0	0	0	0	30.01	23	9.8	10.2	17	24	7.7	52	4	5	27
28	93	69	81	8	64	0	1	0	0	0	0	29.92	20	6.1	9.6	14	13	4.0	27	7	7	28
29	86	70	78	5	64	0	1	0	0	0	0	29.83	22	6.1	9.1	13	27	5.1	34	8	7	29
30	91	68	80	7	59	0	1	0	0	0	0	29.87	22	1.2	8.3	14	12	13.6	91	0	0	30

Sum	Sum	Total	Dep	Temperature	Total	Total	For the month	Total	Sum	Sum
2476	1737	4213	28	Number of days	1.87	0	29.98	22	2.8	6.5
Avg	Avg	Avg	Dep	Avg	Season to date	Dep	Dep	Date: 16	Possible	month
82.5	57.9	70.2	0.2	58	5684	789	0	9	0	0
Extremes for the month: May be the last of more than one occurrence										
Below zero temperatures or negative departure from normal										
T In columns 9, 10, and 11 and in the Hourly Precipitation table indicates an amount too small to measure.										
X Heavy fog - visibility 1/4 mile or less.										
Greatest in 24 hours and dates										
Precipitation Snow, Sleet										
Greatest depth on ground of snow, sleet or ice and date										
1.24 16 0										
T 5° or below at Alaskan stations + Also on an earlier date, or dates.										

HOURLY PRECIPITATION (Liquid in Inches)

A. M. Hour ending at												P. M. Hour ending at												
1	2	3	4	5	6	7	8	9	10	11	12	1	2	3	4	5	6	7	8	9	10	11	12	
1																								1
2																								2
3																								3
4																								4
5																								5
6																								6
7																								7
8																								8
9																								9
10																								10
11																								11
12																								12
13	T	T	.03	.01	T	.01	T	T	.02	.02	.01	.01	.02	T	T	.01	T	T		.01	T	T	T	13
14																								14
15																								15
16																								16
17																								17
18																								18
19	T	T	T	.02	.07	.05	.05	.01	T	T														19
20																								20
21																								21
22																								22
23																								23
24																								24
25																								25
26	T	T	T																					26
27																								27
28																								28
29	T	T																						29
30																								30

Data in columns 6, 12, 13, 14, and 15 are based on 4 observations per day at 3-hour intervals. Wind directions are those from which the wind blows. Resultant wind is the vector sum of wind directions and speeds divided by the number of observations. Figures for directions are tens of degrees from true North, i.e., 09 = East, 18 = South, 27 = West, 36 = North, and 00 = Calm. When directions are in tens of degrees in Col. 17, entries in Col. 16 are fastest observed 1 minute speeds. If the Z appears in Col. 17, speeds are gusts. Any errors detected will be corrected and changes in summary data will be annotated in the annual summary if published.

Subscription Price: Local Climatological Data \$1.00 per year including annual summary if published. Single copy 10 cents for monthly summary, 15 cents for annual summary. Checks or money orders should be made payable and remittances and correspondence should be sent to the Superintendent of Documents, U. S. Government Printing Office, Washington, D. C. 20462.

I certify that this is an official publication of the Environmental Science Services Administration, and is compiled from records on file at the National Weather Records Center, Asheville, North Carolina 28801.

William J. Haggard
Acting Director, National Weather Records Center

AVERAGES BY HOURS												Resultant	
Hour	Max	Min	Avg	Max	Min	Avg	Max	Min	Avg	Max	Min	Wind	Speed
01	5	29.99	62	59	86	57	6.8	26	2.3				
06	5	29.98	61	58	87	56	6.5	27	1.6				
07	5	30.01	66	61	77	58	9.2	27	2.8				
10	5	30.01	74	66	57	59	10.6	28	2.9				
13	6	29.98	81	67	48	58	13.0	22	3.5				
16	6	29.96	78	66	55	59	13.0	08	6.7				
19	6	29.97	71	66	68	59	9.6	18	6.8				
22	6	29.99	65	62	81	59	7.7	21	6.3				
USCOMM - ESSA - ASHEVILLE 225													

Figure 62 A

[illegible]

CEILING COLUMN
UNL indicates an unlimited ceiling.
CLR indicates a continuous clearing of unknown height.

WEATHER COLUMN —
T Tornado
Q Fog
R Rain
RW Rain showers
ZR Freezing rain
L Drizzle
ZL Freezing drizzle
S Snow
SP Snow pellets
I Ice crystals
SW Snow showers
SG Snow grains
A Mist
AP Misty haze
F Fog
IF Ice fog
GF Ground fog
BD Blowing dust
DS Blowing sand
BS Blowing snow
BYS Blowing sprs.
S Smoke
H Haze
D Dust

Directions are those from which the wind blows, indicated in terms of degrees from true North. 1 e. 00 for East, 18 for South, 27 for West. Entry of 00 in the direction column indicates calm.

Speed is expressed in knots, multiply by 1.15 to convert to miles per hour.

Other observational data contained in records on file can be furnished at cost via microfilm or microfiche copies of the original records. Inquiries as to availability and costs should be addressed to:

Director
National Weather Records Center
Federal Building
Asheville, N. C. 28801

Figure 62 B

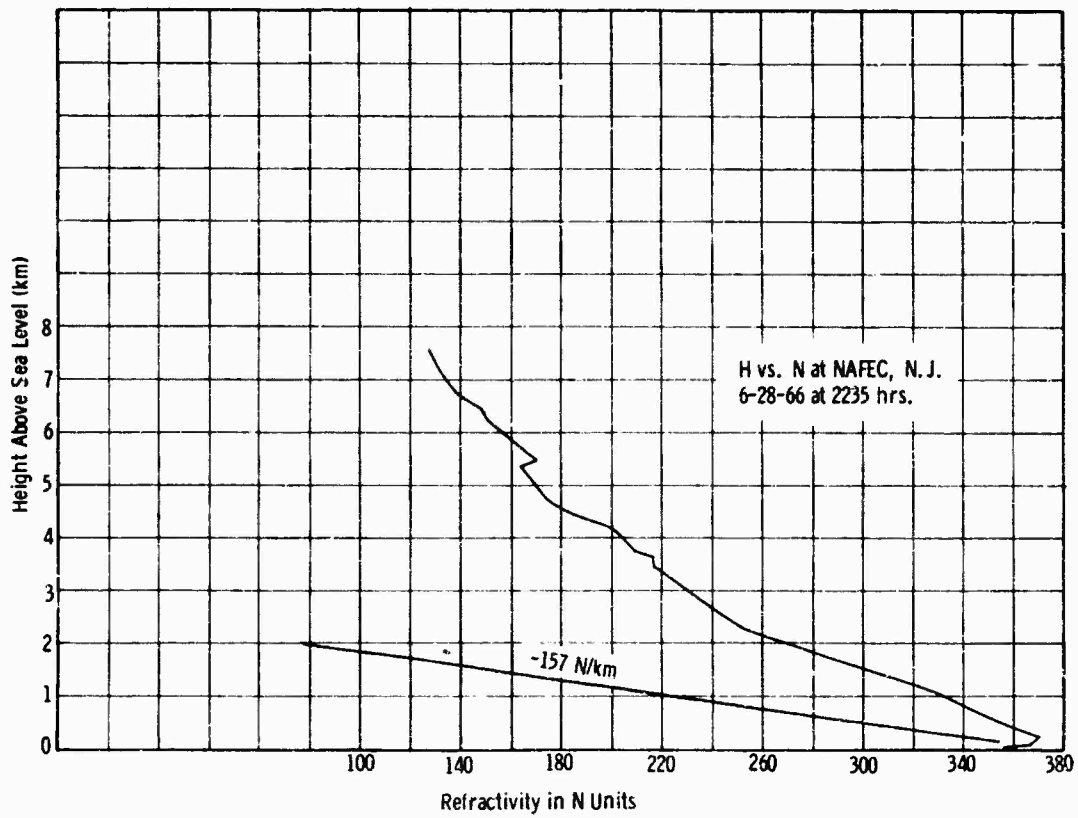
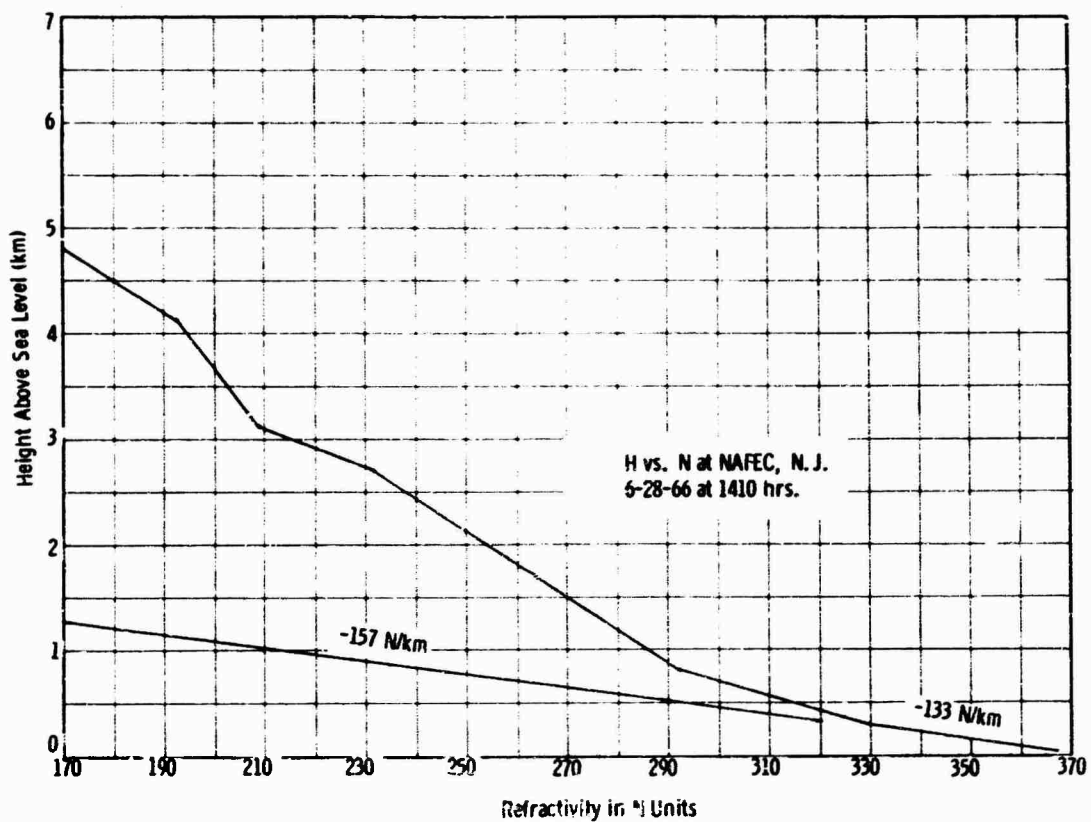


Figure 63

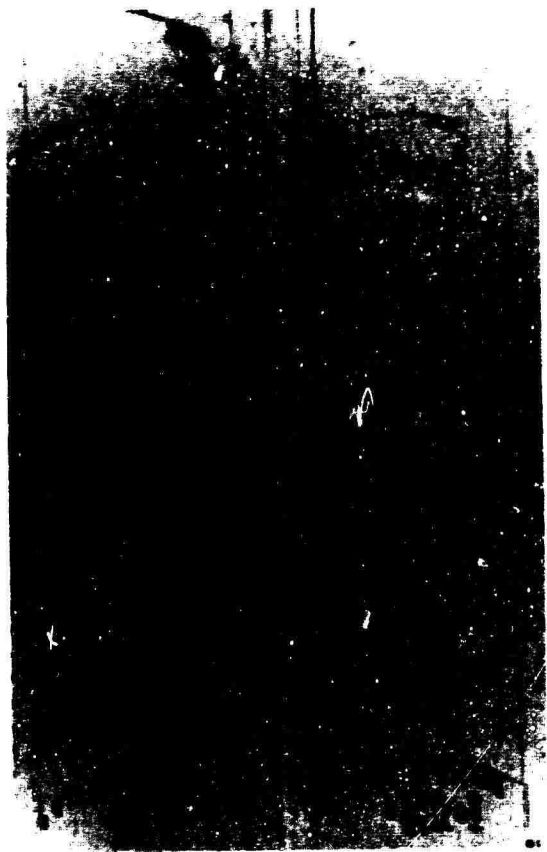


Figure 64A

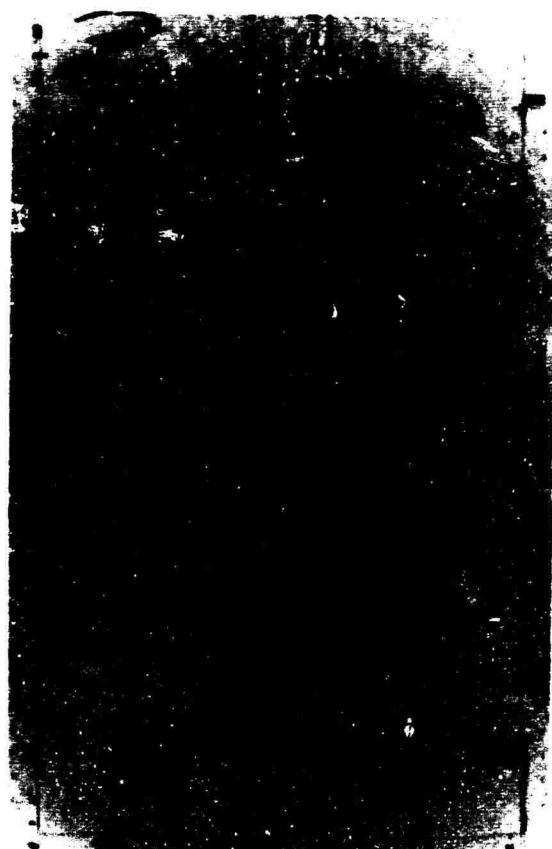


Figure 64B

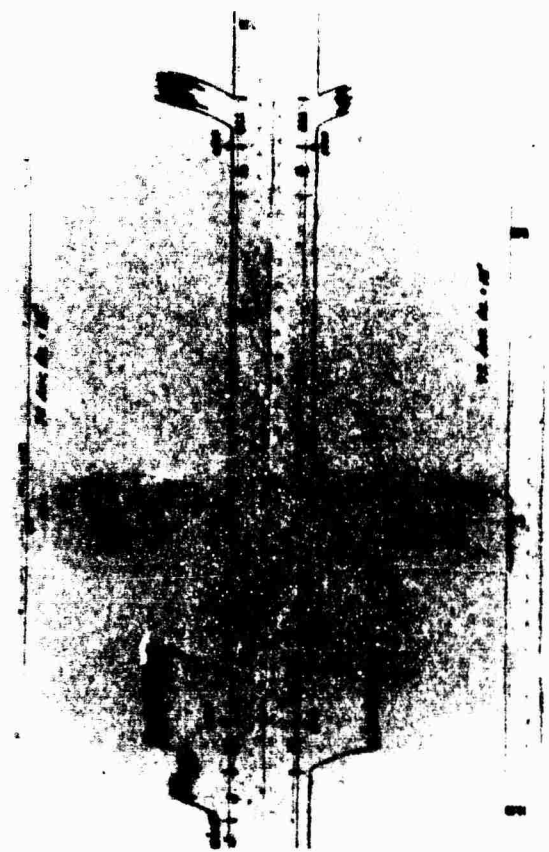


Figure 64C

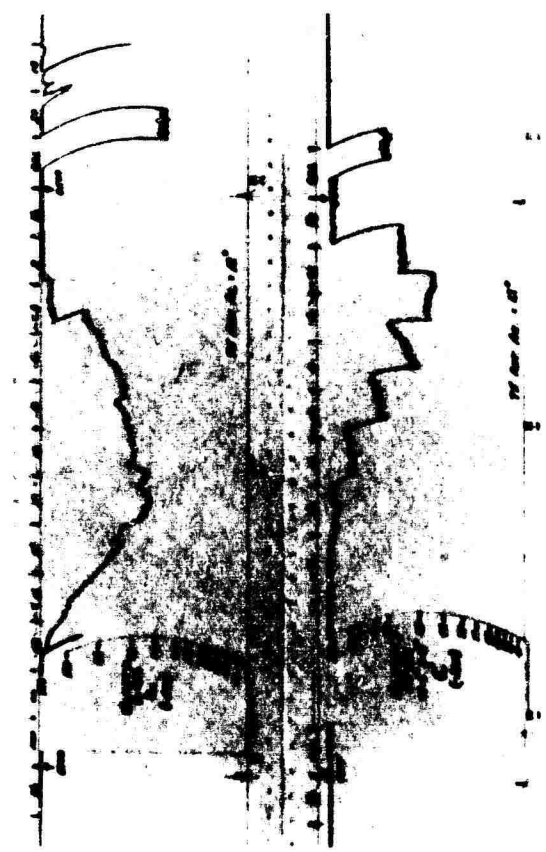
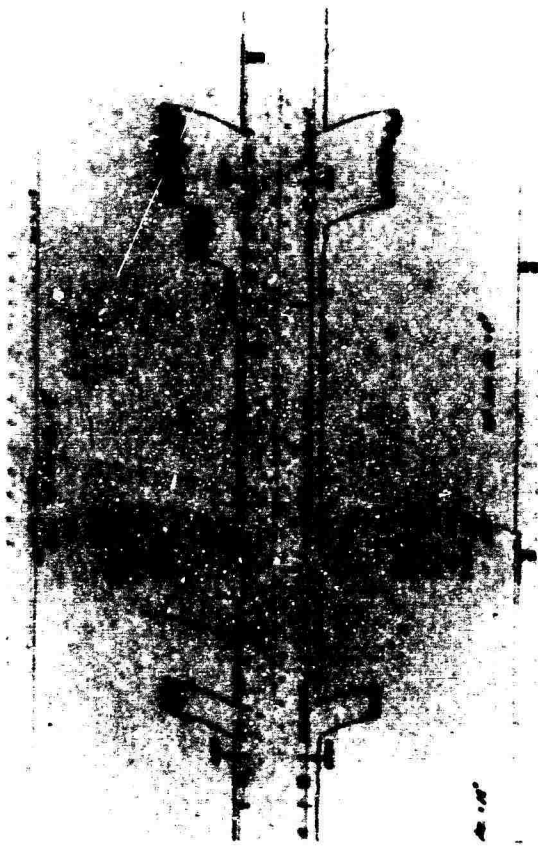


Figure 64D

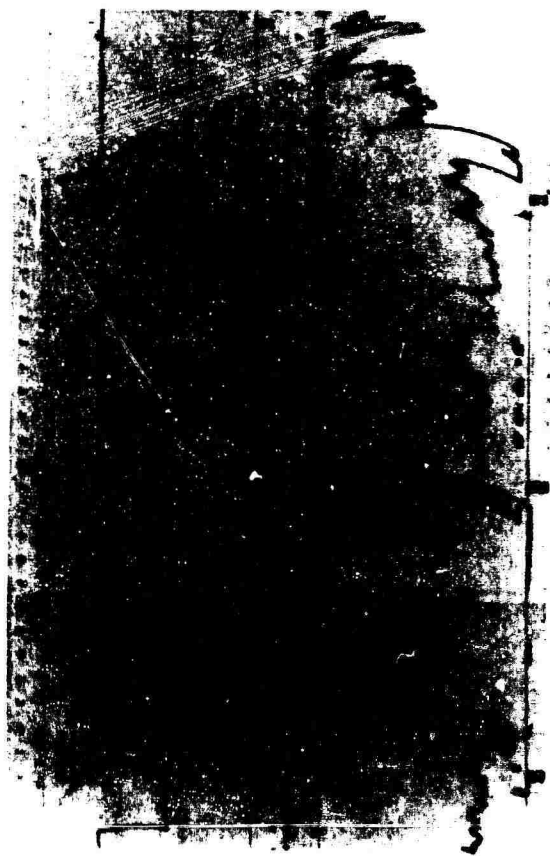
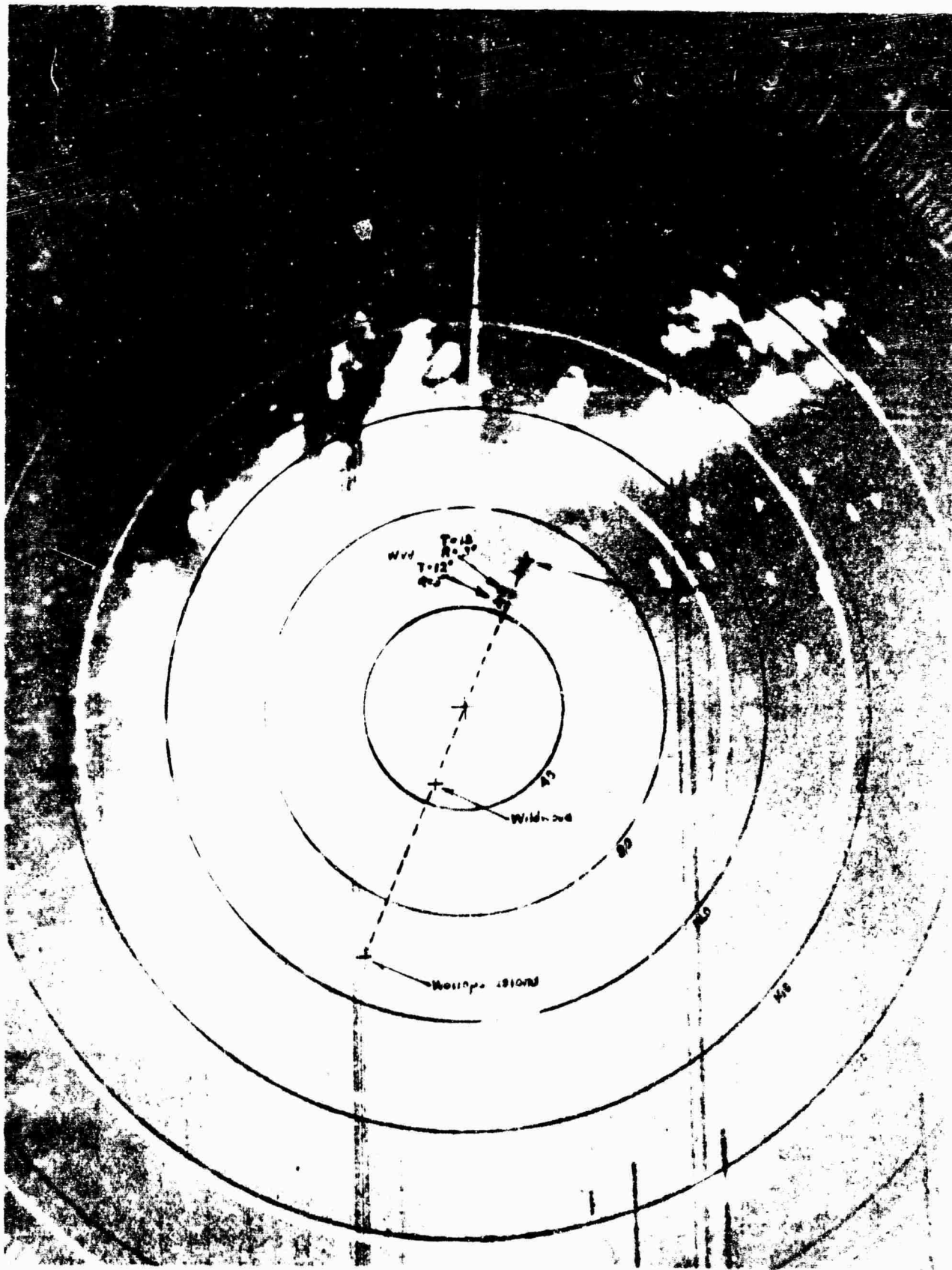


Figure 65



2200 10/15/66 No Att. FIG. 66 A



No Att.

Figure 66B



No Att.

Figure 66C



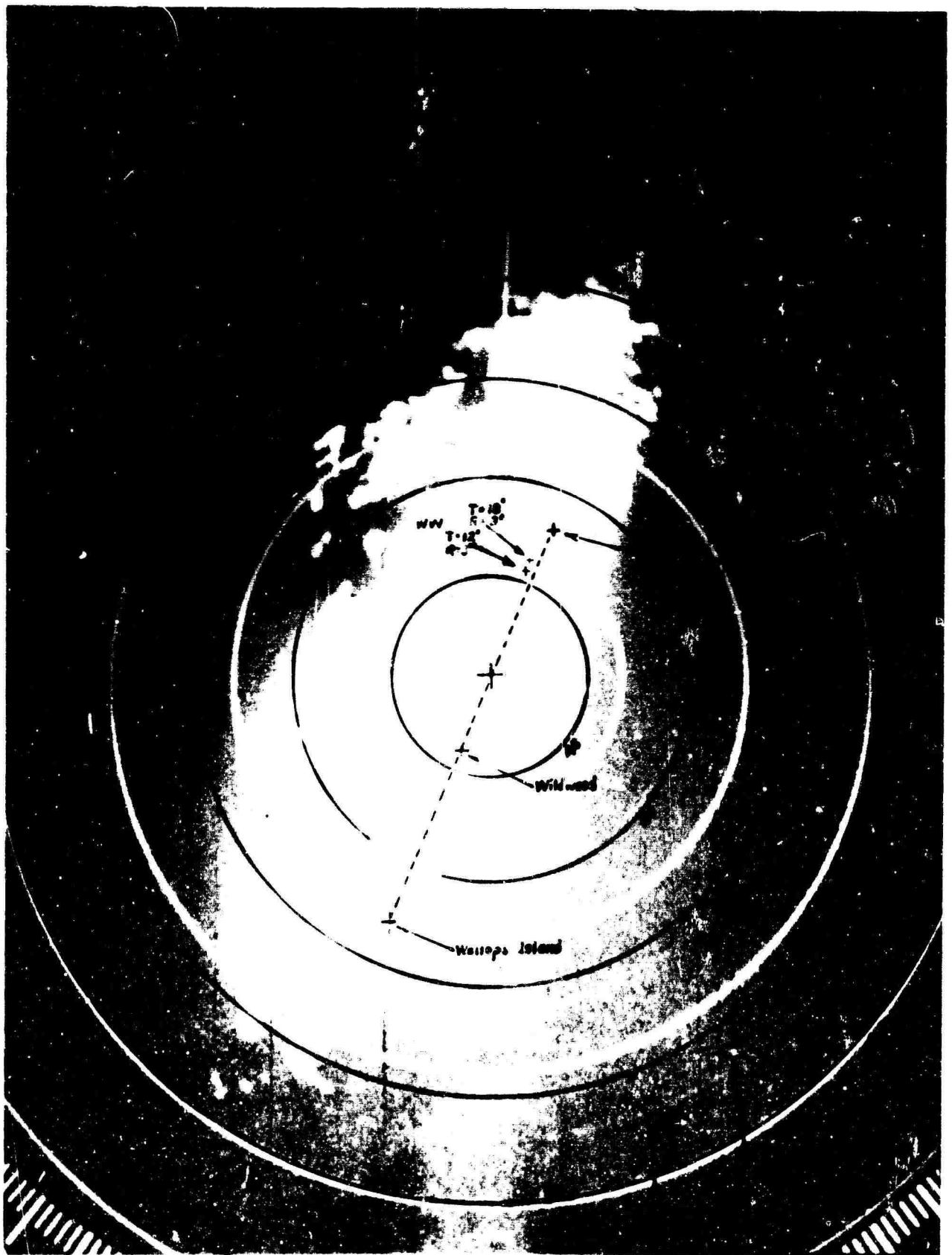
0030 10/16/66 No Att.

Figure 66E



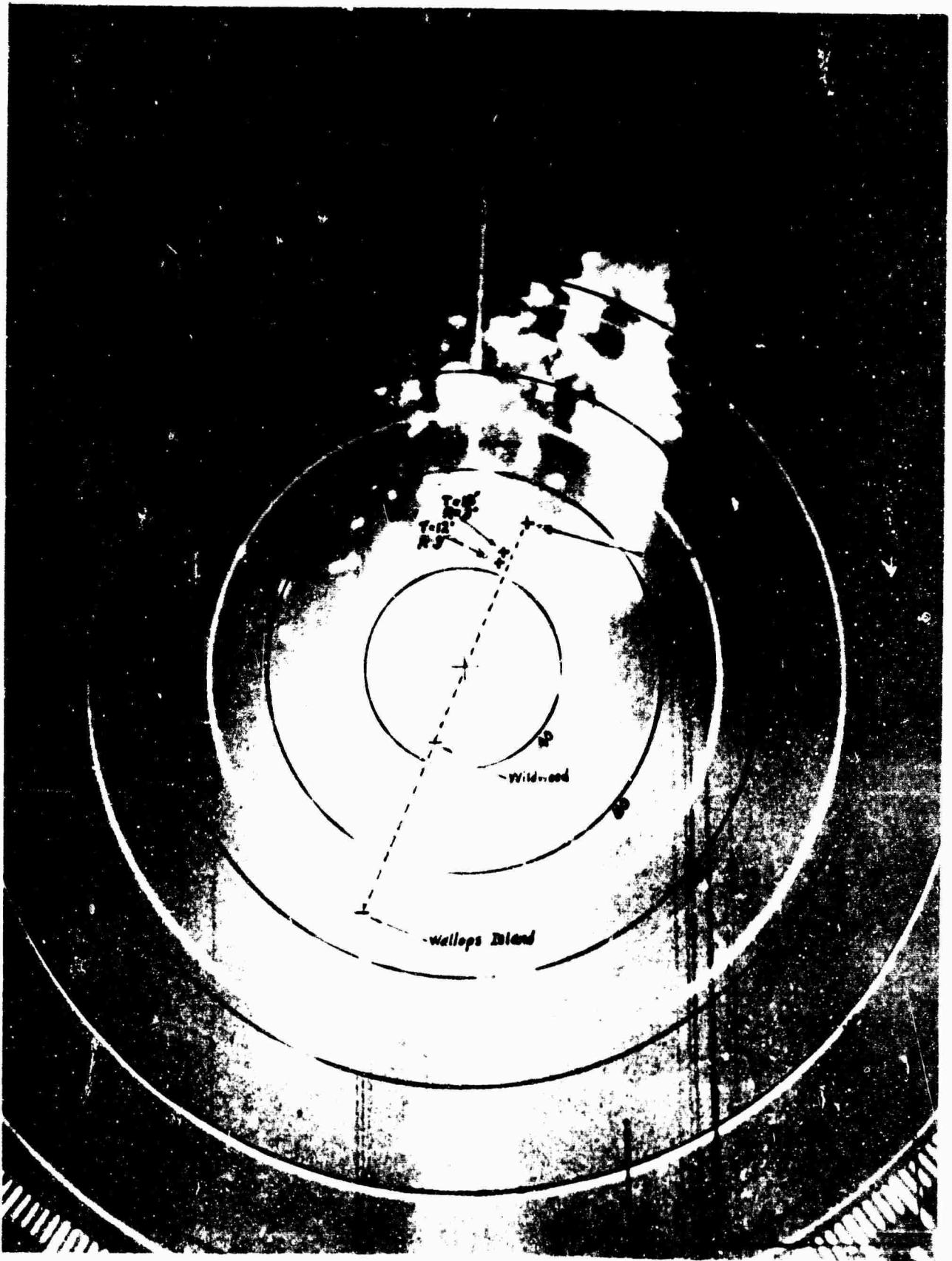
No Att.

Figure 66F



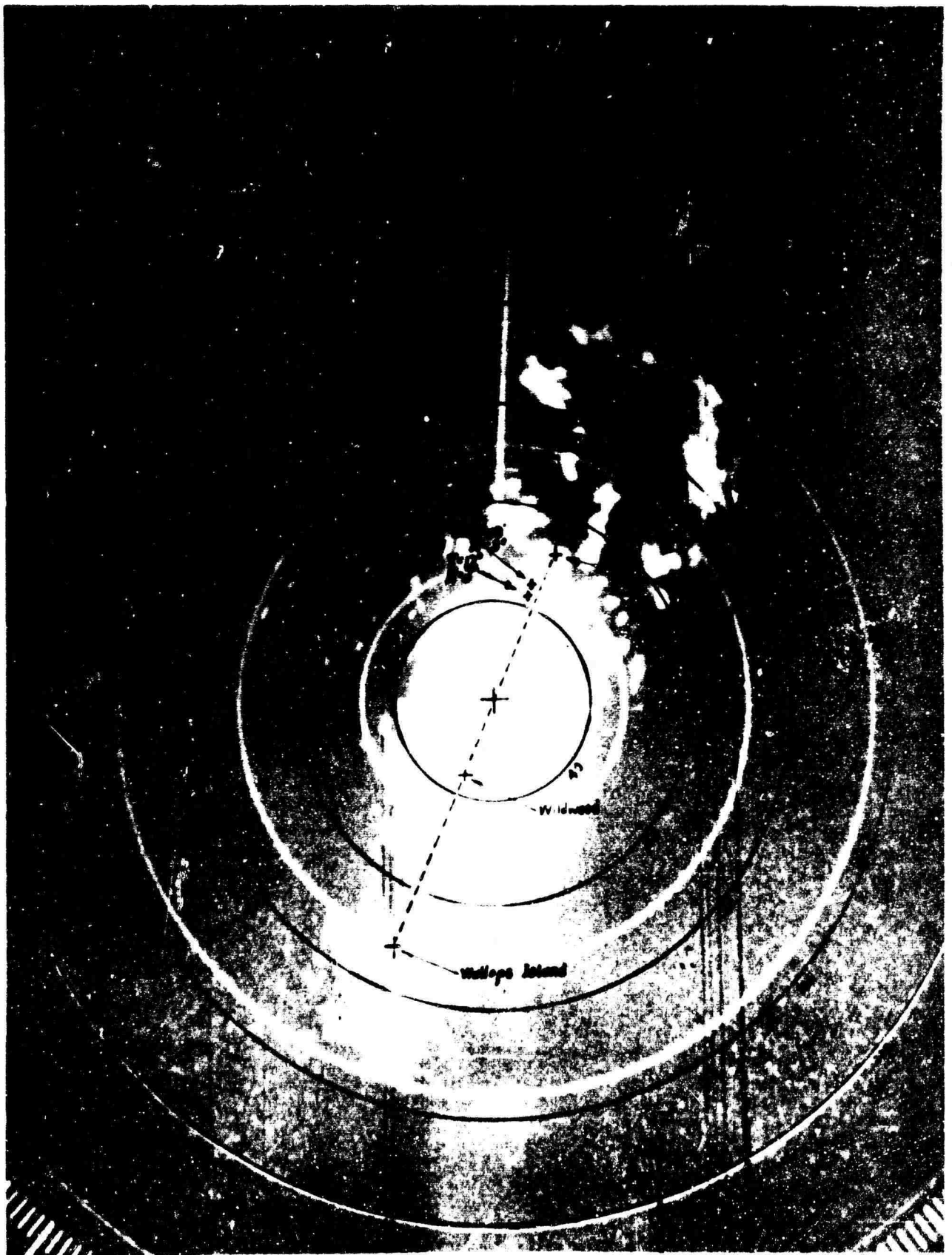
No Att.

Figure 66G



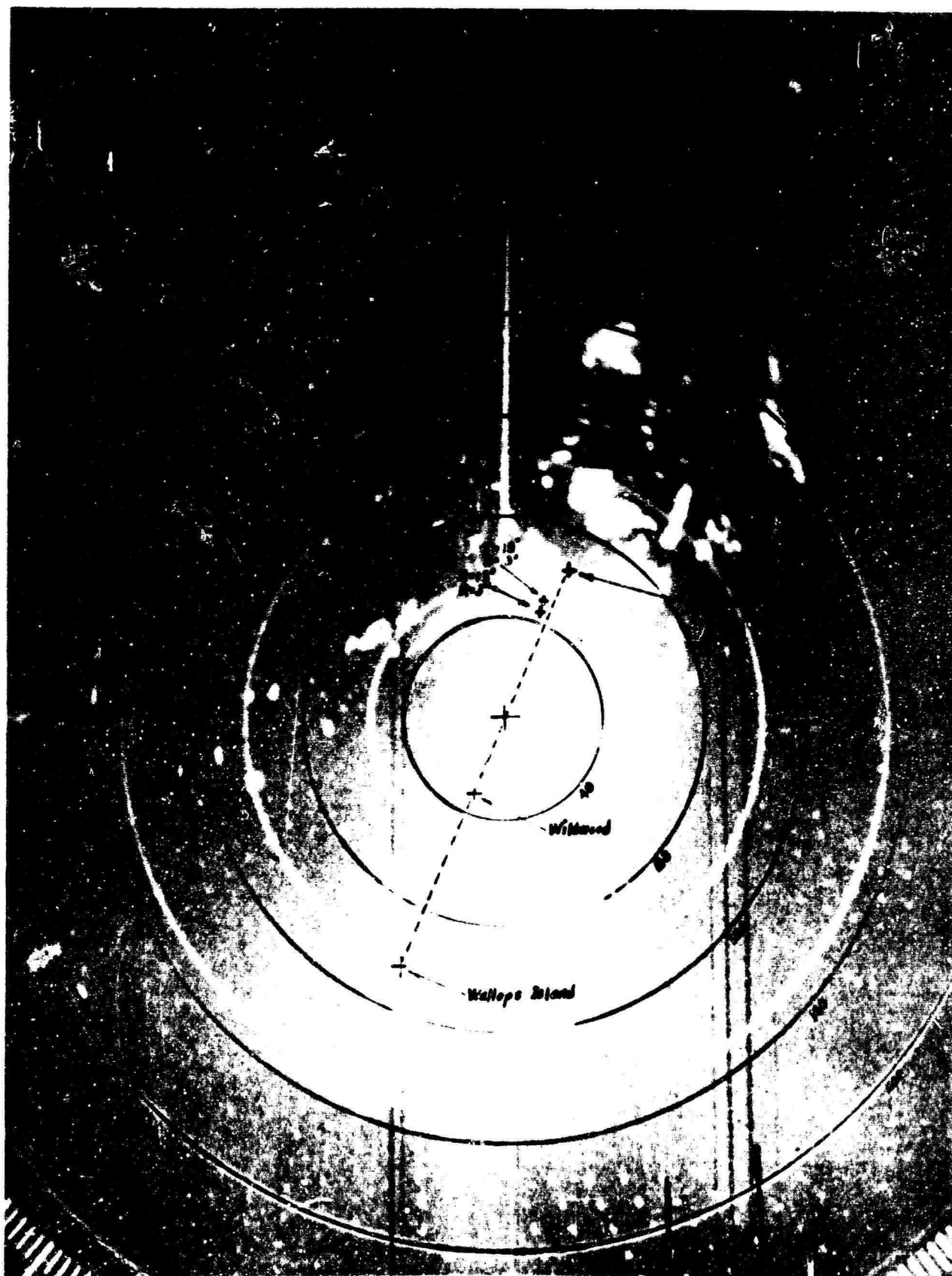
No Att.

Figure 66H



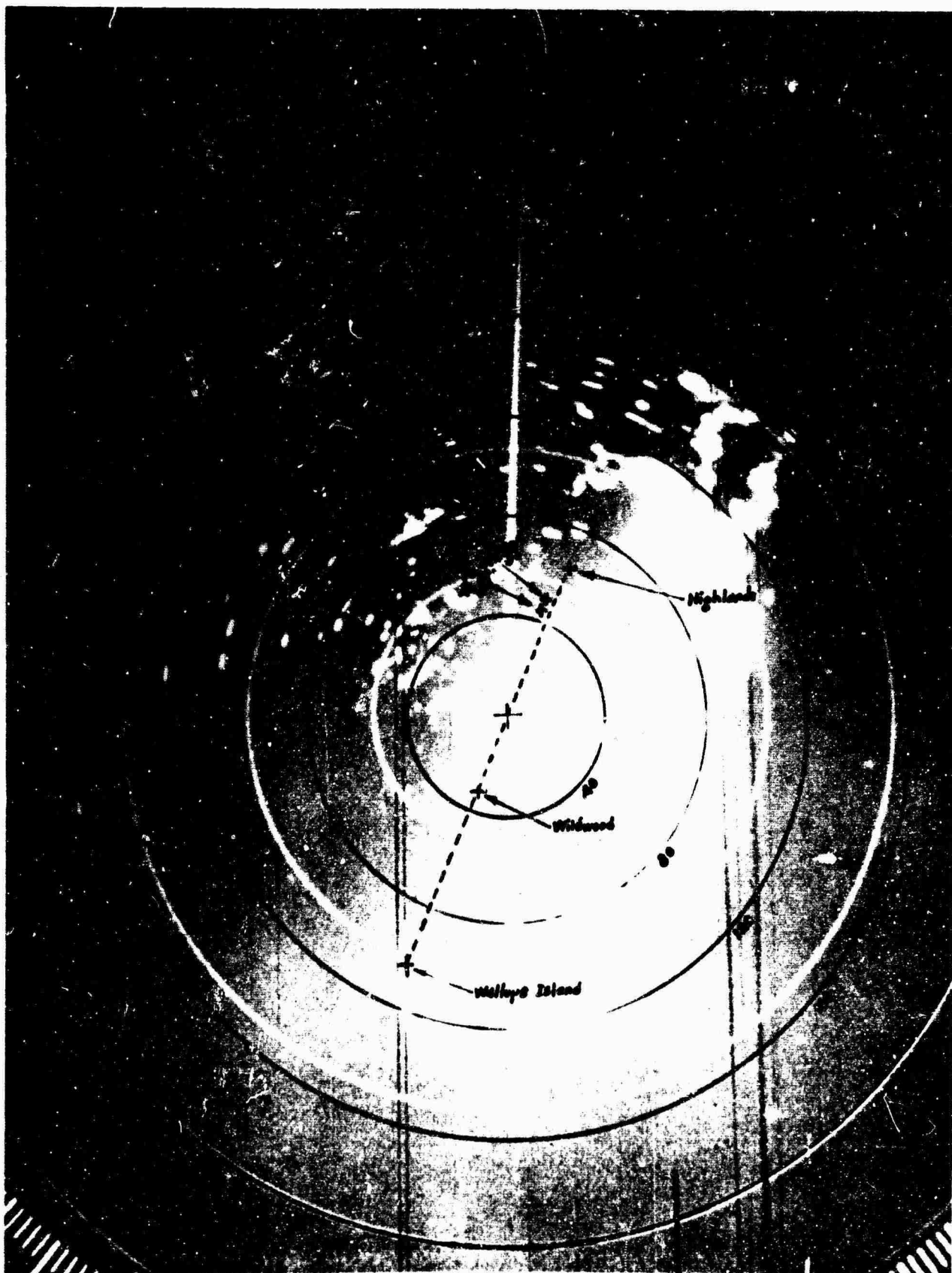
No Att.

Figure 661



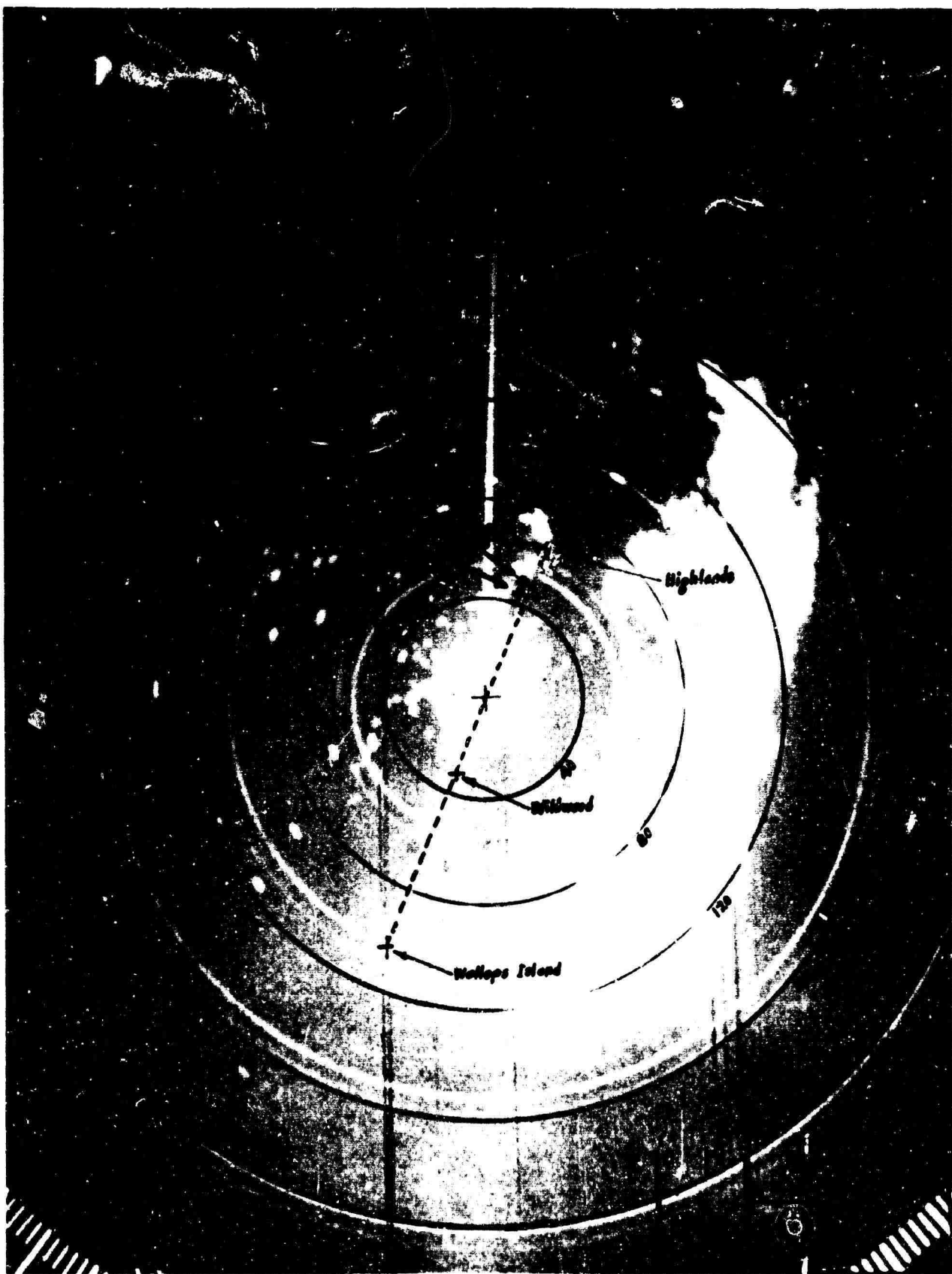
No Att.

Figure 66J



No Att.

Figure 66K



0600 10/16/66 No Att.

Figure 66L

F.C.C. - Washington, D. C.

00007-1

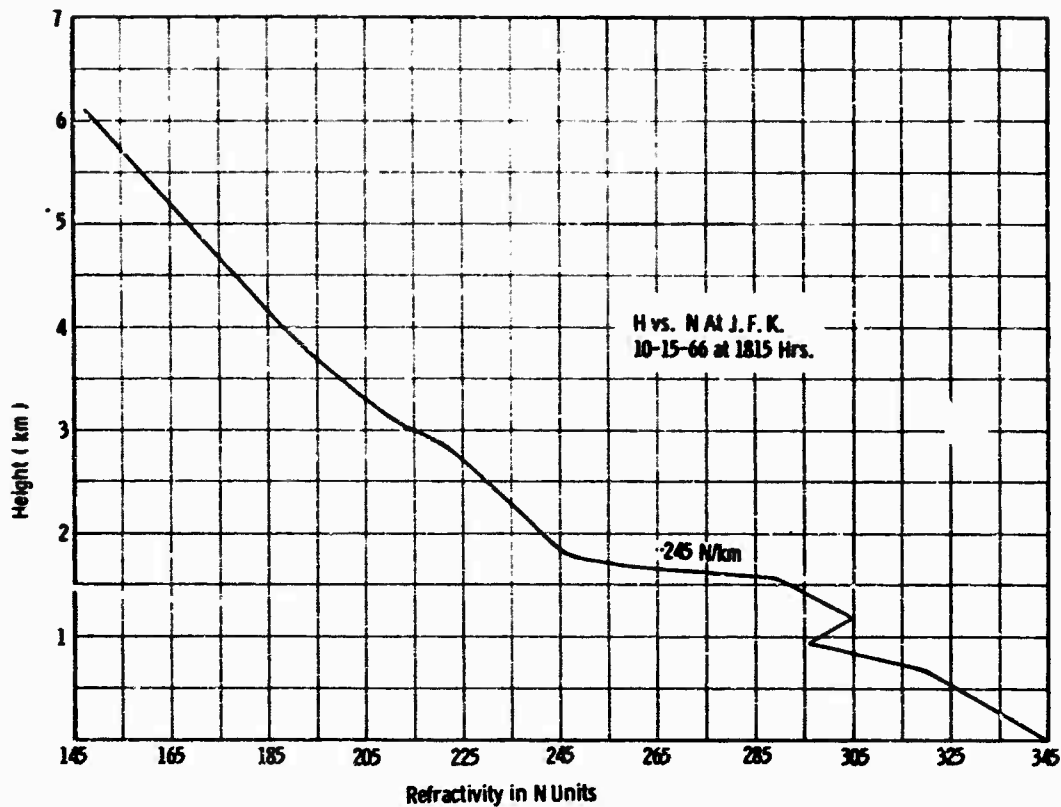


Figure 67A

F.C.C. - Washington, D. C.

00007-1

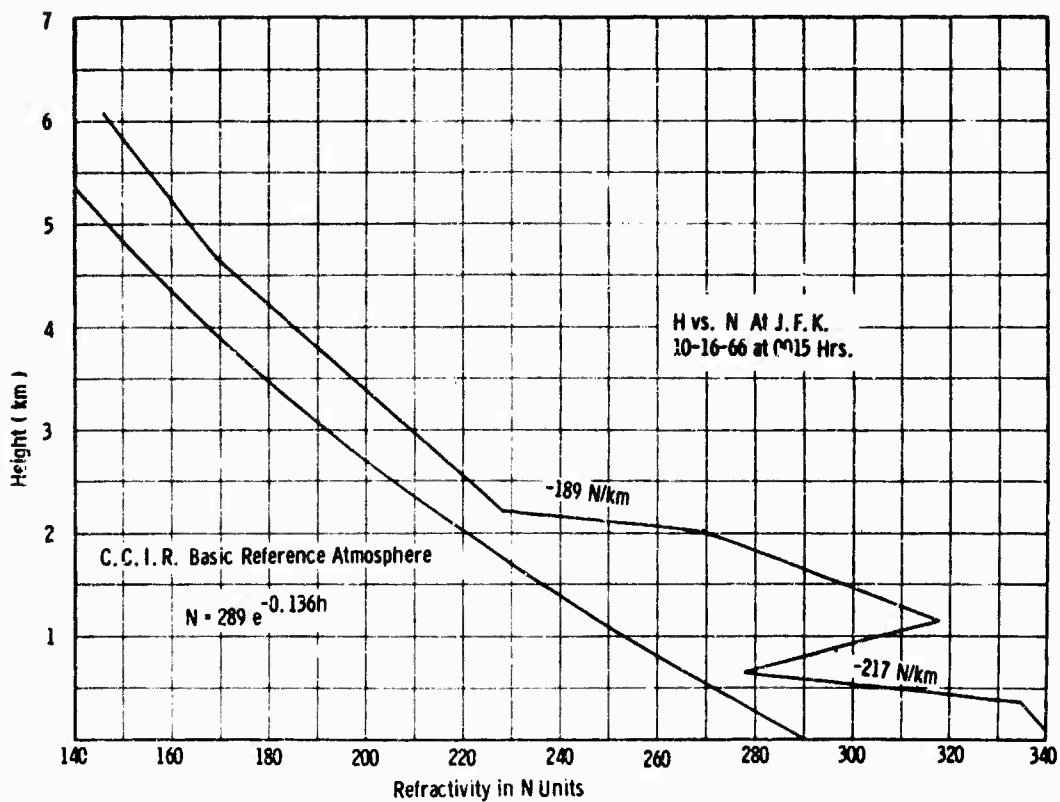


Figure 67B

F.C.C. - Washington, D. C.

66007-1

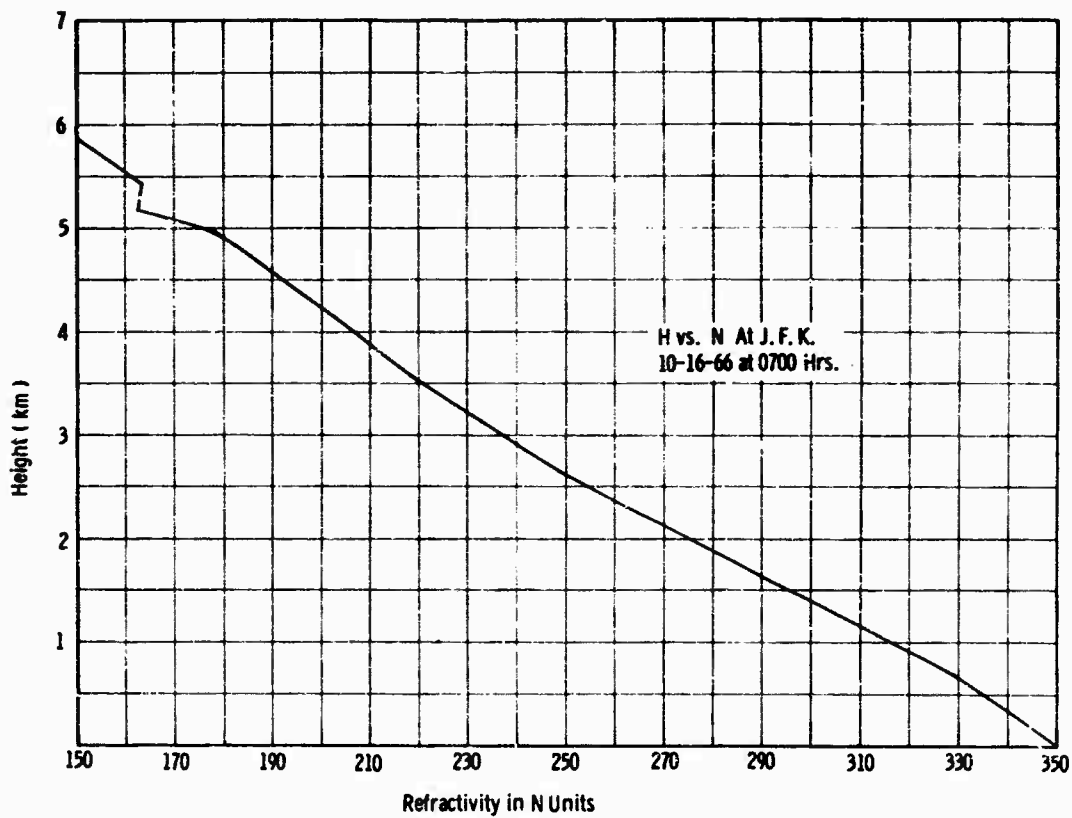


Figure 67C

AD-667 422

POPSI Project Report

Errata Sheet

Page	Line	
Title	4	Delete: "Annex \"
2	last line	Delete: "B"
3	6	Change: "opperate" to "operate"
4	11	Change: "6" to "5"; and add: ", and a typical receiver installation is shown in Figure 6."
10	7 lines from bottom	Insert "52" between "Figure" and "D."

RAPI